# HERMES
# (THE COMMUNICATIONS TECHNOLOGY SATELLITE)
# ITS PERFORMANCE AND APPLICATIONS

## VOLUME 2



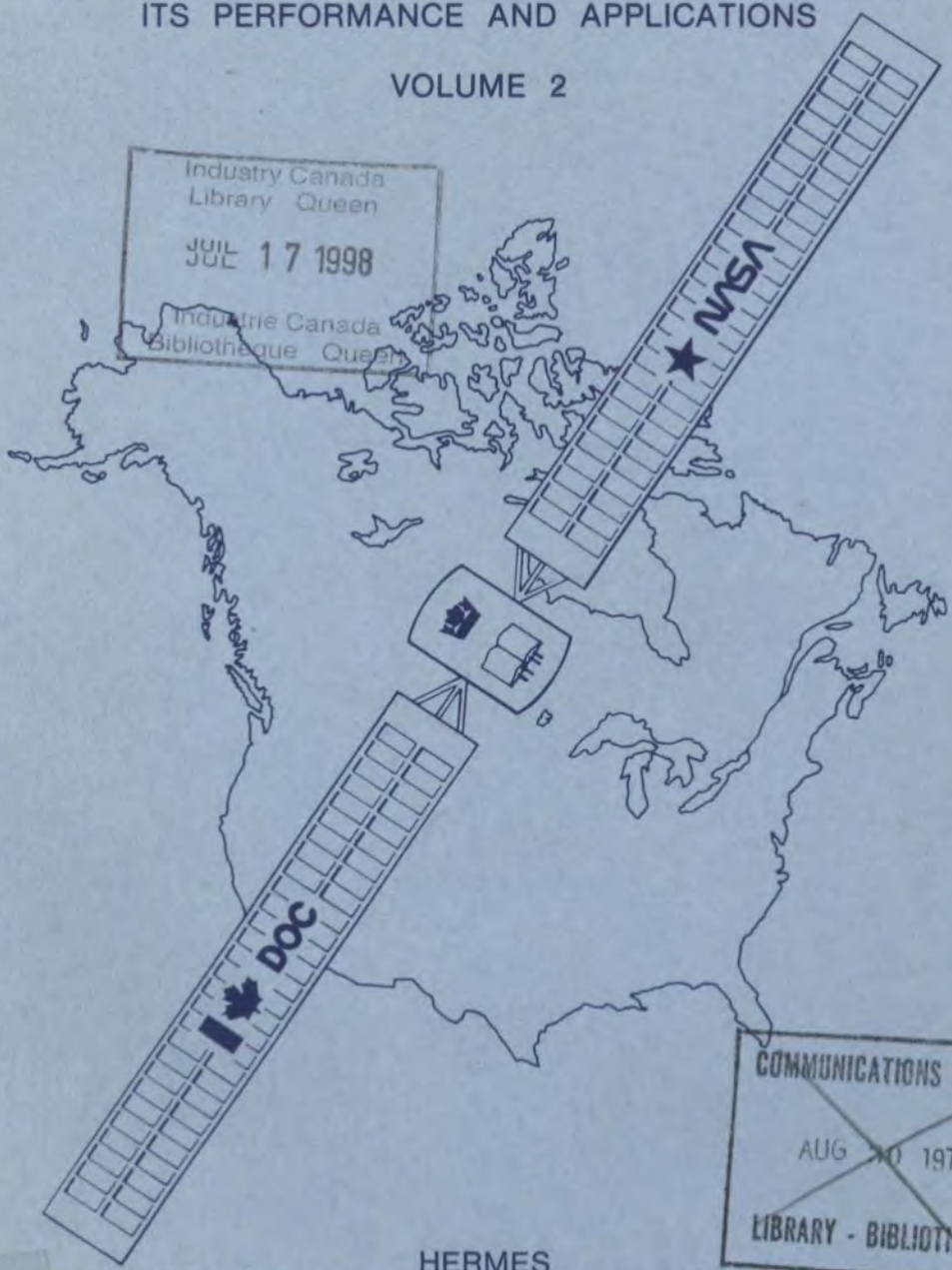




# HERMES
# (LE SATELLITE TECHNOLOGIQUE DE TELECOMMUNICATIONS)
# SON FONCTIONNEMENT ET SES APPLICATIONS

## TOME 2

IRVINE PAGHIS EDITOR/EDITEUR

THE ROYAL SOCIETY OF CANADA
Twentieth Symposium

LA SOCIETE ROYALE DU CANADA
vingtième colloque

# HERMES

## (THE COMMUNICATIONS TECHNOLOGY SATELLITE):

## ITS PERFORMANCE AND APPLICATIONS

# HERMES

## (LE SATELLITE TECHNOLOGIQUE DE TELECOMMUNICATIONS):

## SON FONCTIONNEMENT ET SES APPLICATIONS

in cooperation with:

THE DEPARTMENT OF COMMUNICATIONS CANADA

and

THE NATIONAL AERONAUTICS AND SPACE ADMINISTRATION (NASA) UNITED STATES OF AMERICA

de concert avec:

LE MINISTERE DES COMMUNICATIONS CANADA

et

L'ADMINISTRATION NATIONALE AERONAUTIQUE ET SPATIALE (NASA) ETATS-UNIS D'AMERIQUE

29-30 November,
1 December 1977

in the

National Library

29-30 novembre,
1 décembre 1977

dans la

Bibliothèque Nationale

Ottawa, Canada

Copies available from:
The Royal Society of Canada
344 Wellington
Ottawa, Ontario
K1A 0N4

Exemplaires obtenus de:
La Société royale du Canada

Price: $25.00 for three volumes

Prix: $25.00 pour les trois tomes

ISBN 0-920064-12-4

# TABLE OF CONTENTS/TABLE DES MATIERES

## VOLUME 2 - TOME 2

Page

SCIENCE AND TECHNICAL APPLICATIONS/
LA SCIENCE ET LES APPLICATIONS TECHNIQUES

*Chairman/Président: D. Wright*



## VOLUME 1 - TOME 1



## VOLUME 3 - TOME 3

*SPECIAL ADDRESS/COMMUNICATION SPECIALE*

# SPACECRAFT AND COMMUNICATIONS TECHNOLOGY

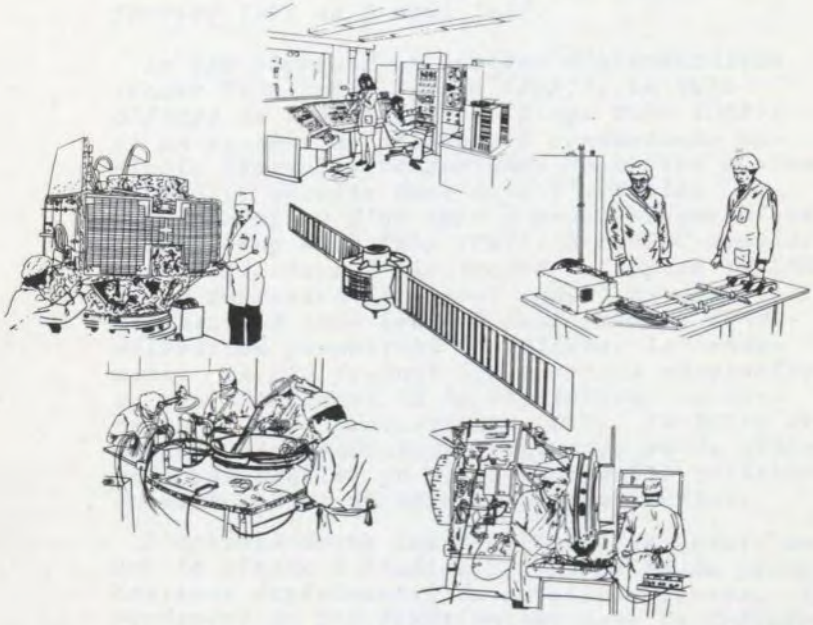

# LA TECHNOLOGIE DES VEHICULES SPATIAUX ET DES COMMUNICATIONS

# PERFORMANCE OF THE 12 GHz, 200 WATT TRANSMITTER EXPERIMENT PACKAGE FOR THE HERMES SATELLITE

Robert E. Alexovich

NASA-Lewis Research Center

Cleveland, U.S.A.

*Evaluation du rendement du groupe émetteur expérimental (Transmitter Experiment Package (TEP)) du satellite Hermès lors d'essais en orbite. Les essais ont été effectués du 8 février 1976 au 8 août 1977.*

*Le TEP comprend un système d'alimentation (Power Processing System (PPS)), un tube d'étage de sortie (Output Stage Tube (OST)) et un système de caloducs à conductance variable (Variable Conductance Heat Pipe System (VCHPS)), décrits dans dans l'article. Le OST se compose d'un tube à ondes progressives (Travelling Wave Tube (TWT)) à cavité couplée, d'un collecteur à électrodes multiples (Multistage Depressed Collector (MDC)) et d'une structure à onde lente à deux paliers de décélération permettant d'améliorer le rendement. Le PPS fournit les tensions nécessaires au fonctionnement, à la régulation, au contrôle et à la protection du OST. Le VCHPS se compose d'un radiateur à ailettes et de trois caloducs doubles en acier inoxydable contenant du méthanol et un mélange de gaz inertes.*

*L'article donne les résultats des essais en orbite visant à étudier l'efficacité du groupe émetteur expérimental du satellite Hermès. Le rendement du OST fonctionnant dans la fréquence centrale de la bande et avec une puissance de sortie en régime de saturation est de 50.75%. Les puissances de sortie rf et d'alimentation en DC du OST étaient respectivement de 233.4 et 463.9 watts. Il n'y a pas eu de baisse appréciable du rendement attribuable au lancement, à la phase précédant la mise sur orbite et à l'environnement spatial. D'autre part aucune diminution n'a été notée pendant les 8830 heures de fonctionnement de l'émetteur réparties sur une période de 568 jours en orbite.*

*L'anomalie thermique survenue pendant l'équinoxe de printemps n'a pas influencé irrémédiablement ou de façon permanente le rendement du TEP. Au terme des essais, le 8 août 1977, les anomalies thermiques ont été attribuées aux facteurs suivants:*

*a. désamorçage inexpliqué du VCHPS, ou*

*b. changements réversibles au niveau des échanges thermiques entre le OST et le VCHPS.*

*En conclusion:*

1. *Le lancement, la phase précédant la mise sur orbite et l'environnement spatial n'entraînent pas de baisse appréciable du rendement électrique du TEP.*

2. *La cause de l'anomalie thermique la plus plausible n'a pas influencé irrémédiablement ou de façon permanente le rendement du TEP.*

3. *On prévoit que le groupe émetteur aura une durée de vie utile de deux ans (environ 18,000 heures) sans baisse appréciable du rendement.*

## Introduction

The Communications Technology Satellite (CTS) or Hermes was developed in a joint U.S.-Canadian program by the National Aeronautics and Space Administration (NASA) and the Canadian Department of Communications (DOC) and was launched by NASA on 17 January 1976. One of the major responsibilities of the United States in this joint program was to provide a 200 watt, 12 GHz, 50% efficient high power transmitter for the spacecraft.

Before Hermes, microwave amplifiers for space applications were limited to frequencies below 8 GHz, power levels of 50 watts and efficiencies of 10 to 25%. These relatively low efficiencies represent an unnecessary waste of power which results in increased satellite weight and cost and a reduction in reliability; the latter being the result of excessive waste heat.

The key to future uses of higher rf powers for communication satellite applications is the development of high-power microwave amplifiers with high efficiency. As rf power output increases, the importance of high efficiency is emphasized. For high-power satellites, the efficiency of the transmitter is a major factor in determining the size of the solar array, the complexity and size of the thermal control system, and the weight of the power-processing system for the transmitter output amplifier. With the launching of Hermes, the era of high power (200w) and high efficiency (50%) space amplifiers has begun.

The Transmitter Experiment Package (TEP) for Hermes has a measured rf output of 233 watts and an overall efficiency of 50.75% at a center band frequency of 12.080 GHz. The operating bandwidth of the TEP is 85 MHz. It consists of the Output Stage Tube (OST), the Power Processing System (PPS) and the Variable Conductance Heat Pipe System (VCHPS).

The principal technological objectives of the TEP development are:

1. To demonstrate in space an amplifier operating with an efficiency $\geq$ 40 percent and a saturated rf output power $\geq$ 180 watts at a frequency of 12 GHz.

2. To demonstrate reliable high-efficiency performance for a transmitter experiment package for two years in a space environment.

3. To obtain fundamental data for further advancement in the state-of-the-art of high-power microwave amplifier operations in space.

This paper presents a description of the TEP, its unique design characteristics, and a summary of the on-orbit evaluation of the TEP performance.

## TRANSMITTER EXPERIMENT PACKAGE

The TEP is used as an output power amplifier in the Hermes transponder (Fig. 1) to amplify signals in the RB1/TB1 signal path. The communications requirements of the TEP are given in Table I. The TEP consists of a nominal 200 watt Output Stage Tube (OST), a supporting Power Processing System (PPS), and a Variable Conductance Heat Pipe System (VCHPS).

The TEP is mounted within the spacecraft on the south panel as shown in figure 2. The OST is mounted on the evaporator saddle of the VCHPS which in turn is mounted on the PPS baseplate; this whole assembly is then mounted on the spacecraft south panel. The OST is located such that the multistage depressed-collector enclosure protrudes through the aft section of the spacecraft, to permit direct thermal radiation from the collector enclosure.

## OUTPUT STAGE TUBE

The OST (Kosmahl et al, 1974) is a coupled-cavity Traveling Wave Tube (TWT) augmented with a Multistage Depressed Collector (MDC) as shown schematically in figure 3. This class of linear-beam microwave amplifier converts the kinetic energy of an electron beam into rf energy.

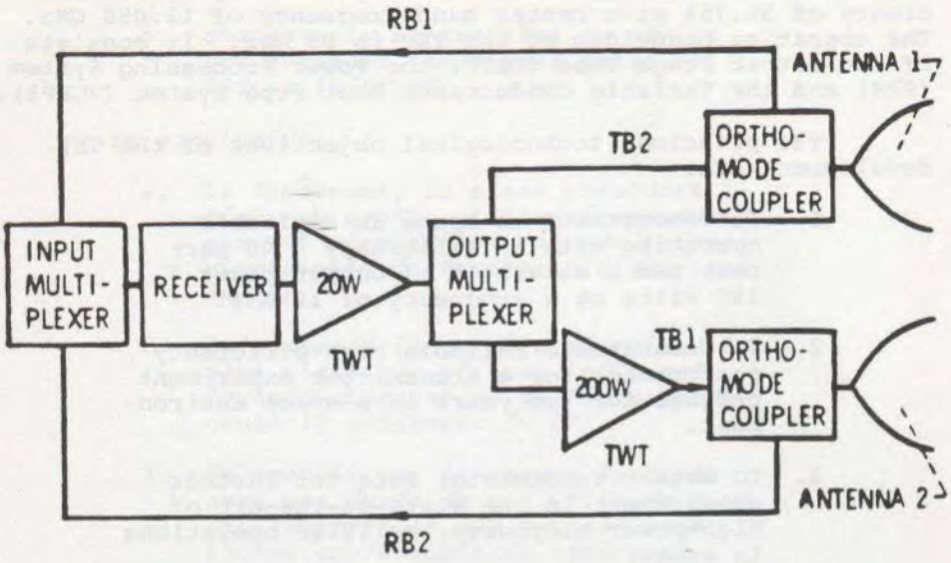


RB - Receiver Band TB - Transmitter Band

Figure 1. Simplified diagram of the Hermes spacecraft transponder.

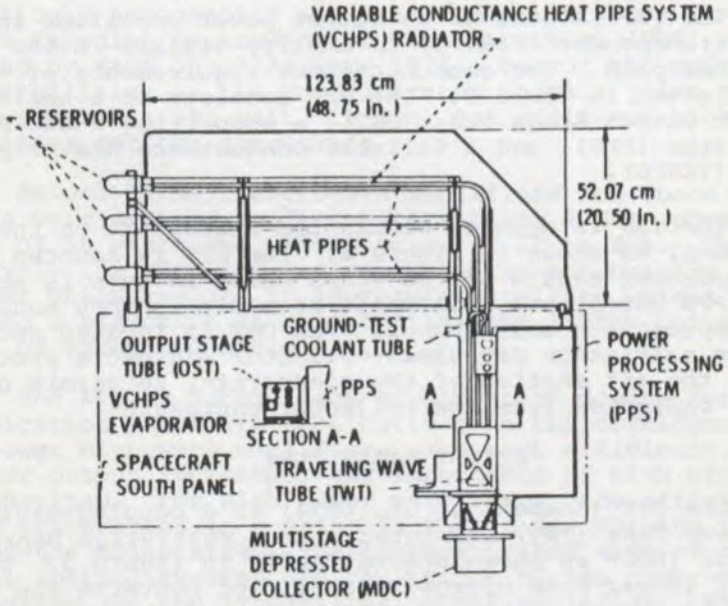


Figure 2. Hermes transmitter experiment package (TEP).

TABLE I

TEP COMMUNICATIONS REQUIREMENTS

| | |
|---|---|
| Minimum Output Power (Average Across Band), Watts | 180 |
| Efficiency Goal, Percent | 50 |
| Gain, Saturated, dB | 30 +2-1 |
| Band Width, GHz | 12.038 - 12.123 |
| Differential Gain, dB | ± 1.5 |
| Maximum Gain Ripple, dB Peak to Peak | 5 |
| Maximum Group Delay, Nanoseconds Peak to Peak | 8 |
| Noise Figure, dB | 40 |
| Maximum Load, VSWR | 1.25 |
| Design Life, Years | 2 |

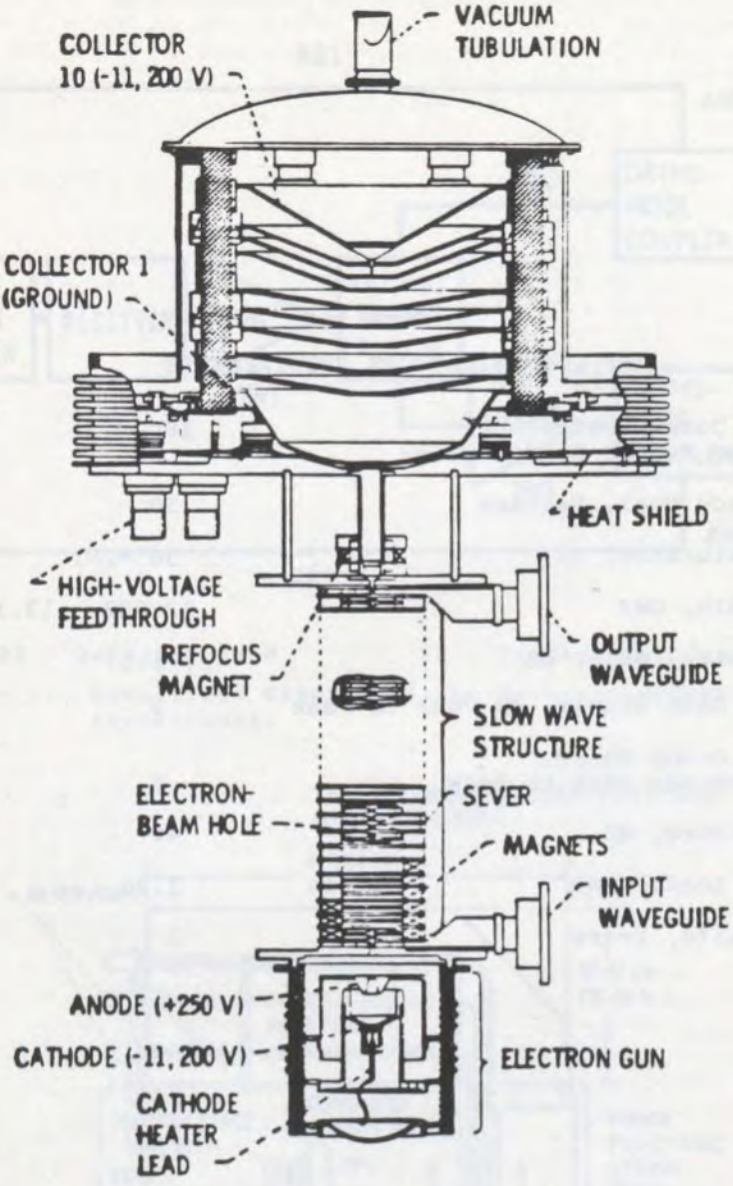


Figure 3. Hermes travelling wave tube with multistage depressed collector.

An electron beam is formed by convergent optics in the electron gun. Electrons, emitted by a thermionic cathode, are accelerated to approximately 1/5 the speed of light by the potential difference between the cathode and the anode. The cathode and anode voltages with respect to the TWT body are - 11,200 volts and 250 volts respectively. The electrons pass through an interaction region of the TWT located between the input and output waveguides. This region of the TWT is composed of cylindrical cavities, coupled to form a lumped-element transmission line or slow-wave structure. It contains three line sections separated by terminations (or severs). Beam focussing is accomplished by magnets placed outside of the cavity structure along the transmission line. The rf wave, in the transmission line, interacts with the electron beam as it passes through each cavity. The kinetic energy of the electron beam is converted to rf energy by fringing rf fields in each cavity which interact with the electron beam.

The output section utilizes cavities with physical dimensions designed to reduce the velocity of the rf wave in the transmission line. The velocity reduction is done in two steps to maintain synchronism between the rf wave and the electron beam as the electron velocities are reduced. This velocity tapering of the output section produces an interaction efficiency of 26%. As the beam exits from the coupled-cavity region of the TWT, it enters the MDC. Magnetic refocusing of the electron beam (Kosmahl, 1971) (see Fig. 3) establishes the desired electron entry conditions into the MDC.

The MDC (Kosmahl, 1971) is used to convert kinetic energy remaining in the electron beam to potential energy and thereby reduce the power required to operate the TWT. The MDC is composed of ten collector electrodes or plates. Each, with the exception of the tenth collector, has a centrally-located hole which allows the electron beam to penetrate the collector region. The tenth collector has a centrally located spike as shown in figure 3. The depth of penetration of an electron is determined by its entry velocity or remaining kinetic energy. Electrons are collected by specific plates, depending on their kinetic energies. High-energy electrons are collected by the tenth and its neighboring plates, while low-energy electrons are collected by the first and its neighboring plates. The shapes of the collector electrodes are designed to produce equipotential surfaces and an electric field configuration necessary to sort and collect electrons in accordance with their entry velocities. The electrons, therefore, are collected near the apex of their trajectories where they have near-zero velocity. In this manner, the electron kinetic energy is converted to potential energy and returned to the PPS. This reduces the power required to operate the OST. The tenth collector is connected to cathode potential; the collector electrodes from the tenth through the second are connected to descending voltages, each differing from its

neighboring electrode by 1/10 of the cathode voltage. The use of the MDC results in reduced input power, and therefore, increased efficiency for all rf output powers up to and including saturation.

Heat produced in the MDC due to residual velocities of the collected electrons is radiated to the collector enclosure and in turn radiated to space. A combination of internal heat shields and a bellows-type external heat choke is used to reduce the heat flow back to the interaction section of the TWT. The packaged OST is shown in figure 4.

## POWER PROCESSING SYSTEM

Electrical power for operation of the TEP is delivered to the PPS at nominal supply voltages of 76 VDC and 27.5 VDC, respectively. The PPS (Farber et al, 1975) performs the following functions for TEP operations:

1. Develops proper operating voltages for the TWT and MDC.
2. Regulates supply voltages.
3. Provides fault sensing and protection.
4. Provides command control and sequencing for remote operation.

The electrical interface between the PPS and the OST and the spacecraft electrical systems is shown in figure 5. The collector and body currents are a function of rf output power and frequency. The values given are typical of center band saturated output operation. The sum of body and collector currents is constant and equal to the cathode current, 76 mA, for all operating conditions. Separate inverters are used for the cathode-collector, anode, and cathode heater supplies.

A simplified schematic of the basic PPS cathode-collector supply which supplies the main operating power for the OST, is shown in figure 6. This supply provides high-voltage power for operation of the OST. Input power from the 76v bus passes through an input filter and chopper pre-regulator. This power is converted to high voltage DC by a transistor chopper converter and high-voltage transformer. There are multiple secondary windings each connected to a bridge rectifier as shown. The DC outputs of the bridge rectifiers are series connected to provide a -11.2KV cathode supply and intermediate voltages for the MDC electrodes. Only the sum of these voltages or the cathode voltage is regulated. It is measured and compared to a reference. The resulting error is used to control the input pre-regulator. The switching frequency of the inverter is 10KHz. An active AC filter is used in the cathode voltage supply to meet minimum ripple requirements without exceeding stored-energy limits that would be damaging to internal OST structure during internal arcs.

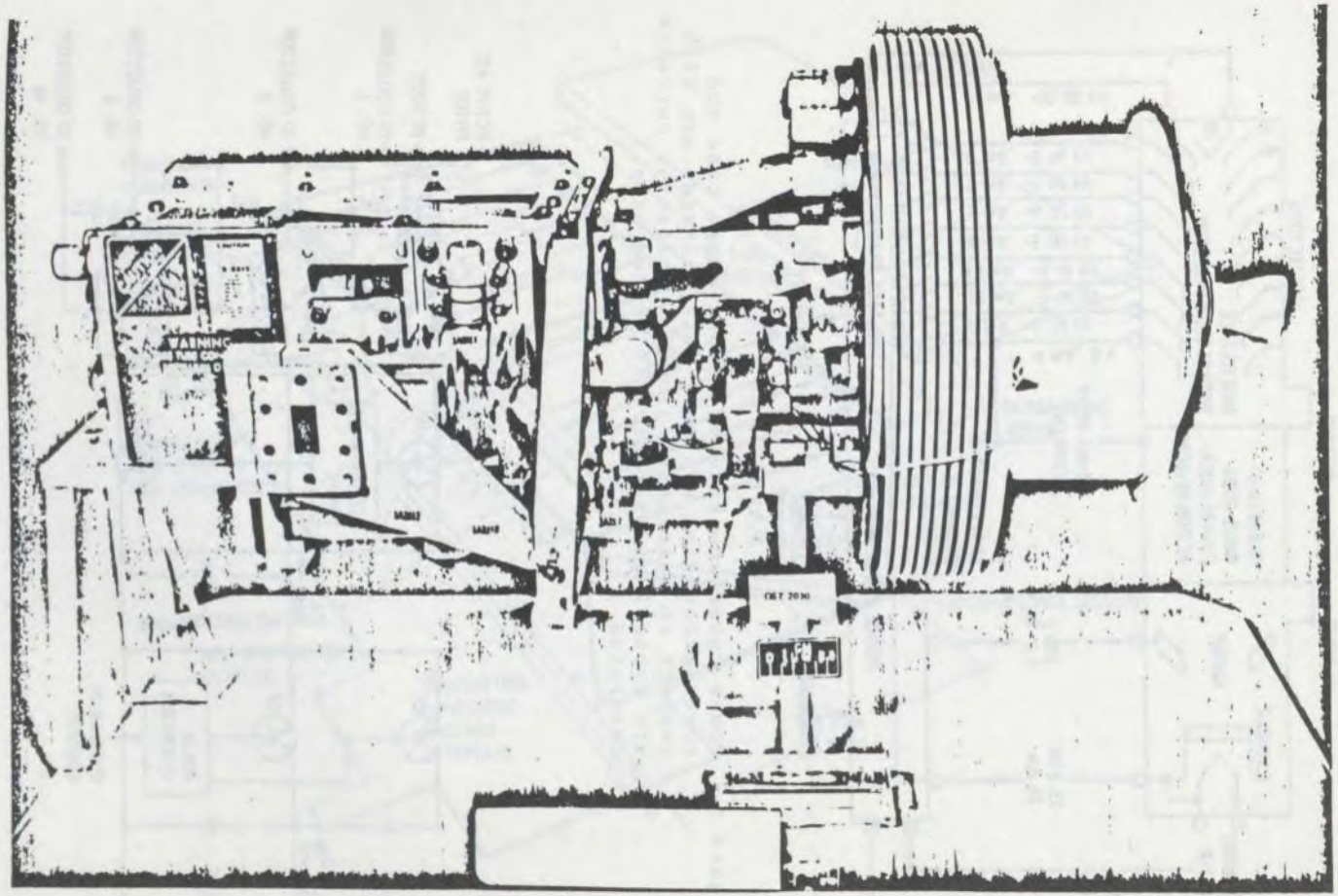

Figure 4. Packaged OST.

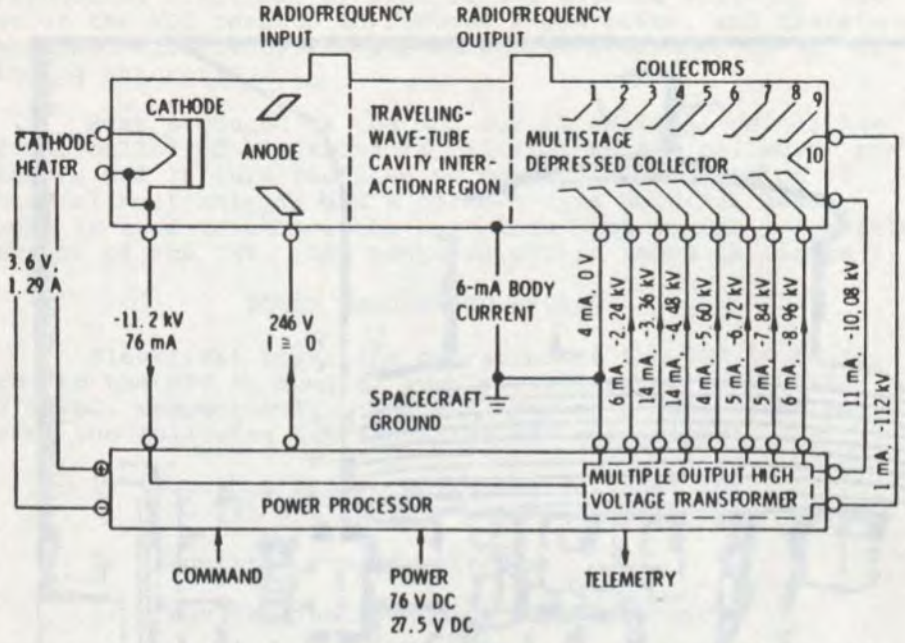


Figure 5. Power interface between output stage tube and power processing system. (All voltages are with respect to spacecraft ground. Collector currents are typical of operation at center band, saturated.)

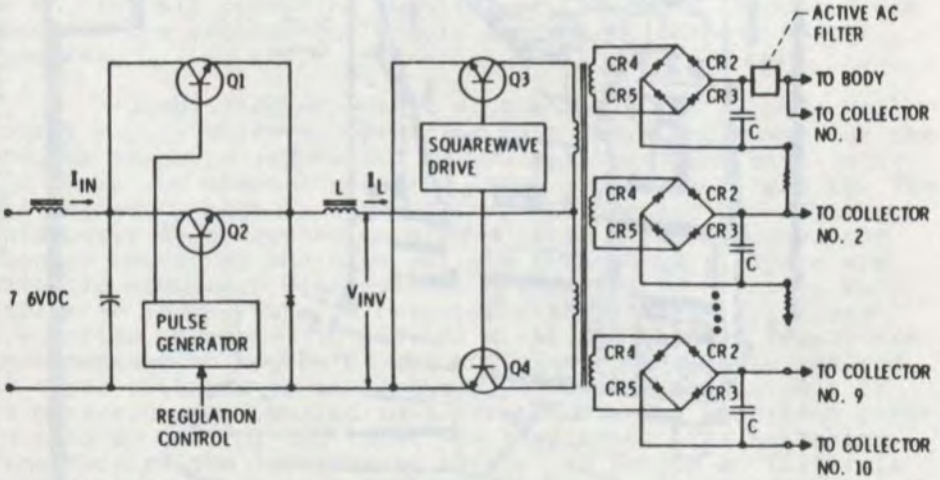


Figure 6. Current source chopper preregulator/squarewave inverter used for collector, cathode supply.

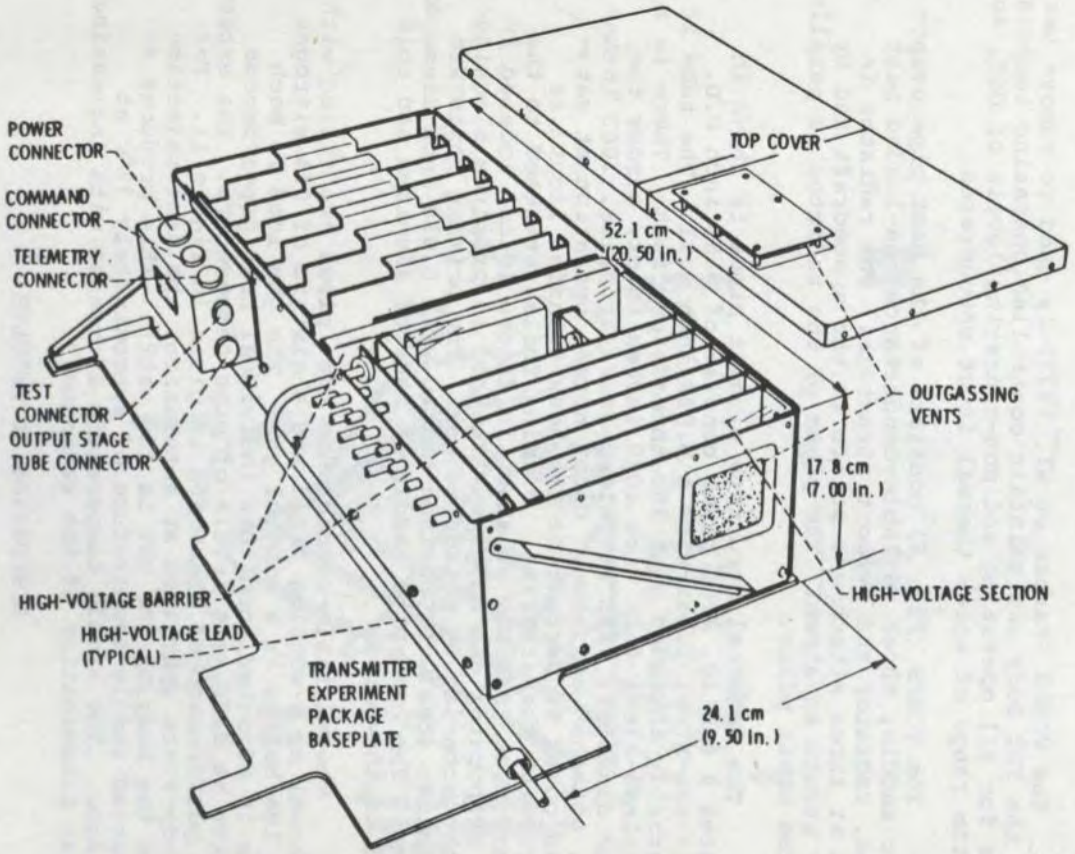


Figure 7. Power processing system.

An exploded schematic of the PPS package is shown in figure 7. The package has outgassing vents in the top cover and side as shown and the high-voltage and low-voltage sections are separated within the package. Heat developed within the PPS is conducted to the TEP base-plate and to the south panel.

## VARIABLE CONDUCTANCE HEAT PIPE SYSTEM

The VCHPS (Farber et al, 1977) is used to remove heat from the TWT body and maintain controlled operating temperatures for all operating and non-operating levels of OST, and for the range of solar thermal input encountered.

The VCHPS (Fig. 8) consists of the heat pipe evaporator saddle, three variable-conductance gas-loaded heat pipes, radiator and support structure. The radiator is held at three attachment points to the spacecraft and by four struts as shown. The plane of the radiator is parallel to the orbit plane.

The internal structure of heat pipes is shown in figures 9 and 10. The pipes consist of 0.50 inch O.D. stainless-steel tubes with a 0.028 inch wall. The tube is internally threaded with 100 threads per inch. There is a stainless-steel felt wick .020 inches thick, across the inner diameter, with stainless-steel arteries, .063 inches I.D. attached as shown. Under normal operation at saturated power 90 percent of the heat-transfer liquid is carried by the arteries. Priming foils, attached to the artery wick assembly as shown in figure 10 and located in the evaporator end of pipes are used to preclude blocking of the arteries by entrapped gas. The priming foils are stainless steel, 0.005 inch thick, with 0.010 inch diameter holes. The heat-pipe saddle is made of aluminum and soldered to the pipes.

The variable-conductance heat pipes are filled with methanol as a working fluid and a mixture of 90% nitrogen and 10% helium as a control gas. The gas load in each pipe is adjusted such that individual heat pipes become active at different levels of pipe temperature. The expected performance of the VCHPS is given in figure 11. For steady-state operation at saturation, the heat rejection from the body of the OST is 155 watts. This produces an expected saddle temperature of approximately 37°C at equinox. The saddle temperature increases with increasing solar illumination of the radiator.

## DISCUSSION OF RESULTS

### DC and RF Performance of the TEP

The results presented comprise on-orbit test results from June 14, 1976 through August 8, 1977, including results of the first TEP operation during the season of eclipse by the Earth. The TEP was not operated during

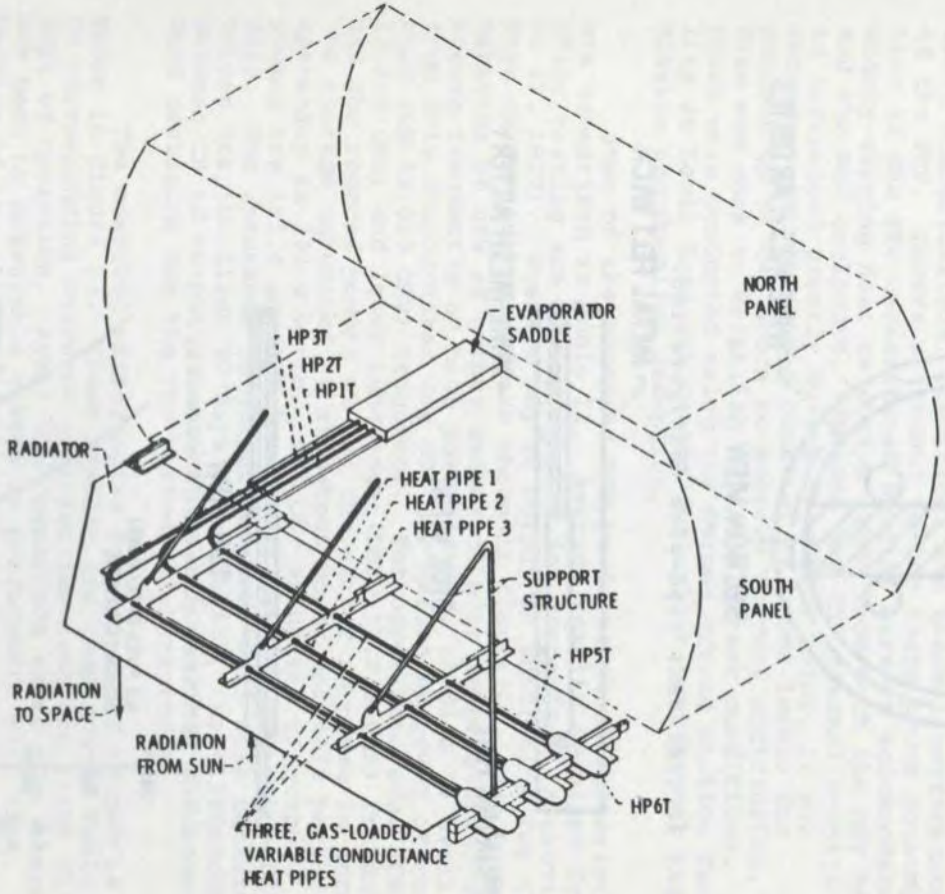


Figure 8. Variable conductance heat pipe system.

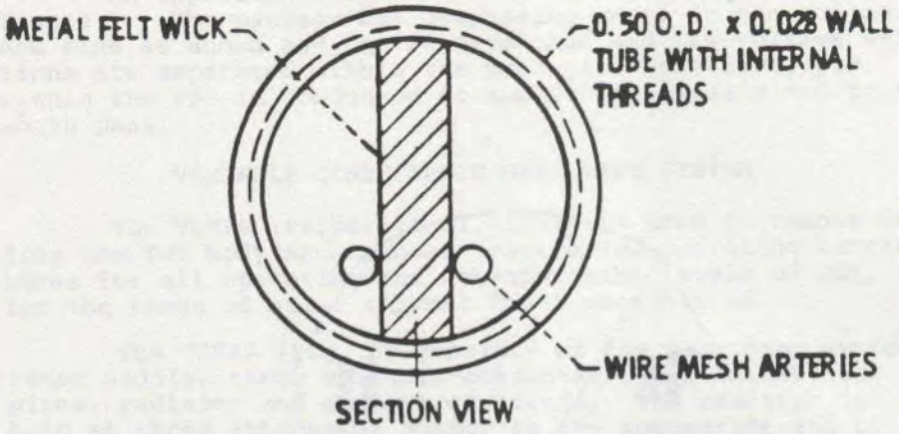


Figure 9. TEP heat pipe wick configuration.

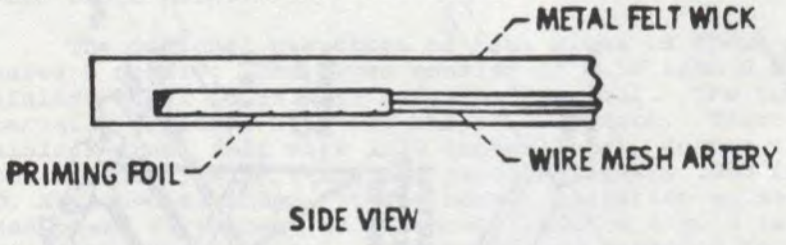


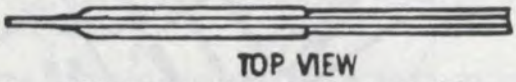


Figure 10. TEP heat pipe wick assembly.

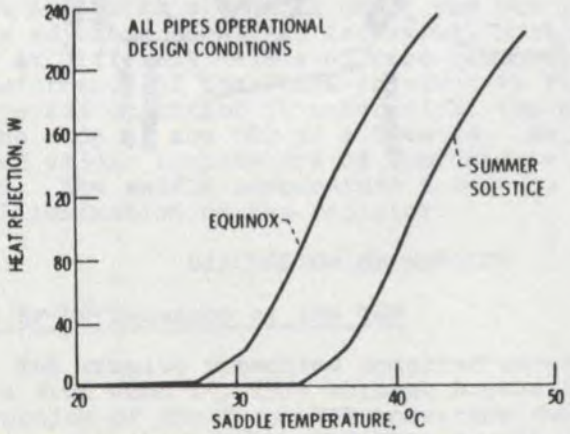


Figure 11. VCHP system expected performance.

prior eclipse seasons due to failure in the spacecraft power subsystem. As of August 8, 1977, the TEP had been operated for 8,830 hours. The results obtained from tests during this period are compared to initial on-orbit test results from February 8 through June 13, 1976 (Alexovich et al, 1977).

A series of tests were conducted to determine on-orbit communications, electrical and thermal performance of the TEP. Losses attendant to the large power consumption of the TEP necessitated special care to accommodate widely-varying heat rejection rates from both the OST body and the MDC enclosure. Because the TEP thermal condition is influenced greatly by its operating point, it was necessary to operate at constant rf power levels for periods up to two hours to achieve thermal equilibrium. This was done to establish repeatable test conditions. All tests were conducted using the Hermes ground station facility at Lewis Research Center for uplink test signal transmission and downlink reception.

Some of the observed TEP performance characteristics are summarized in Table II. Average results obtained from prior testing are also presented for comparison (Alexovich et al, 1977). Average OST rf output at saturation for the days of TEP operations are shown in figure 12. Due to erratic behavior of the rf output sensor at high temperatures, which occurs frequently at high power levels, no data is available from this source after day 300 for saturated power at center band (CB 12.080 GHz) frequency. For upper band edge (UBE, 12.123 GHz) and lower band edge (LBE, 12.038 GHz) frequencies and for reduced powers at CB, the sensor response is normal. The average saturated CB rf output power for this period of operation is 233.4 watts. The OST saturated rf output powers are 151.4 and 185.5 watts at UBE and LBE respectively. The saturated rf output compares well with measured values for the first 90 days of operation, the difference between CB rf output at saturation being within the standard deviation for the two periods of measurement.

The measured efficiencies for saturated output is shown in figure 13. These results are compared in Table II to corresponding measured efficiencies from the first 90 days of operation. Again the comparison shows that there has been no measurable change in performance with time. Because of the failure of the output power sensor at high temperatures no data is available for CB saturated power output. However, the energy recovery of the MDC is sensitive to spent beam characteristics. As a result, an indication of rf output power extracted from the electron beam can be derived from the MDC electron-velocity distributions and OST DC input power. Based on the constancy of OST DC input power, figure 14, and collector current distributions, it is concluded that saturated rf output power has not changed in the time period after day 70, 1977.

The OST beam focusing utilizes samarium-cobalt

permanent magnets. Stability of the focusing field distribution can be derived from observations of beam interception or body current. Body current for saturated rf and for 100 watts rf output power at CB, and for zero rf or DC operation is given in figure 15. A comparison of this data with values obtained from earlier test results, Table II, shows that there has been no measurable effect due to environment or thermal cycling in spite of the 8,830 hours of operation.

The cathode-heater supply is current regulated and provides constant heater power, and both the cathode and anode voltages are regulated and continuously monitored. The change in beam current, figure 16, is due to a change in emission from the cathode. This drop in beam current is well within design limits necessary to achieve two years of operating life. The expected effects of this reduction in beam current on DC input power, rf output power and body current are too small to be observable. It is therefore expected that two years operating life (18,000 hours) will be achieved without significant degradation in performance.

OST Thermal Anomaly

On day 75, March 16, 1977, at 19:25 GMT, the OST body temperature in the region of the rf output unexpectedly began to increase. Figure 17 shows the body time-temperature-profile on day 75 during the anomaly period. At 340 minutes, the body temperature increased from its normal operating temperature of 56°C, to 75°C at 377 minutes. At this time rf output power was reduced and body temperature was reduced. Figure 18 shows the OST DC input power history for the same period on day 75. It can be seen that from 250 minutes, when rf power was reduced, the input power was essentially constant. RF output power during this time was also constant, therefore, internal losses resulting in waste heat rejected by the TEP thermal control system were also constant. Changes in input or output power, failure in measurement, and solar illumination were readily discounted as possible causes for the thermal anomaly. It was concluded that the anomalous increase in OST body temperature was caused by a change in:

1. Thermal conducting paths of the OST or

2. Performance of the VCHPS.

As of August 8, 1977, there have been three OST thermal anomalies, day 75, day 82, and day 101. Figure 19 shows the Sun angles and eclipse durations for the anomaly days. All three days occurred during the eclipse season and during the period of near zero or positive Sun angles. Figure 20 shows the orbital position of the spacecraft at the time of each anomaly. The orientation of the spacecraft at the time of each anomaly was such that the heat-pipe radiator and gas reservoirs are shadowed by the spacecraft, (see also Fig. 8). The resultant shadowing

TABLE II

OBSERVED TEP PERFORMANCE CHARACTERISTICS

| | February 8 - June 13, 1976 Average | Standard Deviation | June 13, 1976 August 8, 1977 Average | Standard Deviation |
|---|---|---|---|---|
| SATURATED EFFICIENCY, PERCENT | | | | |
| CB (Center band freq., 12.080 GHz) | 51.52 | 1.85 | 50.75 | 1.75 |
| UBE (Upper band edge freq., 12.123 GHz) | 37.0 | 1.22 | 37.80 | 3.34 |
| LBE (Lower band edge freq., 12.038 GHz) | 38.5 | 1.22 | 38.14 | 1.01 |
| SATURATED RF OUTPUT, WATTS | | | | |
| CB | 241.1 | 8.68 | 233.4 | 7.26 |
| UBE | 151.3 | 6.96 | 151.4 | 11.51 |
| LBE | 185.7 | 5.76 | 185.5 | 1.09 |
| SATURATED TEP POWER, WATTS | | | | |
| CB | 469.9 | 6.6 | 463.9 | 8.12 |
| UBE | 406.1 | 5.7 | 401.9 | 1.81 |
| LBE | 482.6 | 8.8 | 475.3 | 9.46 |
| BODY CURRENT, mA | | | | |
| CB, SATURATED | 6.43 | 0.27 | 6.32 | 0.34 |
| CB, 100W | 2.37 | 0.15 | 2.56 | 0.11 |
| DC | 1.64 | 0.10 | 1.62 | 0.05 |
| BEAM CURRENT, mA | 76.35 | -- | 76.2 | -- |

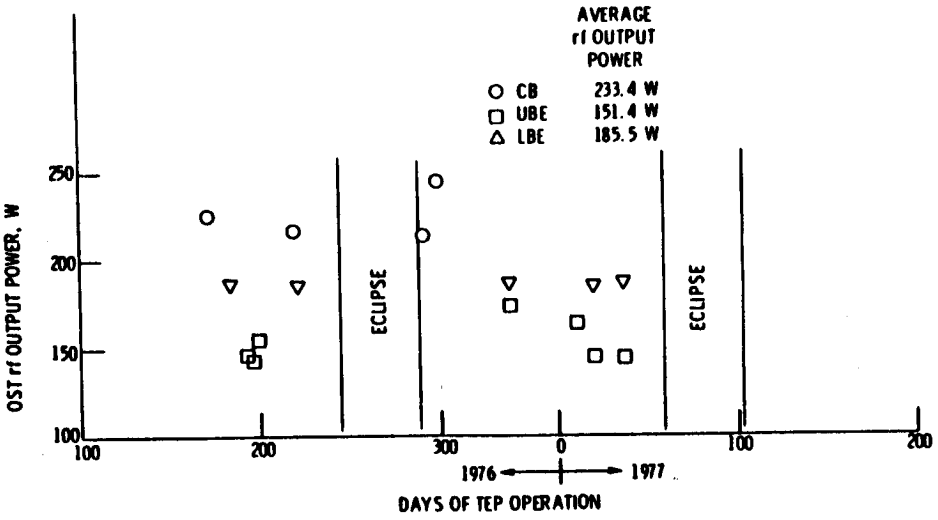


Figure 12. Hermes OST saturated rf output power at center band, upper band edge, and lower band edge frequencies.

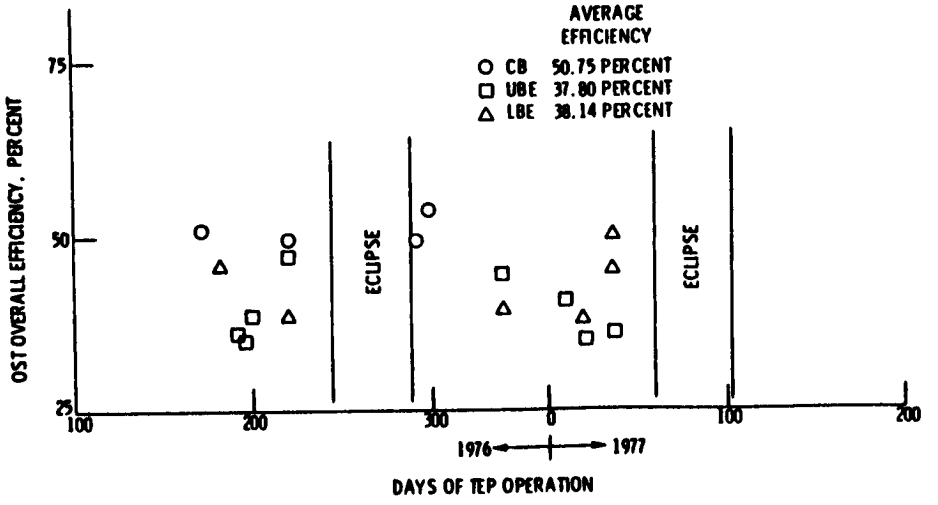


Figure 13. Hermes OST overall efficiency at saturated rf output power at center band, upper band edge, and lower band edge frequencies.

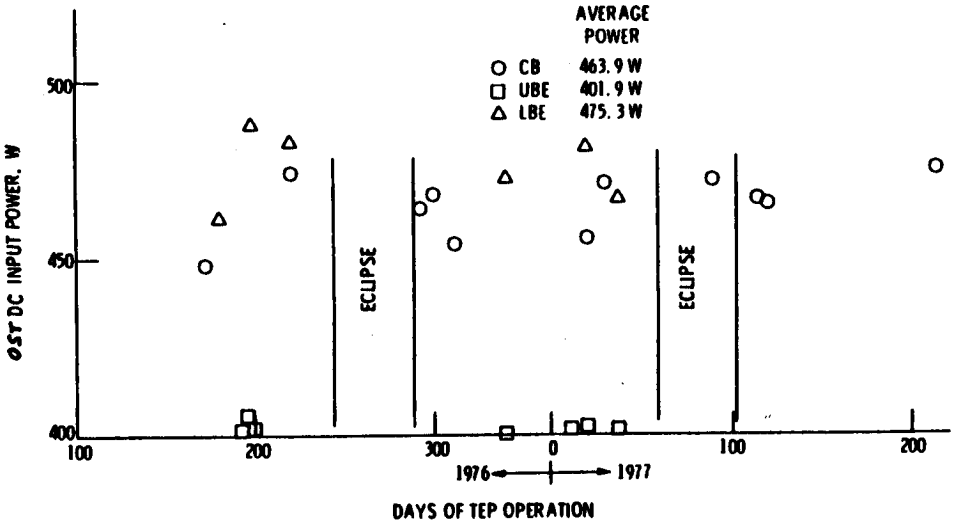


Figure 14. Hermes OST DC input power for saturated rf output at center band, upper band edge, and lower band edge frequencies.

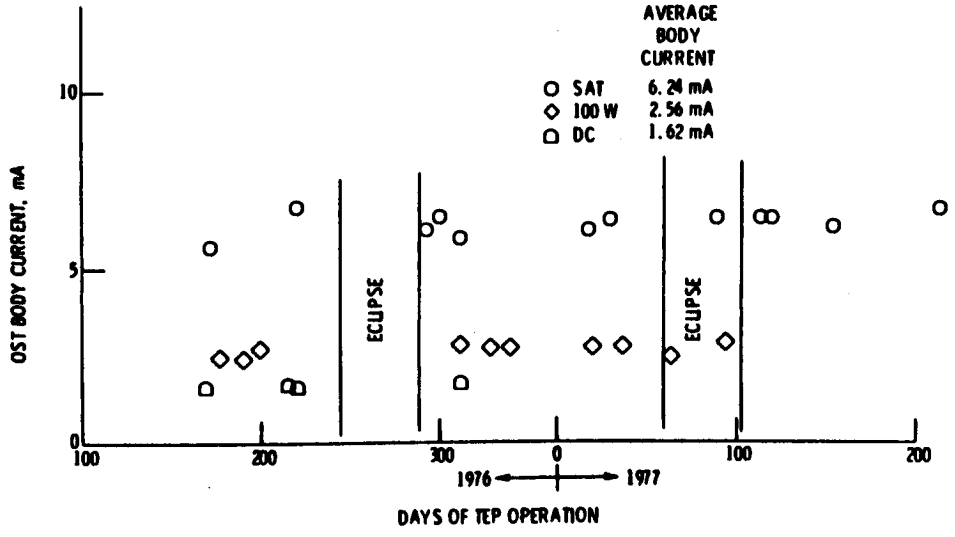


Figure 15. Hermes OST body current for saturated rf and 100 W rf output at center band frequency and for DC operation.

causes this region of the radiator to fall in temperature to near the freezing point of methanol, (-98°C), see figures 21 and 22. These sensor locations are shown in figure 8.

The thermal conducting path for removal of body-loss heat is shown in figure 23. The OST is supported by an input and output saddle. The larger saddle is located at the output end because skin effect and beam interception losses are largest in this region of the body. The saddles are mounted on the OST baseplate which then is mounted on the heat-pipe saddle. The whole assembly is then mounted on the PPS baseplate and the south panel of the spacecraft. The sensors that indicated abnormally high temperatures during each anomaly are located in the region of the OST output port. Figure 24, a section through AA of figure 23, shows the conducting paths from the OST body to the heat-pipe saddle and spacecraft south panel. Indium foil shims are used in the thermal interfaces between the copper bus to the aluminum saddle, and aluminum saddle to OST baseplate. The remaining interfaces use RTV silicone elastomer as shown.

A detailed analysis of data from the anomalies has revealed the following:

1. The turn-on signature as indicated by the adiabatic temperatures of heat pipes 1, 2, and 3, shown in figures 25, 26, and 27 respectively, are normal. They turn on in sequence and their initial steady-state temperatures are normal.

2. The difference between heat pipe 3 and heat pipe 1 adiabatic temperatures, figure 28, prior to the anomaly and during the anomaly exceeds the normal difference by 1 to 2°C.

3. The anomalies in OST body temperature (see Fig. 29 for day 75) are characterized by a sudden drop to a low value of heat rejection (Point A), an exponential recovery (A-B) to a constant rate of heat removal depicted by the straight-line section of the temperature rise (B-C) The constant value determined by this linear rise in all anomalies was 104 to 109 watts.

4. The thermal system recovers completely, without any measurable change, after each anomaly.

Based on ground tests with the VCHPS, it has been found that the abnormal difference between the adiabatic section temperatures of heat pipe 3 and heat pipe 1 can be duplicated by heat pipe depriming.

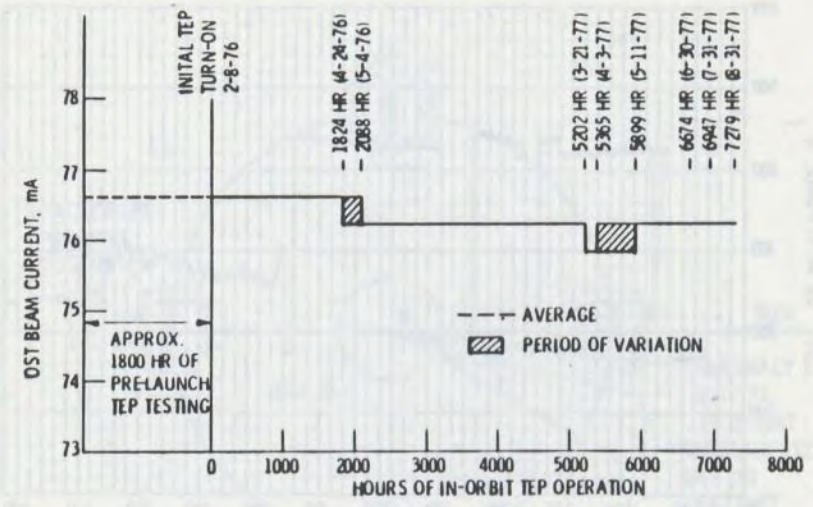


Figure 16. Hermes OST beam current history to date.

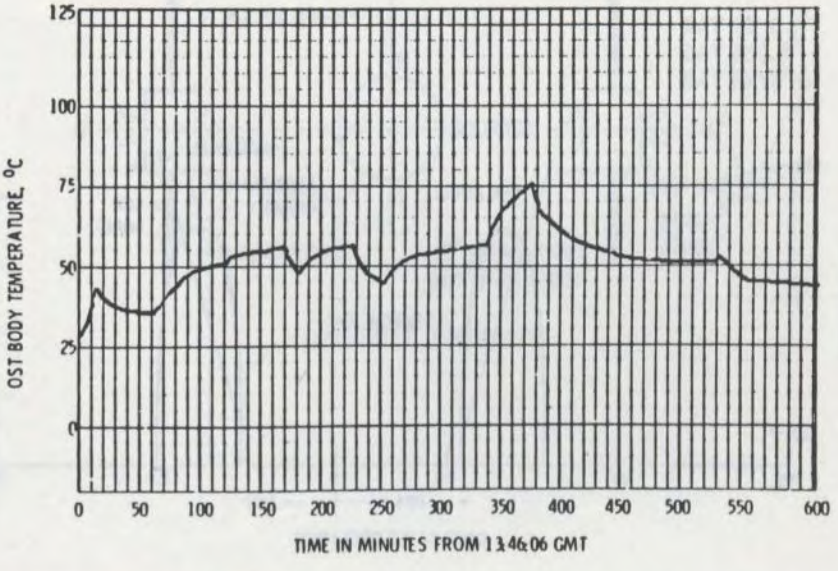


Figure 17. OST body temperature response to input power changes for day 75.

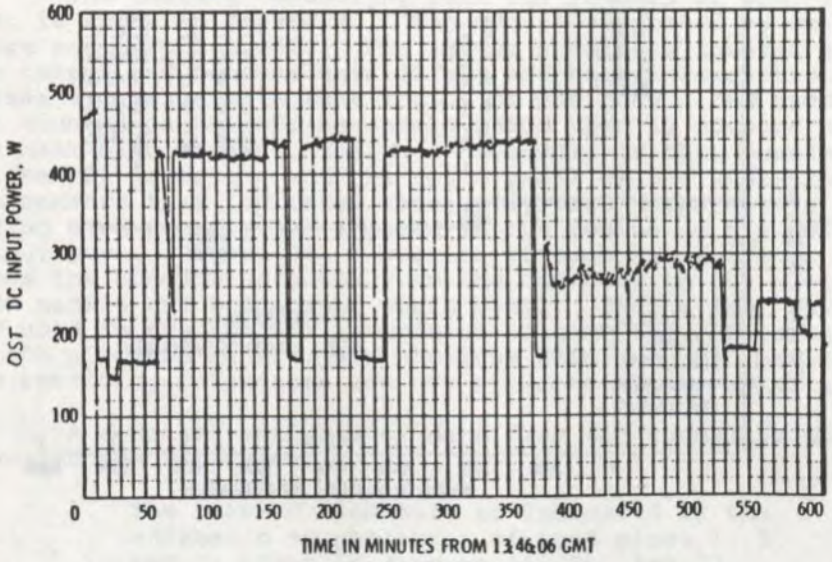


Figure 18. Electrical input power to OST for day 75.

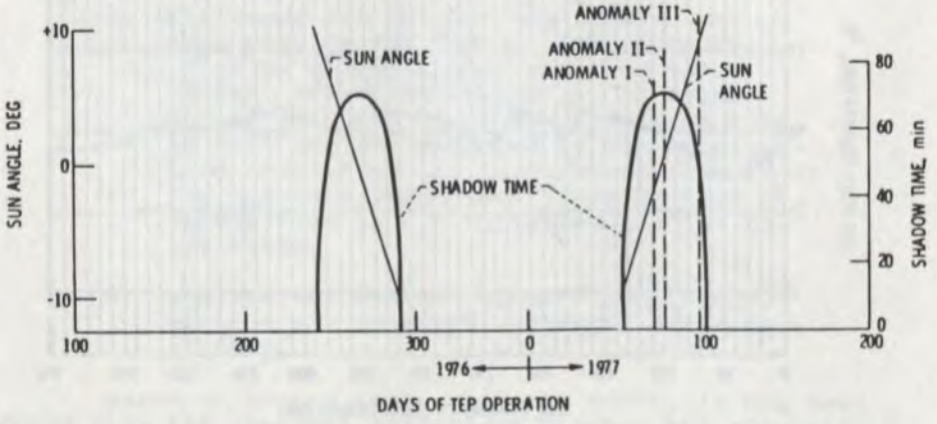


Figure 19. Eclipse shadow duration and sun angles with respect to spacecraft orbit plane for TEP thermal anomaly days.

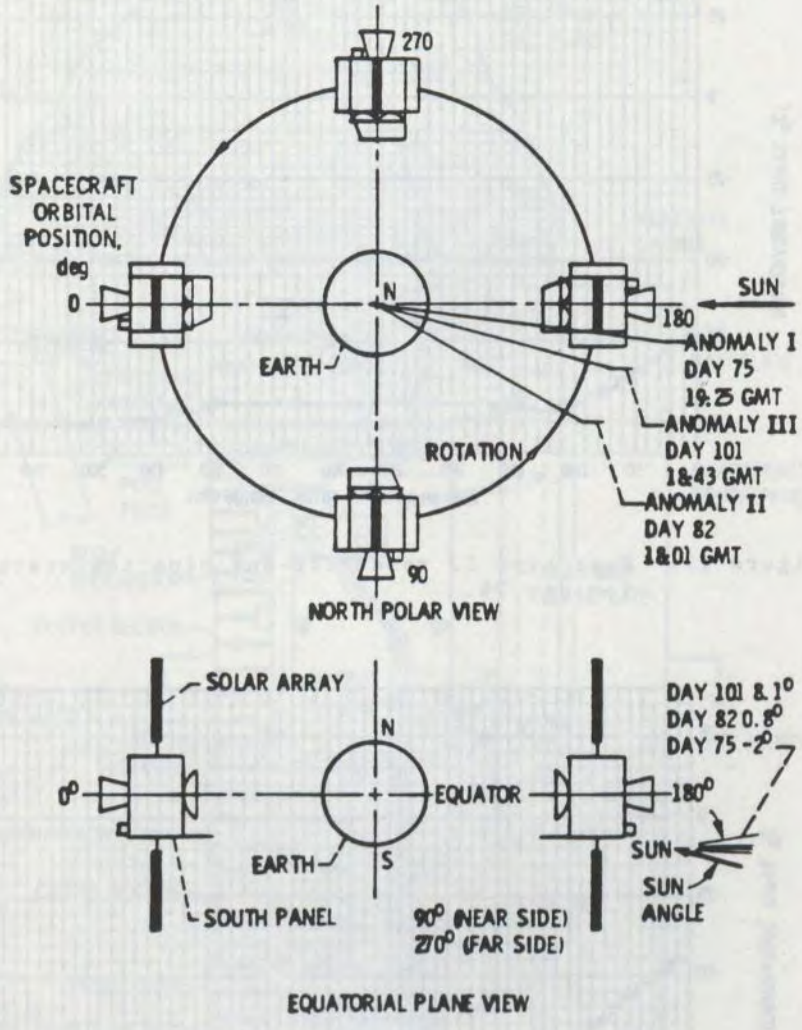


Figure 20. Hermes spacecraft orbital position and orientation with aspect to sun illumination for each thermal anomaly day.

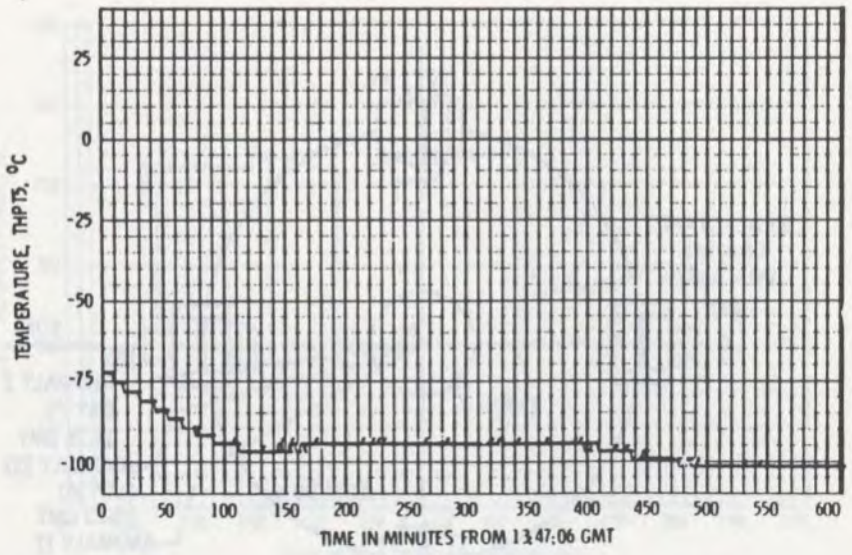


Figure 21. Heat pipe 1, reservoir-end pipe temperature for day 75.

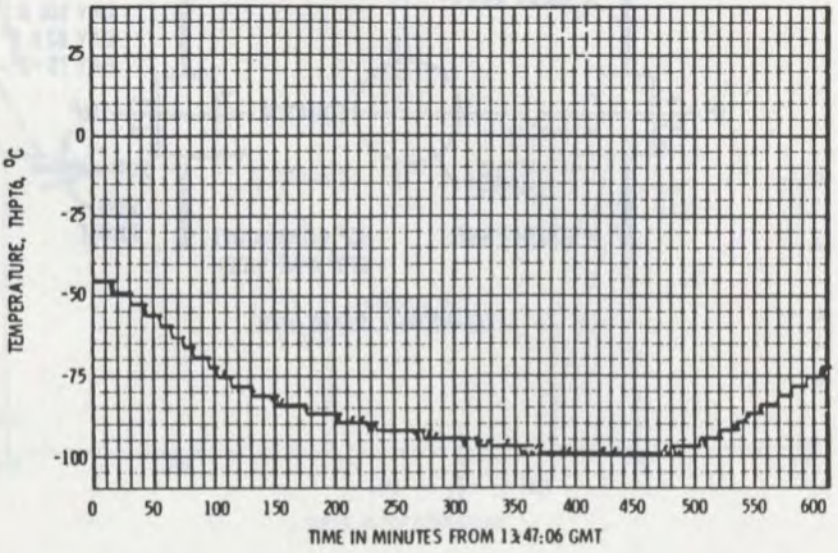


Figure 22. Heat pipe 1, gas reservoir temperature for day 75.

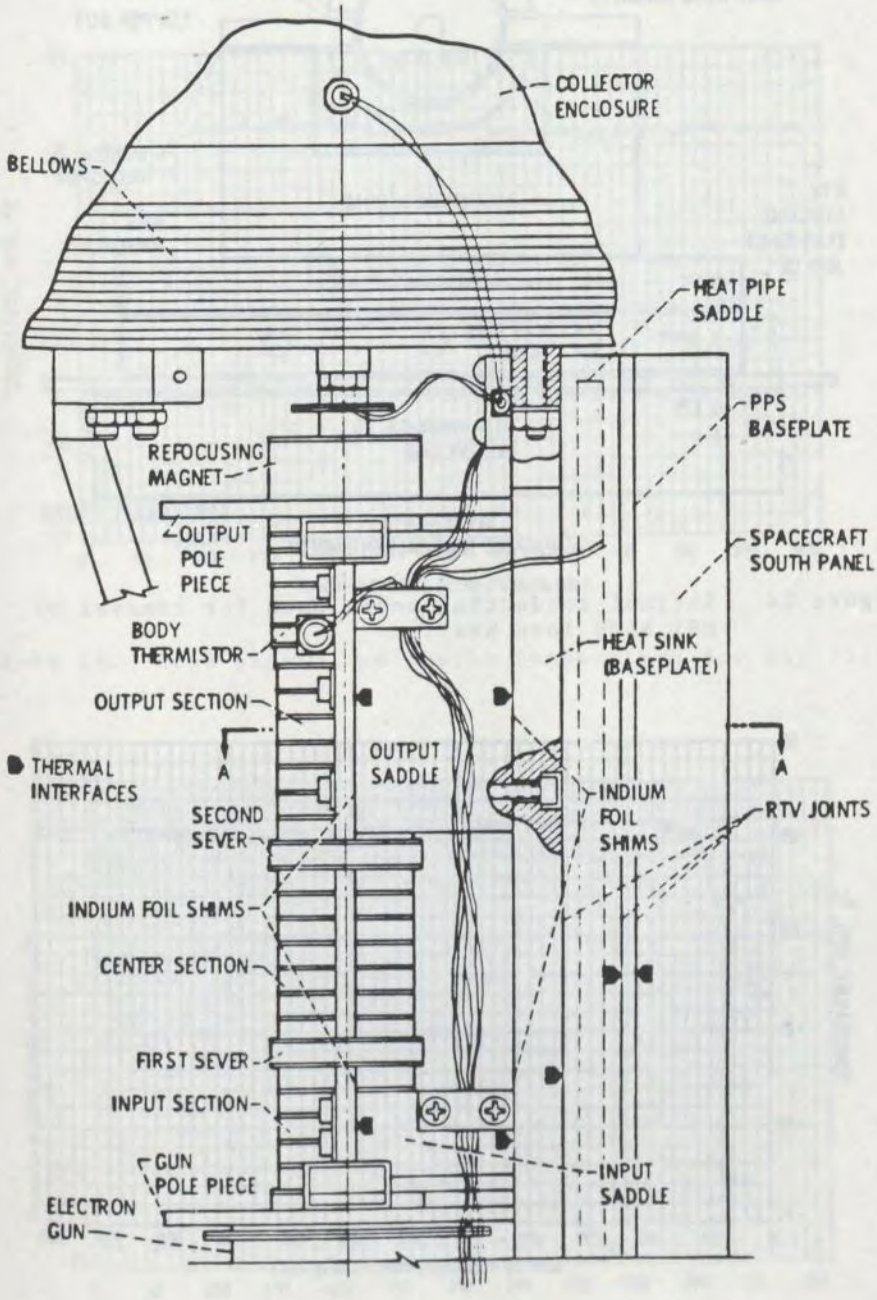


Figure 23. Mounted OST.

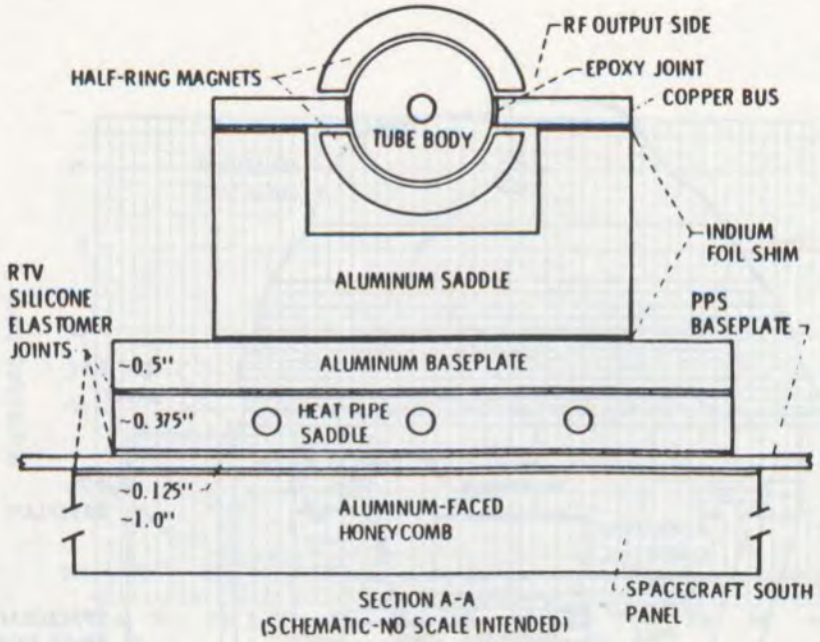


Figure 24. Thermal conducting mount used for removal of OST body loss heat.

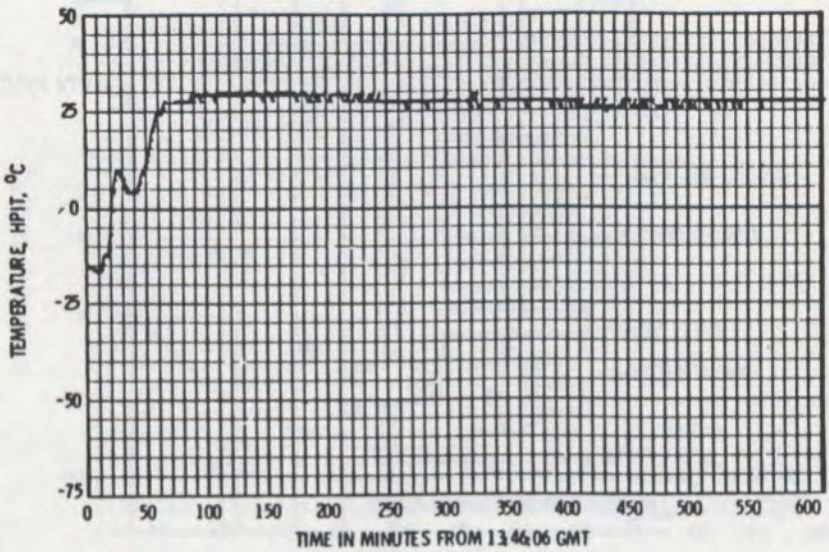


Figure 25. Heat pipe 1, adiabatic temperature for day 75.

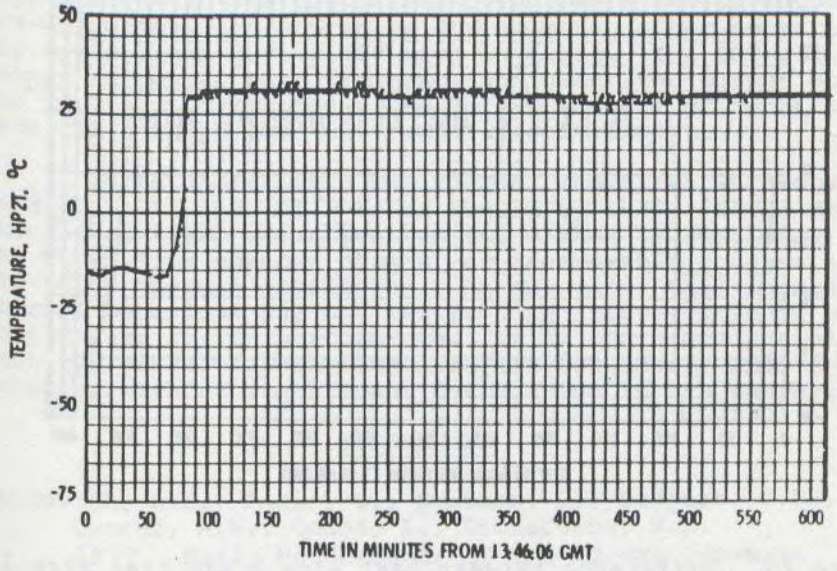


Figure 26. Heat pipe 2, adiabatic temperature for day 75.

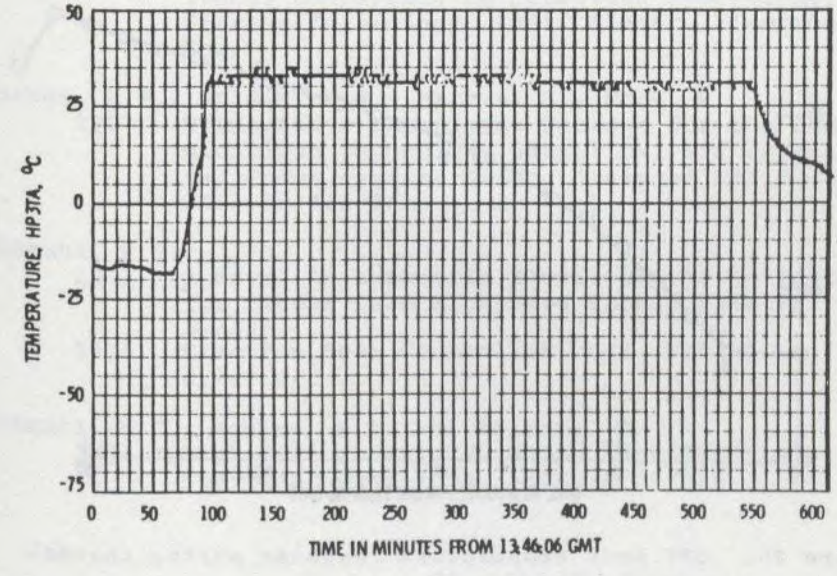


Figure 27. Heat pipe 3, adiabatic temperature for day 75.

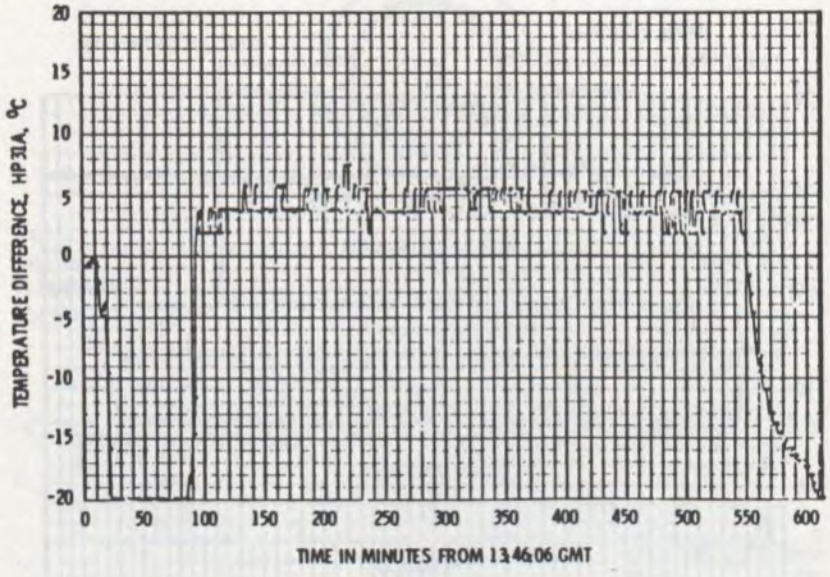


Figure 28. Difference between heat pipe 3 and heat pipe 1, adiabatic temperatures for day 75.

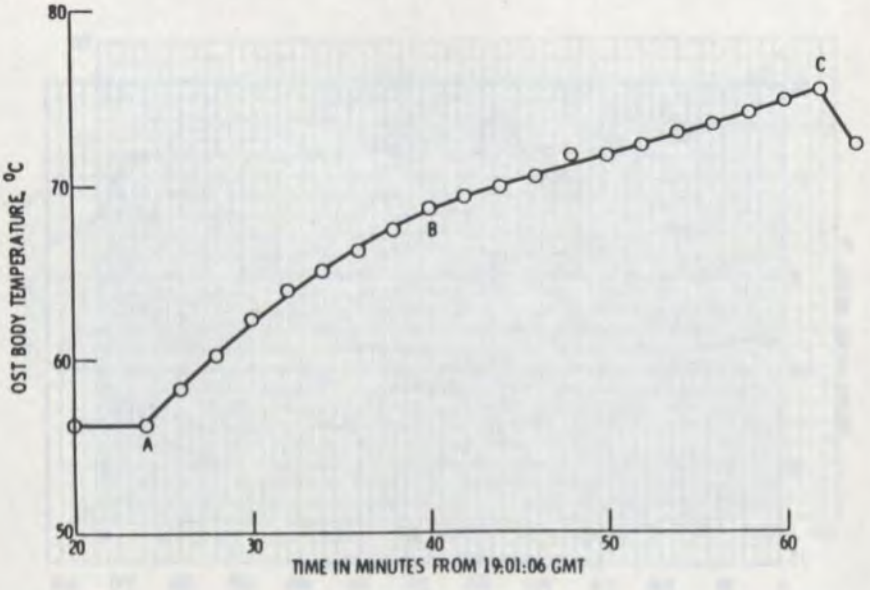


Figure 29. OST body temperature response during thermal anomaly for day 75.

## CONCLUDING REMARKS

On-orbit tests were conducted to evaluate the performance of the Hermes TEP. There were no observable degradations in TEP electrical performance due to launch, pre-injection, and operating environments after operating for 8,830 hours during 568 days in orbit. The OST efficiency at center band frequency and saturated output power was 50.75%. Corresponding rf output and OST DC input powers were 233.4 watts and 463.9 watts respectively.

Three short-lived OST thermal anomalies were observed on day 75, 82 and 101. As of August 8, 1977, it was determined that these anomalies are due either to depriming of the VCHPS from unknown causes, or recoverable changes in OST-VCHPS thermal interfaces. In any case, this anomalous thermal behaviour has not resulted in irreversible or permanent change in TEP performance. It is therefore anticipated that two years of operating life (18,000 hours) will be achieved without significant degradation in TEP performance.

## REFERENCES


Alexovich, R.E., Anzic, C., Smetana, G., Siegert, C.E., Curren, A.N., Gedon, L., Richardson, M.E.
1977 Early Performance of the 12-GHz 200-Watt Transmitter Experiment Package in the Communications Technology Satellite, *NASA TM X-3555.*

Farber, B.F., Schoenfeld, A.D., Thollot, P.A.
1975 Power Processing System for a 200w Communication Satellite Transmitter, in *IEEE International Conference on Satellite Communications Systems Technology,* Inst. Electr. Electron. Eng.

Farber, B.F., Goldin, D.S., Marcus, B., Mock, P.
1977 Transmitter Experiment Package for the Communications Technology Satellite, *TRW Defense and Space Systems Group, Contract NAS 3-15839, NASA CR-135035.*

Kosmahl, H.G.
1971 A Novel Axisymmetric Electrostatic Collector for Linear Beam Microwave Tubes, *NASA TN D-6093.*
1973 Electron Beam Controller, *U.S. Patent 3,764,850.*

Kosmahl, H.G., McNary, B.D. and Sauseng, O.
1974 High-Efficiency, 200 Watt, 12-Gigahertz Traveling Wave Tube, *NASA TN D-7709.*

# THE FLIGHT PERFORMANCE OF THE HERMES POWER SUBSYSTEM AND FLEXIBLE SOLAR ARRAYS

J.V. Gore

Communications Research Centre, Ottawa, Canada

K.P. Bogus

European Space Technology Centre,

Noordwijk, The Netherlands

*Le satellite technologique de télécommunications (STT) Hermès est un satellite expérimental géostationnaire qui a été lancé dans le cadre d'un programme conjoint du Ministère des communications et de la NASA. L'Agence spatiale européenne a également apporté son concours à sa fabrication en fournissant certains de ses équipement essentiels. Hermès devait servir à des essais de télécommunication SHF et à des expériences technologiques. Les principaux objectifs visés étaient:*

1. *la mise au point et l'essai sur orbite d'un groupe émetteur expérimental (TEP) de 200 watts fonctionnant sur le 12 GHz;*
2. *la mise au point et l'essai sur orbite d'un ensemble de panneaux solaires déployables d'une puissance en début de vie supérieure à 1,000 watts;*
3. *la mise au point et l'essai sur orbite d'un système de stabilisation triaxial pour un vaisseau spatial à structure non rigide;*
4. *la mise à l'épreuve d'un système de télécommunication opérant dans la gamme de fréquence 12/14 GHz.*

*Hermès a atteint ses objectifs technologiques. Dans plusieurs domaines les techniques utilisées étaient inédites, dans le sens qu'elles ont été spécialement conçues pour le programme Hermès. Ce vol spatial nous a donc permis d'assister à plusieurs premières dans le domaine des sous-systèmes d'alimentation d'un vaisseau spatial. Les panneaux solaires déployables ont été les premiers panneaux flexibles à fonctionner sur une orbite synchrone. Hermès a permis d'effectuer une expérience unique touchant la technologie des photopiles, expérience faisant usage d'instruments d'évaluation du rendement mécanique et électrique des panneaux solaires. La puissance en début de vie des*

*réseaux de piles solaires était de 1,110 watts pour les télécommunications SHF et de 270 watts pour la maintenance interne des systèmes. Les réseaux de piles solaires fixés sur la structure du satellite et servant à l'alimentation des sous-systèmes de maintenance interne des systèmes pendant les 15 premiers jours, lorsque le satellite était en rotation, utilisaient les plus récentes photopiles solaires Helios de la firme Heliotek.*

*L'article fait état du rendement sur orbite des réseaux de piles solaires et contient un rapport succinct sur le sous-système d'alimentation et les piles.*

## Introduction

The Communication Technology Satellite (CTS) or Hermes is an experimental geosynchronous communication satellite. Hermes was launched as a joint project between the Department of Communications (DOC) and the National Aeronautics and Space Agency (NASA) with some major components supplied by the European Space Agency (ESA). Hermes' purpose was to act as a test vehicle for SHF communications and technological experiments. The prime objectives were:

1. To develop and flight test a high efficiency 200w 12 GHz transmitter experiment package (TEP).

2. To develop and flight test lightweight deployable solar arrays with a beginning of life (BOL) power capability in excess of 1000w.

3. To develop and flight test a 3-axes stabilized control system capable of controlling a flexible spacecraft.

4. To conduct communications experiments in the 12/14 GHz band.

Hermes has met its technological objectives. In many areas, the technology was new, developed specifically for Hermes, and several firsts in the spacecraft power subsystem field were established with the flight of Hermes. The deployable solar arrays were the first flexible substrate arrays to be flown in synchronous orbit; Hermes carried a unique Solar Array Technology Experiment (SATE) that included instrumentation to evaluate the mechanical and electrical performance of the deployable arrays. The BOL power capability of these flexible arrays was 1110w for the SHF experiments plus 270w for the housekeeping functions. The body-mounted solar arrays, that provided power to housekeeping subsystems for the first 15 days while the spacecraft was in spinning attitude, used the latest Helios solar cells from Heliotek.

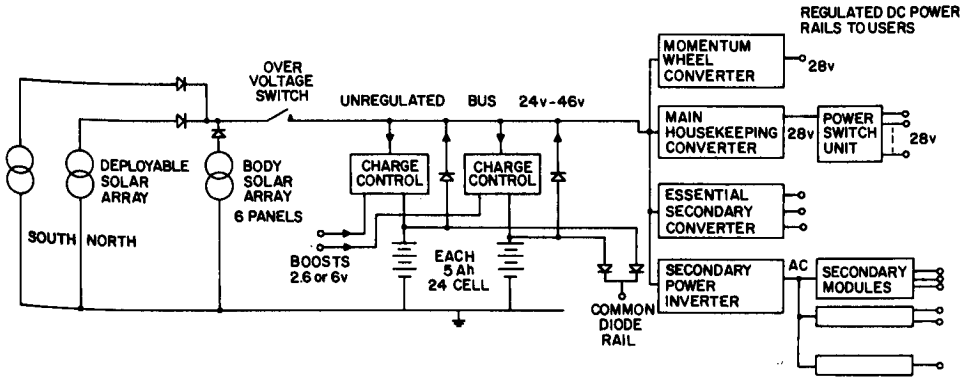


Figure 1a. Housekeeping Section.

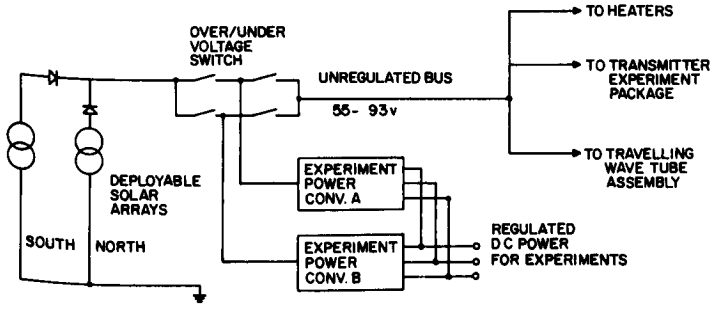


Figure 1b. Experiment Section.

This paper describes the flight performance of the solar arrays and presents a capsule report on the present status of the power subsystem and the batteries. As background, the following section describes briefly the power subsystem as it relates to the solar arrays and the batteries.

## 2. The Power Subsystem

The power subsystem is divided into two independent sections: housekeeping and experiments. The housekeeping section, which supplies regulated power to the housekeeping subsystems, obtains its power from the body array, a part of the flexible array, and two Nickel-Cadmium batteries as shown in figure 1a. The experiment section (Fig. 1b) which supplies power to the SHF communications subsystem, obtains its power exclusively from the experiment section of the flexible solar array.

### 2.1 The Housekeeping Section

The body and flexible solar arrays and the batteries are connected to an unregulated power bus via isolating diodes. Switching converters with overcurrent protection supply regulated voltages to other subsystems.

The interaction between the solar arrays, batteries, battery chargers, and loads is dynamic and complex. Ideally, for maximum power utilization from the arrays, the battery voltage should be equal to the voltage of the solar arrays at their maximum power output condition. However, the battery voltage changes considerably depending on its state of charge, and the charge or discharge current. The array voltage also changes with sun angle and age; therefore, the ideal condition cannot be maintained and the maximum power output cannot be obtained from the arrays. A computer simulation program was used to develop the best designs for the body and flexible arrays. Calculations showed that typically about 95% of the body array power could be realized.

The diode connections of the power sources to the unregulated bus permit stable load sharing between the arrays and the batteries. The battery charge controllers normally provide a constant-charge current. The controllers, however, will charge at a reduced current when the arrays cannot support the spacecraft loads plus the full-charge current. These two features result in the best possible utilization of the arrays when their power output is marginal.

### 2.2 The Experiment Section

The experiment section, figure 1b, obtains power exclusively from the flexible solar array and has no long-term energy storage. Therefore, the Hermes SHF experiments cannot be operated in eclipse. The TEP and the 20w TWTs have their own power conditioners and take power directly from the

unregulated bus, the voltage of which is determined entirely by the load and the voltage-current characteristics of the array. The transponder and antenna controllers are provided with regulated power from one of two redundant experiment power converters (EPC). On March 4, 1976, EPC A failed because of the malfunction of one of the over-voltage/under-voltage (OV/UV) relays. EPC B has been in use and has performed nominally since that time.

This arrangement of two independent power buses was natural for Hermes because no long-term energy storage was provided for the experiment section, but there are also other advantages. Conducted electromagnetic interference is minimized between the two sections.

Housekeeping subsystems generally require lower voltages and the converters operate more efficiently from a low-voltage bus, whereas the 200 and 20 watt TWT's need high voltage and their converters operate more efficiently from the higher voltage experiment bus. Also the overall spacecraft reliability is improved. This has proven to be important because of two major faults in the experiments power system: the OV/UV relay malfunction and a short circuit on the array on June 8, 1976 (see section 6.1).

### 3. The Body Mounted Solar Arrays

From launch through transfer and drift orbit (15 days) with the spacecraft spinning, power was obtained from the batteries and the body-mounted solar arrays. These arrays, manufactured and tested by Spectrolab in Sylmar, California, used 5460 of the latest 150 μm Helios solar cells with 100 μm ceria-doped coverglass. The Helios cell is Heliotek's equivalent to the COMSAT violet cell. The use of these thin cells and coverglasses, instead of the conventional 200 μm cell and 200 μm fused silica coverglass, saved about 1.0 Kg of weight while providing 14% more power. The best estimates of the power output of the body array in drift orbit was 103w, 6% higher than preflight calculations.

The body arrays remained connected to the unregulated bus after deployment of the flexible arrays, but when the spacecraft is in its 3-axes stabilized mode, the body arrays provide negligible power.

### 4. The Deployable Solar Arrays (DSA) Subsystem

The DSA subsystem consists of solar array mechanical assemblies (SAMA's) designed and manufactured by SPAR Aerospace, Toronto, and Flexible Solar Arrays (blankets) designed and manufactured by AEG Telefunken, West Germany, under contract to ESA. The complete solar array subsystem consists of two fold-up DSA's each of which when deployed is approximately 7.21 m long by 1.31 m wide. A DSA consists of a flexible blanket upon which are mounted the solar cells and wiring for power and instrumentation, a single BISTEM stainless-steel boom and deployment actuator, an inboard pallet,

and outboard pressure plate, instrumentation, a drive and track mechanism, a slip ring assembly, and related structure and associated equipment (Fig. 2). The drive and track mechanism rotates the array about the spacecraft pitch (north-south) axis and maintains the array normal to the sun in azimuth in a sun track or a clocked mode.

5. The Solar Array Technology Experiment (SATE)- Test Patch and Electronics

The SATE package includes: accelerometers, deflection sensors, load cells and blanket tension monitors to measure mechanical performance of the arrays in flight (Paulsen et al, 1974). The SATE also includes five platinum resistance temperature sensors to measure blanket temperatures; these sensors were placed under small, covered, open-circuit solar cells. Their range is -200°C to +75°C. Four additional temperature sensors are about mid-way along the south blanket and one is mounted next to a solar cell test patch. This test patch is a module of 3 X 9 solar cells just inboard of the housekeeping section on the north blanket. Inside the spacecraft, an Array Experiment Electronics (AEE) package provides: resistance bridges for the temperature sensors; commutation of 6 load conditions on the test patch; and determination of the test patch voltage and current at the 6 load conditions. The AEE, also contains a first-failure-proof subcommutator and logic circuit for control of the measurement functions and for sequencing the temperature, current and voltage data onto a telemetry channel.

The AEE provided the primary data on the performance of the AEG Telefunken solar cells. These data are used for calculation of the array housekeeping and experiment power capability.

The beginning of life datum on the test-patch power output was obtained immediately after array deployment. In an earlier paper (Gore, 1976) it was reported that the flight values of short-circuit current and maximum power were 4.3% and 5.9% respectively below preflight prediction. A re-examination of the solar cell calibration procedures at the European Space Technology Center (ESTEC) showed that the ground calibration was 2% high(Bogus et al, 1977). Two independent re-assessments of the flight data and the preflight calibrations showed a difference in the values of the test-patch currents of 1%. The lower figure is listed in Table I.

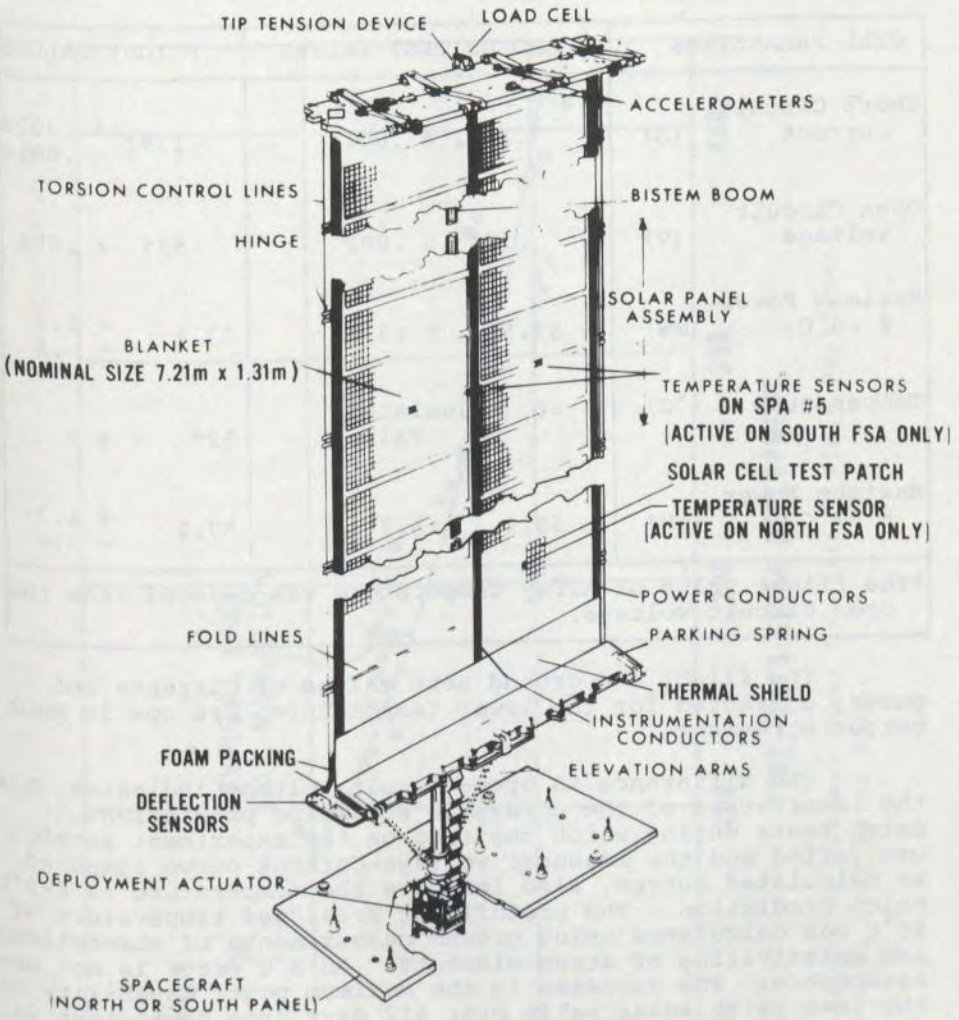


Figure 2. The Deployable Solar Array

TABLE I

Comparisons between Ground Test Data and Flight Data for the Solar Cell Test Patch (Values are given for normal-to-the-sun conditions.)

| CELL PARAMETERS | GROUND TEST VALUES | FLIGHT VALUES |
|---|---|---|
| Short Circuit Current (A) | .1422 ± .0014 | .1391 + .0028 − .0014 |
| Open Circuit Voltage (V) | .538 ± .002 | .545 ± .004 |
| Maximum Power @ 60°C (mW) | 57.5 ± .7 | 57.2 + 1.2 − .6 |
| Temperature (°C) | 60 (Calculated Value) | 52* ± 2 |
| Maximum Power @ 52°C (mW) | 59.4 ± .7 | 57.2 + 1.2 − .6 |

*The flight value of Array Temperature was deduced from the open circuit voltage.

The flight and ground test values of currents and power, corrected for the lower temperature, are now in much better agreement.

The difference in open-circuit voltage indicates that the temperature of the arrays is 8°C below predictions. Later tests during which the load on the experiment section was varied and the measured voltage-current curve compared to calculated curves, also indicate the temperature is 8-9°C below prediction. The protoflight predicted temperature of 60°C was calculated using ground measurements of absorptions and emissivities of array elements. An 8°C error is not unreasonable. The decrease in the maximum power capability of the test patch solar cells over 412 days from deployment is shown in figure 3. The decrease of about 1% shortly after deployment may be caused by the expected darkening of the coverglass and adhesives or by photon degradation as reported by Fischer and Pschunder, 1973. The amount of the subsequent degradation, caused by electron and proton radiation, is consistent with the low solar proton flare levels observed since launch.

The AEE and test patch provided data until March 20th, 1977, when a malfunction in a unit powered by the secondary module associated with the SATE resulted in the permanent loss of all SATE instrumentation data.

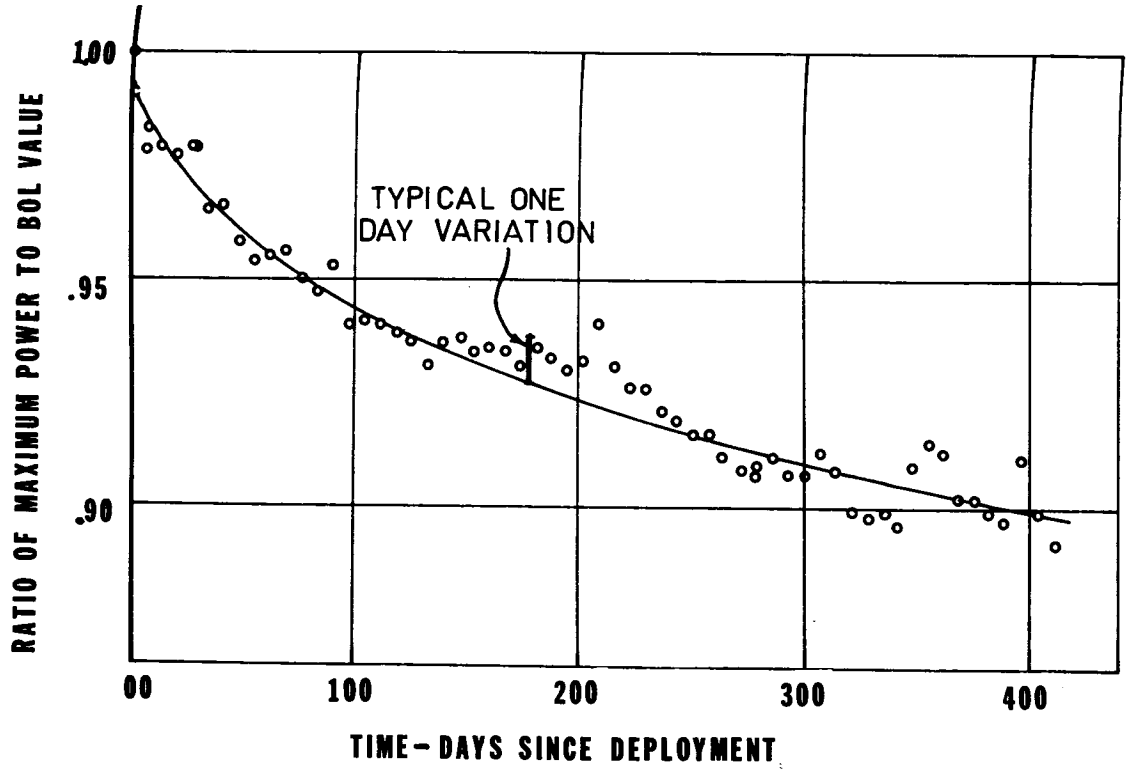


Figure 3. Degradation of Maximum Power Capability since Deployment - Solar Cell Test Patch Data

## 6. The Flexible Solar Arrays

The construction of the flexible array blankets has been described in detail by other authors (Buhs, 1974; Paulsen et al, 1974; Reinhartz et al, 1976). The flexible substrate is a laminate of 25 μm kapton and 35 μm fiberglass in polyester. The solar cells are 2 cm X 2 cm X 200 μm. The interconnects are 25 μm silver mesh welded to the cells. Coverglasses, completely covering the cells, are Pilkington Perkin Elmer 100 μm ceria-doped glass. The cells are bonded to the substrate by RTV 560 adhesive. By careful masking techniques, the adhesive covered >90% of the cell area with very little adhesive spread into the gaps between the cells, thereby providing excellent thermal contact to the substrate for efficient cooling while maintaining maximum flexibility and stress relief. Printed-circuit power and instrumentation wiring is mounted on the sunward side of the blanket.

### 6.1 Electrical Performance

The electrical connections on one flexible blanket are drawn schematically in figure 4. On the two flexible blankets, the total number of solar cells in the experiments sections is 20,412, and in the housekeeping sections is 4,860.

The power capabilities of the experiment and housekeeping sections of the arrays were calculated from the solar cell test patch BOL datum and the smoothed degradation values, as shown in figure 5. On June 21, 1977, a test was run where the load on the experiment unregulated bus was varied over its maximum range (220w to 746w). From this test, maximum power capability of the experiment section was calculated to be 792w, in excellent agreement with predictions based on test patch data.

On June 8, 1976, at 06.45 GMT a short circuit occurred on the experiment section of the north deployable solar array. Immediately the short circuit occurred, the OV/UV relay opened, isolating the arrays from the spacecraft. The short lasted 24 seconds, then apparently burned itself out. Following this anomaly, best estimates were that 6 panels, 14% of the experiment section, were no longer in the circuit.

The short could have occurred in two possible locations: on a board containing isolating diodes, located just under each array and exposed to the external environment, or on a flexible blanket. It was first thought (Gore, 1976) that the latter hypothesis was unlikely because it required prior failure of three specific isolating diodes. However, ground tests on a large section of flexible array (Bogus, 1978) revealed that electrostatic charging and subsequent discharges result in shorting failures of the isolating diodes. It now seems more likely that the short did occur on a blanket, and that the initiating arc resulted from electrostatic charging.

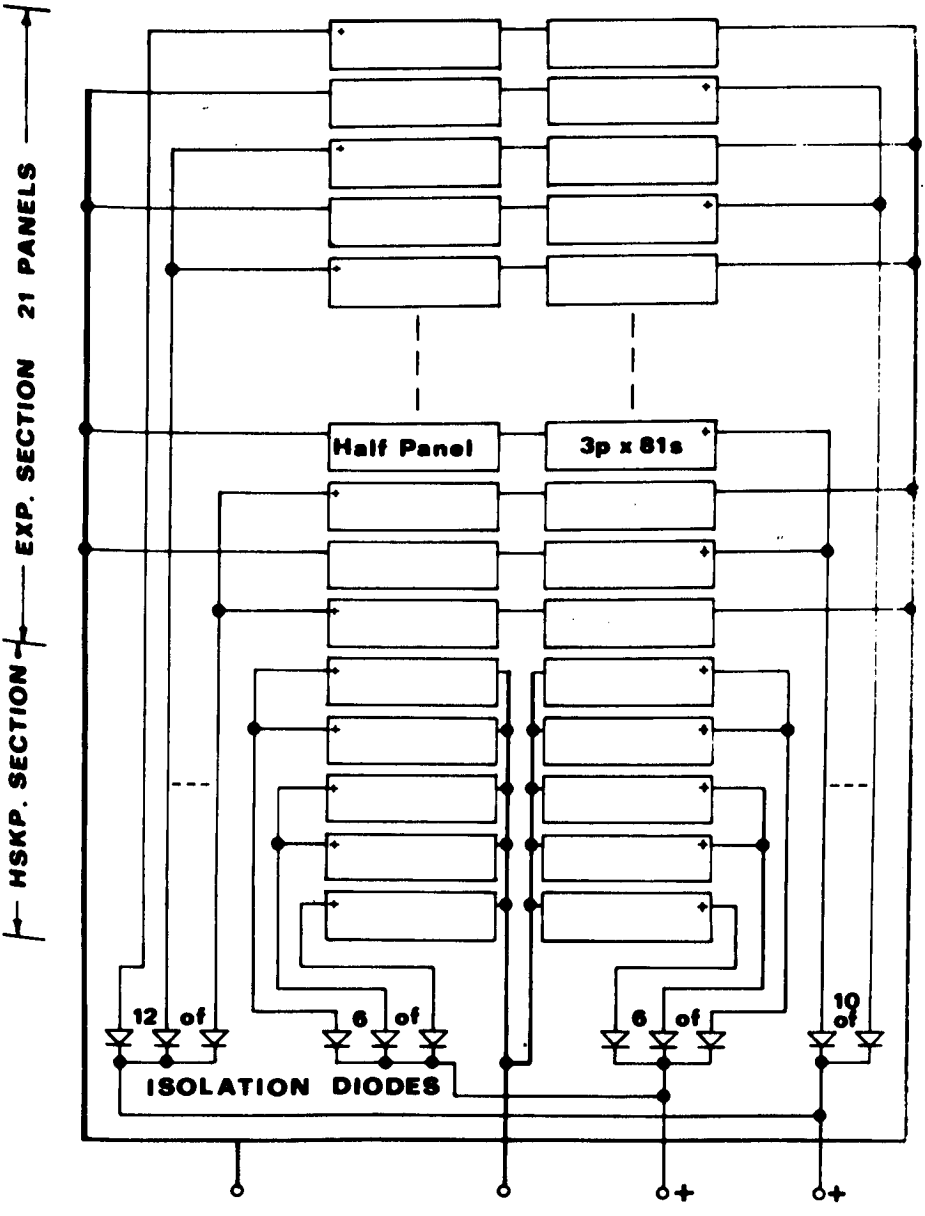


Figure 4. Block Diagram of the Electrical Connections on One Flexible Solar Array Blanket

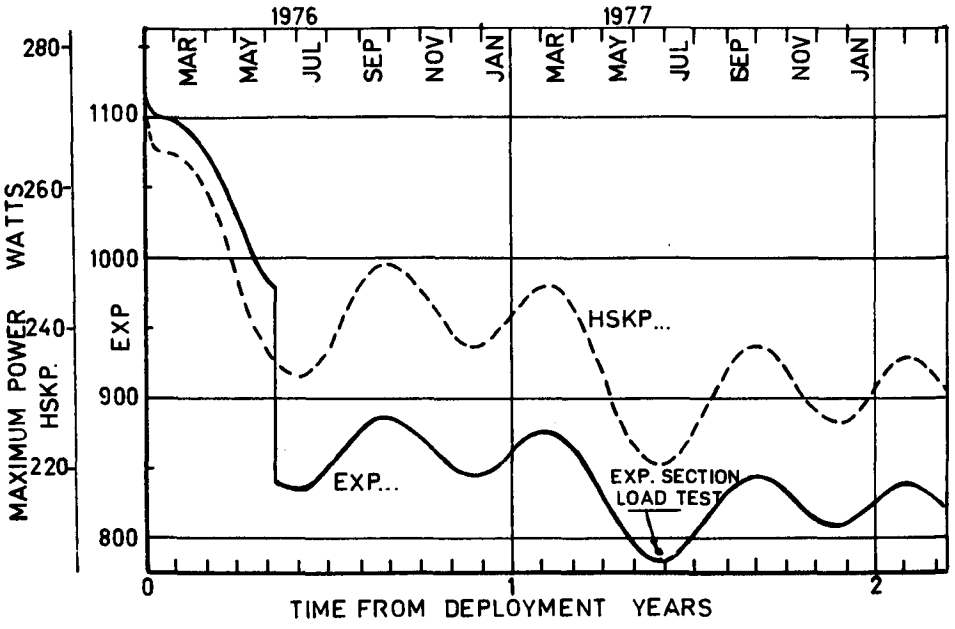


Figure 5. Maximum Power Capability of the Housekeeping and Experiment Sections of the Flexible Solar Arrays.

## 7. Nickel Cadmium Batteries

During eclipses, the housekeeping subsystems obtain power from the two 24 cell 5 Ampere hour (Ah) (Name Plate Capacity) Nickel-Cadmium batteries.

One of the two batteries on Hermes has not performed well. A capsule summary is presented here and some recommendations are given in the next section. The flight batteries were installed on Hermes during the spacecraft integration phase. During the integration and test phases, the batteries were subjected to random periods of charge, discharge and open-circuit stand. After launch, the main use of the batteries has been for housekeeping power during transfer-orbit eclipses and for the synchronous-orbit eclipse seasons, 48 days each spring and fall. Between eclipse seasons, the batteries continually supply a 50mA current and are recharged daily. No low current (about 125mA) charge rate was available on Hermes to supply this current and to trickle charge the batteries.

During the ground test phase, the battery temperatures were usually above 20°C. In transfer orbit battery temperature often exceeded 25°C, and in synchronous orbit, summer season the batteries operate at temperatures as high as 30°C.

Periodically during the test phase and about 4 times per year after launch, the batteries were reconditioned by one or more deep discharges, followed by an immediate recharge. The histories of the batteries' capacities for each discharge are listed in Tables IIa and IIb. The attainable Ampere-hour capacity is the value listed for a battery voltage of 26.2 volts. (Undervoltage protection circuits cut off all but essential housekeeping loads at slightly below 26.2 volts.)

In Table IIa, the listed capacities for battery A show two things: that the decrease in capacity has been gradual; and that the recovery by reconditioning has been quite successful.

In Table IIb, the listed capacities for battery B show; a sudden decrease in capacity as revealed by the February 7, 1977 recondition; recondition cycles are not able to recover capacity. The problem is apparently one or more low-capacity cells.

For the long eclipses near spring and fall equinoxes the batteries must supply 2.8 Ampere-hours. The present capacities of batteries A and B, 4.0 and 2.5 Ah respectively, are adequate but uncomfortably close to the limit.

TABLE IIa

BATTERY A Ampere Hour Capacity as determined by Recondition Cycles

| Date | Comments | Ampere Hour Capacity at 26.2V | Ampere Hour Capacity At end of Discharge | Voltage at end of Discharge |
|---|---|---|---|---|
| Sept. 8/75 | Thermal Vacuum Test | 4.30 | 4.77 | 24.0 |
| Sept. 21/75 | Thermal Vacuum Test | 5.52 | 5.72 | 24.0 |
| Dec. 11/75 | Launch Site | 4.95 | 5.30 | 24.0 |
| Jan. 8/76 | Launch Site (Pad) | 4.50 | 4.52 | 26.1 |
| Feb. 16/76 | First Flight | 4.73 | 5.25 | 24.0 |
| Apr. 19/76 | First Cycle - Post-Eclipse | 4.46 | 4.90 | 24.0 |
| May 10/76 | Second Cycle | 4.58 | 5.30 | 24.0 |
| Aug. 15/76 | Second Cycle - Pre-Eclipse | 4.07 | 5.17 | 24.0 |
| Oct. 20/76 | First Cycle - Post-Eclipse | 3.95 | 5.07 | 21.6 |
| Nov. 3/76 | Second Cycle | 4.25 | 5.15 | 21.6 |
| Feb. 10/77 | Second Cycle - Pre-Eclipse | 4.20 | 5.48 | 21.6 |
| Apr. 22/77 | First Cycle - Post-Eclipse | 3.88 | 4.90 | 22.3 |
| Apr. 23/77 | Second Cycle - note recovery | 4.75 | 5.50 | 22.3 |
| Aug. 22/77 | Second Cycle - Pre-Eclipse | 3.10 | 4.81 | 21.4 |
| Aug. 23/77 | Second Cycle - recovery at 26.2V | 4.05 | 4.81 | 21.4 |
| Oct. 20/77 | Second Cycle - Post-Eclipse | 2.85 | 4.25 | 21.6 |
| Oct. 21/77 | Second Cycle - note recovery | 4.05 | 5.18 | 21.6 |

TABLE IIb

BATTERY B Ampere Hour Capacity as Determined by Recondition Cycles

| Date | Comments | Ampere Hour Capacity at 26.2V | Ampere Hour Capacity At end of Discharge | Voltage at end of Discharge |
|---|---|---|---|---|
| Sept. 9/75 | Thermal Vacuum Tests | 4.22 | 4.55 | 24.0 |
| Sept. 28/75 | Thermal Vacuum Tests | 5.18 | 5.36 | 24.3 |
| Dec. 12/75 | Launch Site | 4.62 | 4.98 | 24.4 |
| Dec. 15/75 | Launch Site | 4.81 | 4.98 | 24.4 |
| Jan. 9/76 | Launch Site (Pad) | 4.55 | 4.63 | 25.6 |
| Feb. 15/76 | First Flight | 4.85 | 5.30 | 24.0 |
| Apr. 29/76 | First Cycle/First Sign of Serious Degradation - Post Eclipse | 4.15 | 4.25 | 26.0<br>24.0 |
| May 13/76 | Second Cycle | 4.60 | 5.18 | |
| Aug. 17/76 | Second Cycle - Pre Eclipse | 4.37 | 5.20 | 24.0 |
| Oct. 22/76 | First Cycle - Post Eclipse | 4.48 | 5.65 | 21.6 |
| Nov. 5/76 | Second Cycle - Note decrease | 4.37 | 5.10 | 21.6 |
| Feb. 7/77 | First Cycle - Serious Trouble | --- | 1.25 | 27.9 |
| Feb. 8/77 | Reported | --- | 1.82 | 27.5 |
| Feb. 11/77 | Attempts | --- | 2.05 | 27.0 |
| Feb. 12/77 | to Recover Capacity | --- | 2.31 | 27.2 |
| Feb. 21/77 | First Cycle - Recovery Attempt | | 1.81 | 27.1 |
| Feb. 22/77 | Back-to-Back Cycle* Successful | 4.15 | 4.45 | 24.6 |
| Apr. 19/77 | Back-to-Back Cycle Post Eclipse | --- | 1.82 | 26.8 |
| Apr. 20/77 | Second Cycle - Small Recovery | --- | 2.12 | 26.9 |
| Aug. 19/77 | Second Cycle - Pre Eclipse | --- | 1.50 | 26.6 |
| Aug. 20/77 | Second Cycle | 1.88 | 1.88 | 26.2 |
| Aug. 21/77 | Third Cycle - Small Recovery | 2.05 | 2.10 | 25.8 |
| Oct. 17/77 | Third Cycle - Post Eclipse | 1.90 | 2.10 | 25.2 |
| Oct. 18/77 | Second Cycle - Small Recovery | 2.48 | 2.98 | 24.0 |

*A "back-to-back" cycle is one with no break between the first recharge cycle and the second discharge.

## 8. Recommendations and Conclusions

Hermes is an advanced technology satellite and has provided valuable in-orbit experience. Based on this experience, the following observations and recommendations are made in the areas of power subsystems and power sources.

### 8.1 Flexible Solar Arrays

The flexible solar arrays have performed beyond expectation. Except for the short circuit in June 1976, there have been no malfunctions. The low decrease in power output indicates that there have been no observable losses due to cell or interconnect breakage or fatigue through 4 eclipse seasons. However, the authors would caution that this type of flexible blanket, with large areas of dielectric in shadow, is susceptible to charging by high-energy electrons (Bogus, 1978), and that in future the blankets should be designed to prevent charge accumulation. One method being investigated by AEG Telefunken is to have a conductive layer on the shadowed side of the blankets. Generally, the spacecraft-charging problem has not been solved and electronic circuits must be protected against the fast transients that are generated by static discharges.

### 8.2 Batteries

One of the batteries on Hermes has degraded rather badly but we feel that a few improvements would prevent a similar experience.

- The flight batteries must not be subjected to the integration and test phase. They should be installed on the flight spacecraft as late as possible, preferably at the launch site.

- The battery's temperature should be maintained in the range 10° ±5°C for all mission operations.

- The battery charge controllers should supply at least two levels of charge current, C/10 or higher (where C is the battery name-plate capacity), and a trickle charge, C/50 to C/100. The trickle charge is a maintenance charge for the solstice season. Some form of automatic charge control should be incorporated on the spacecraft.

- Provision for reconditioning is mandatory and it is desirable to be able to discharge each battery cell to less than .2 volts. Monitoring of individual cell voltages is desirable.

## REFERENCES

Bogus, K.P.
1978 Electrostatic Charging Effects on Deployable Solar Arrays, *Proceedings of the Royal Society Symposium on Hermes*, November 29, 30, December 1, 1977.

Bogus, K.P., Larue, J.C., and Crabb, R.L.
1977 Solar Cell Calibration: Recent Experiences at ESTEC and Proposals of a Combined Space and Terrestrial Calibration Procedures, *Proc. of the 1977 Photovoltaic Solar Energy Conference*, Luxemburg, September.

Buhs, R.
1974 Layout and Technology of the CTS Solar Array Blanket, presented at *the 10th Photovoltaic Specialists Conf., IEEE*, Palo Alto.

Fischer, H. and Pschunder, W.
1973 Investigation of Photon and Thermal Induced Changes in Silicon Solar Cells, *Proc. of the 10th Photovoltaic Specialists Conference*, November.

Gore, J.V.
1976 The Flight Performance of the CTS Body Mounted and Deployable Solar Arrays, *Proceedings of the 12th Photovoltaic Specialists Conference*, Baton Rouge, November.

Paulsen, P., Woodcock, W. and Sachs, P.
1974 Design and Qualification of the CTS Solar Cell Blanket, *Proc. of International Conference on Photovoltaic Power Generation*, Hamburg.

Reinhartz, K.K., Paulsen, P. and Buhs, R.
1976 European Flexible Solar Cell Blanket on the Canadian/U.S. Communications Technology Satellite, *ESA Bulletin*, August.

# ELECTROSTATIC CHARGING EFFECTS ON THE HERMES SOLAR ARRAY

K.P. Bogus

The European Space Technology Centre,

Noordwijk, The Netherlands

*Lorsque des satellites sur orbite géostationnaire sont soumis à des sous-orages magnétiques des charges différentielles peuvent s'accumuler sur la surface de divers matériaux, donner lieu à d'importantes tensions électriques et provoquer la création d'arcs électriques si le seuil de claquage est dépassé.*

*Comme le réseau de piles solaires du STT est constamment tourné vers le soleil, sa paroi arrière, toujours à l'ombre, est faite d'un matériau isolant. Ce réseau constitue donc un des principaux sièges où des décharges sont susceptibles de se produire.*

*Dans le cadre d'un programme d'essais au sol après lancement, on a étudié en profondeur les phénomènes de charge électrostatique du réseau, en tentant d'établir des rapports entre les résultats des essais et le comportement du satellite sur orbite.*

*Il s'est avéré que le matériel expérimental électrique du réseau de piles, qui s'intègre aux techniques expérimentales employées, ne pourrait pas supporter une décharge électrique dans la région de l'unité d'essai incorporée au panneau Nord. Jusqu'à avril 1977, le matériel sur orbite n'a présenté aucune anomalie.*

*Le 160e jour de 1976, on a toutefois constaté une défaillance temporaire de la barre omnibus servant à l'alimentation principale du matériel. Toute explication plausible de l'anomalie, qui suppose la création d'un arc de décharge sur le réseau de piles, devait nécessairement se fonder sur le court-circuit d'au moins un groupe de diodes de blocage du réseau. Une simulation au sol a en effet permis de démontrer que des décharges sur le réseau de piles, causées par des sous-orages magnétiques, avaient presque toujours pour effet de court-circuiter certaines de ces diodes.*

*Les résultats d'essais au sol supplémentaires portant sur l'incidence des dimensions de la zone d'échantillonnage ont fait ressortir encore*

*plus les dangers que présentent les charges et décharges d'électricité statique. Il a été démontré que l'énergie d'une impulsion de décharge augmente linéairement en fonction des dimensions de la zone d'échantillonnage, jusqu'à au moins 3,6000 cm$^2$, superficie à laquelle des impulsions d'une énergie de 5 joules et d'une intensité crête supérieure à 300 ampères ont été mesurées.*

*Les futurs réseaux de piles solaires devront donc être convenablement protégés contre les charges sur orbite géostationnaire. En Europe, on met au point actuellement des réseaux de conception nouvelle, composés de couches dont la paroi arrière sera conductrice (faite par exemple de fibre de carbone) et pourra être mise au potentiel de la masse du satellite afin d'empêcher la création de charges différentielles.*

## 1. Introduction

Satellites in geostationary orbit and under magnetic substorm conditions are known to be subject to differential charging of different material surfaces leading to high values of electrical stress. Arc discharges occur if the threshold for electrical breakdown is surpassed. The highest electric stress is expected on insulating material surfaces which are not sun-illuminated and therefore cannot equilibrate at low potentials by photo emission of electrons. The rear-side of sun-oriented deployable solar arrays is shaded permanently and therefore constitutes a principal source of discharge if the rear surface conductivity is low.

The Communications Technology Satellite (CTS) or Hermes, has a sun-oriented 2-wing solar array using a kapton-glass fibre-compound flexible substrate 75 microns thick which provides an insulating rear surface. Electrostatic-charging phenomena on this solar array have been extensively investigated in a post-launch ground test program where the magnetic substorm environment was simulated by a 5 to 20 kV electron beam in a space environment simulation chamber. The results of the final test series are described in this paper and an interpretation of the in-orbit performance is attempted.

Moreover, the test results give useful information on more general charging phenomena, such as the sample-size dependence of discharge intensity and the influence of temperature and illumination on the discharge characteristics.

## 2. Summary of Previous Test Results

A first series of charging tests had been performed in the 2.5m Space Simulation Chamber of the Deutsche Fors-

chungs-und Versuchsanstalt für Luft-und Raumfahrt (DFVLR) at Porz-Wahn (Fig. 1). The test specimen consisted of a Hermes solar cell test patch (Fig. 2) with an area of about 80 $cm^2$ together with the appertaining electronics unit (AEE). Details of these tests are given in Bogus, 1976.

The major results obtained from these tests were as follows:

I Discharges due to electrostatic charging of the sample rearside occur at electron beam energies above 15kV if the sample is not illuminated.

II The discharge rate depends strongly on the sample equilibrium temperature. Discharges are obtained only below a threshold temperature of about 30°C. Moreover, illumination of the sample front side reduces the threshhold temperature. Consequently, under solar illumination, the discharge rate decreases to zero as the sample temperature rises above -50°C.

III The AEE electronics unit will not survive a severe discharge in the test patch area of the solar array.

IV The measured dissipated discharge-pulse energy is only slightly less than the electrostatic-charge energy of the entire sample area. From this it can be assumed that the entire sample surface is discharged in one discharge pulse.

## 3. Objectives of the Second Test Series

The results derived from the first test series had indicated a direct correlation between discharge-pulse energy and sample size. Therefore tests with larger samples became desirable in order to better understand the behaviour of large solar cell panels in magnetic substorms.

Moreover, after several months in orbit, Hermes had experienced a significant anomaly in the power subsystem (the "day 160 anomaly") for which no explanation had been found. Therefore tests had to be performed to investigate electrostatic charging and discharging as potential sources of the anomaly.

## 4. The Sample Size Effect

To study the influence of the sample size on the discharge pulse characteristics two CTS samples T01 and T04 (Figs. 2 and 3) with an area of 3600 $cm^2$ and 180 $cm^2$, respectively, were used. As sample area, only the area with conductive (i.e. solar cells and wiring) front surface is considered here. However, the area ratio of the two samples would be about the same if the entire sample area had been considered.

Typical high-energy discharge pulses are shown in

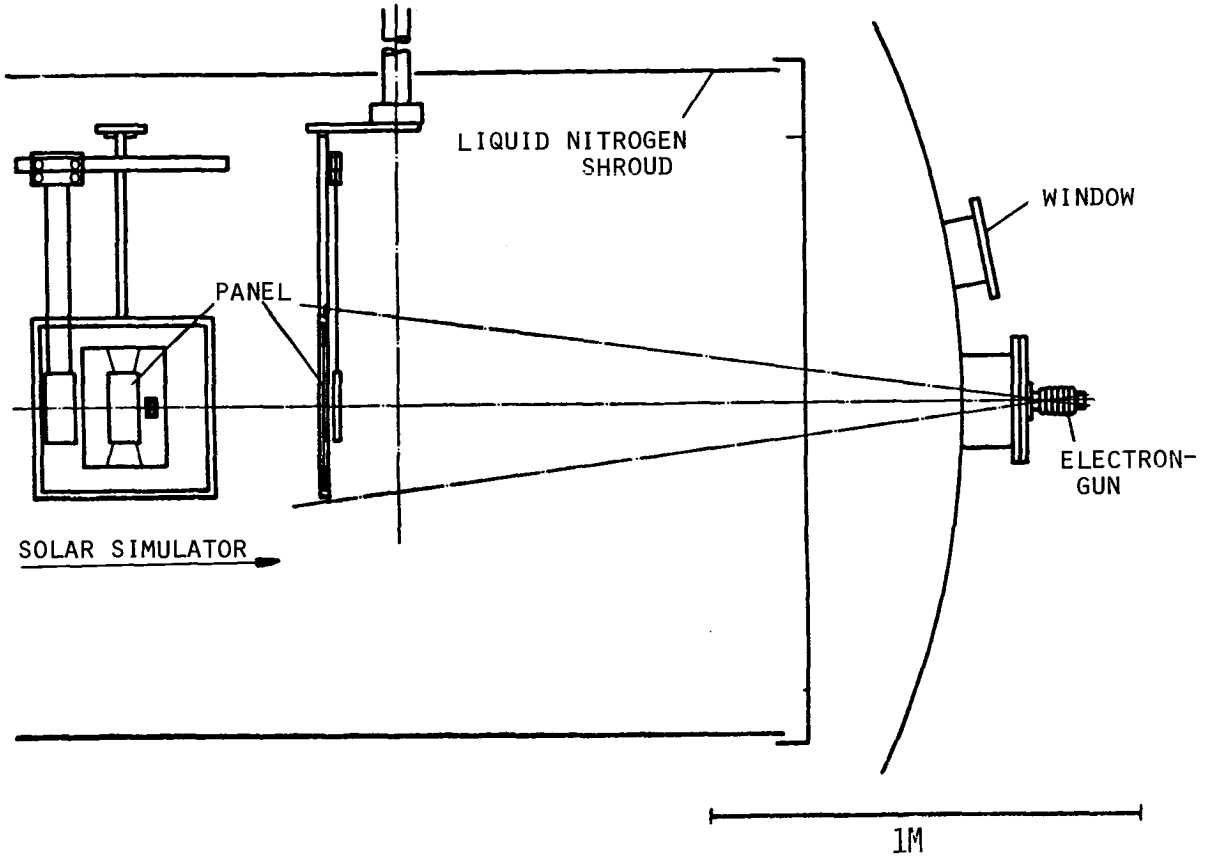


Figure 1. The Geomagnetic Substorm Simulation Facility at DFVLR.

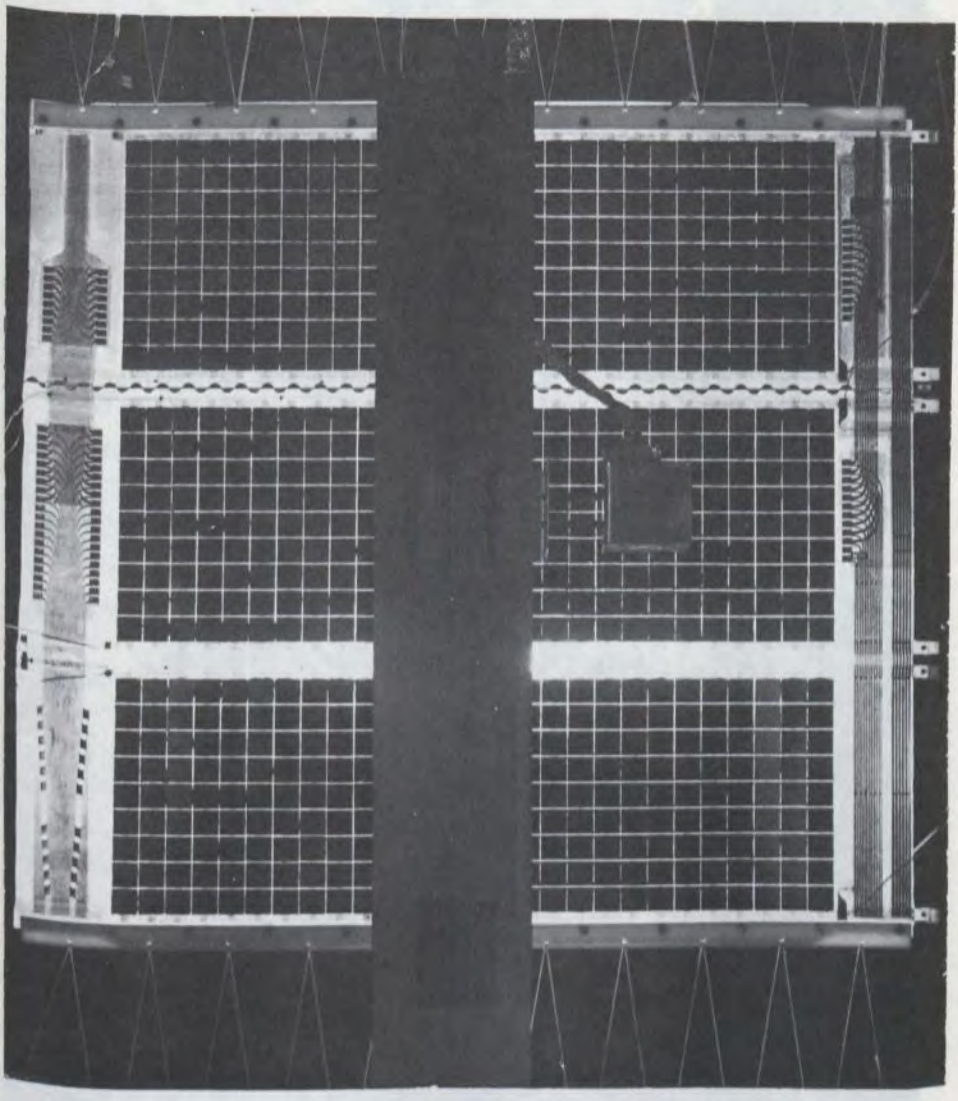

Figure 2. Hermes Solar Cell Test Patch T01 (70 x 70 cm).

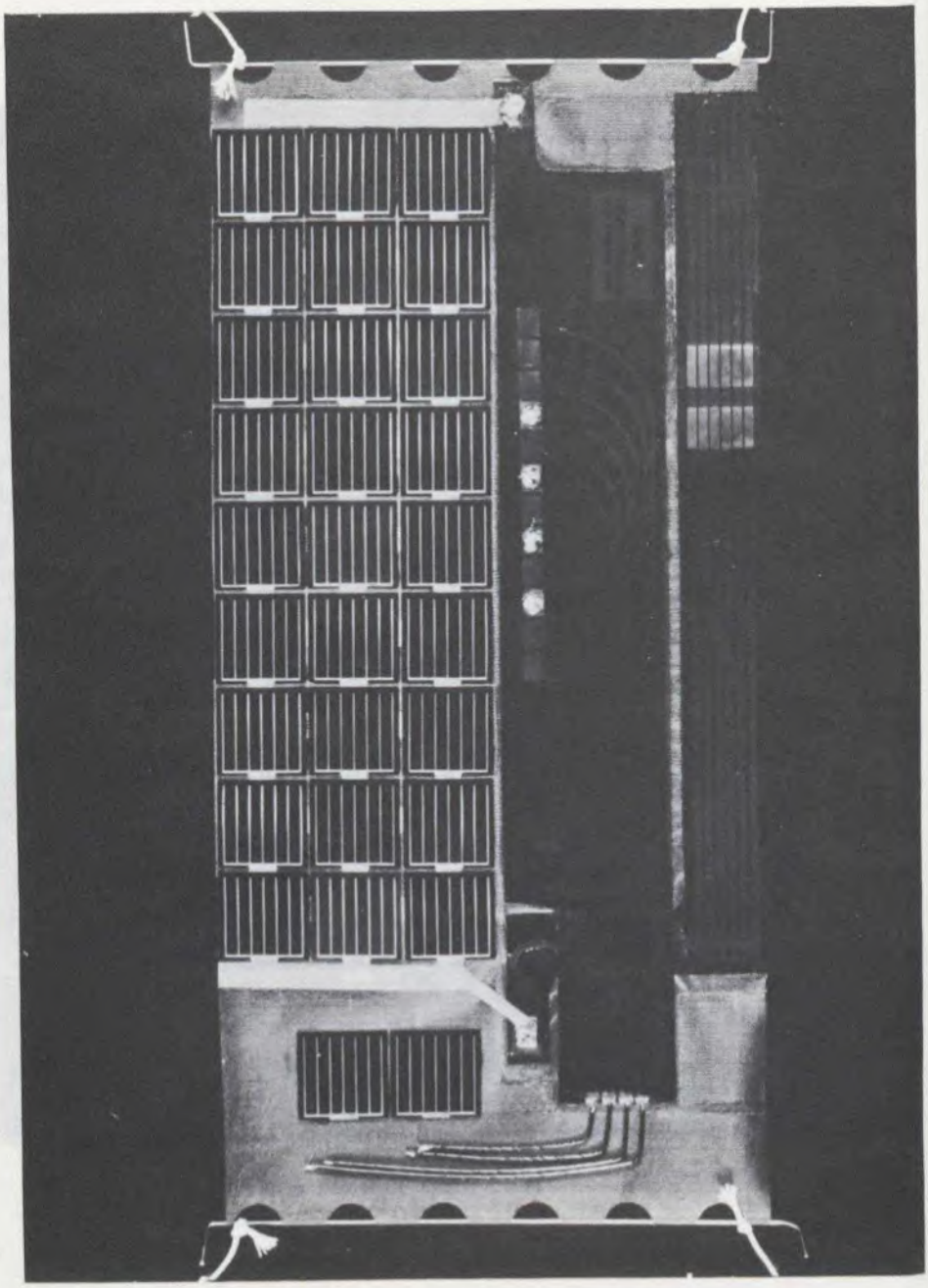

Figure 3. Hermes Solar Cell Test Patch T04 (12 x 25 cm).

figures 4 and 5. The pulses were recorded by a Tektronix P6021 current probe and a transient recorder at the solar cell module terminal wires which were connected to ground.

A comparison of the most important pulse parameters is given in figure 6. The listed values for the peak discharge current, and consequently all other derived data, are average values of a large number of pulses obtained without sample illumination.

The comparison clearly shows that the discharge pulse energy is proportional to the sample area even for sample sizes up to several thousand $cm^2$. Moreover, it can be seen that the pulse energy is about a factor of 4 lower than the energy stored in the flat-plate capacitor represented by the charged rear surface of the sample and the grounded conductive front side.

From these results it can be concluded that the entire sample surface is involved in each major discharge. This is also reflected in the frequency distribution of the discharge events as shown in figure 7. In case of locally-limited discharges of random distribution, a statistical distribution p(n) would be expected. In case of constant intervals between the discharges, the distribution r(n) would be observed. As can be seen, the actual distribution w(n) is not random, but rather close to constant intervals between the discharges. From the electron-beam current density and the time interval, the charge stored on the sample between the discharges is calculated to be about 700 μCb assuming 100% absorption of the arriving electrons. This figure is in good agreement with the values given in figure 6.

## 5. The Influence of Temperature and Illumination

As previous tests on the small Hermes sample had shown, temperature and illumination have a strong influence on the discharge frequency. For convenience, the essential results of these tests are shown once more in figures 8 and 9.

The same solar cycle tests were performed on the large sample. The results are shown in figure 10 in a slightly different fashion. The right-hand curve represents the electron-beam current density per 40 $cm^2$ detector area; the left-hand curve shows the total leakage current through the substrate as collected by the front-side solar cells and wiring. Discharges are indicated by the superimposed spikes originating from electromagnetic pick-up of the electron beam detector and the displacement current through the leakage-current-measuring circuit.

Parts A and B show the sample behaviour before the start of a solar illumination cycle. In A we see the effect of rear-side electron irradiation (25KV acceleration voltage, 10nA/$cm^2$ beam density) at room temperature in the dark; in B the chamber has been cooled to liquid nitrogen temperature. Evidently, the discharge frequency and intensity increase at

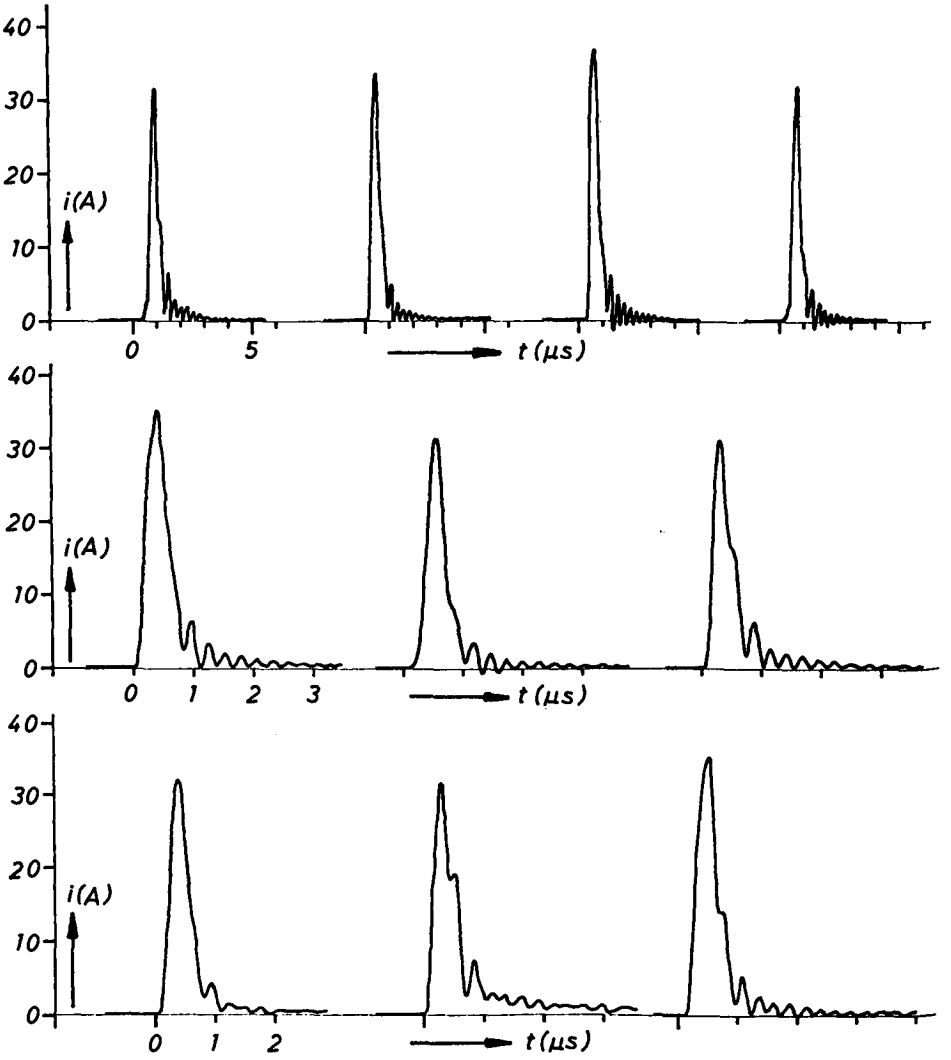


Figure 4. CTS Solar Array T04 Discharge Pulses

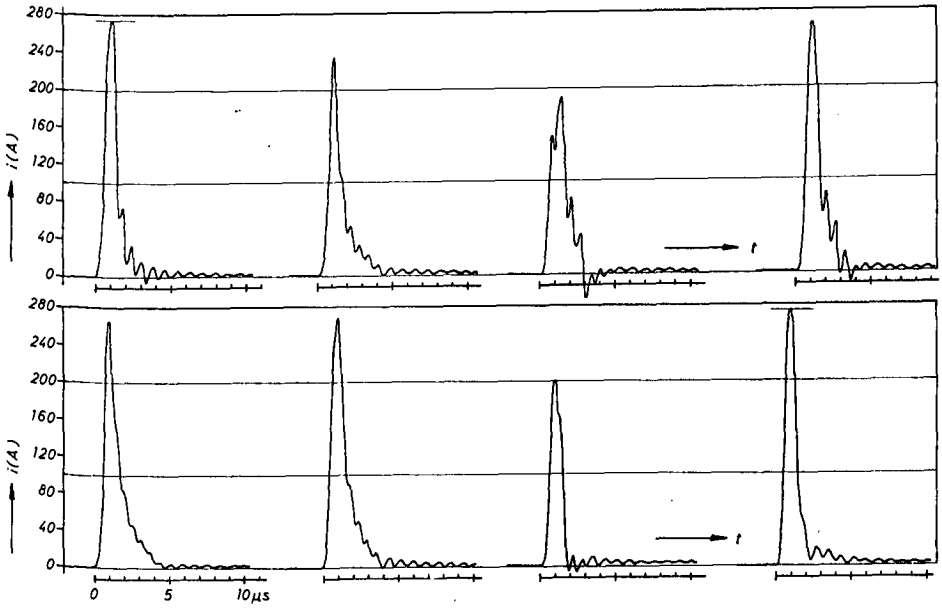


Figure 5. CTS Solar Array T.O.1 - Discharge Pulses.

| | T.O.4 | T.O.1 | RATIO |
|---|---|---|---|
| "ACTIVE" AREA | 180 $CM^2$ | 3600 $CM^2$ | 20 |
| PEAK DISCHARGE CURRENT | 30–40 A | 200–300 A | ~ 7 |
| CHARGE PER PULSE | 20–30 $\mu$Cb | 400–600 $\mu$ Cb | ~20 |
| PEAK PULSE ENERGY | 0.25 JOULE | 5 JOULE | ~20 |
| GEOM. CAPACITANCE | 7 n F | 140 n F | ~20 |
| STORED ENERGY | 1 JOULE | 20 JOULE | ~20 |

Figure 6. Sample Size Effect.

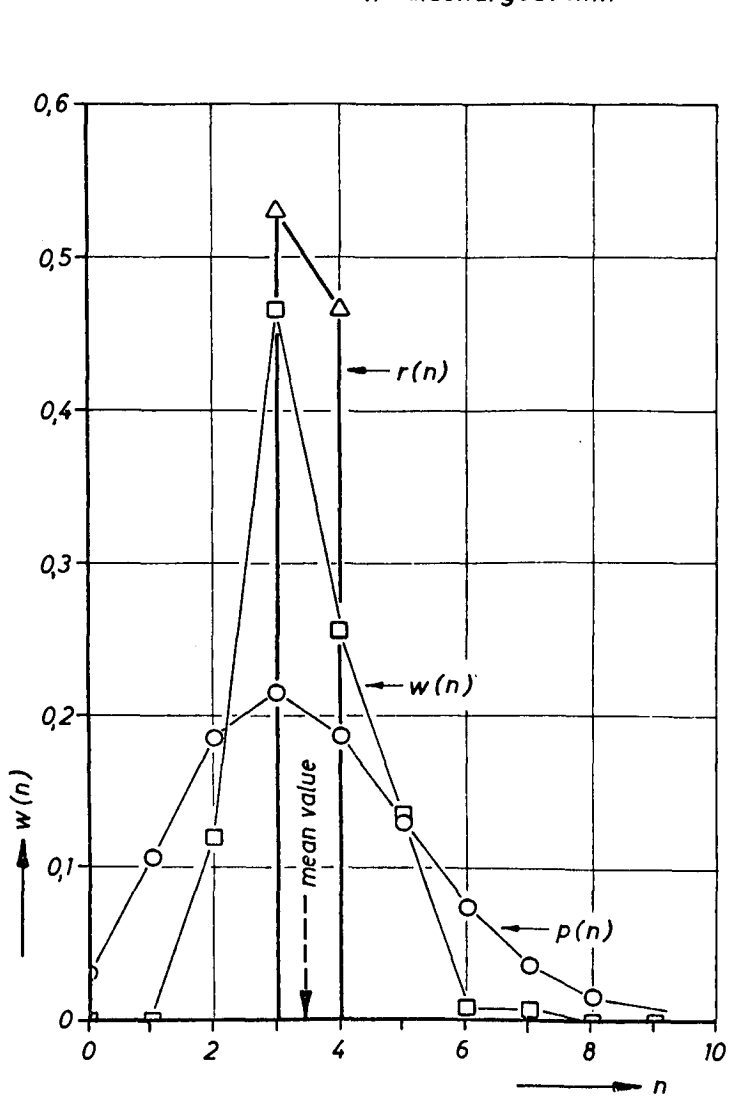


Figure 7. CTS Solar Array T.O.1.
Discharge Pulse Frequency Distribution.

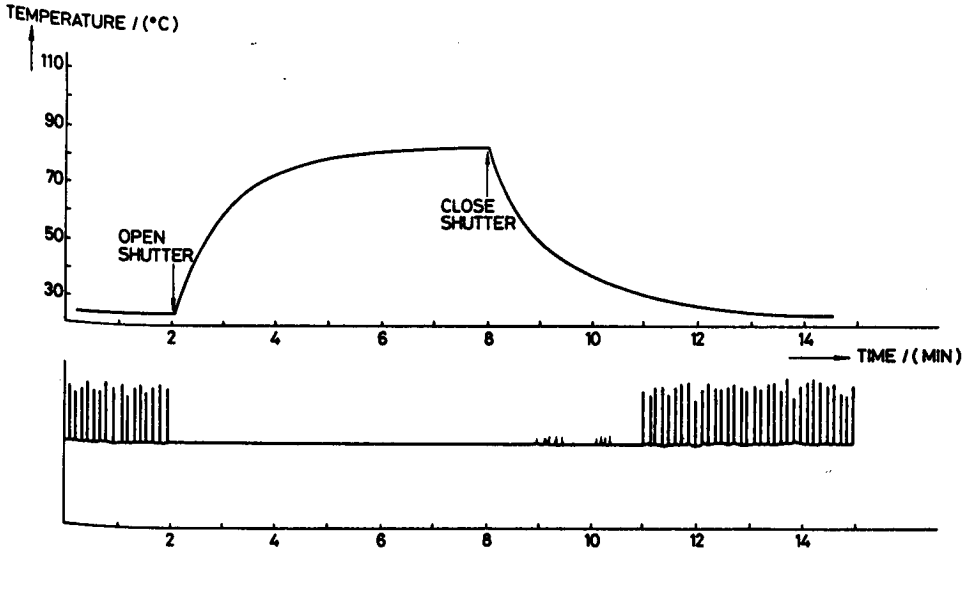


Figure 8. Discharge Rate on Sample T04 During Illumination Transient Without Chamber Cooling.

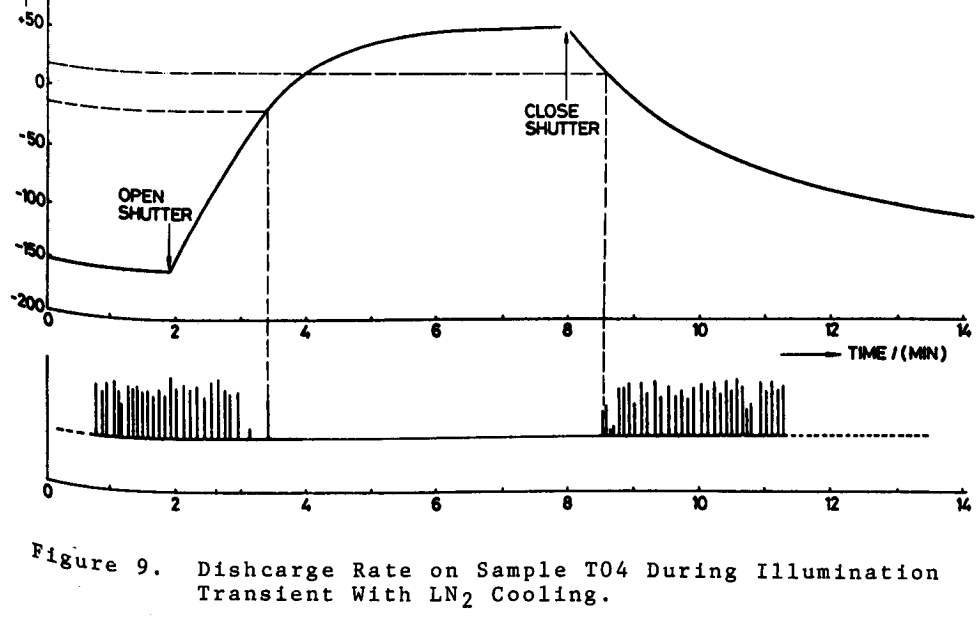


Figure 9. Dishcarge Rate on Sample T04 During Illumination Transient With $LN_2$ Cooling.

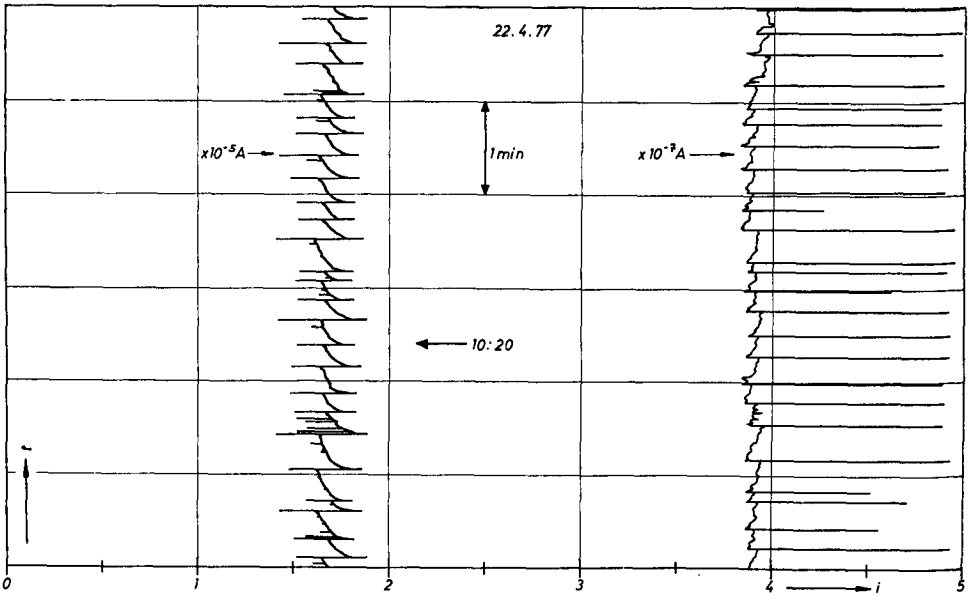


Figure 10a. No illumination, room temperature.

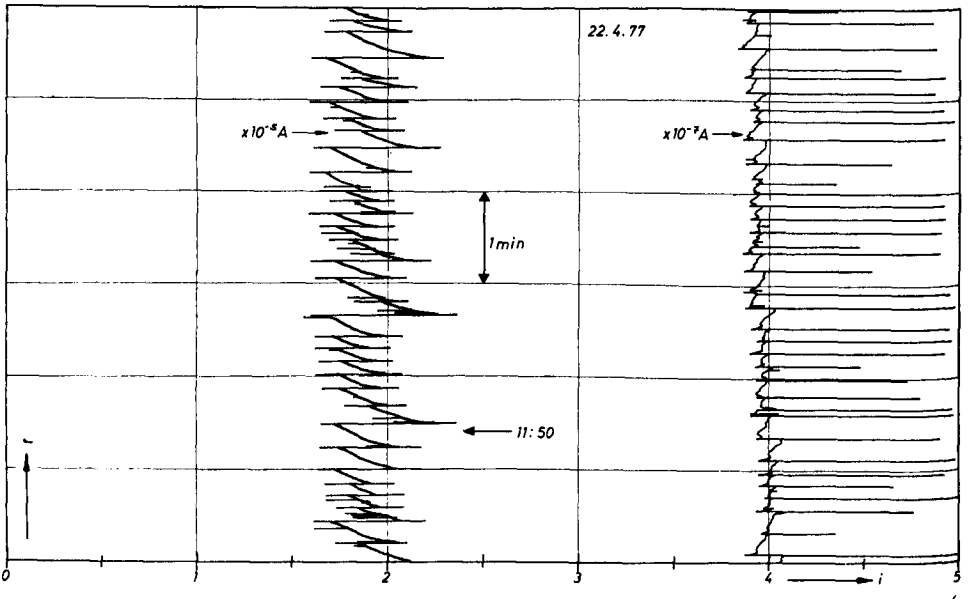


Figure 10b. No illumination, $LN_2$-temperature.

low temperatures. In Part C, the beginning of the sun phase is shown in which the sample temperature increases from about -160°C to +50°C. The temperature of the sample as a function of time is not recorded in this figure since it is the same as presented in figure 9.

In contrast to results with the small sample, the discharges do not completely cease in the sun phase, as can be seen in Part D of figure 10. The continuing discharge activity in the sun phase is of a different nature, however. The discharge energy is much smaller, as can be seen from the reduced displacement current. A measure for the displacement current is the deviation from the flat equilibrium line of the leakage current curve ($10^{-5}$A scale) between two discharge spikes. Moreover, the discharge frequency is considerably reduced and of random nature as judged from the probability distribution. Hence, it appears that these discharges are locally limited and do not involve the full blanket area as in the case of discharges in the dark.

Part E of figure 10 shows the end of the sun phase. After turn-off of the solar simulation, the discharge frequency and intensity increases to the equilibrium situation in the dark, with a time constant of about 1 minute. The leakage current also returns to its initial level with about the same time constant.

The contradictory results on the small and large test samples are difficult to understand since the test conditions were similar in both cases. The only difference is in the electron beam: for the small sample monoenergetic electrons were used (Bogus, 1976) whereas for the large sample a 2 μm aluminum scattering foil had been introduced in front of the electron-gun exit to achieve the required intensity uniformity of ± 30% over the larger area. As a consequence, the monoenergetic beam incident on the foil was transformed into a broad-spectrum beam typical for a scattered-electron energy distribution.

A useful piece of information for the explanation of the apparent discrepancy is found in the recording of the rear-surface potential which was measured with a calibrated Eltek E-field meter. Figures 11 and 12 show the rear surface potential across the width of the sample. In figure 11 the sample was not illuminated. During the scan erratic discharges and associated decreases of the surface potential occurred. The degree of potential decrease may be determined by the distance between the potential probe and the point from where the discharge originates and/or by the energy content of the discharge pulse. The equilibrium potential lies between 13kV and 16kV. In figure 12 the sample was illuminated. The surface potential is reduced to about 5kV in the inner part of the sample. At the edges, however, the potential remains at 12kV. The actual peak potential may be even higher in narrow edge regions, since the recorded potential is an average value over an area determined by the spatial resolution of the potential probe.

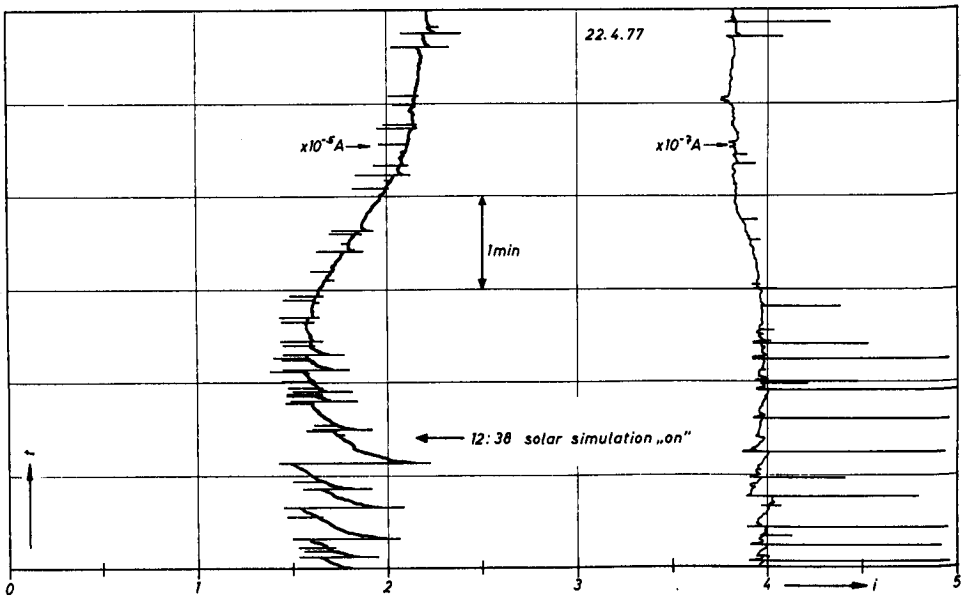


Figure 10c. Turn-on of Solar Simulator.

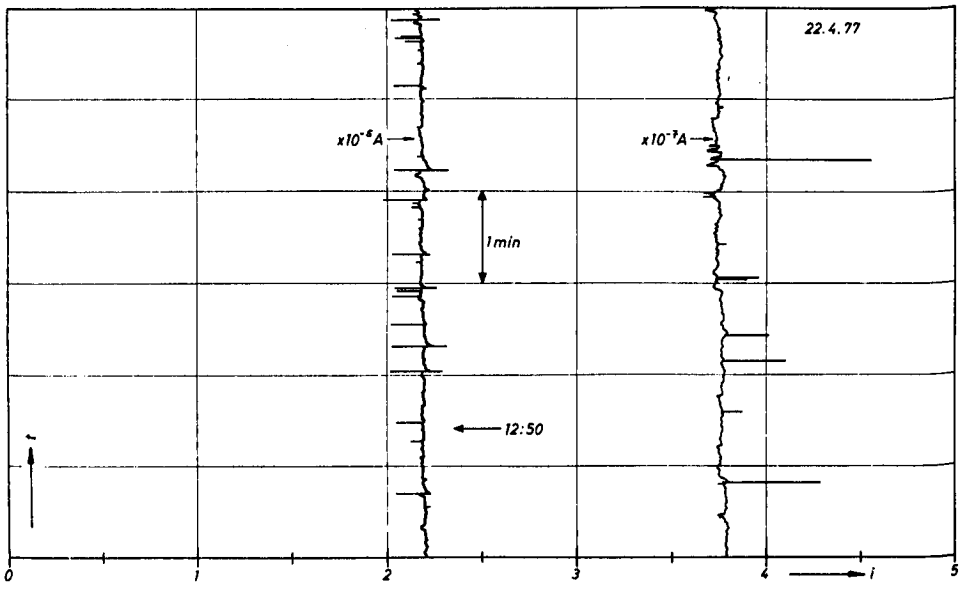


Figure 10d. Illumination, $LN_2$-temperature.

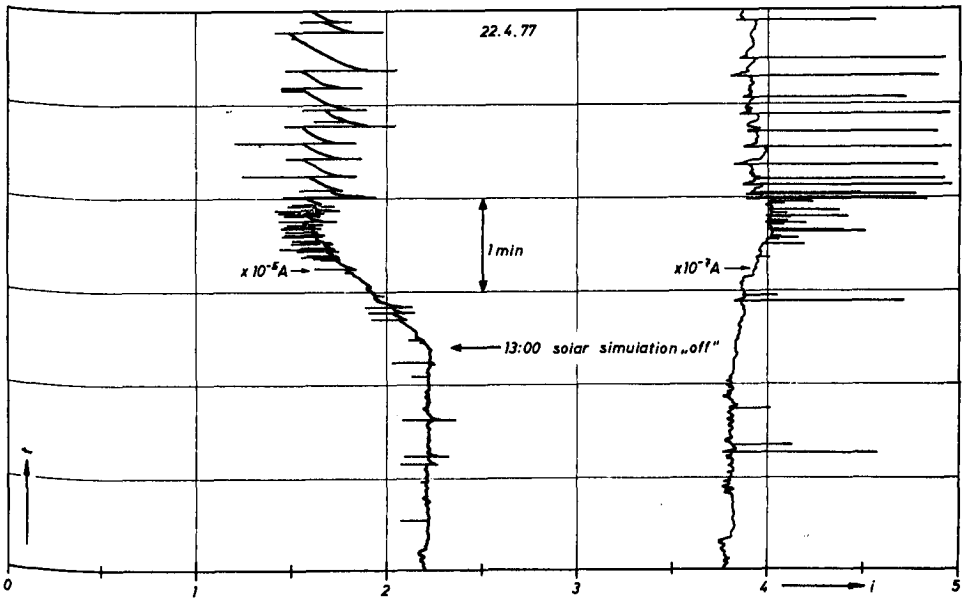


Figure 10e. Turn-off of Solar Simulator.

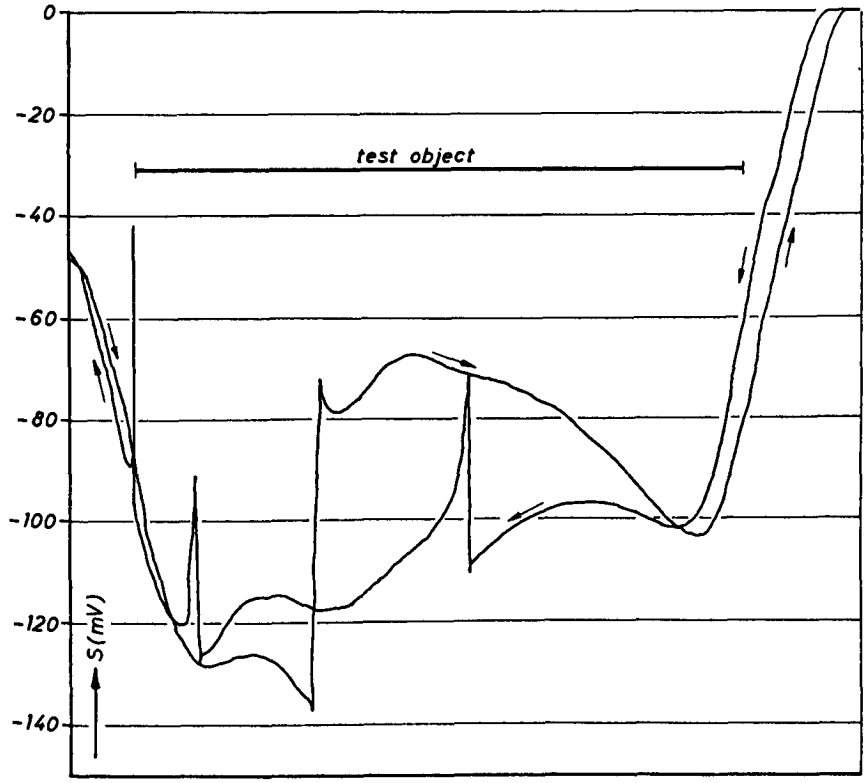


Figure 11. Rear Surface Potential of T01 in the Dark (Scaling Factor: 8.2mV ≙ 1kV).

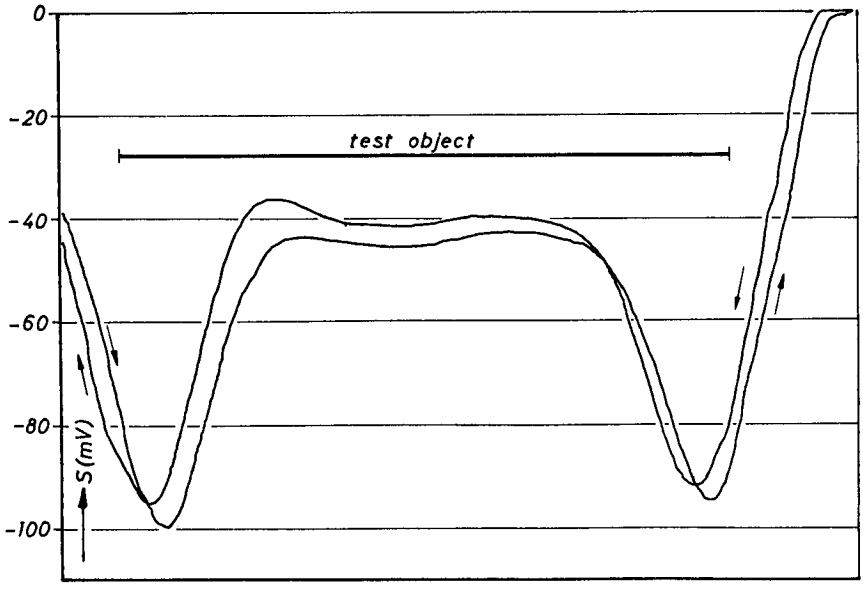


Figure 12. Rear Surface Potential of T01 in Sunlight (8.2mV ≙ 1kV).

The elevated potential at the sample edges was not found with the small sample where it could have been only partly masked by the limited resolution of the probe. It appears plausible that the low energy discharges observed on the large sample T01 occur in the edge areas which are considerably larger than those of sample T04. The different behaviour of the two samples is not yet fully understood.

The available test data still are not sufficient to distinguish between the influence of temperature and illumination. An additional test with internal heating of the sample by passing a forward current through the solar cells failed because the temperature across the sample turned out to be extremely non-uniform.

## 6. In-Orbit Performance of the Hermes Solar Array

138 days after in-orbit deployment of the Hermes solar array, on day 160 of 1976, a short circuit occurred on the experiment primary power bus (Gore, 1976). The voltage dropped from 86 Volts to 19 Volts and varied between this value and up to 42 Volts for the next 24 seconds. Then, it jumped back to full voltage again. Thereafter the array operated normally, but at a current capability about 15% lower than before the anomaly, which is equivalent to the loss of 6 out of 42 solar-cell panels which constitute the experiment section of the Hermes solar array (Gore and Bogus, 1978). This corresponds to the loss of 3 electrical sections of 2 panels each. Each electrical section has a pair of isolation diodes which protect the main bus in case of short circuit on one section.

The voltage levels during the breakdown and a slight attitude disturbance registered during the event indicate that the breakdown was caused by an arc that burnt itself out after 24 seconds. The arc could have occurred on the solar array or on the diode board on which solar array blocking diodes are positioned. The blocking diodes are there to protect the main bus from breakdown in case of a local short circuit in one of the electrical sections. If the arc occurred on the array side of the blocking diodes, it must be assumed that at least one of the diode sets was short-circuit damaged before or during the time of the anomaly.

Originally this hypothesis was considered as rather unlikely since the blocking diodes are hefty, high current devices. A simulation test, however, revealed a high probability that these blocking diodes would be damaged by discharges on the solar array. The test was performed with the sample T01, the solar cell strings being connected to ground on the ground side and connected through the diodes (outside the simulation chamber) to ground on the other side. Several common diode types (UES 304, UTR 6410 and UR 225 from Unitrode) were tested in this configuration under simulated magnetic substorm conditions. They were all short-circuit damaged after the first discharges on the test sample.

The results support the hypothesis that the day 160 anomaly was caused by an arc discharge on the solar array. This could have happened in two different ways:

An electrostatic discharge occurred on the solar array at the onset of the anomaly and created a low-impedance path for the solar cell power of at least one electrical section. Simultaneously, the blocking diodes of this section were short-circuit damaged. This caused the current of all the other parallel sections (totalling more than 8A) to flow into the low-impedance path. Then the short circuit burnt itself out and, as a consequence, 3 electrical sections (i.e. 6 panels) were disconnected from the main bus.

An electrostatic discharge occurred at any time before the anomaly and caused the short circuit of the blocking diode(s). This could not be noticed until, at the time of the anomaly, a short circuit was generated on the array in the area of a section with a short-circuited diode, leading to a breakdown of the main bus voltage. In this hypothesis, the short circuit at the time of the anomaly could have been due to causes other than an electrostatic discharge.

Surprisingly, the electrical solar-array-experiment equipment, which had been shown to be discharge sensitive in earlier tests (Bogus, 1976), was not affected by the anomaly. The solar cells of the array experiment are located on the north wing of the solar array. The short circuit probably occurred on this wing. It has to be borne in mind, however,

that the solar cells of the array experiment are at the in-board part of the wing, whereas the short-circuited array sections are at the out-board part.

## 7. Conclusion

The test results presented in this paper demonstrate that electrostatic charging of sun-oriented solar arrays with insulating rear surfaces in geomagnetic substorms leads to high energy arc discharges which can destroy electronic components and equipment connected to the charged array.

Additional evidence is presented for the hypothesis that the primary power breakdown on CTS on day 160 in 1976 was at least partly caused by discharges on the solar array.

The hazards arising from electrostatic charging are further emphasized by the results of ground tests on the influence of sample size on the discharge pulse parameters. It has been demonstrated that the pulse energy increases linearly with the sample area up to at least 3600 $cm^2$ where pulse energies of 5 Joule and peak current values above 300A were registered.

Future sun-oriented arrays have to be adequately protected against charging in order to avoid considerable hazards for missions in geostationary orbit.

## REFERENCES

Bogus, K.P.
1976 The CTS Solar Cell Test Patch Under Simulated Geomagnetic Substorm Charging Conditions, *Proc. Spacecr. Charging Tech. Conf.*, Air Force Academy, Colorado Springs, Oct. (in print).

Gore, J.V.
1976 Design, Construction and Testing of the CTS - Protection Against Spacecraft Charging, ibid

Gore, J.V. and Bogus, K.P.
1978 Electrical Performance of the Hermes Flexible Solar Array, *Royal Society of Canada Hermes Symposium*, Ottawa, Canada, November 29, 30, December 1, 1977.

# STRUCTURAL DYNAMICS FOR HERMES - MODELLING AND MEASUREMENT

F.R. Vigneron and P.C. Hughes

University of Toronto, Toronto, Canada

*Un des objectifs technologiques du programme Hermès était de "mettre au point et de faire l'essai en orbite d'un système de stabilisation triaxial assurant la précision du pointage de l'antenne d'un vaisseau spatial à bras flexibles." La communication décrit les épreuves réalisées et présente les conclusions générales tirées d'un élément clé de l'expérience, à savoir l'interaction entre la dynamique structurale et les systèmes de commande du satellite.*

*La structure d'Hermès est non-rigide étant donné son réseau important de piles solaires. L'étude au sol des propriétés dynamiques de la structure ne peut se faire que dans des limites très étroites, cette dernière ne possédant pas de mécanismes propres de sustentation qui permettrait son déploiement à terre. Pour permettre des essais sur orbite, Hermès était doté d'accéléromètres et d'autres capteurs spéciaux.*

*L'article analyse les données de 1971-72 sur le profil dynamique du satellite et les indications numériques correspondant aux principaux paramètres (fréquences d'oscillation des divers éléments, gains et amortissement) qui avaient été définis avant l'assemblage des éléments mécaniques d'Hermès. Les auteurs étudient ensuite les résultats préliminaires des essais au sol simulant le vol orbital, et décrivent les modifications apportées avant le lancement, en 1974-75, aux prévisions concernant le comportement dynamique de l'engin. Enfin, ils résument les résultats généraux des essais en orbite et de l'interaction entre la dynamique structurale et les systèmes de commande, puis comparent le comportement dynamique après le lancement avec les données de 1971-72 et de 1974-75.*

*La communication présente également les conclusions quant au modèle qui correspond le mieux aux applications du satellite Hermès, au rôle et à l'utilité des essais au sol, au degré d'interaction entre la dynamique structurale et*

*les systèmes de commande et, enfin, à la précision des résultats d'études dynamiques effectuées à différentes étapes de l'évolution du satellite.*

## Introduction

One objective of the Communications Technology Satellite (CTS) or Hermes program was "to develop and flight test a 3-axis stabilization system to maintain accurate antenna boresight pointing on a spacecraft with flexible appendages" (Vigneron and Millar, 1976). This paper provides an overview of experience gained and of the general conclusions obtained relative to a key sub-topic of this objective, namely spacecraft structural dynamics and the related control-system interactions.

Hermes is structurally non-rigid as a result of its large lightweight solar array. Ground-based dynamical testing was possible to only a limited extent because the configuration is not structurally self-supporting in Earth's gravity. Design and pre-launch performance prediction is heavily reliant on mathematical modelling, computer simulation, and ground testing of developmental hardware. At the outset of the program (1970), the state-of-the-art of this technology could not provide definitive answers to the following types of questions for the Hermes class of spacecraft.

a) Of the many mathematical methods available for analyzing flexible satellites (e.g., multibody, finite element, classical continuum mechanics), which is the most suitable?

b) How accurate are the methods for determining structural frequencies and modal characteristics?

c) How does one quantify structural damping, and to what extent can it be predicted prior to launch?

d) What is the role of ground testing in determining structural dynamics properties prior to launch?

In the course of the Hermes Project, answers (or, in some cases, partial answers) to these queries evolved. This paper provides an overview of this experience and the corresponding general conclusions.

## SPACECRAFT DESCRIPTION AND INSTRUMENTATION

Earlier publications provide a comprehensive description of Hermes (Vigneron and Millar, 1976; Harrison et al, 1976; Vigneron and Millar, 1977; Franklin and Davidson, 1973; Raine, 1976; and Bassett, 1976). A brief outline of relevant areas is included here. Of the various configurations which Hermes had during the mission, of special interest in this paper is the "array fully deployed" state (Fig. 1).

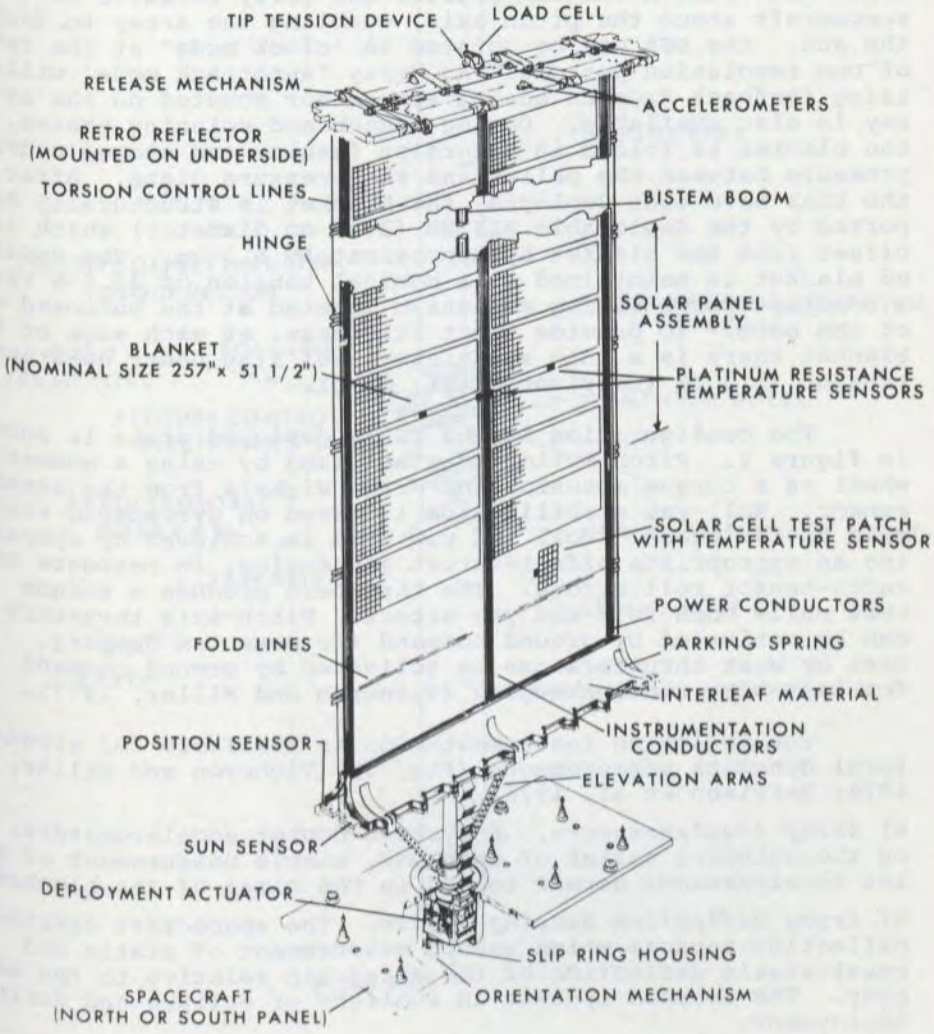


Figure 1. HERMES DEPLOYABLE SOLAR ARRAY (DSA)

The solar array consists of two fold-up deployable solar array units (DSA's), each when deployed is 7.2m long and 1.3m wide. Each DSA has a flexible blanket upon which are mounted the solar cells and wiring, a steel boom (BISTEM), a deployment actuator, an inboard pallet, an outboard pressure plate, a slip-ring assembly, and related structure. A drive-and-track mechanism rotates the array relative to the spacecraft about the pitch axis, enabling the array to face the sun. The DSA may be rotated in 'clock mode' at the rate of one revolution per day. An array 'autotrack mode' utilizing feedback from an analog sun sensor mounted on the array is also available. During launch and spinning phases, the blanket is folded in accordion fashion and stowed under pressure between the pallet and the pressure plate. After the DSAs have been deployed, the blanket is structurally supported by the deployable BISTEM (3.40 cm diameter) which is offset from the blanket by approximately 6.3 cm. The deployed blanket is maintained at a nominal tension of 35.6 N via a constant-force spring mechanism located at the outboard end of the boom. To provide twist stiffness, at each edge of the blanket there is a thin stainless-steel line under constant tension (1.3 N) (Harrison et al, 1976).

The configuration in the fully deployed state is shown in figure 2. Pitch motion is stabilized by using a momentum wheel as a torque actuator and error signals from the earth-sensor. Roll-yaw stabilization is based on gyroscopic stiffness of the wheel. Roll and yaw trim is achieved by operating an appropriate offset-thrust jet engine, in response to earth-sensor roll errors. The thrusters produce a torque that nulls both roll and yaw errors. Pitch-axis thrusters can be activated by ground command for momentum dumping. East or West thrusters can be activated by ground command for East-West stationkeeping (Vigneron and Millar, 1977).

The following instrumentation is available for structural dynamics measurements (Fig. 3) (Vigneron and Millar, 1976; Harrison et al, 1976).

a) *Array Accelerometers.* 6 Systron-Donner accelerometers, 3 on the outboard pallet of each DSA, enable measurement of pallet accelerations normal to and in the plane of the blanket.

b) *Array Deflection Sensing System.* The spacecraft carries 4 deflection sensors which enable measurement of static and quasi-static deflection of the array tip relative to the main body. The sensors operate in sunlight or eclipse and during deployment.

c) *Array Temperature Sensors.* 5 platinum-resistance thermometer temperature sensors are mounted on the blankets.

d) *Array Tension Load Cell.* A specially-designed strain-gaged beam is incorporated into each DSA at the outboard pallet, and enables measurement of DSA tension.

In addition, a number of sensors which support spacecraft operations are used as instruments for flight evaluation. These are boom-length potentiometers, potentiometers

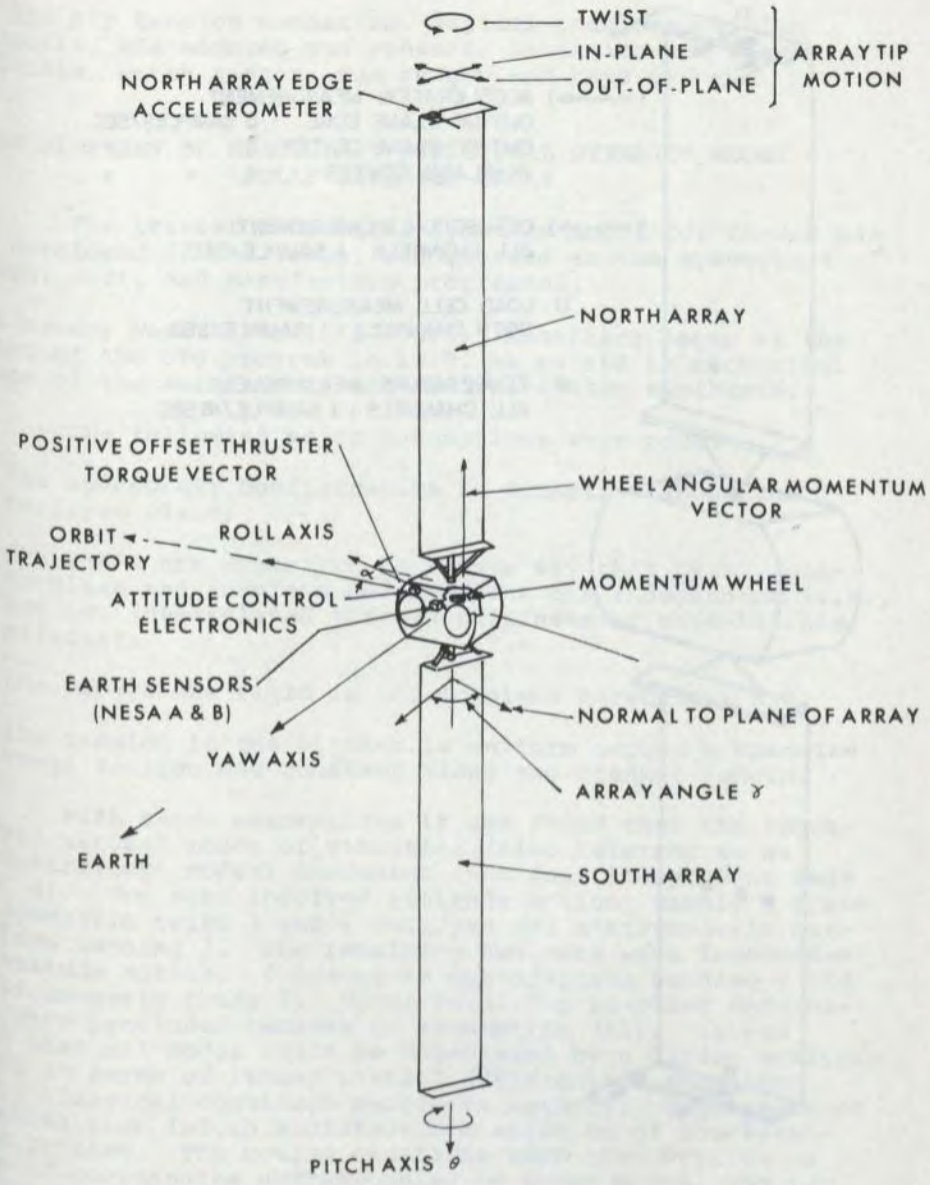


Figure 2. Hermes on-station configuration.

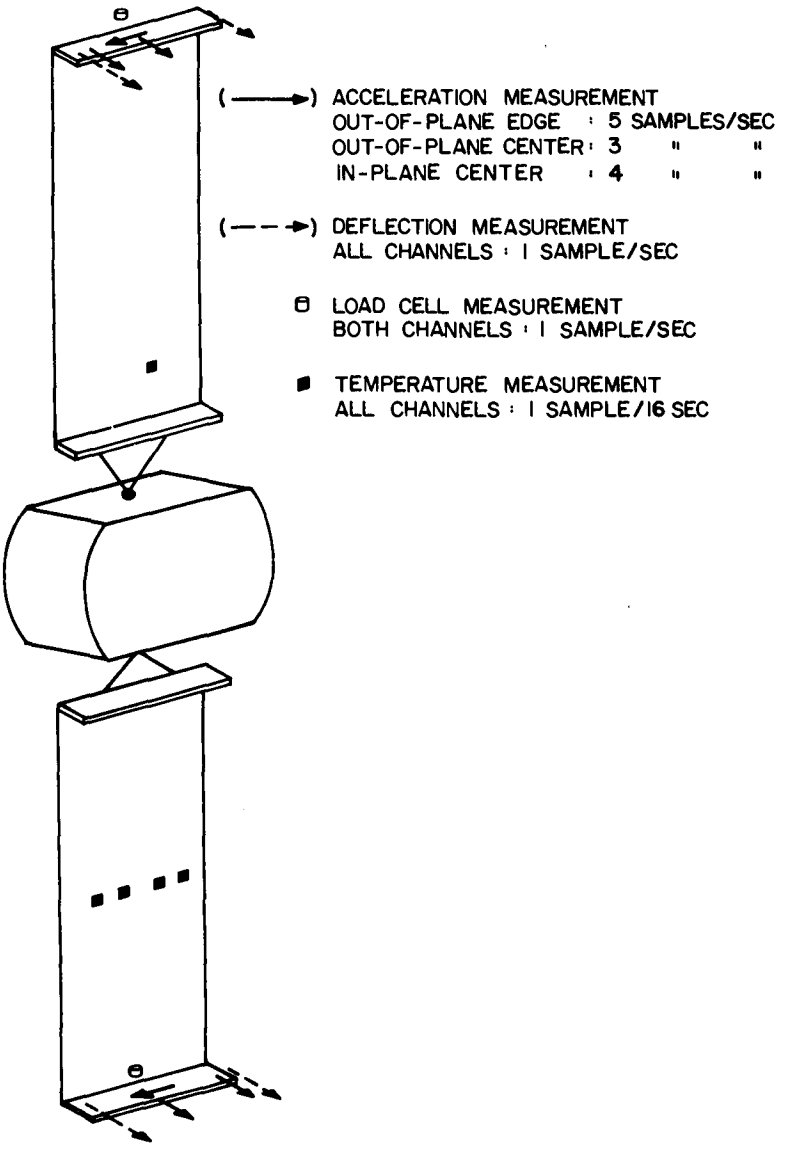


Figure 3. Schematic representation of instrumentation.

in the tip tension mechanism, digital angular-position encoders, DSA-mounted sun sensors, extension-arm micro-switches, earth sensor, sun sensor and rate gyros.

## DEVELOPMENT OF SPACECRAFT STRUCTURAL DYNAMICS MODEL - FULLY DEPLOYED ARRAY

The present structural dynamics model for Hermes was not developed in one stage, but evolved as the spacecraft design, test, and manufacture progressed.

*Preliminary Work - the 1971 Model.* Modelling began at the outset of the CTS program in 1970, as an aid to mechanical design of the solar array and control-system synthesis.

The following major assumptions were made:

A1) the spacecraft configuration is symmetric about the roll/yaw plane;

A2) the DSA's are symmetric in such a way that twist, out-of-plane and in-plane deformations are independent (i.e., are not interrelated through stiffness or mass-balance effects);

A3) the arrays are rigid in the in-plane direction; and

A4) the tension in the blanket is uniform across a spanwise cross section and constant along the blanket length.

With these assumptions it was found that the spacecrafts' natural modes of vibration (also referred to as 'unconstrained' modes) uncoupled into four independent sets (Fig. 4). Two sets involved attitude motion, namely { pitch and symmetric twist } and { roll/yaw and antisymmetric out-of-plane bending }. The remaining two sets were independent of attitude motion: { symmetric out-of-plane bending } and { antisymmetric twist }. Modes involving in-plane deformation were precluded because of assumption (A3). It was found that all modes could be formulated by a direct analytic method in terms of linear partial differential equations (i.e., classical continuum mechanics method). Separation of variables then led to a closed-form solution of the eigenvalue problem. The motion equations were then written in terms of coordinates corresponding to those modes, and expressed in the block diagram forms given in figures 5 and 6. (Hughes and Garg, 1973; Hughes, 1972; Hughes 1972). In calculating these modes, the effect of wheel angular momentum was included but the 24-hour rotation rate in synchronous orbit was disregarded. For Hermes' parameters, the influence of stored momentum on the modes was also found to be small, and could be ignored for design purposes. A conceptual approximation to the mode shapes is depicted in figure 4 (also shown are in-plane modes, to be discussed subsequently).

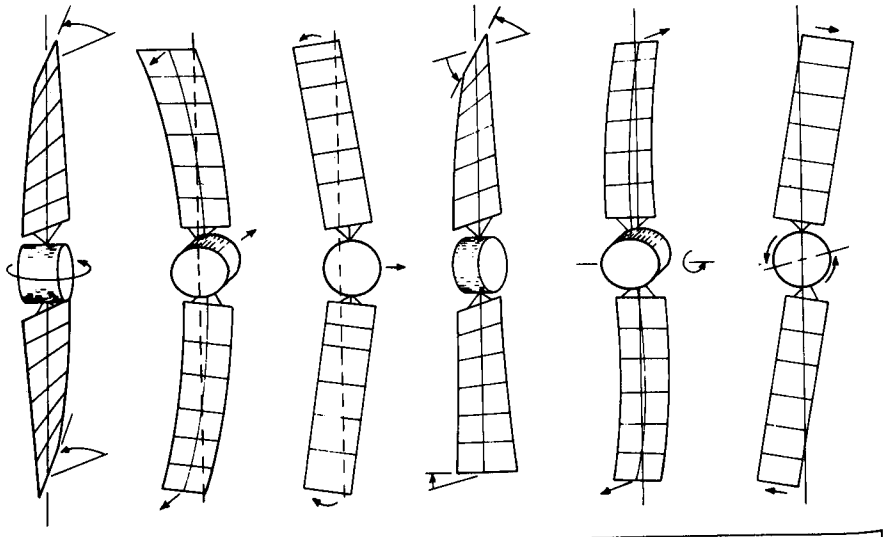

| SYMMETRIC (EVEN) (Hz) | | | ANTISYMMETRIC (ODD) (Hz) | | |
|---|---|---|---|---|---|
| PREDOMINANT TWIST | PREDOMINANT OUT-OF-PLANE | PREDOMINANT IN-PLANE | PREDOMINANT TWIST | PREDOMINANT OUT-OF-PLANE | PREDOMINANT IN-PLANE |

Figure 4. Major Natural (Unconstrained) Structural Modes of Vibration.

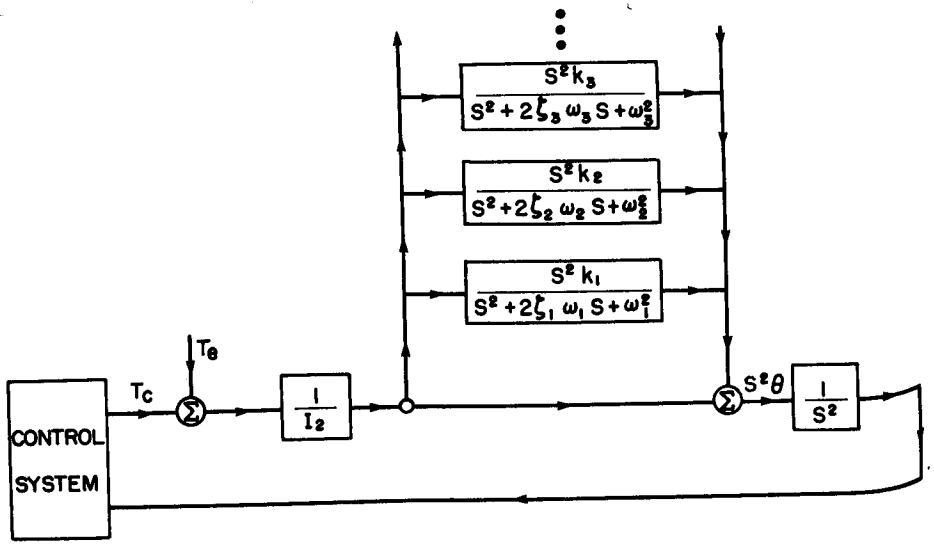


Figure 5. Flexibility Modelled Using Unconstrained Modes.

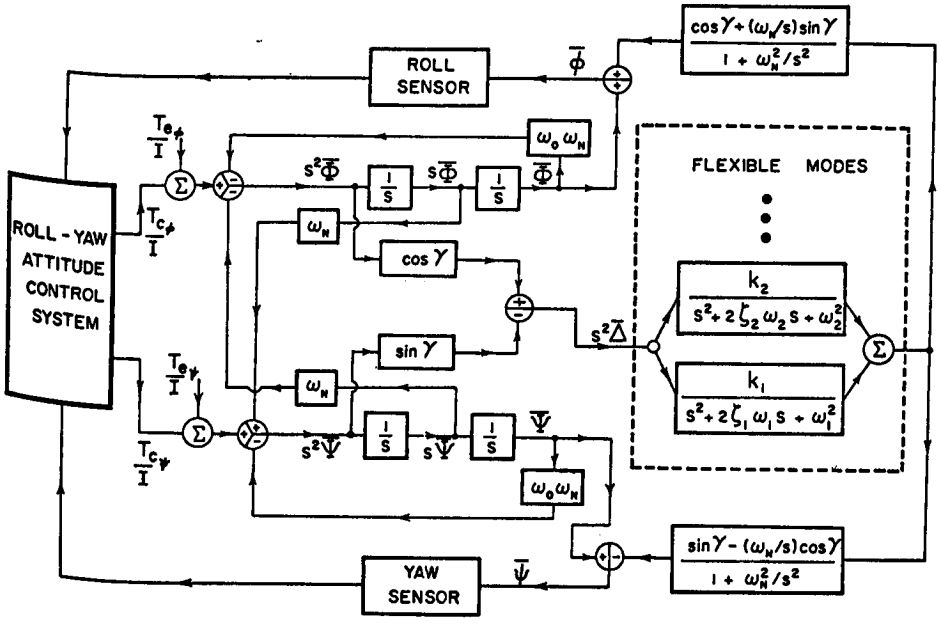


Figure 6. Incorporation of Flexibility Simulation into Roll-Yaw Control System Block Diagram (1971 model).

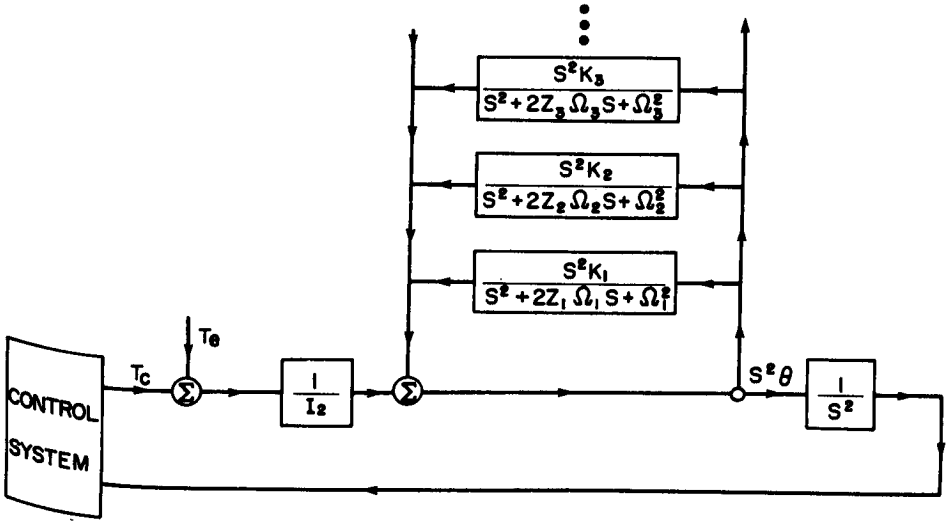


Figure 7. Flexibility Modelled Using Constrained Modes.

The assumptions were known to be idealizations, and were made in part with a view to generating an easily tractable mathematical model. The design of the solar array was in a state of evolution, and modelling which would have led to greater analytical complexity was not justifiable at that time.

The modal frequencies and gains calculated in 1972 based on the above model are given in Table I. (The modal gain is basically a measure of the mass associated with a mode, i.e. the larger the gain, the larger the amount of mass which participates in the modal vibration.) The array at that stage consisted of a detailed definition in terms of engineering drawings and partial existing hardware, and was continually subject to changes of detail. Reliable information on damping factors was not available. Factors of 0.001 were chosen, because it was felt that the structure would be highly underdamped and 0.001 was regarded as a conservative value from a control systems viewpoint.

At the same time, characteristics for symmetric modes were calculated by the Ontario Research Foundation, using the finite element method and the above four assumptions. (Yao, 1971). Results were in general agreement with Table I, and confirmed methods and software. Later, attitude-related modes were also verified at the University of Toronto Institute for Aerospace Studies (UTIAS) by the finite element method (Nguyen and Hughes, 1976).

The unconstrained modes model of figures 5 and 6 formed the basis for several large and detailed digital simulations used in the design and qualification of the attitude control system; SPARCON (Lang et al, 1974) and its derivatives (CRCCON, a DOC-developed program, and GARCON, a UTIAS-developed program).

The dynamics equations were also expressed in terms of 'cantilever' modes ('constrained' or 'hybrid' modes), and with these modes the block diagram for pitch takes the form shown in figure 7 (Hughes and Garg, 1973). It is significant to note that the unconstrained (vehicle) modes lead to a block diagram which is 'feed forward', whereas the constrained (cantilever) modes lead to a 'feed back' type. The forms of figures 5 and 7 are mathematically equivalent; (Hughes, 1974) however they differ significantly in their utility. Discussion of this aspect will follow in a later section.

Analytical studies during 1970-73 explored assumptions (A2), (A3), and other minor effects (e.g., freeplay, BISTEM root stiffness) (Hughes, 1970; Cherchas, 1973), none of which resulted in changes to the main model of Hughes and Garg, 1973 and SPARCON.

*Finite Element Analysis.* During 1973-75, the finite-element method was used by SPAR, ESA and CRC, primarily to determine stresses in the array blanket and solar cells.

*TABLE I*

*STRUCTURAL DYNAMICS PARAMETERS DURING HERMES PROGRAM*

| DESCRIPTION | | 1971 ESTIMATE (before manufacture/ground test) | | | 1975 ESTIMATE (after manufacture/ground test) | | | HERMES FLIGHT DATA | | |
|---|---|---|---|---|---|---|---|---|---|---|
| | | | $k_n$ | $\zeta_n$ | $\omega_n$ (Hz) | $k_n$ | $\zeta_n$ | $\omega_n$ (Hz) | $k_n$ | $\zeta_n$ |
| Sym. | Out-of-Plane First | 0.15 | N/A | 0.001 | 0.16 | N/A | 0.003-0.006 | 0.15 | N/A | 0.020-0.030 |
| Sym. | In-Plane First | ∞ | - | - | 0.34 | N/A | 0.014-0.02 | 0.31 | N/A | 0.02-0.03 |
| Sym. | Twist First | 0.13 | 0.025 | 0.001 | 0.17 | 0.031 | 0.09-0.16 | 0.20 | ** | 0.06-0.08 |
| | Second | 0.41 | 0.003 | 0.001 | 0.50 | 0.003 | 0.01-0.02 | 0.49 | | |
| Anti-Sym. | Out-of-Plane First | 0.40 | 0.63 | 0.001 | 0.38 | 7.69 | 0.005-0.009 | 0.45 | ** | 0.02-0.04 |
| | Second | 0.46 | 6.04 | 0.001 | 0.50 | 0.40 | No estimate | 0.50 | ** | 0.007(?) |
| Anti-Sym. | In-Plane First | ∞ | - | - | .75 | 7.45 | No estimate | 0.91 | ** | 0.016 |

NOTES: (1) Flight Values of damping are amplitude dependent
(2) ** - not yet evaluated

## LIST OF MAJOR SYMBOLS

| | | |
|---|---|---|
| $\omega_n$, $k_n$, $\zeta_n$ | - | frequency, gain, and damping, respectively, for the n'th mode of the unconstrained (natural) modes model |
| $\Omega_n$, $K_n$, $Z_n$ | - | frequency, gain, and damping, respectively, for the n'th mode of the constrained modes model |
| $S$ | - | Laplace transform parameter |
| $\Theta$ | - | pitch angle of spacecraft |
| $\phi$, $\Psi$ | - | roll and yaw angle of spacecraft |
| $\gamma$ | - | array angle (see Fig. 2). |

SPAR, using computer programs STARDYN (Gossain, 1973), and ESA (Fournier-Sicre, 1973) calculated the static-stress distribution and found that it was not uniform chordwise or constant spanwise in contradiction to assumption A4. Dynamic analysis was not done because it was beyond the capability of STARDYN and ESA's software. However, it was recognized that non-uniform tension could have a major effect on twist modes (Gossain, 1973).

At the Communications Research Centre (CRC), both the statics and the dynamics of the array were analyzed using NASTRAN (Vigneron et al, 1976). The non-uniform static-stress distribution and its effect on natural frequency in twist were demonstrated. It was found that NASTRAN provided a very large volume of detailed information and that it required a corresponding great deal of computer time and analyst effort. The work was terminated at a relatively incomplete stage because the computer costs were not justifiable when compared with other methods.

*Ground Testing*. Tests on developmental model hardware in an ambient vacuum (Harrison, 1975; Sincarsin, 1976) and on flight-spare hardware in thermal vacuum (Harrison et al, 1975) were made in 1974 and 1975. In parallel, dynamical models were extended to include gravity (Vigneron, 1975; Sincarsin, 1977; Sincarsin and Hughes, 1977). The test program showed the following:

a) With regard to the four assumptions:

   i) cross coupling between excitation and motion occurred to some extent for all vibration modes. Modal frequencies calculated using A2 were reasonable approximations, but mode shapes were influenced to a significant extent;

   ii) the array had a significant in-plane flexibility, to an extent which necessitated modification of assumption A3;

   iii) a variation in twist frequency was observed with differing sets of hardware, an effect which was felt to be related to non-uniform tension distribution in the blanket (assumption A4); and

   iv) classes of modes (i.e., blanket modes) were observed which were completely precluded by assumption A4;

b) Dynamics effects were observed which were beyond the scope of the modelling, and were believed to be due to superharmonic excitation phenomena (it has also been suggested that they might have been caused by distortions in the harmonic excitation);

c) Damping values based on measurement were obtained. They

were amplitude dependent, and also dependent on hardware (development model or qualification unit). Damping for major modes was insensitive to temperature.

Effects a)(iv) and b) were considered of minor importance since they were localized, and the amount of energy associated with them was relatively small. Effect a)(iv) was demonstrated to be associated with blanket-tension variations by finite-element method analysis (Vigneron et al, 1976).

The effect of blanket-tension variations on twist frequency (effect a(iii)) was demonstrated to be potentially important by finite-element modelling and by extension to the classical continuum-mechanics modelling (Vigneron et al, 1976). Later in static tests of the flight-spare hardware (Plewes, 1975), it was noted that the physical connection between the blanket and pressure plate did not correspond fully with the modelling of the finite element, and that the finite-element-predicted variations in tension distribution (variation from constant tension) were likely somewhat exaggerated. This work led to the belief that the constant-tension distribution (assumption A4) was probably reasonable for calculation of twist frequency. Dynamics tests of the flight-spare hardware supported this view.

The stiffness and mass properties were tailored to include the major mechanisms of a)(i-iii) (in addition to the basics of Hughes and Garg, 1973), and modelling then emulated the data well (Vigneron, 1975; Sincarsin and Hughes, 1977).

1975 Revision to Spacecraft Dynamics Model In 1975, the dynamic equations of Hughes and Garg, 1973; Hughes, 1972a,b, were revised to reflect major discrepancies found in ground testing (in-plane flexibility and mass imbalances), the revised spacecraft mass properties, and the nonrigidity of the DSA at the BISTEM root (Hughes, 1975). The spacecraft modes and frequencies were calculated and a sensitivity study performed (Hughes and Sincarsin, 1975). Projected values for on-orbit operation are given in Table I.

It was also desired to extrapolate the damping data to the on-orbit situation. This proved to be a task well beyond standard engineering practice; however, (unproven) methods were devised (Hughes, 1975; Vigneron, 1975 and 1977) and projected values were as given in Table I.

*Flight Measurements.* Hermes was launched in January 1976, and during the first year some modal data became known from analysis of incidental structural excitation that accompanied normal operations (Harrison et al, 1976; Vigneron, 1977). These operations included deployment, momentum dumping, East-West stationkeeping, and array slewing. To fill in certain missing data (modal gains, for example), and to make the modal parameters already available more precise, a 'special

excitation' experiment was designed and carried out (Garg, 1976; Garg et al, in press). The values obtained from flight data are shown in Table I.

*Discussion.* Table I shows the progression of modal estimates made over the course of the program and illustrates the degree of accuracy at various stages.

Modes and frequencies adopted at the outset of the program (on the basis of detailed 'paper' design and partial existing hardware) bear some resemblance to flight values, but there are significant differences. These differences are due to design changes subsequent to 1972, and inaccurate assumptions or estimates of stiffness and mass properties. Damping estimates made in 1972 were guesses, and proved to be an order of magnitude too low.

Comparison of the flight values with the 1975 estimates shows that the test program served to enable good modal identification. The differences in frequencies between flight values are due to:

a) parameter differences between the 1975 configuration and the configuration actually launched (late in the program extra fuel and balance weights were added and minor hardware substitutions were made);

b) unavoidable parameter errors (e.g., the elevation arm stiffness is difficult to measure and is conceivably in error by ±30%);

c) errors or oversimplifications associated with the mathematical modelling.

By post-launch recalculation using an adjusted set of parameters, one can virtually match software results and flight data, and this indicates that factors (a) and (b) are the major sources of the discrepancies.

Damping factors estimated from values of ground tests are within one order of magnitude of the flight values. Although this is in accord with current state-of-the-art, clearly there is a need for further improvement in this area.

## STRUCTURAL FLEXIBILITY AND CONTROL SYSTEM DESIGN

*Design Philosophy in 1971.* In 1971 it became apparent that the spacecraft structural resonant frequencies would be outside the desired control-system bandwidth by a factor of five or greater (Hughes and Garg, 1973; Hughes, 1972a,b). Further, it seemed feasible to avoid exciting the spacecraft at its resonant frequencies during momentum dumping, E-W station-keeping array autotrack operation, etc.. Consequently the control-system design approach adopted was to assume that the spacecraft was rigid for purposes of synthesis and initial design, and then to verify and finalize the design with flexibility included via detailed simulation results from SPARCON

(Lang et al, 1974). On this basis a proportional-integral-derivative controller was evolved for pitch control, and a dual-time-constant pseudorate controller was evolved for yaw control (Lang et al, 1974).

*Pitch Instability.* In 1973 it was discovered by SPARCON simulation that the pitch-control loop exhibited a structural-dynamics-related instability. It was shown that a linearized model of the loop was unstable for low damping ($\zeta < 0.004$) and for certain values of loop time delay (associated with sampling periods in the controller) when structural flexibility was included in the model; however, it was stable when only rigid body dynamics was considered (Trudel et al, 1974). The mechanism was clarified in an analysis wherein the dynamics was represented in 'feed forward' form, and mode-separability principles combined with Routhian and root-locus techniques were utilized (Millar and Vigneron, 1975). The addition of a passive damper was considered for solution to the problem (Hughes, 1974). The problem was averted by adjusting parameters (gains) in the controller electronics. The influence of time delays was investigated subsequently, using sampled data theory (Garg, 1977).

*Roll-Yaw Instability.* In 1974 it was found by computer simulation with GARCON and CRCCON (derivatives of SPARCON, Lang et al, 1974 that the roll/yaw control loop exhibited a structural-dynamics-related instability for certain control-electronics configurations. Ultimately, analysis showed that the pseudorate controller could interact with structural flexibility to produce instability for large-angle capture conditions, if certain combinations of loop time delay and low modal damping ($\zeta < 0.004$) were assumed. An analysis which demonstrated the mechanisms with clarity utilized the feed-forward form of the dynamics model, and the describing-function technique for linearization of the non-linear pseudorate controller (Millar and Vigneron, 1976; Millar and Vigneron, 1977).

Prior to launch, it was concluded that the probability of instability was about 5% and that workable non-standard flight procedures were available for such an event. On this basis no changes were made to the spacecraft.

*Flight Performance.* Hermes has performed with no detectable structural dynamics/control system interaction (Vigneron and Millar, 1977).

A lack of significant interaction was expected, since the structural frequencies are outside the control system bandwidth. The damping factors experienced in flight are somewhat higher than the ground-based forecasts (Table I) and this has also contributed significantly to the lessening of interactions.

Solar array autotrack operation, momentum dumping and E-W stationkeeping excite the structural modes to an extent easily measurable by the array accelerometers and other in-

struments, (Harrison et al, 1976; Vigneron and Millar, 1977) but there is no measurable interaction with the control system.

*Discussion.* The policy of assuming the spacecraft rigid for synthesis and initial design led to a successful controller design for Hermes. During the project this method provided an engineering solution to an otherwise very complex problem, and allowed control-system design to progress on schedule. However, it has also been learned that stability problems can arise even though the controller bandwidth is significantly below the structural resonant frequencies, if such structural frequencies are detectable by the sensors in the control loop (as per pitch and roll/yaw controller instabilities).

$\Omega_n$, $K_n$, $Z_n$ As regards to "feedforward, $\omega_n$, $k_n$, $\zeta_n$" and "feedback, $\Omega_n$, $K_n$, $Z_n$" (Figs. 5-7) ways of configuring the dynamics equations, it was not clear which way was preferable at the outset of the program.

The following points are noted:

a) The feedforward version is well adapted to enabling a physical understanding of the control-loop behaviour. Control-system performance correlates directly with $\omega_n$, $k_n$ and $\zeta_n$, whereas there is no correlation (as a rule) with $\Omega_n$, $K_n$ and $Z_n$.

b) The feedforward version lends itself directly to mode separation and/or describing function techniques, and thus leads to approximate functional relationships which describe system performance.

c) In the feedback form the equations are not conveniently integrated in closed form, and would normally be integrated by Runge-Kutta or other numerical methods. For the feedforward form a closed-form solution is readily available, and this is usually preferable to numerical integration since it is more accurate and computationally efficient.

d) Derivation of the feedback version is more direct, since it depends on the appendage alone. An additional computer code is then required to convert from $\{\Omega_n, K_n\}$ to $\{\omega_n, k_n\}$. However, this conversion is not especially difficult and need only be made once for a specific configuration.

e) Results of ground-testing do not correspond directly to the in-space values of either $\{\Omega_n, K_n\}$ or $\{\omega_n, k_n\}$ if the structure is sufficiently flexible to be affected by Earth's gravity. Ground-testing of the whole spacecraft (not done with Hermes) would give values of $\omega_n$ and $k_n$ as modified by gravity. Ground-testing of an appendage (as done with Hermes) gives values of $\Omega_n$ and

$K_n$ as modified by gravity. In either case, a dynamical model is clearly required to extrapolate from one-g to zero-g.

f) As the number of modes considered increases, the difference between the feedforward and feedback results becomes negligible. However, the spacecraft responses of interest (i.e., large responses) can be studied with fewer feedforward loops.

All things considered, there is a definite preference for the 'feedforward' representation for the Hermes class of spacecraft.

## GENERAL CONCLUSIONS AND REMARKS

With regard to Hermes, the calculation of frequencies and gains was clearly well in hand prior to launch. Ground testing played a key role. The prediction of damping factors using current techniques was less satisfactory, and final damping factors in flight are higher than expected. If damping could have been predicted accurately in 1974, a substantial amount of simulation, analysis, project review, and pitch controller changes probably would have been averted.

With regard to future spacecraft of this generic class, the following general conclusions appear evident:

a) For appendages like the Hermes solar array that are relatively simple geometrically, a 'continuum mechanics' analysis (Hughes and Garg, 1973; Hughes, 1975) is adequate. Due to its simplicity and cost effectiveness, it is the preferred approach to calculating modal frequencies and gains, at least for spacecraft of this class.

b) The finite element method is well suited for analysis of static stress of the solar array (Gossain, 1973; Fournier-Sicre, 1973).

c) The major discrepancies between flight results and results calculated at a time prior to launch are due to:

(i) model being based on incomplete or inaccurate definition of hardware;

(ii) errors in masses and stiffness due to limitations of component-measurement techniques;

(iii) inevitable changes to parameters as spacecraft design and manufacture progresses. Ground testing of the array subsystem substantially minimizes these errors. Pre-flight calculation can predict fundamental frequencies and gains to within 10% of flight values without major testing, if the structure is sufficiently simple or perhaps if it has been previously flown and thus well characterized. However, if accuracy of greater than 10-15% is critical to controller performance, a ground-testing program is recommended.

d) There are no reliable theoretical methods for making sufficiently accurate predictions of structural damping; moreover, it is difficult to make accurate extrapolations from ground tests. The only engineering solutions appear to be either to design controllers that are stable with effectively zero structural damping (Millar and Vigneron, 1975), or to add a passive damping device to the appendage to provide a known amount of damping (Hughes, 1974).

e) Successful techniques for the analysis and design of proportional-integral-derivative and pseudorate controllers include mode separation and describing-function techniques.

Thus the technology base (i.e., proven theory, techniques, design guidelines, and software) appears to be in place to permit the reliable synthesis and design of controllers for spacecraft similar to Hermes. Indeed, the experience described here will enable controllers to be designed with confidence for spacecraft whose pointing requirements and structural flexibility are significantly more demanding than Hermes.

## REFERENCES


Bassett, D.A.
1976 Ground Controlled Conversion of Communications Technology Satellite (CTS) from Spinning to Three-Axis Stabilized State, *AIAA* Paper No. 76-1928, *AIAA Guidance and Control Conference*, 16-18 Aug.

Cherchas, D.B.
1973 Coupled Bending-Twisting Vibrations of a Single Boom Flexible Solar Array and Spacecraft, *CASI Transactions*, Vol. 6, No. 1, March.

Fournier-Sicre, A.
1973 CTS Blanket Tension Distribution Analysis, *ESTEC Memorandum, TSS/APFS/483*, July.

Franklin, C.A. and Davidson, E.H.
1973 A High Power Communications Technology Satellite for the 12 and 14 GHz Bands, *AIAA Progress in Aeronautics and Astronautics*.

Garg, S.C.
1976 Near Resonant Vibration Tests of an Orbiting Flexible Spacecraft: Theory, Design and Simulation, *UTIAS Report* No. 204, Nov.
1977 Stability Analysis of a Flexible Satellite with a Sampled-Data Attitude Sensor, *Symposium on Dynamics and Control of Large Flexible Spacecraft*, 13-15 June, Blacksburg, Virginia, U.S.A.

Garg, S.C., Hughes, P.C.; Millar, R.A. and Vigneron, F.R.
Flight Results on Structural Dynamics from Hermes, in press.

Gossain, D.
1973 Tension Distribution in DSA Blanket and the Effect of Non-Uniform Tension Distribution on Twisting Frequency of the Array, *SPAR TM* 985.

Harrison, T.D.
1975 Communications Technology Satellite Deployed Solar Array Dynamics Tests, *CRC Report* No. 1264, *Department of Communications*, Jan.

Harrison, T.D., Buckingham, R. and Vigneron, F.R.
1975 Functional and Dynamics Testing of the Flexible Solar Array for the Communications Technology Satellite, Paper No. 24, in *NASA SP-379*, Nov.

Harrison, T.D., Lang, G.B., Gore, J.V., Vigneron, F.R. and Quittner, E.
1976 In Orbit Characteristics of the Communications Technology Satellite Deployable Solar Array, *Eleventh Intersociety Engineering Conference*, Las Vegas, U.S.A., 12-17 Sept.

Hughes, P.C.
1970 Flexible Motions of the CTS Solar Array in the Plane of the Array, *Aercol Report* No. 70-41-2, Dec.
1972a Flexibility Considerations for Pitch Attitude Control of the Communications Technology Satellite, *CASI Transactions*, Vol. 5, No. 1.
1972b Attitude Dynamics of a Three-Axis Stabilized Satellite with a Large Flexible Solar Array, *Journal of Ast. Sci.*, Vol. 20, No. 3, pp. 166-189.
1974a Dynamics of Flexible Vehicles with Active Attitude Control, *Celestial Mechanics*, Vol. 9, pp. 21-39.
1974b Analysis of Two Passive Dampers for Reducing Controller/Flexibility Interaction on CTS, *AIAA* Paper No. 74-1268, *CASI/AIAA Joint Meeting*, Toronto, Canada, Oct.
1975 A Model for the Attitude Dynamics of CTS with Reference to Attitude Control System Design, *Aerospace Engineering and Consultants Ltd*, *AERCOL Report* No. 75-14-4, March.

Hughes, P.C. and Garg, S.C.
1973 Dynamics of Large Flexible Solar Arrays and Application to Spacecraft Attitude Control System Design, University of Toronto, *UTIAS Report* No. 179, Feb.

Hughes, P.C. and Sincarsin, G.
1975 Numerical Results of the Updated Dynamics Model for the Flexible CTS Spacecraft, *Aerospace Engineering and Research Consultants, Ltd*, *AERCOL Report* No. 75-14-5, March.

Lang, G.B., Trudel, C.P.R. and Staley, D.A.
1974 Program SPARCON, Description and Operating Procedure, *SPAR - ST.118, SPAR Aerospace Products Ltd,* Toronto, Canada, (July 1973), Issue A, Oct. 1974, Ammendment 1, March.

Millar, R.A. and Vigneron, F.R.
1975 The Effect of Structural Flexibility on the Stability of Pitch for the Communications Technology Satellite, *Proc. 1975, Conference on Automatic Control,* University of British Columbia, Canada, 23-24 June.
1976 Attitude Stability of Flexible Spacecraft Which Use Dual Time Constant Feedback Lag Network Pseudorate Control, *AIAA* Paper No. 76-266, *AIAA/CASI 6th Communications Satellite Systems Conference,* Montreal, Canada, 5-8 April.
1977 Attitude Stability and Structural Flexibility in Roll Yaw for the Communications Technology Satellite, *Symposium on Dynamics and Control of Large Flexible Spacecraft, AIAA Guidance and Control Technical Committee,* Blacksburg, Virginia, U.S.A., 13-15 June.

Nguyen, P.K. and Hughes, P.C.
1976 Finite Element Analysis of CTS-Like Flexible Spacecraft, *UTIAS Report* No. 205, University of Toronto, Institute for Aerospace Studies, June.

Plewes, J.
1975 CTS Solar Blanket Tension Distribution Tests, *Internal Report, Communications Research Centre,* Aug.

Raine, H.R.
1976 The Communications Technology Satellite Flight Performance, *International Astronautical Federation* Paper No. 76-223, *27th Congress,* Anaheim, 10-16 Oct.

Sincarsin, G.B.
1976 Dynamics Tests of the Communications Technology Satellite Developmental Model Solar Array, *UTIAS Technical Note* No. 200, April.
1977 Dynamical Model for the CTS Developmental Model Solar Array Under the Influence of Gravity, *UTIAS Technical Note* No. 206, May.

Sincarsin, G.B. and Hughes, P.C.
1977 Dynamic Ground Testing of the CTS Development Model Solar Array: Theory and Experiment, *Symposium on Dynamics and Control of Large Flexible Spacecraft,* 13-15 June.

Trudel, C.P., Staley, D and Ruta, R.
1974 Pitch Loop Stability Investigation, *SPAR R-624, SPAR Aerospace Products Ltd,* July.

Vigneron, F.R.
1975a A Structural Dynamics Model for Flexible Solar Arrays of the CTS Class, *CRC Report* No. 1268, Department of Communications, Ottawa, Canada, March.
1975b Extrapolation of Structural Damping Coefficients Measured in Ground Test (Due-G) Environment to the On-Orbit (Zero- ) Environment, *Internal Publication*, April 1975, on File CRC 6666-15-2, 6 May.
1977 Ground-Test Derived and Flight Values of Damping for a Flexible Spacecraft, *Symposium on Dynamics and Control of Non-Rigid Spacecraft*, European Space Agency, ESA SP-117, May, pp. 325-333.

Vigneron, F.R. and Millar, R.A.
1976 Plan for Flight Evaluation of Attitude Stabilization and Flexible Solar Array Dynamics for the Communications Technology Satellite, *Proceedings of the 26th International Astronautical Congress*, Edited by L.G. Napolitano, Pergamon Press-Oxford and New York, pp. 91-111.
1977 Flight Performance of the Three-Axis Stabilization System of the Communications Technology Satellite, *AIAA* Paper No. 77-1059, *AIAA Guidance and Control Conference*, 8-10 Aug.

Vigneron, F.R., Parthasarathy, A. and Harrison, T.D.
1976 Analysis of the Structural Dynamics of a Flexible Solar Array and Correlation with Ground Testing, *AIAA* Paper No. 76-242, *AIAA/CASI 6th Communications Satellite Systems Conference*, 5-8 April.

Yao, C.C.
1971 Interim Results of CTS Solar Array and Boom Normal Mode and Frequency Analysis, *Eng. R -71-39, Ontario Research Foundation*, April. Also *Eng. R-71-2* and *Eng. R-71-38*.

# RAIN ATTENUATION AND COMMUNICATIONS LINK CHARACTERIZATION WITH HERMES

L.J. Ippolito

NASA/Goddard Space Flight Center

Greenbelt, Maryland, U.S.A.

*Le Centre des vols spatiaux Goddard (GSFC) de la National Aeronautics and Space Administration (NASA) effectue actuellement une expérience avec Hermès, le Satellite technologique de télécommunications (STT), en vue de mesurer et de caractériser d'importants phénomènes de propagation radioélectrique pour les liaisons terre-espace dans les bandes des 12/14 GHz. Cette expérience comprend l'évaluation d'un bon nombre de paramètres intéressants, notamment l'atténuation des signaux, l'évanouissement et la scintillation causés par la pluie, les effets de dépolarisation, l'angle d'arrivée des ondes et la transmission de caractérisation des liaisons par vidéo.*

*La majeure partie des données sur la propagation sont obtenues à l'aide du radiophare d'Hermès fonctionnant sur 11,7 GHz ainsi que des stations au sol situées à Greenbelt, Maryland; Rosman, Caroline du Nord; Blacksburg, Virginie; Columbus, Ohio et Austin, Texas. Les données sur les liaisons vidéo proviennent des stations émettrices-réceptrices de la NASA situées à Greenbelt et Rosman, qui peuvent fonctionner en duplex complet dans l'une ou l'autre des bandes du répondeur d'Hermès.*

*On donne également des statistiques sur l'atténuation causée par la pluie, établies à Greenbelt (GSFC) et Rosman pour les pires mois de 1976 et 1977 et pour la période de juin 1976 à mai 1977. Les rapports entre l'intensité des pluies mesurée et l'atténuation des signaux sont évalués et comparés avec des modèles théoriques.*

*Les stations de Blacksburg et de Austin ont observé et analysé l'effet de la pluie et des cristaux de glace sur la dépolarisation du radiophare polarisé en cercle de Hermès. Les données de l'angle d'arrivée et de la scintillation obtenues à Columbus sont les premières captées d'un satellite en orbite. Ces données ont mené à la création d'un modèle de la dégradation de l'amplification d'antenne qui permet de voir le nombre et l'angle d'élévation des scintillations dans la ligne terre-espace.*

*Pour conclure, l'auteur évalue l'impact des données sur la propagation et les caractéristiques des liaisons sur le dessin du modèle et la performance des systèmes spatiaux de télécommunication en 12/14 GHz, présents et futurs.*

## 1. Introduction

In the design of space communications systems at millimeter wavelengths, consideration must be given to the effects of the earth's atmosphere on the space propagation path. At frequencies above 10 GHz, absorption and scattering caused by rain, hail, or wet snow can cause large reductions in signal level (attenuation) which reduce the reliability of the communications link. Other effects caused by precipitation include: depolarization, amplitude, and phase scintillations, and bandwidth decoherence. All of these factors can have a degrading effect on space communications systems. Very little experimental data presently exists on the effects of rain on earth-satellite signals in the 12 and 14 GHz bands. Previous measurements at 15.3, 20, and 30 GHz using the Applications Technology Satellites (ATS) showed that extrapolation from one frequency to another or from one location to another in the determination of rain attenuation effects can lead to misleading and often incorrect conclusions (Ippolito, 1971 and 1975).

The Goddard Space Flight Center (GSFC) of the National Aeronautics and Space Administration (NASA) is performing an experiment with Hermes (The Communications Technology Satellite, CTS) designed to measure and characterize the radio propagation phenomena important to earth/space applications in the 12/14 GHz frequency bands. This Communications Link Characterization Experiment (CLCE) includes evaluation of many parameters of interest, including signal attenuation, fading and scintillation caused by rain, depolarization effects, angle of arrival, and video link characterization.

The major propagation data are developed from measurements with the CTS 11.7 GHz beacon with ground terminals located at Greenbelt, Maryland; Rosman, North Carolina; Blacksburg, Virginia; Columbus, Ohio; and Austin, Texas. Video link data are obtained from NASA receive-transmit terminals at Greenbelt and Rosman, which can operate full duplex through either of the Hermes transponder bands. Figure 1 shows the overall elements of the CLCE, including the ground terminals and central data processing locations.

The major characteristics of the CLCE ground terminals and the primary measurements accomplished at each site are listed in Table I. Detailed descriptions of the data re-

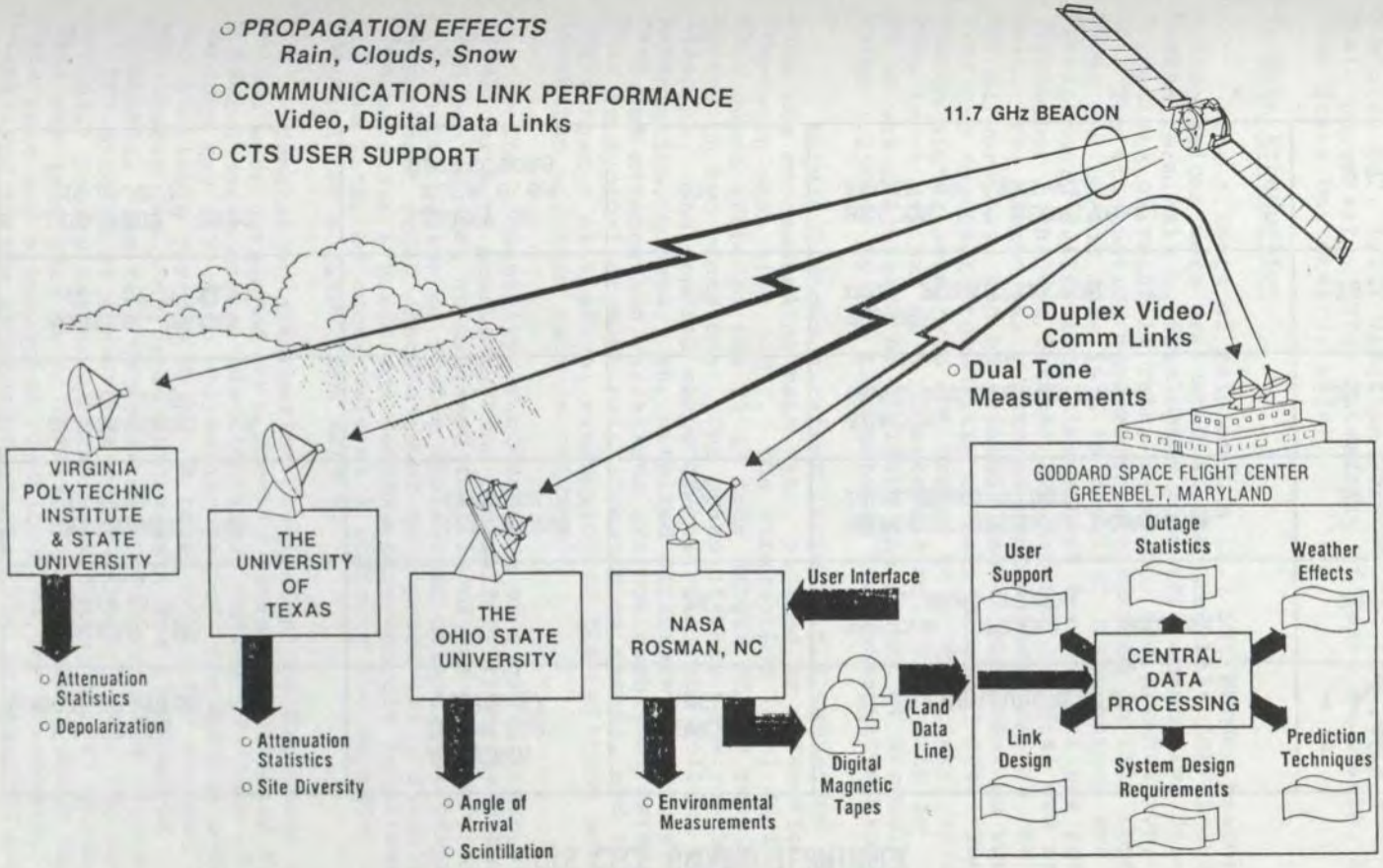


Figure 1. Principal Elements of the CTS Communications Link Characterization Experiment (CLCE).

TABLE I

## CTS CLCE GROUND TERMINALS

| LOCATION (ORGANIZATION) | ANTENNA DIAMETER (METERS) | ELEVATION ANGLE | MEASUREMENTS | $\frac{G}{T}\left(\frac{dB}{°K}\right)$ |
|---|---|---|---|---|
| 1. ROSMAN, NC (GSFC) | 4.6 | 36° | BEACON, UPLINK, DOWNLINK, DUAL BAND VIDEO | 26 |
| 2. GREENBELT, MD (GSFC) | 4.6 (RECEIVE)<br>3 (TRANSMIT) | 29° | BEACON, UPLINK, DOWNLINK, DUAL BAND VIDEO | 26.5 |
| 3. BLACKSBURG, VA (VPI & SU) | 3.7 | 33° | BEACON, DUAL POLARIZATION | 21.2 |
| 4. AUSTIN, TEXAS (U. OF TEXAS) | 3 | 49° | BEACON, DUAL POLARIZATION | 18.2 |
| 5. COLUMBUS, OHIO (O.S.U.) | ARRAY OF FOUR 0.6M REFLECTORS | 33° | BEACON, (4 RECEIVERS) ANGLE OF ARRIVAL | 8.3 |

duction and analysis procedures, and the ground terminal configurations used are presented elsewhere (Westinghouse Electric Co., 1975; Virginia Polytechnic Institute and State University, 1976; University of Texas at Austin, 1977; Ohio State University, 1976).

2. Rain Attenuation

The effects of rain on the 11.7 GHz Hermes beacon transmissions were evaluated at the Greenbelt (GSFC) and Rosman terminals by developing long-term cumulative distributions of rainfall rate, in mm/hr, and attenuation, in dB. The attenuation measurements discussed in this report cover the period June 1976 to May 1977. The beacon was on continuously during this time except for one eclipse period (September 1 through October 16), where no signal was available. The beacon was monitored continuously during the normal work day, and on weekends and in the evenings whenever the forecast probability of rain exceeded 40%. The beacon signal level was calibrated to a "clear sky" reference level defined as 0 dB attenuation. Rain rate in mm/hr was calculated by dividing the amount of accumulated water (.250mm) by the time between two consecutive tips.

Figure 2 shows a rather large rain attenuation event, with the corresponding rain rate, plotted as a function of Greenwich mean time (GMT). The attenuation level during this event exceeded the 31 dB fade margin of the receiver system on two occasions. The peaks of rain rate reached 183mm/hr. The general shape of the rain rate follows the attenuation, however, the detailed structure of the rain rate and attenuation variations are noticeably different. This is typical of most rain attenuation events, and suggests that a statistical evaluation of the relation between attenuation and rain rate is required.

The probability of occurrence of a given attenuation level, or more precisely, the probability that the attenuation has equaled or exceeded that level, is extremely useful in the design of system where rain attenuation plays a significant role. Knowledge of this probability distribution provides a basis for setting power-margin requirements for the link, or conversely will indicate the expected outage time for a given link margin.

Cumulative attenuation statistics for Greenbelt and Rosman were developed on a monthly basis, and totaled for a twelve month annual distribution. During the June 1976 through May 1977 data collection period, the Hermes beacon was available for 318 days. A total of 14,647 minutes of measurable (>0.5 dB) attenuation data was recorded at Greenbelt. The rain gauge at Greenbelt recorded a total of 11,587 minutes of measurable rain (>1mm/hr) over the same period. Precipitation at Greenbelt during the 47 unrecorded days was less than 3% of this total. Figure 3 shows the rain rate and attenuation distributions for Greenbelt, normalized to the attenuation time. The attenuation exceeded

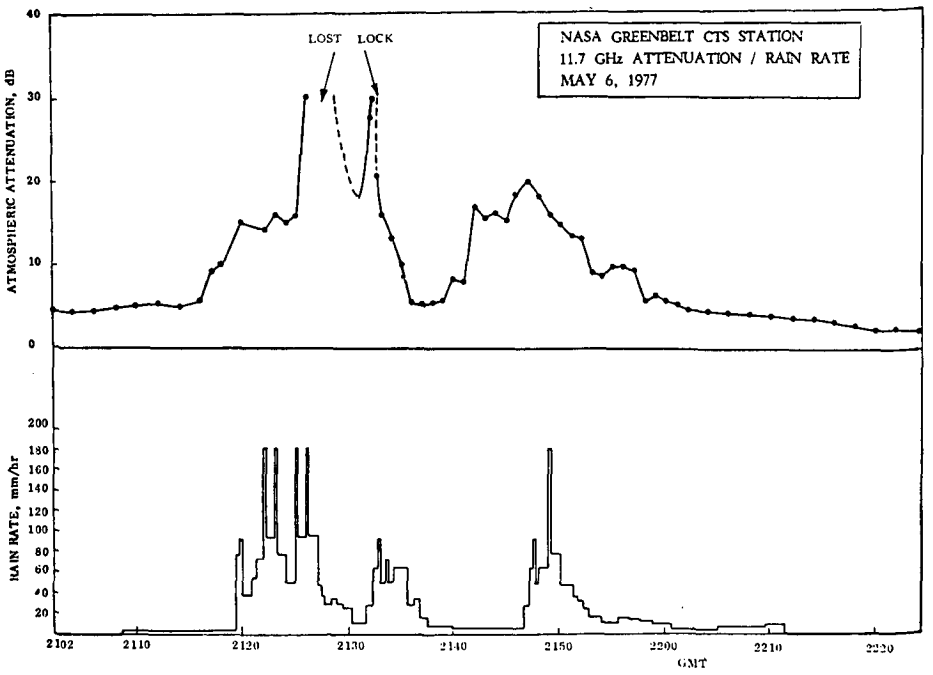


Figure 2. Attenuation Event, Greenbelt, May 6, 1977.

10 dB for over 45 minutes, 20 dB for 10 minutes, and 30 dB for 6 minutes. Rain rate excedence for the same three time periods was 42mm/hr, 76mm/hr, and 82mm/hr, respectively.

The attenuation measurements obtained at Rosman were less extensive than those for Greenbelt. The station was not operated on a continuous basis and during most of 1976 beacon monitoring was accomplished only during week days. The beacon signal level was recorded on a digital tape at the rate of one sample per second. Rosman has ten rain gauges located along the azimuth ground track of the earth-satellite path. The distances from the receiver antenna to the ten rain gauges were 0, 310, 524, 670, 937, 1204, 1151, 1764, 2057, and 2454 meters. Each gauge was sampled once per second, and rain rate computed on the basis of the time between tips, as was done for Greenbelt, Two rain-rate distributions were developed from the rain gauge data, the near-bucket rain rate, corresponding to the single gauge located at the receiver antenna, and the ground average of the rain rates measured at each of the ten gauges.

Attenuation and rain-rate measurements at Rosman for the thirteen month period of June 1, 1976 through June 30, 1977 will be discussed in this report. During this period 4148 minutes of measurable attenuation were recorded. Measurable rain rate totaled 5012 minutes for the near gauge, and 6521 minutes for the ground average (>1mm/hr in *any* gauge). The longer ground average time was due to

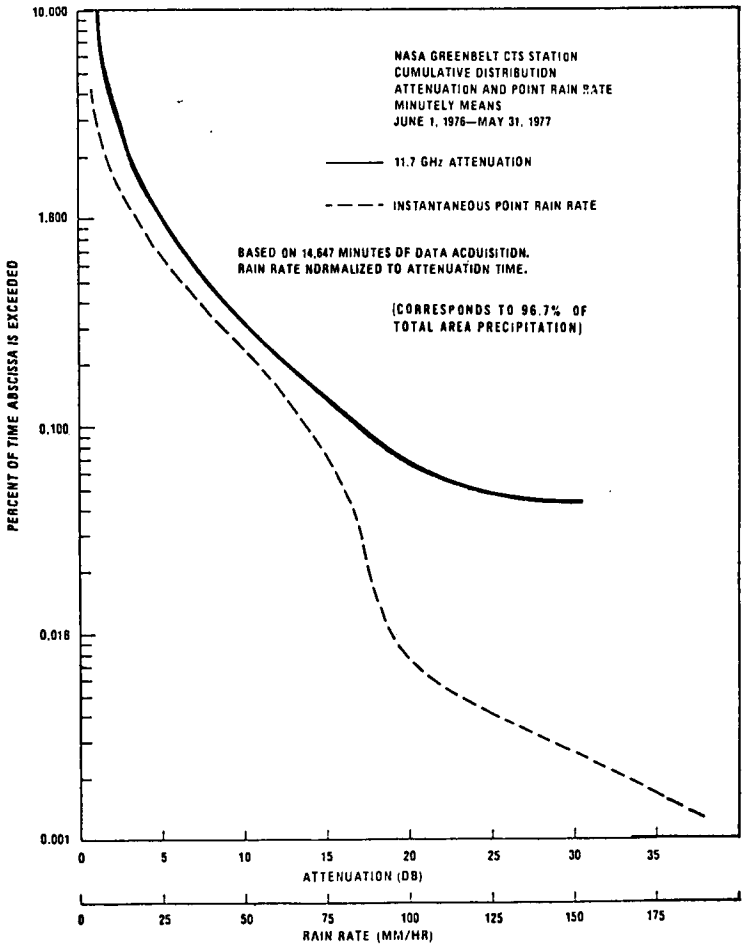


Figure 3. Long Term Attenuation and Rain Rate Distributions, Greenbelt, June 1, 1976 to May 31, 1977.

those periods when precipitation was present in at least one of the other nine rain gauges, but not present at the receiver terminal location. The measurements indicate that precipitation present in the path was not recorded by the near bucket for over 23% of the time that measurable rain rate was observed somewhere along the path. This result highlights one of the limitations in employing only a single rain gauge for rain attenuation studies.

Rain rate and attenuation distributions at Rosman for the total thirteen month period are presented in figure 4. The attenuation distribution reached a maximum of 23 dB for 1.16 minutes. Attenuation exceeded 10 and 20 dB for 33.6 minutes and 7.47 minutes, respectively. Note that the attenuation and rain rates are plotted as four second mean values, which reduces the amount of data reduction time but still produces a physically meaningful

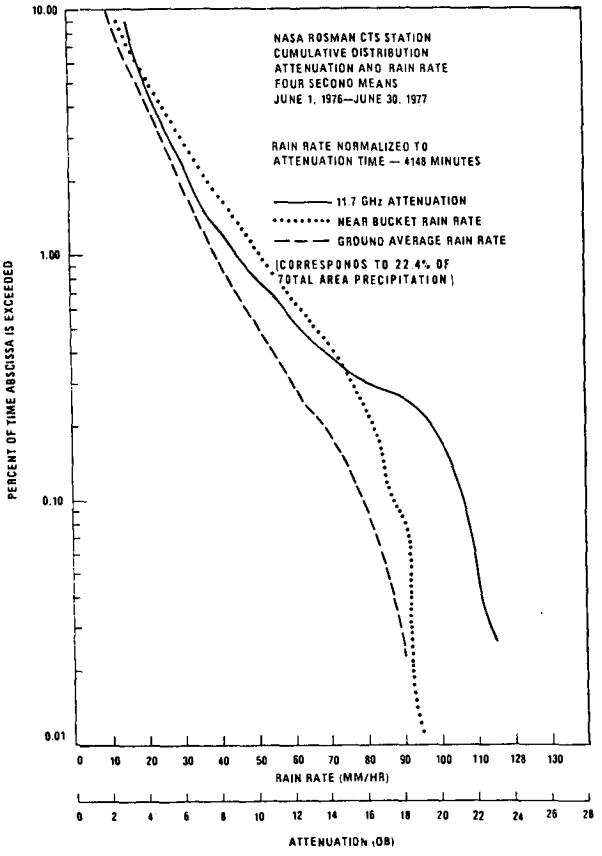


Figure 4. Long Term Attenuation and Rain Rate Distributions, Rosman, June 1, 1976 to June 30, 1977.

distribution. The ground-averaged rain-rate tends to be about 10-15mm/hr less, for a given percentage time, over the range of 10 to 90mm/hr, and the distribution tends to be smoothed out by the averaging process.

Precipitation at Rosman during the attenuation measurements was 18.4 inches, or 22.4% of the total accumulated precipitation of 82.2 inches during this period. The precipitation values were accumulated by a single rain gauge placed at the receiver antenna.

The "worst month" attenuation month, defined here as the actual calendar month with the highest percentage of time of attenuation exceeding 10 dB, were August 1976 and May 1977 for Greenbelt, and June 1977 for Rosman. Figure 5 presents these worst month attenuation distributions, normalized to the total month period. The large attenuation event of May 6, 1977 (Fig. 2) produced the "tail" in the May 1977 Greenbelt distribution.

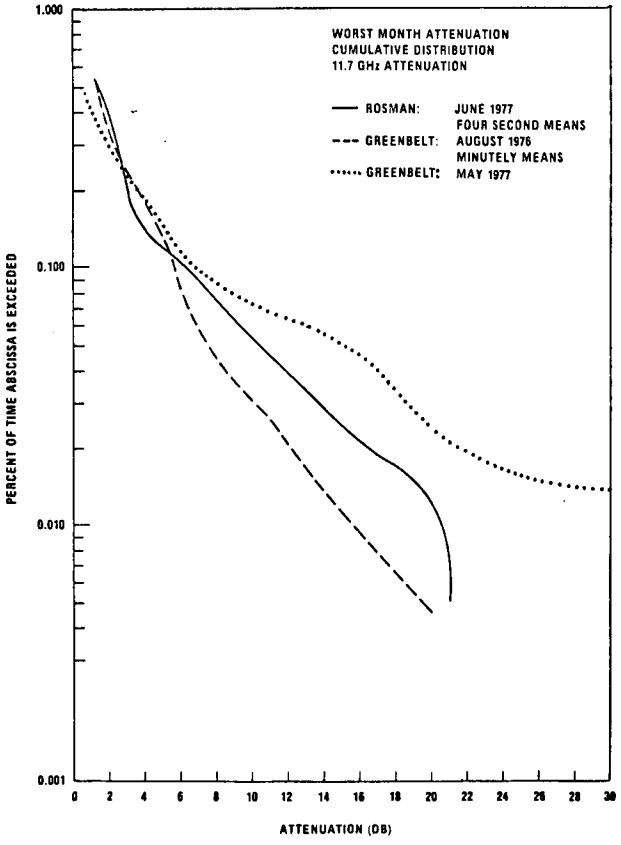


Figure 5. Worst Month Attenuation Distributions for Rosman and Greenbelt.

Summaries of the Greenbelt and Rosman distributions are presented in Tables II and III for three representative percentage factors, 0.1%, 0.01%, and .005%. These values correspond to about 8.75 hours, 53 minutes, and 26 minutes, respectively for the yearly distributions, and about 45 minutes, 4.5 minutes, and 2.25 minutes for the worst-month distributions. Note that the yearly data collected at Greenbelt was over three times greater than at Rosman, however, it is interesting to note that for the worst-month statistics the data collected at Rosman was twice the data obtained at Greenbelt. It is also noticed that the 4 second averaging of the rain rate at Rosman drastically reduces the peak rain-rate values relative to those obtained at Greenbelt which employs instantaneous values. This occurs because high rain-rate values involve the time between bucket tips that are on the order of a few seconds. Hence, averaging even over a few seconds can affect the rain rate at the high peak values.

TABLE II

SUMMARY OF RAIN RATE STATISTICS

| | PERCENTAGE VALUES | | | | | |
|---|---|---|---|---|---|---|
| | 0.1% | | 0.01% | | 0.005% | |
| | NB (MM/HR) | GA (MM/HR) | NB (MM/HR) | GA (MM/HR) | NB (MM/HR) | GA (MM/HR) |
| Rosman (4 Sec. Mean) | 11 | 12 | 49 | 41 | 65 | 54 |
| Yearly NB = 5012<br>GA = 6521 Minutes<br>22.4% of total precipitation* | | | | | | |
| Worst Month June 1977<br>NB = 414 Minutes<br>GA = 934 Minutes | 22 | 32 | 75 | 75 | 82 | 82 |
| Greenbelt (Minutely Mean) | 21 | | 82 | | 147 | |
| Yearly 11587 Minutes<br>96.7% of total precipitation* | | | | | | |
| Worst Month August 1976<br>597 Minutes | 20 | | 112.5 | | 140 | |
| Worst Month May 1977<br>178 Minutes | 10 | | 110 | | — | |

*Corresponds to total area precipitation.

TABLE III

SUMMARY OF 11.7 GHz ATTENUATION STATISTICS

| | PERCENTAGE VALUES | | |
|---|---|---|---|
| | 0.1% | 0.01% | 0.005% |
| Rosman (4 Sec. Mean)<br>Yearly = 4148 Minutes<br>22.4% of Total Precipitation* | 2.2 dB | 8 dB | 11.2 dB |
| Worst Month June 1977<br>689 Minutes | 6.4 dB | 20.2 dB | 21.2 dB |
| Greenbelt (Minutely Mean)<br>Yearly = 14647 Minutes<br>96.7% of Total Precipitation* | 2.1 dB | 10 dB | 15 dB |
| Worst Month August 1976<br>351 Minutes | 5 dB | 15.6 dB | 19.4 dB |
| Worst Month May 1977<br>227 Minutes | 6.5 dB | >30 dB | —— |

*Corresponds to total area precipitation.

The yearly distributions indicate that for a maximum allowable outage of one hour per year caused by rain, margins of 8.5 dB at Greenbelt and 7.3 dB at Rosman would have been required.

3. Depolarization

The recent interest in the use of dual-polarized communications links for increasing the information transmission capabilities of the transmission path has highlighted the need for measurements and evaluation of the depolarization properties of the earth's atmosphere. Dual-polarized communications systems require a high degree of isolation between channels to avoid cross-channel interference. Above 10 GHz the propagation medium, particularly when rain, hail, ice crystals, or wet snow are present, will cause depolarization and a reduction in the channel isolation.

The Hermes 11.7 GHz circularly polarized beacon has been used for depolarization measurements at Blacksburg, Virginia and Austin, Texas since spring 1976 as part of the CLCE. Detailed descriptions of the experimental systems and measurements are reported elsewhere, (Virginia Polytechnic Institute and State University, 1977a, b; University of Texas at Austin, 1977) and a summary of the major results is presented here.

The depolarization measurements at Blacksburg, Virginia have provided the first look at long-term isolation statistics from an orbiting spacecraft. Isolation is defined as the ratio of received power in the co-polarized (direct) channel to the received power in the cross-polarized channel. During the summer of 1976 over sixty "events" were observed where measurable depolarization occurred on the CTS 11.7 GHz beacon signal, nearly all associated with observed precipitation on the earth-space path. (See below for discussion of "anomalous depolarization".) Figure 6 shows an example from four of the most intense events of the isolation reduction as a function of direct attenuation. Clear weather isolation variations typically were about 1 dB peak-to-peak, and the average value of isolation was between 30 and 40 dB, caused by small pointing errors in the ground antenna tracking program. Figure 6 shows that as the rain attenuation increases, the isolation decreases. For example, for a 10 dB direct attenuation, isolation has been reduced by nearly 20 dB from the clear weather value, and for a 25 dB attenuation isolation has been reduced by nearly 30 dB.

The dashed curves on the figure are based on theoretical calculations of isolation versus attenuation developed from Oguchi's 11 GHz scattering coefficients at a 40° elevation angle for oblate drops (Oguchi and Hosoya, 1974), and Morrison and Cross' coefficients for spherical drops (Morrison and Cross, 1974). The upper curve assumes that 60% of the drops are oblate spheroids, and the lower curve assumes 100% oblate spheroids. The curves assume perfect

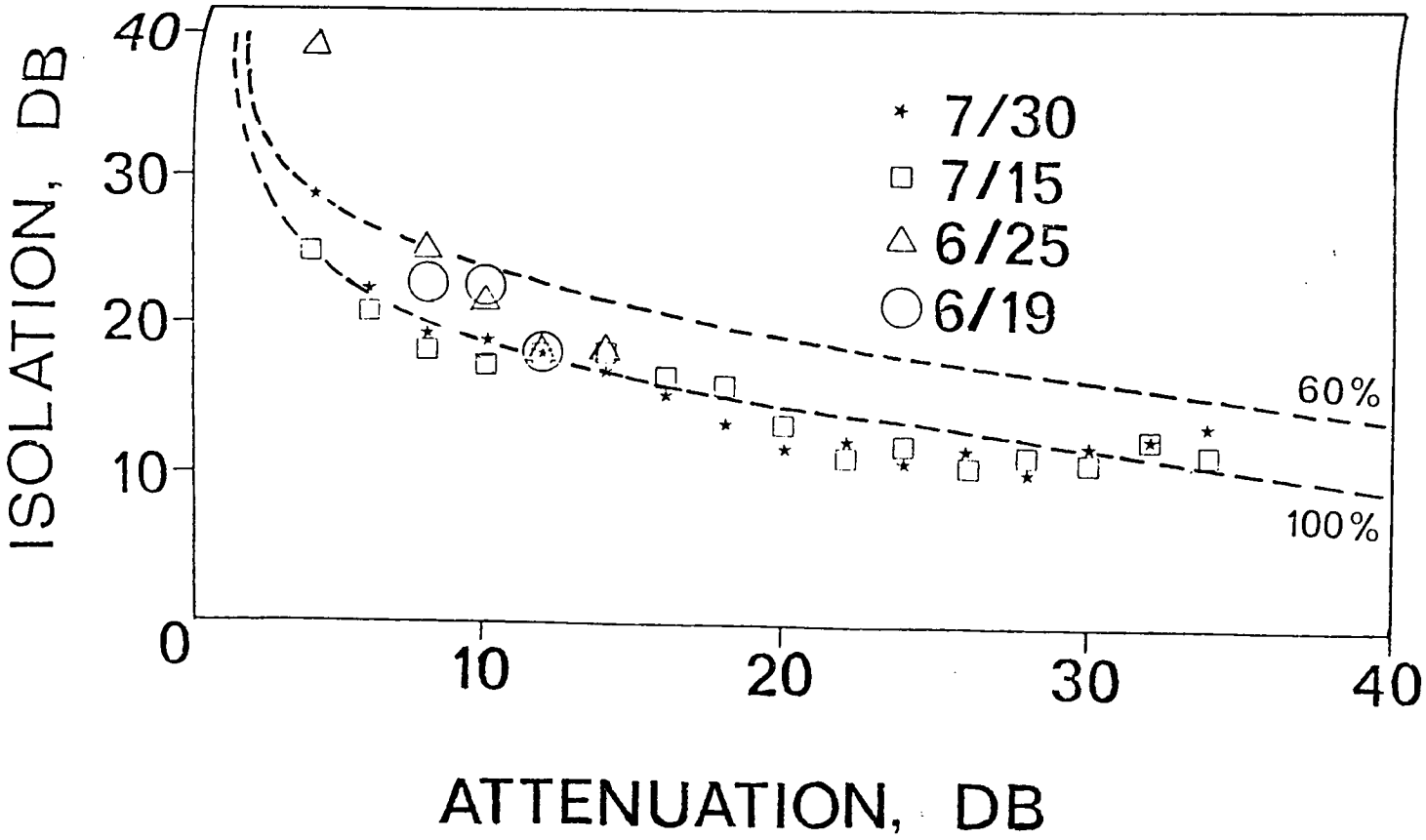


Figure 6. 11.7 GHz Depolarization Measurements at Blacksburg Va., Summer 1976.

circular polarization for the satellite and ground antennas, and a rain height of 2.5 km with an elevation angle of 33 degrees. The theoretical curves are seen to agree quite well with the measured data throughout the attenuation range.

Another propagation factor observed during the Hermes beacon measurements was the presence of depolarization in the absence of direct attenuation in the path. This behavior, sometimes referred to as "anomalous depolarization", is generally observed in conjunction with thunderstorms, which is an indication of ice formation in the path. The anisotropic phaseshift introduced to the transmitted wave by the frozen ice particles results in a change of polarization with very little accompanying attenuation.

Figure 7 shows an example of an event of this type observed at Austin, Texas in June of 1976. A strongly fluctuating cross-polarization signal power was observed for more than ten minutes before the attenuation peak occurred, and the character of the cross-polarization fluctuations changed noticeably when the attenuation finally occurred.

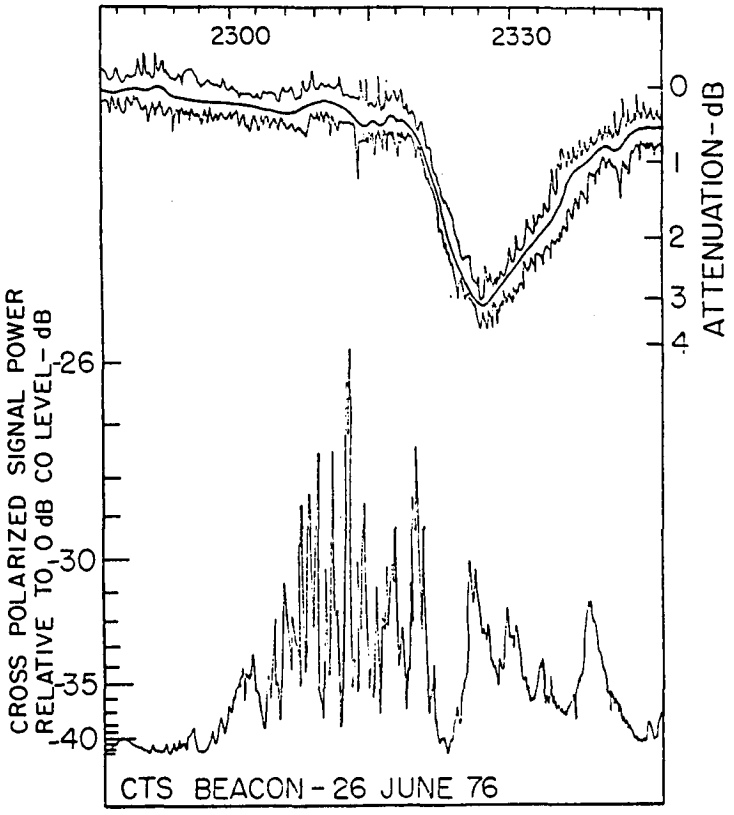


Figure 7. Ice Depolarization Event at Austin, Texas, June 26, 1976.

The relative importance of ice depolarization was considered for the Austin measurements by determining the percent of time of observed depolarization measurements (306 days) when the attenuation was less than 1 dB (Vogel and Straiton, 1977).

The results are summarized as follows:

| Observed Isolation | % of Total Due to Ice Depolarization |
|---|---|
| 25 | 5% |
| 30 | 15% |
| 35 | 38% |

Thus, for systems requiring a 25 dB isolation margin over this (or similar) propagation paths, ice-crystal depolarization is of small concern. For a 35 dB requirement this is no longer true because a substantial portion, nearly 40%, of the isolation loss is caused by ice effects. These first results on the significance of ice depolarization point out the difficulty in using rain attenuation statistics to predict isolation at 11.7 GHz, particularly for isolation values above 25 dB.

The long-term isolation statistics for Blacksburg and Austin are summarized in Table IV. The isolation versus attenuation least-square error equations are listed for the total available data base, as listed. The results for both locations are similar, and, since both include any ice depolarization effects present, they represent a "prediction" equation for 11.7 GHz isolation at these locations. The applicability of the results to other locations with different meteorological profiles must be investigated further.

4. Other Measurements

The Hermes CLCE consists of a whole range of experiments and measurements involving propagation and communications link characterization.

In addition to the attenuation and depolarization measurements described above, angle-of-arrival measurements utilizing four 0.6 meter reflectors on a single antenna mount, spaced one meter apart center-to-center, are underway at Columbus, Ohio (Ohio State University, 1976). A self-phased array receiver measures four amplitude signals and four differential phase signals which can be used to determine the angle of arrival of the propagating wave from the satellite. Measurements are in progress and the initial results are expected to be published early in 1978.

Several days of Hermes communications link characterization tests have been conducted from Rosman and Greenbelt, using both the 200w and 20w transponders. The tests in-

TABLE IV

11.7 GHz DEPOLARIZATION VERSUS ATTENUATION FOR BLACKSBURG, VA. AND AUSTIN, TEXAS.

| LOCATION | MEASUREMENT PERIOD | ISOLATION- ATTENUATION LEAST SQUARE ERROR EQUATION (dB) |
|---|---|---|
| Blacksburg, Va. | Summer 1976 (60 days) | I = 41.11 - 20.86 log A |
| | Summer 1977 (60 days) | I = 39.51 - 19.64 log A |
| | June 1976 - Aug 1977 (120 days) | I = 40.31 - 20.25 log A |
| Austin, Texas | June 1976 - June 1977 (306 days) | I = 44.1 - 21.5 log A |

cluded satellite transponder linearity, two-carrier intermodulation, two-carrier compression, carrier-to-noise and video test-tone-to-noise ratios, audio signal-to-noise, and baseband-frequency-response. All tests were conducted in clear weather conditions, and the results were nominal and as expected (Westinghouse Electric Co., 1977). It was hoped that some of the scheduled link tests would be accompanied by precipitation so that the links could be evaluated during attenuation periods, but the weather did not cooperate. Scheduled link tests are continuing at Greenbelt.

Meteorological support measurements and studies employing a dual-frequency radar system at Rosman have been conducted. The radar, operating at 3 GHz and 8.75 GHz, is directed along the earth-to-Hermes path during precipitation, and simultaneous measurements of 11.7 GHz attenuation, 3 GHz and 8.75 GHz backscatter, and rain rate from ten rain gauges are used for channel definition and modelling (Westinghouse Electric Co., 1977).

The CLCE measurements program will continue into the third year of Hermes operations at all of the ground terminal locations.

## 5. Summary

This paper has presented the major results of the first sixteen months of measurements of the Hermes Communications Link Characterization Experiment (CLCE).

Long-term attenuation measurements at Rosman and Greenbelt have shown that for a one hour per year allowable outage due to rain, power margins of 7.3 dB and 8.5 dB would be required, respectively. Looking at it another way, if 11.7 GHz satellite communications links were operating with 10 dB power margins at Rosman and Goddard, the links could have been expected to be out due to rain for 37 minutes at Rosman and for 53 minutes at Greenbelt during the one year measurement period.

Worst-month statistics developed for the two locations show a wide variability, ranging from 16 minutes to 36 minutes outage at the 10 dB level, and from 1-1/2 minutes to 11 minutes at a 20 dB level. Attenuation events at Greenbelt have exceeded 30 dB on three occasions, resulting in a total of five minutes in excess of 30 dB. In general, the attenuation observed at 11.7 GHz has been statistically as expected, however, individual events with very high attenuation levels, particularly during thunderstorm activity, have been observed.

Depolarization caused by precipitation and by ice particles has been observed with the Hermes beacon, however, the direct attenuation generally predominates over the depolarization, for moderate attenuation levels. For example, a frequency-reuse link employing dual polarization in operation at Blacksburg, with a clear weather isolation of 40

dB, would suffer a 10 dB loss in isolation during a 5 dB attenuation event. The resultant 30 dB isolation would still be acceptable for link operation. The measurements indicate that isolation remains acceptable up to about 10 dB levels of attenuation which is probably the upper limit to consider for practical space communications systems design. The importance of ice depolarization on systems design at 11.7 GHz requires further measurements; however, initial observation at Austin, Texas indicates that only 5% of all observed events resulting in an isolation of less than 25 dB between channels could be attributed to ice depolarization.

## REFERENCES


Ippolito, L.J.

1971 Effects of Precipitation on 15.3 and 31.65 GHz Earth Space Transmissions with the ATS-5 Satellite, *Proc. IEEE*, Vol. 59, pp. 189-205, February.

1975 ATS-6 Millimeter Wave Propagation and Communications Experiment at 20 and 30 GHz, *IEEE Trans. on Aerospace and Electronic Systems*, Vol. AES-11, No. 6, November.

Morrison, J.A. and Cross, M.J.

1974 Scattering of a Plane Electromagnetic Wave by Axisymmetric Raindrops. *Bell System Technical Journal*, Vol. 53, pp. 955-1019, August.

Oguchi, T. and Hosoya, Y.

1974 Scattering Properties of Oblate Raindrops and Cross-Polarization of Radiowaves due to Rains (Part II); Calculations at Microwave and Millimeter Wave Regions. *J. of Radio Research Laboratories*, Vol. 21, no. 105, pp. 191-259.

Ohio State University

1976 The OSU Self-Phasing Array for Propagation Measurements Using the 11.7 GHz CTS Beacon, *Technical Report 4299-1*, prepared for NASA/ Goddard Space Flight Center, November.

University of Texas, Austin

1977a CTS Attenuation and Cross-Polarization Measurements at 11.7 GHz, prepared for NASA/ Goddard Space Flight Center under Contract NAS 5-22576, April.

1977b CTS Attenuation and Cross-Polarization Measurements at 11.7 GHz, prepared for NASA/ Goddard Space Flight Center, April.

Virginia Polytechnic Institute and State University
1976 A Depolarization and Attenuation Experiment Using the CTS Satellite, Vol. I Experiment Description, prepared for NASA/Goddard Space Flight Center, under Contract NAS 5-22577, November 18.
1977a A Depolarization and Attenuation Experiment Using the CTS Satellite, Vol. 2, Data, prepared for NASA/Goddard Space Flight Center, under Contract NAS 5-22577, February 23.

Virginia Polytechnic Institute and State University
1977b Quarterly Technical Progress Report III (Second Year) on A Depolarization and Attenuation Experiment Using the CTS Satellite, prepared for NASA/Goddard Space Flight Center, under Contract NAS 5-22577, July 19.

Vogel, W. and Straiton, A.
1977 CTS 11.7 GHz Beacon Attenuation and Cross-Polarization Measurements: June 1976 to May 1977, *1977 USNC/URSI Meeting*, Stanford University, Stanford, California, June 22-24.

Westinghouse Electric Co.
1975 CTS CLCE Data Analysis Requirements, *Report No. BF75-0001*, prepared for NASA/Goddard Space Flight Center, under Contract NAS 5-20724, March.
1977 CTS Communications Link Characterization Experiment, *Technical Data Report*, Volume 3, *Report FIS-77-4057*, prepared for NASA/Goddard Space Flight Center, August.

# MEASUREMENTS OF DEPOLARIZATION AND ATTENUATION AT 11.7 GHz USING THE HERMES BEACON

W.L. Nowland*, J. Schlesak,
R.L. Olsen, J.I. Strickland
Communications Research Centre
Ottawa, Canada

*L'article décrit une expérience en cours effectuée par le Centre de recherches sur les communications (CRC) du ministère des Communications et Bell-Northern Research. L'expérience vise à mesurer la dépolarisation et l'atténuation, en divers endroits au Canada, à l'aide du radiophare du satellite technologique de télécommunications (STT-CTS), ou Hermès, émettant un signal dans la bande de fréquence de 11,7 GHz. Les calculs effectués en différents points au Canada permettront une évaluation plus exhaustive de la théorie et apporteront les données nécessaires sur la répartition des gouttes de pluie en fonction de l'angle de chute. Le calcul de l'atténuation directe permettra d'évaluer les données fondées sur le calcul radiométrique de la température du bruit de l'espace.*

## INTRODUCTION

To design a satellite communications system using frequencies above several GHz, it is necessary to evaluate the attenuation of microwave signals by liquid water in the earth's atmosphere. For those satellites which use orthogonal polarizations to increase their capacity, it is also necessary to evaluate the depolarization of signals by non-spherical raindrops, ice particles in clouds, and snow. Since the characteristics of precipitation vary widely across Canada, it is insufficient to study attenuation and depolarization in only one location.

This paper describes a joint experiment being conducted by the Communications Research Centre (CRC) of the Department of Communications and Bell Northern Research to measure the characteristics of depolarization and attenuation at several locations across Canada using the signal received from the 11.7 GHz beacon of the Communications Technology Satellite (CTS) or Hermes. Initial results obtained at Ottawa are summarized.

## BACKGROUND

Measurements of depolarization and attenuation of the Hermes beacon signal have been made at Ottawa since July

*formerly at Bell-Northern Research, Ottawa, Canada.

1976. With support from the Trans-Canada Telephone System and the Department of Communications, this experiment has recently been extended to several locations representative of the various climatic areas of Canada. Equipment was installed at the telephone toll offices in Winnipeg, Toronto, Halifax and St. John's in August and September 1977. The equipment at Winnipeg will be moved to Vancouver in January 1978.

Since satellite earth stations operating in the 12 and 14 GHz bands can be located within cities, the depolarization and attenuation data will be directly applicable to the design of future satellite communications systems which use such stations. The simultaneous measurement of depolarization and attenuation will also assist in understanding the significant depolarization mechanisms in the 12 and 14 GHz bands and their relation to various meteorological quantities. Predictions of depolarization statistics may then be made from existing statistics of other propagation or meteorological quantities. When rain is the dominant depolarization mechanism, a technique has been developed for predicting depolarization statistics from rain attenuation statistics (Nowland et al, 1977a). Since rain attenuation statistics, particularly those obtained with radiometers, are more widely available than depolarization statistics, it is important to evaluate this technique. The measurements described here provide a means of not only evaluating this technique, but also of obtaining the effective parameters of the raindrop canting-angle distribution (i.e., distribution of orientations) which are also required by the prediction technique. At some sites, the combination of depolarization and rainrate measurements will allow the evaluation of techniques for predicting rain depolarization statistics from rainrate statistics (C.C.I.R., DOC, 1977).

## EXPERIMENTAL TECHNIQUES

Attenuation and depolarization data are obtained from measurements of the linear orthogonal components of the circularly-polarized signal from the Hermes beacon. At Ottawa, a 3.7m antenna is employed; 1.9m antennas are used at the other sites. The amplitude and phase of the two orthogonal linearly-polarized components (nominally horizontal (H) and vertical (V)) are coherently detected by a special phase-lock receiver whose block diagram is given in figure 1. The differential attenuation $\Delta A$ (in dB) and differential phase $\Delta\beta$ (in radians) between these orthogonal components are calculated from the demodulator outputs, Q and I, using

$$\Delta A = 10 \log \left( \frac{(Q-Q_o)^2 + (I-I_o)^2}{(Q_{cs}-Q_o)^2 + (I_{cs}-I_o)^2} \right) \quad \text{(dB)}$$

$$\Delta\beta = \tan^{-1} \left( \frac{I-I_o}{Q-Q_o} - \tan^{-1} \frac{I_{cs}-I_o}{Q_{cs}-Q_o} \right) \quad \text{(radians)}$$

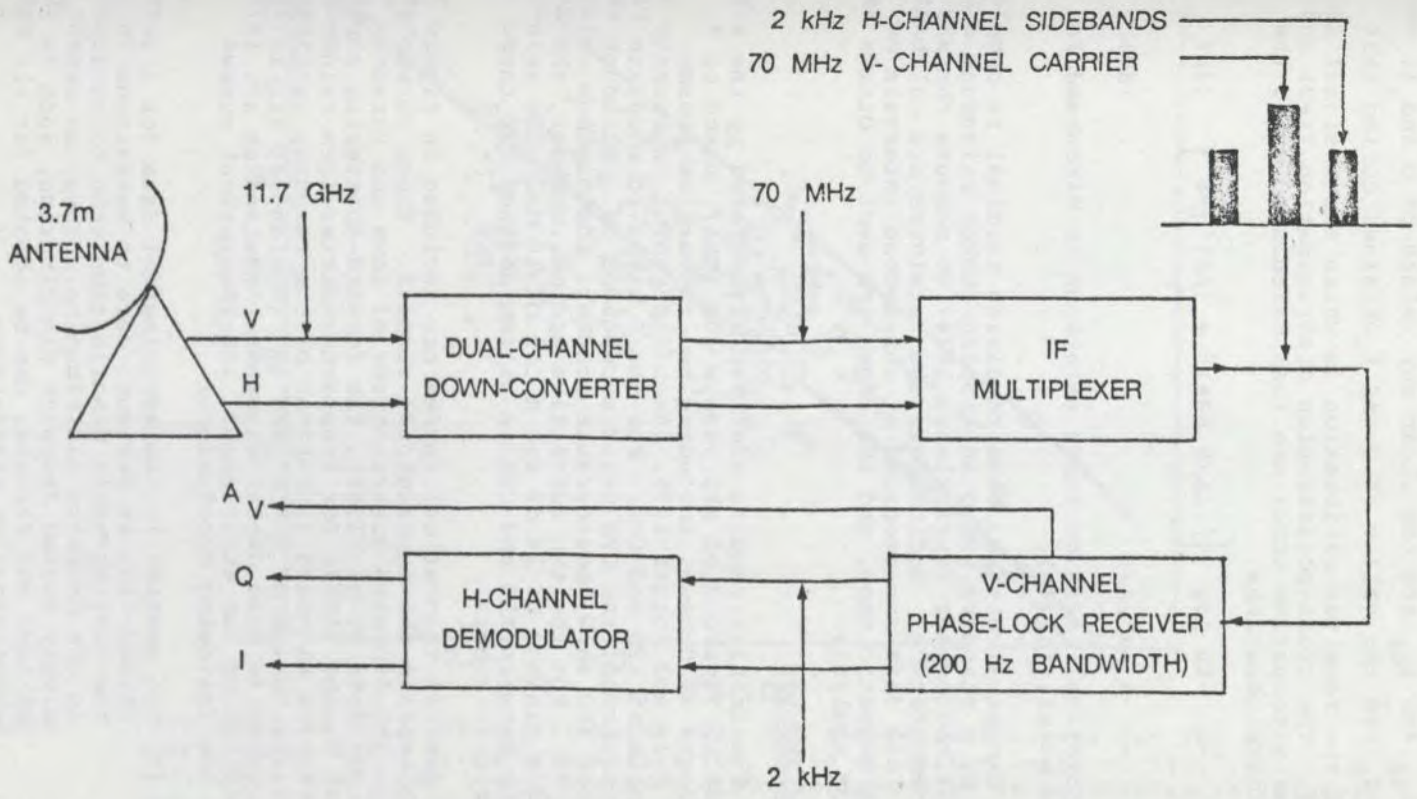


Figure 1: Block diagram of the Hermes cross-polarization receiving system.

where $Q_{cs}$ and $I_{cs}$ are the clear sky values of Q and I, and $Q_o$ and $I_o$ are the values of Q and I obtained during that part of the receiver calibration in which the H signal is removed. The cross-polarization discrimination (XPD) and co-polar attenuation (CPA) are then calculated using the approximate relations

$$XPD \simeq -10 \log \left\{ [(\Delta A/8.686)^2 + (\Delta\beta)^2]/4 \right\} \quad (dB)$$

$$CPA \simeq A_v + \Delta A/2 \quad (dB)$$

The theoretical basis of these relations is discussed in Nowland et al, (1977a).

Except at Ottawa, each receiving terminal is complemented by a standard Canadian tipping-bucket raingauge and a 13 GHz radiometer (Strickland, 1974) to measure the sky noise temperature. Radiometers and receivers are calibrated daily. All data are recorded at one-second intervals on digital magnetic tape, and the tapes are sent to Ottawa each week for analysis.

## INITIAL RESULTS

The initial results are best illustrated by the scatter plot in figure 2 of XPD versus log (CPA), based on 8 rain events at Ottawa, including two convective storms, during July and August 1976. Each data point represents a 10s sample of XPD and CPA. For the 6 light to moderate rain events observed, the CPA never exceeded 3 dB. Although the values of XPD show considerable scatter, the minimum value was 20 dB. For the two convective storms, however, the XPD reached a minimum of 14 dB for a CPA of 10 dB. The relationship between XPD and CPA is better defined for these heavier rain events.

Several theoretical curves are included in figure 2 to help explain the experimental results. These curves are based on the dropsize distributions of Laws and Parsons (1943) and Joss et al (1968), the forward-scattering amplitudes of Oguchi (1977) for Pruppacher-Pitter-form raindrops, and effective standard deviations of the raindrop canting-angle distribution of $\sigma = 0°$ and $40°$ (Nowland et al, 1977a). As discussed in more detail elsewhere (Nowland et al, 1977b), a comparison of the experimental and theoretical curves yields the following conclusions:

(i) The scatter in the experimental data for a given attenuation is due much more to variations in the canting-angle distribution than to variations in the dropsize distribution. Thus, an extensively tested dropsize distribution, such as that of Laws and Parsons, can be adopted for all rain depolarization predictions.

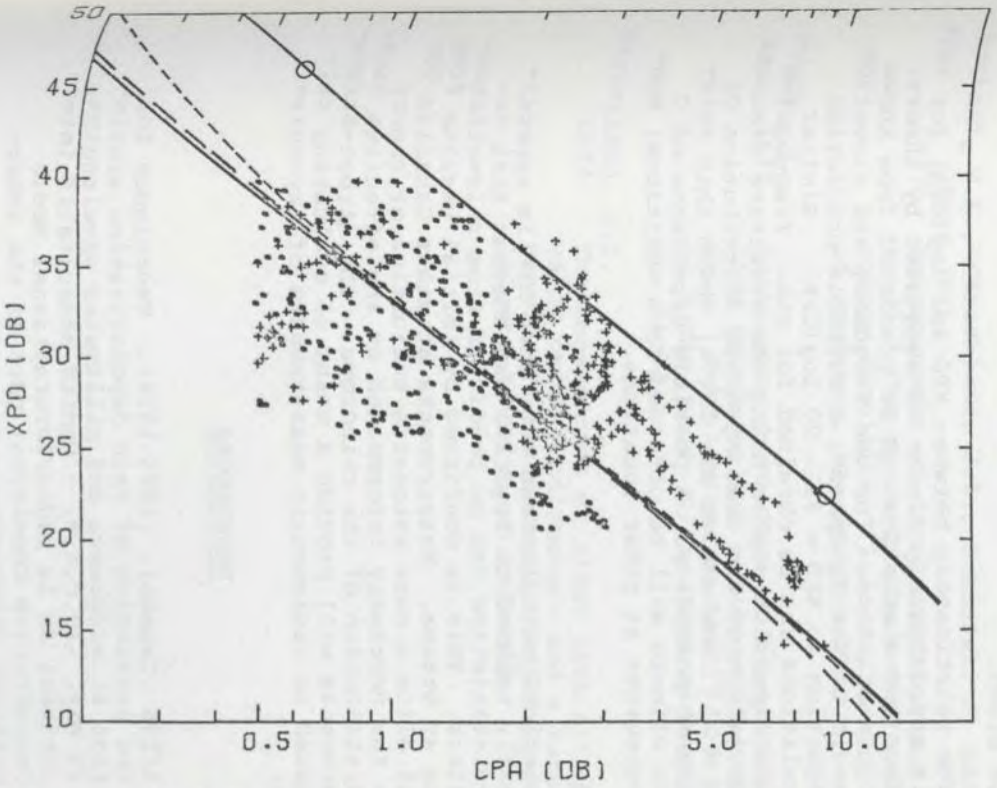


Figure 2. Comparison of 11.7 GHz experimental data and theoretical curves for XPD as functions of CPA. Circular polarization, path elevation angle of 24.6°. ——LP, — — —J-T, and ---J-D dropsize distributions with an equi-oriented raindrop model. —o— LP dropsize distribution and random canting-angle model with $\sigma = 40°$. Data for the two consecutive storms are shown as crosses; the remaining data are shown as dots.

(ii) At least for the events analyzed, rain depolarization at 11.7 GHz seems to be more significant than depolarization due to other hydrometeors along the path. Thus, depolarization predictions based only on rain effects may be valid in the 12 and 14 GHz bands. However, additional measurements are required, particularly for other climates, before a more definite conclusion can be drawn.

(iii) The relationship between XPD and log(CPA) for rain is approximately linear as suggested by theory. Thus XPD statistics can be predicted from known CPA statistics. For the frequency and elevation angle of the equipment, a suitable prediction equation is XPD = 35 - 20 log(CPA). Similar relations can be obtained for other frequencies and elevation angles using the effective standard deviation of the canting-angle distribution of $\sigma = 25°$ (Nowland et al, 1977a) which this relationship implies. A possible dependence of $\sigma$ on climate will be obtained from additional measurements at other locations.

## CONCLUSIONS

Theoretical calculations show that XPD is approximately linearly related to log(CPA) and suggest that depolarization statistics can be predicted from rain-attenuation statistics. This is confirmed by initial results from measurements at Ottawa. Measurements at other Canadian locations will allow a more extensive evaluation of theory and provide the necessary information on the effective canting-angle distribution of the raindrops. The direct-attenuation measurements will provide a means of evaluating calculations based on radiometric measurements of sky-noise temperature.

## REFERENCES

C.C.I.R.
1977 5/206 (Canada), (1974-1978). Techniques for the prediction of rain depolarization statistics at microwave and millimeter wavelengths, 20 May. (C.C.I.R. - Comité consultatif international de la radio/International Radio Consultative Committee; part of the International Telecommunications Union.)

Joss, J., Thams, J.C. and Waldvogel, A.
1968 The variation of raindrop size distributions at Locarno, *Proc. of the International Conference on Cloud Physics*, Toronto, Canada, pp. 369-373.

Laws, J.O. and Parsons, D.A.
1943 The relation of raindrop-size to intensity, *Trans. Am. Geophys. Union*, 24, pp. 452-460.

Nowland, W.L., Olsen, R.L. and Shkarofsky, I.P.
1977a Theoretical relationship between rain depolarization and attenuation, *Electron, Lett.*, 27 October, 13, pp. 676-678.

Nowland, W.L., Strickland, J.I., Schlesak, J. and Olsen, R.L.
1977b Measurements of depolarization and attenuation at 11.7 GHz by using the Communications Technology Satellite, *Electron, Lett.*, 24 November, 13, pp. 750-751.

Oguchi, T.
1977 Scattering properties of Pruppacher-and-Pitter-form raindrops and cross-polarization due to rain: Calculations at 11, 13, 19.3, and 34.8 GHz, *Radio Sci.*, January-February, 12, pp. 41-51.

Strickland, J.I.
1974 The measurement of slant path attenuation using radar, radiometers and a satellite beacon, *J. Recherches Atmosphériques*, January-June, 8, pp. 347-358.

# HERMES EXPERIMENTS ON CENTRALIZED SYNCHRONIZATION AND RANGING (CENSAR) FOR TIME-DIVISION MULTIPLE-ACCESS (TDMA) SYSTEMS, AND FOR SATELLITE ORBIT PERTURBATION MEASUREMENTS (OPME)

P.P. Nuspl and R. Mamen

Communications Research Centre

Ottawa, Canada

*Cet article donne un compte rendu des épreuves de synchronisation mettant en jeu les systèmes d'accès multiple par répartition dans le temps (Time-Division Multiple-Access (TDMA)) des satellites de télécommunications, ainsi que les résultats d'une expérience connexe sur le calcul de la perturbation des orbites (Orbit-Perturbation Measurements Experiment (OPME)). La première partie de l'article, traitant de l'accès multiple par répartition dans le temps (TDMA), embrasse les principes de base d'un nouveau concept, touchant la synchronisation et la télémétrie centralisée (Centralized Synchronization and Ranging (CENSAR)) et en explique les servitudes techniques. On décrit les éléments matériels et logiciels de la mise en application du système, et on détaille et analyse ensuite les résultats. Une constatation importante est que la synchronisation en boucle ouverte est possible avec des temps de garde inférieurs à 30 ns. La deuxième partie traite de l'expérience sur le calcul de la perturbation des orbites (OPME) effectuée dans le cadre du projet mixte et qui permet d'obtenir les données orbitales après traitement des données de la synchronisation. Les prévisions relatives au système, découlant des analyses et des informations numériques, sont présentées après une description des objectifs. Les résultats d'expériences récentes démontrent que l'excellente définition et la fréquence des données du TDMA permettent un repérage précis de la position du satellite et constituent un instrument de haute-précision pour le calcul de l'orbite et des perturbations de celle-ci. Il s'agit donc d'un outil virtuellement supérieur à ceux utilisés jusqu'ici. Les auteurs de l'article donnent enfin les conclusions et les recommandations relatives au TDMA et à l'OPME.*

## 1. INTRODUCTION

Early in 1971, the Department of Communications recognized the desirability for digital communications experiments to be conducted with the Communications Technology Satellite (CTS), now named Hermes. General guidelines in this embryonic period were to investigate new concepts, to develop advanced techniques and to promote work in high-speed technology in Canada. This paper reports on experiments in synchronization for Time-Division Multiple-Access (TDMA) systems for satellite communications and on a closely-related experiment in orbit perturbation measurements (OPME).

The paper consists of Part I and II, dealing with TDMA and OPME respectively. Part I covers the basic principles of the new centralized synchronization and ranging (CENSAR) concept and explains the technological requirements. Hardware and software features of the implementation are described and the results are discussed. Part II describes how the satellite position is derived from the TDMA synchronization data. It compares the experimental results with analytic predictions, and examines accuracy, sensitivity, and possible sources of discrepancies. The conclusions and recommendations from the TDMA and OPME parts conclude the paper.

# PART I - CENTRALIZED SYNCHRONIZATION FOR TDMA SYSTEMS

## 2. SYNCHRONIZATION FOR TDMA

TDMA technologies for geosynchronous communications satellite applications have had about a decade of intense development by numerous organizations in several countries, with expectations of high capacities, greater efficiencies, system flexibility and inter-connectivity in the associated communications systems. Compatibility with the use of spot-beam antennas and satellite switching is also a major factor in creating interest in the techniques. However, there are only a few TDMA systems in operation, suggesting that further developments and cost reductions are needed before TDMA will be competitive with the more mature Frequency Division Multiple Access (FDMA) approach. The initial impetus in TDMA technology development was for INTELSAT applications, but recent activities are aimed at regional and domestic systems, sometimes with special-purpose (e.g., data only) applications.

TDMA is the shared use of a satellite repeater by several user stations transmitting bursts timed so as to interleave without overlap at the satellite. Since high utilization efficiency is usually a requirement, small guard times, which are deliberate gaps between bursts, are allocated; and since the satellite moves about its nominal position, there is a continuing need for synchronization which is the availability of required timing at all stations in the network. Timing accuracies of better than 100 ns are usually expected.

A new synchronization sub-system for TDMA (deBuda, 1972) has been given the acronym CENSAR, derived from CENtralized Synchronization And Ranging. The objectives of the Hermes CENSAR experiment included demonstration of technical feasibility and assessments of timing accuracies and guard times. In a parallel operation, synchronization data was recorded for OPME studies.

The experimental CENSAR system discussed in this paper consists of a central control station, three ranging stations and a single user station from a possible network of stations. This system and stations were designed for use with a geosynchronous communications satellite with spot-beam antennas, such as Hermes. The control station sends short bursts of microwave radio signals having wide bandwidth and carrying control data via the satellite, to all stations. Each ranging station sends back a ranging burst at a time specified by the control data. The control station measures the total transmission delays (elapsed time) from the three stations, estimates its own delay to the satellite and corrects the control data accordingly. Because each user station calculates its own delay from a knowledge of the station co-ordinates and from the control data, and thus achieves synchronization without any transmissions of its own, CENSAR is in the class of 'open-loop' synchronization systems.

Section 3 contains concise statements of CENSAR principles and discussions of them. Computer algorithms are treated in Section 4, whereas the specific implementations for the experiment are discussed in Section 5.

## 3. PRINCIPLES AND FEATURES OF CENSAR

The CENSAR concept is based on four principles:

### (a) Measure Effective Delays Through Three Satellite Links

Delay measurements are made at a central control station, with the co-operation of stations called ranging stations. From the geometry illustrated in figure 1, it will be apparent that only three measurements are necessary. These are best done by transmitting and receiving broadband signals in a burst mode (synchronization and ranging bursts), yielding full information on actual propagation delays through the equipment, propagation paths and the repeater. Each ranging station responds to control data for its use only, establishing three very precise delay-lock loops. The ranging bursts do not interfere with user stations. The required measurements can be made at a central control station with only moderate requirements in signal processing and computation.

### (b) Broadcast Relevant Information to the Network

The control station uses a very small capacity synchronization burst to send the necessary data to all stations.

(c) Recover Frame and Symbol Timing

Each station receives the synchronization burst, recovers frame timing and demodulates the control data in this burst. It is a significant principle of CENSAR that network symbol timing is recovered from the synchronization data bursts; the network is said to be bit synchronous.

(d) Calculate the Transmission Delay at Each Station

Through a deliberate choice of unique basis vectors, since each user station is given its precise co-ordinates and receives the control data, each station calculates its own delay to the satellite.

From these principles flow some basic features of CENSAR systems, regardless of implementation. Centralized control can be used in practical applications, with the measurements and computations done at a single control station, in co-operation with only three remote stations.

CENSAR is in the class of 'open-loop' synchronization systems. This has been alternately expressed as passive synchronization, because the user stations achieve complete and precise synchronization without transmissions of their own. They are initially synchronized when all synchronization data is received.

Thirdly, through the use of short bursts, with a minimum number of measurements and control data, high efficiencies are achievable even for large numbers of accesses. The remote regeneration of network symbol timing keeps the preamble requirements very low. For example, it has been projected that it is feasible to have 30 accesses at 97% efficient use of available capacity.

It is also noteworthy that CENSAR is compatible with present-generation satellite technology and would also be compatible with future spot-beam systems and satellite-switched TDMA (wherein fast switches in the satellite redirect bursts to designated beams).

Since most applications of TDMA are very sensitive to costs, the potential economies of CENSAR must be emphasized. With only simple equipment of small size and high technology, but requiring no trained operators, a cost-effective TDMA network can be envisioned.

## 4. COMPUTER ALGORITHMS

In the development and understanding of the computational procedures, it is very useful to view the problem as geometrical. A geocentric cartesian co-ordinate system is selected and the locations of all stations are found by accurate surveys. Other small effects temporarily put aside, the requirement is to solve for the position of the satellite.

In a system having spot-beams, it is usually the case that a station cannot receive its own signals. This implies that two-hop signalling is necessary between pairs of stations. In CENSAR, the control station and a ranging station are foci of an ellipse; the satellite lies on the ellipse defined by the sum distance of $T_1+T_K$, where K = 2,3,4, in figure 1. The satellite resides on the ellipsoid of rotation obtained by rotation of the ellipse about its major axis. Three such ellipsoids with foci carefully selected to provide independent information are necessary and sufficient; in principle, the satellite is at the intersection of the ellipsoids.

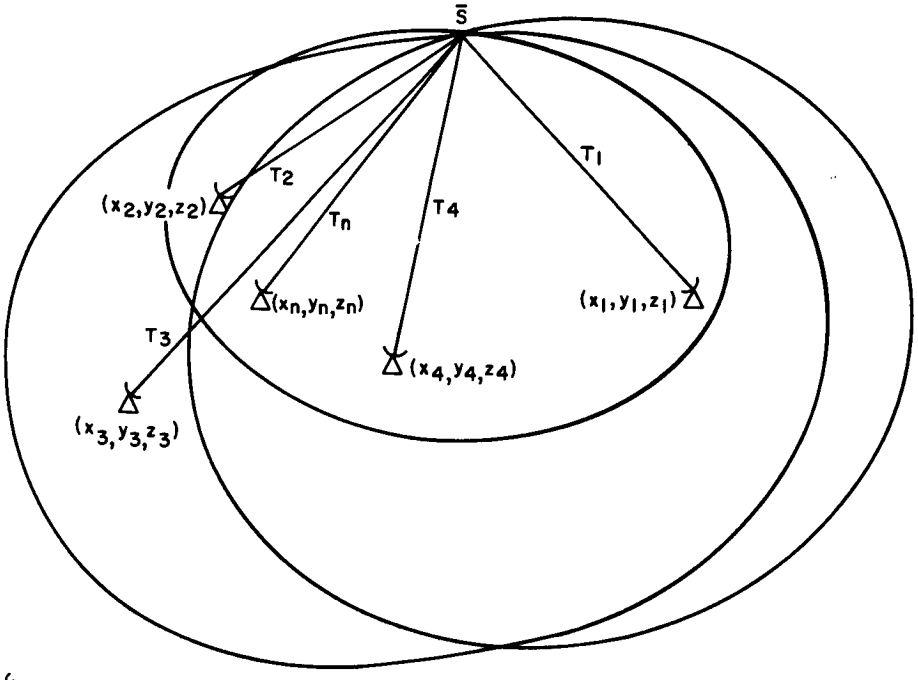


$(x_1, y_1, z_1)$ and $(x_k, y_k, z_k)$ are foci of ellipsoids of rotation.
S, satellite is on the surface of each ellipsoid.
Check system with a fourth measurement

Figure 1: Geometry for Spot Beams

A direct solution is unattractive due to computational requirements. Indeed, the viability of the CENSAR concept is attributed to vector algebraic transformations which yield tractable formulations (Nuspl and deBuda, 1974). The first of these starts with survey data and computes coefficients for use in the other algorithms. Such calculations are done off-line, with high precisions and accuracies; they are required only once for a given network. Another related off-line processing consists of calculation of CENSAR coordinates for each of the user stations.

Real-time algorithms have been devised to achieve high accuracies and yet be programmed for the modest resources of a mini-computer. At the control station only, the main procedures are the control of the delay-lock loops and the calculation of the delay ($T_1+T_1$) (which cannot be measured in a spot-beam system). There are numerous other housekeeping, data logging and check functions performed also. At each user station, a simple computation with known coefficients and received data yields the required burst delay for the station.

## 5. IMPLEMENTATION OF THE EXPERIMENT

Whereas the above has discussed principles and algorithms applicable generally, the following sections describe the technical preparations for the experiment with Hermes and ground stations in Canada. In all phases of the experiment, the central control station was in Ottawa at the Hermes 9m station. The required three ranging stations were located at London (Ontario), Rouyn and Quebec City (Quebec) in Phase I and at Brandon, Thompson, (Manitoba) and Thunder Bay (Ontario) in Phase II, the latter illustrated in figure 2. A convenient method of evaluating the accuracy of the synchronization technique was to measure the burst-timing error of the signals from a fifth station which utilized only the broadcast synchronization data, thereby simulating one of the many user stations of a CENSAR-timed network. The design of the experiment included calculations in real-time and off-line of the difference between predicted timing and measured timing for the station.

In comparison to a satellite system optimized for the CENSAR concept, there were severe constraints in this implementation. The Hermes transponder was configured with two separate channels and two spot-beams, which resulted in requirements for new algorithms and for different signal types. The ground stations were also selected, in number, type, and function, according to general requirements; however, their transmit power was increased from about 2W to 20W to improve ranging station performance. Nevertheless, ranging bursts had to be longer than in an operational system and structured with redundancy and bandwidth in order to achieve the desired time-resolution at the control station. Some additional problems and delays were caused by the need to co-locate and to share the stations with other experimenters.

Accurate station surveys are necessary for precise open-loop synchronization and for satellite position determination. Through the co-operation of the geodesy group of the Department of Energy, Mines and Resources, all locations were eventually surveyed to accuracies of about ±5m in each co-ordinate.

### 5.1 Measurements

Measurements of delay time $T_1+T_K$, K = 2,3,4,5 are ob-

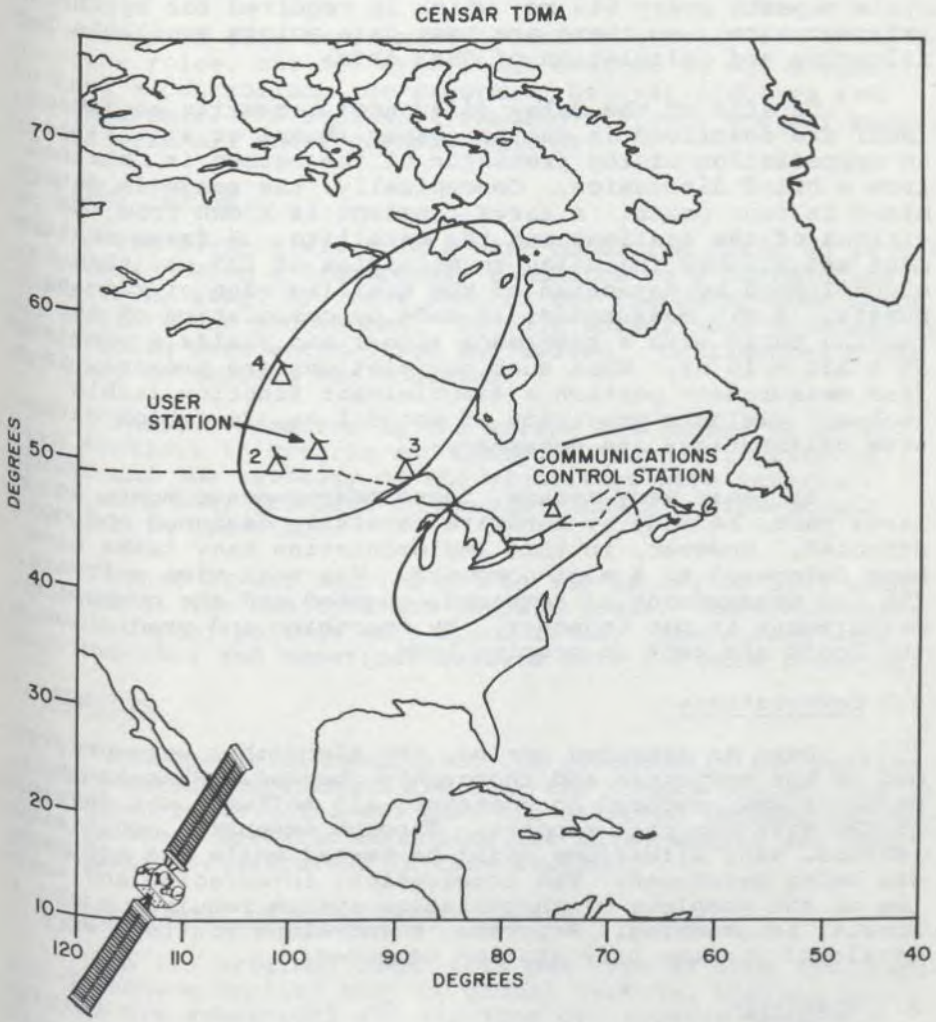


Figure 2. Typical Regional Coverage and Sample TDMA Network.

tained from four delay-lock loops. Each loop is identical but is processed in its own quarter of the cycle. The fundamental purpose of each loop is to maintain a precise arrival time of a ranging burst, which is suitably observed and controlled at the control station. The control data in each loop are independent and are the required measurements. A cycle repeats every 640 ms, which is required for synchronization control, so there are many data points available for filtering and calculation of OPME data.

Details of the delay (distance) measuring equipment (DME) are described in another paper (Nuspl et al, 1975); an appreciation of the precision of the method is obtained from a brief discussion. Conceptually, the range is determined in four parts. A large constant is known from the positions of the stations and the satellite. A frame measurement establishes the delay to multiples of 125 μs; this is accomplished by detection of the trailing edge of ranging bursts. A bit measurement is made by correlation of the ranging burst with a reference signal and yields a precision of 1 bit = 15 ns. When such correlations are present, in a fine measurement portion a discriminant function (table look-up) yields a precision of about 1 ns, for which extensive calibrations are necessary.

By their very nature, these measurements must, in large part, be made by hardware carefully designed and constructed. However, in this implementation many tasks have been delegated to a mini-computer. Via real-time software, the raw measurement is acquired, checked and the composite measurement is put together. By smoothing and prediction the loops are kept in precise lock.

## 5.2 Computations

Over an extended period, the algorithms were programmed on the computers and thoroughly checked. Whereas the hardware was procured on contract, all software was developed at CRC with contract support. Through extensive orbit simulations, many situations could be tested while the software was being developed. The integration, interfacing and testing of the complete synchronization system required much special programming. Separate, stand-alone routines were developed for the user station computer.

## 5.3 Start-up

The CENSAR concept does not require orbital information, so a very important procedure is start-up, by which the synchronization network becomes operational. It was possible to develop procedures by which fully automatic start-up is achieved with up to four ranging stations simultaneously. Typically, the four loops become locked in less than 10 seconds and seldom require more than 30 seconds.

## 5.4 Data-Log and Control Functions

A set of new measurements are made every 640 ms; for post-processing in TDMA and OPME studies, a concise data set is written on magnetic tape. This facility has enabled many repeated processings of interesting data.

The events in this experiment occur too quickly for detailed operator roles, but for experiment control it was desirable to have a control/monitor program. Digital displays and pen recorders, the status of ranging stations and key parameters were all under console control.

## 6. FIELD TRIALS

The first field trials were conducted prior to launch of Hermes. With a transponder simulator on a boresighted tower 15 km away, RF tests checked out the delay-lock loops and calibration procedures. In this phase, many problems in interfacing were encountered and solved. Confidence in the expected accuracies was achieved.

Phase I occurred in the spring and summer of 1976, with stations in Ontario and Quebec. The feasibility of CENSAR and the validity of the algorithms were verified. There were many problems in keeping CENSAR equipment and stations in operation.

Phase II was carried out in the spring of 1977 with stations in the Manitoba and Ontario areas. More extensive data in longer periods were accumulated. Operations were much smoother and numerical results were yet more pleasing.

## 7. RESULTS

The essential results of the synchronization portion of this Hermes experiment are that the CENSAR concept had been shown to be valid and that the selected implementation is feasible. Specific technological advancements and technical data are discussed in this section.

## 7.1 Development of the CENSAR Concept

In its original form, this new type of TDMA synchronization scheme applied only to global systems, wherein geometries are spheroidal and stations can receive their own signals. By extension of the concept to spot-beam satellites (deBuda, 1972), the scope of potential applications was considerably widened. The advent of satellite switching is expected to increase interest in centralized synchronization.

## 7.2 Algorithms

Computational procedures have been developed for spheroidal and ellipsoidal geometries. The satellite is at the intersection of three of these surfaces; since a direct

solution in real-time is not viable (Nuspl et al, 1975), an algorithm which solves this problem is a key constituent of CENSAR. Algorithms have also been designed to control the delay-lock loops and the open-loop bursts by user stations. A start-up algorithm is completely automatic and requires no orbit data. All of these algorithms were extensively analyzed, checked in simulations and verified in operations.

### 7.3 Hardware

Equipments have been designed according to CENSAR principles and constructed using modern technology. The new developments include a multi-function synchronization burst generator, timing recovery circuits, burst ranging techniques which have a precision of 1 ns, delay-measuring equipment which is used for four measurements, and interface circuits. Crucial to the performance are the two-hop delay-lock loops which operate independently in a time-share mode with three ranging and one check stations.

### 7.4 Software

Algorithms have been programmed to operate off-line as much as possible, yielding coefficients and parameters for real-time operation. Real-time software was prepared for a modest mini-computer facility (PDP 11 family). These programs include operations control and display, and also data log routines.

### 7.5 Integration

A significant aspect of this project has been the integration of technologies and equipments. The delay measurements are a prime example of effective integration of hardware and software methods. Due attention was paid to interfacing of the computer and the measuring equipment and of the IF and RF equipments. Calibration of the complete system required careful procedures to yield precision and accuracy.

### 7.6 Technical Performance

The performance of the CENSAR system, as implemented for synchronization tests with Hermes, is summarized in Table I. A user station recovered symbol timing to about 2 ns under operating conditions; the self-noise contribution has been measured to be ±0.2 ns rms. The control bits broadcast to all stations were sent in an erasure channel, with erasures at one per minute under operating conditions. From measurable error rates in the signalling system, the calculated error rate for these control bits is 1 in $10^{20}$ approximately. Figure 3 is a typical result of range measurement and figure 4 illustrates system errors from all sources.

### 7.7 Data Base

All data produced during CENSAR operations has been

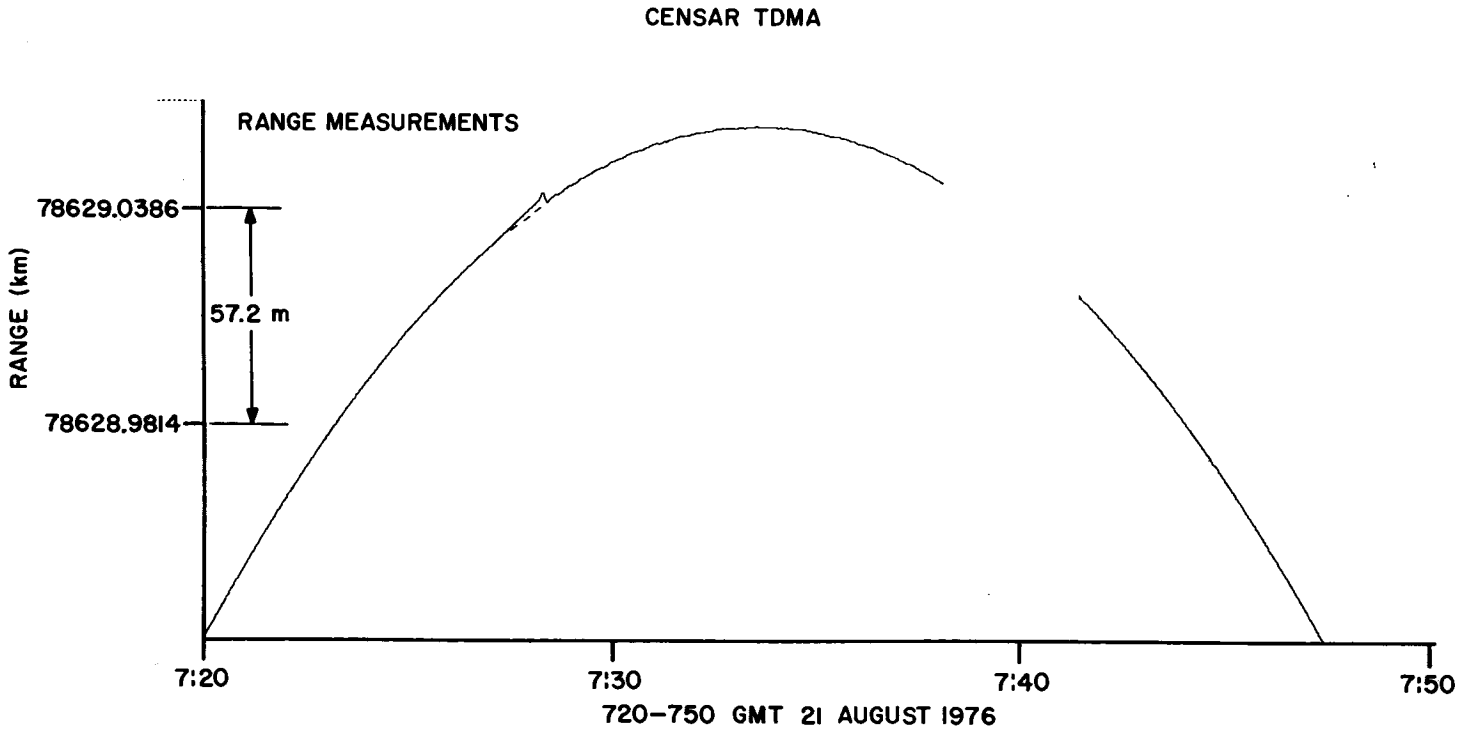


Figure 3. Typical result of range measurement.

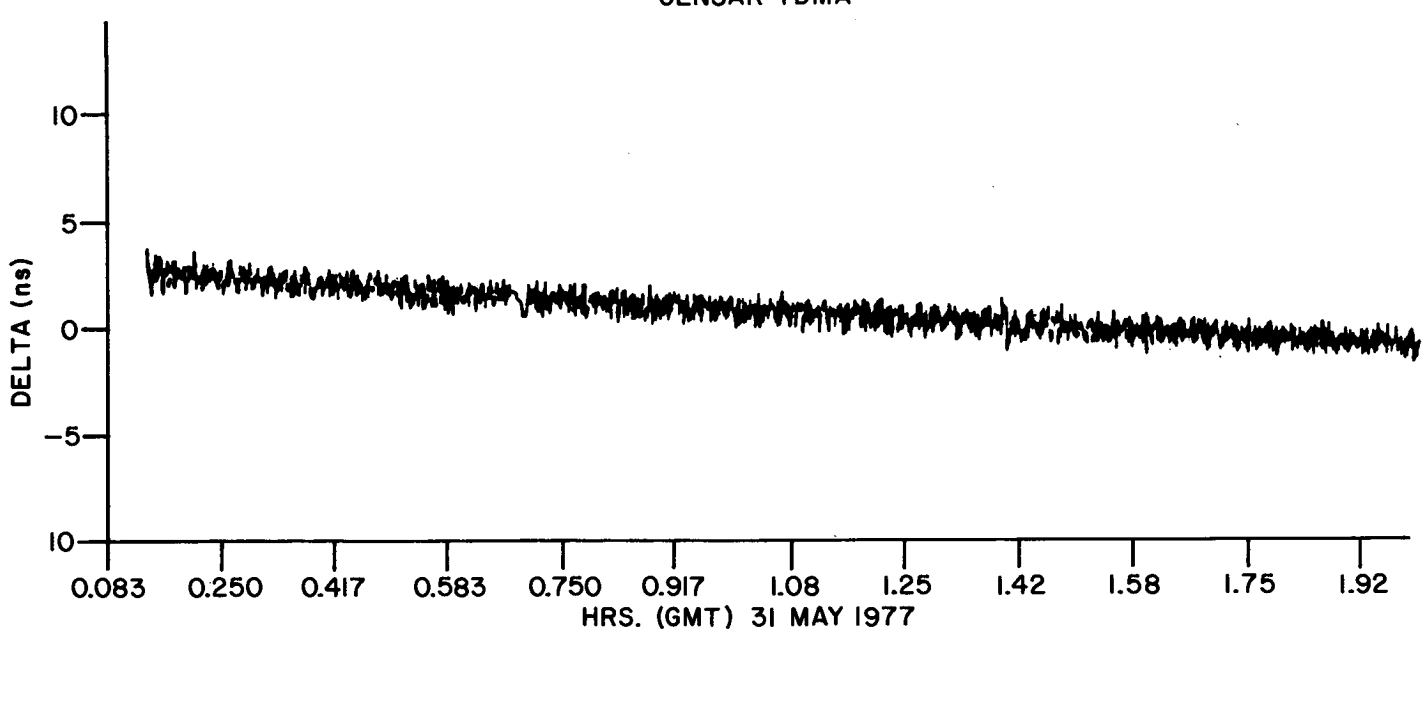


Figure 4. System Eooro (calculated delay-measured delay).

recorded in concise form on a few magnetic tapes. This data base was used in checking the accuracy of the CENSAR system and in the companion OPME studies. Some of the data is also being used to investigate doppler and possible relativistic effects on time transfer.

TABLE I

CENSAR Performance Data

| | |
|---|---|
| Start-Up Time: | typical - 10s |
| | worst case - 30s |
| Symbol Timing Recovery: | accuracy - < 2 ns peak error |
| | ±0.2 ns rms self-noise |
| Control Bit: | erasure rate, typical - 1/min |
| | error rate - < 1 in $10^{20}$ (calculated) |
| Synchronization: | loop precision - ±1 ns |
| | accuracy, short term - ±5 ns |
| | 24 hour - ±20 ns (3σ) |
| | guard time - < 30 ns (2 bit durations) |

## 7.8 TDMA Synchronization Costs

Being experimental and pioneering, the CENSAR experience cannot be expected to yield accurate information on costs for future systems. However, project allocations in dollars and man-years are indicators which can be used for planning and budgetary estimates. For example, IF equipment for five stations was procured for less than $500,000 (1975). DOC staffing ranged from one professional to a high of two professionals plus two technicians before and during operations. Estimated costs for specific-purpose TDMA stations are $25,000 per station (IF equipment for TDMA, in quantity production).

## 7.9 Experience

This CENSAR experiment was a pioneering endeavour in a new approach and has provided 'hands-on' experience with advanced technologies for project staff and for Canadian companies. The operations with Hermes were very interesting; there were several formal demonstrations, and some seminars and briefings to interested groups and presentations at international meetings. The CENSAR synchronization method is widely understood and accepted; INTELSAT is sponsoring open-loop synchronization techniques (Dill, 1977).

## PART II - ORBIT PERTURBATION MEASUREMENTS USING CENSAR DATA

### 8. OBJECTIVES OF THE ORBIT PERTURBATION MEASUREMENT EXPERIMENT (OPME)

As described above, the satellite may be thought of as lying at the intersection of three ellipsoids with foci at the ground stations and with range sums in proportion to the observed values of $T_1+T_k$ $K = 2,3,4,5$. For TDMA synchronization, conversion from time delays to distances need not be performed, but for satellite position determination the conversion is necessary and introduces a host of discrepancies between observed time delay and true range divided by C, the speed of light. With appropriate compensation a single set of TDMA data permits the accurate determination of satellite position in three dimensions, and a sequence enables the satellite orbit to be determined.

The objectives of the OPME portion of this experiment are to demonstrate that the precise time delay measurements of the TDMA experiment permit accurate satellite position (< 100m) and motion determination, and to investigate the potential of this tool for the study of orbital perturbations and satellite stationkeeping. This part of the paper relates principally to the derivation of satellite position from TDMA data and to an examination of the relevant accuracies, sensitivities and performance of this approach which obviates the use of additional conventional tracking. Analytic predictions are compared with actual experimental results and possible sources of discrepancies are described.

### 9. SATELLITE POSITION DETERMINATION

The nominal relationship between satellite position $\bar{S}$ and observed time delay $T_1+T_K$ is given by the following

$$(T_1+T_K)' = (|\bar{S}-\bar{X}_1| + |\bar{S}-\bar{X}_K|)/C, \quad K = 2,3,4 \qquad (1)$$

where $(T_1+T_K)'$ = single hop propagation time delay (nominal)

$\bar{S}$ = satellite position

$\bar{X}_{1,\ldots.4}$ = location of station 1,....4

C = speed of propagation of light (free-space value)

The set of equations (1) does not permit a closed form solution for $\bar{S}$, and a variety of iterative approaches is possible. The selected algorithm (Algo 2; de Buda, 1973) stems from some properties of four spheres centered on the ground stations and passing through the satellite, an algorithm related to the TDMA requirement for synchronizing associated stations automatically.

Rapid convergence of this algorithm has been demon-

strated for the station locations of both experimental phases; initial satellite position errors of hundreds of kilometers reduce to centimeters within four iterations.

The solution for $\bar{S}$ is expressed in terms of an inverse basis which is a function of ranging station locations. An algorithm (Algo 1) has been written to generate a parameter set for each of the two experimental phases; it evaluates the inverse basis as well as several other parameters required for the determination of $\bar{S}$. This algorithm must be executed once per phase, and the parameters stored for use with all observations made with the given ranging and control station geometry. Subsequently the delay data may be processed through Algo 2 to create the satellite position history, which in turn may be input to orbit and/or perturbation determination routines. However, a closer scrutiny of the accuracy of the position solution is in order; sources of error in the observations and in the data processing may be examined separately and compensated as appropriate.

## 10. ERROR SOURCES AND COMPENSATION

Practically, a number of errors contaminate the observations; accordingly a more realistic representation of the observation model becomes:

$$T_1 + T_K = (|\bar{S}-\bar{X}_1| + |\bar{S}-\bar{X}_K|)/C + D_K, \quad K = 2,3,4 \qquad (2)$$

where $D_K$ accounts for all the increase in delay over the ideal free-space propagation delay. A description of the constituents of $D_K$ follows.

### 10.1 Equipment Delays

Transmission delays in the ground station equipment have been measured and form part of a correction to be applied to $T_1+T_K$ before the satellite position is determined. Typical values are 704 to 755 ns. The satellite transponder delay was not measured before launch, and attempts to calculate it from flight data have been basically inaccurate, for reasons to be described below. An estimate of 20 ns has been derived and gives reasonable results.

### 10.2 Propagation Delays

Two effects contribute to increase the actual propagation delay beyond that corresponding to a straight-line free-space value: refraction and propagation-velocity decrease in the ionosphere and the troposphere. Typical elevation angles from ground stations are in the order of 25° to 40°, and the geometric delay (that due to the path length increase above the straight line value) may be shown to be an insignificant fraction of the total excess propagation delay. Of the ionospheric and tropospheric delay effects, the former is about 2% of the latter for the frequencies of interest and is consequently neglected. The excess

tropospheric delay is compensated to a first order by removing the predicted monthly mean value (with elevation angle considered); a typical two-hop excess delay averages 40 ns, with a standard deviation in the order of 1 ns.

### 10.3 Clock Errors

The CENSAR clock may have both bias and drift errors, of which only the latter is relevant for OPME. (The time of each set of data may be related to the time of the first set in one experimental period, thereby removing any effects of clock bias.) Short-term clock stability (at $65.5360_3$ MHz) has been stated to be about one part in $10^7$. The clock errors introduce a small ($\approx$ 5m) discrepancy in absolute position but a negligible error in relative position determination, and are not compensated in our pre-processor.

### 10.4 Satellite Velocity

Satellite velocity relative to the ground stations causes a doppler shift of the received signal and introduces a potential for error because the delay measurements are not made exactly simultaneously. The frequency shift should have no significant effect since two-hop delays are measured, resulting in both positive and negative frequency shifts for each satellite-to-ground station link. The data could be interpolated between successive measurements to produce corrected values at the same time resulting in changes in the order of meters. Such interpolation is not implemented in our current pre-processor.

### 10.5 Ground Station Surveying Errors

The accuracy of the ground station co-ordinates has a fundamental effect on the parameter set and thereby on the absolute accuracy of the resultant solution for satellite position. (Station co-ordinate errors along the direction of the satellite may cause the same relative increase in satellite position errors, as do errors in the delay measurements.) Station co-ordinates have been surveyed to an accuracy of $\pm$ 5m in each parameter, and have been calculated at the focus of each antenna.

With an accurate orbit determination program, one may solve for station location biases as well as satellite orbital elements, but in the present implementation such biases are not computed.

## 11. SENSITIVITY ANALYSIS

Although the major error sources are recognized and the major deterministic components compensated, it is important to understand the effects, both relative and absolute, of uncompensated or stochastic error components. The need for this understanding becomes obvious when one considers the geometry of the satellite and ground station locations. The three ranging terminals are separated by distances of as little as 700 Km, yet the satellite slant

range is approximately 39000 Km. Errors in the short terrestrial baseline or delay measurements can 'tilt' the satellite-ground station triangles by some small angle but the long slant range amplifies the error in the position solution. Phrased alternatively, the three ellipsoids intersect at a very shallow angle, so that a slight shift of one ellipsoid shifts the intersection of the three by up to two orders of magnitude more. A check on the accuracy of the algorithm solving these nearly singular equations is in order before considering errors in station co-ordinates and delay measurements.

For both experimental phases, parameter sets were found using Algo 1 on the given station co-ordinates. Then, with nominal satellite co-ordinates, exact delay 'measurements' were calculated from Equation (1). These delay values were processed by Algo 2 and the resultant solution for $\bar{S}$ compared to the starting value. Within four iterations of Algo 2, the error in $\bar{S}$ shrank from several hundred Km to less than 15 cm.

## 11.1 Effects of $T_1+T_K$ Errors

Subsequently the nominal $T_1+T_K$ values were increased individually by 10m and $\bar{S}$ recalculated by Algo 2 with one 'perturbed' $T_1+T_K$ and two nominal $T_1+T_K$ values. The resultant $|\bar{S}|$ showed a variation of between 500m and 1500m, with the z component displaying greatest sensitivity.

Finally, all three $T_1+T_K$ values were simultaneously increased by 10m and the $|\Delta\bar{S}|$ shrank to almost 5m, approximately radially outward.

These numbers reflect the effects of increases in delay data as processed by Algo 2, including whatever computational errors there are. A more analytic approach is to evaluate the derivatives of $T_1+T_K$ with respect to $\bar{S}$, using Equation (1) or (2). The resultant differentials may be expressed as

$$\Delta\bar{Z} = A\ \Delta\bar{S} \qquad (3)$$

where $\Delta$ denotes a change in a variable

and $\bar{Z}$ = observation vector = $\begin{vmatrix} T_1+T_2 \\ T_1+T_3 \\ T_1+T_4 \end{vmatrix}$

$\bar{S}$ = satellite position = $\begin{vmatrix} S(1) \\ S(2) \\ S(3) \end{vmatrix}$

and $A = \{A_{ij}\}$, where $A_{ij} = \frac{\partial \bar{Z}(i)}{\partial \bar{S}(j)}$, $i,j = 1,2,3$

$$A_{ij} = ((S(1)-X_1(1))^2 + (S(2)-X_1(2))^2 + (S(3)-X_1(3))^2)^{-\frac{1}{2}} (S(j)-X_1(j)) + (S(1)-X_{i+1}(1))^2 + (S(2)-X_{i+1}(2))^2 + (S(3)-X_{i+1}(3))^2)^{-\frac{1}{2}} (S(j)-X_{i+1}(j)) \quad (4)$$

If A is nonsingular, $\Delta\bar{S} = A^{-1}\,\Delta\bar{Z}$ (5)

For Phase 2 station locations and a nominal $\bar{S}$, the eigenvalues, determinant and inverse of A were found to be respectively:

Eigenvalues of A, $\lambda_{1,2,3}$ = (1.61953, $-2.10063\times10^{-2}$, $9.37602\times10^{-3}$)

Determinant of A, $|A| = -3.18975\times10^{-4}$

$$A^{-1} = \begin{vmatrix} -16.6723 & -3.2396 & 20,4070 \\ -20.2886 & -51.4477 & 71.7170 \\ -122.7327 & -5.1235 & 127.7878 \end{vmatrix}$$

These eigenvalues emphasize the near singularity of the equations to be solved for $\bar{S}$, encouraging careful numerical analysis. The elements of $A^{-1}$ support the nonlinear numerical results above; an error in a single component of $\bar{Z}$ may be 'magnified' up to 150 times in the solution for $\bar{S}$. On the other hand, the same error in all components of $\bar{Z}$ causes a nearly radial translation of $\bar{S}$ of only half the magnitude of the error in $\bar{Z}$.

Consider next the state error covariance matrix, with $\bar{S}$ defined as the state vector, and $\bar{Z}$ as the observation vector. For a more general derivation, with $\bar{e}_S$ and $\bar{e}_Z$ as random variables representing the differences between actual and computed state and observation respectively we have:

$$\bar{e}_Z = A\bar{e}_S$$

neglecting higher order terms.

Then $\bar{e}_Z\,\bar{e}_Z^T = A\bar{e}_S\,\bar{e}_S^T\,A^T$

from which we find $\bar{e}_S\,\bar{e}_S^T = (A^T\,(\bar{e}_Z\,\bar{e}_Z^T)^{-1}A)^{-1}$

To evaluate the state error covariance matrix, we assume that observation noise is independent and all observation components have white noise of standard deviation n.

$$\text{Then } E\{\bar{e}_Z\,\bar{e}_Z^T\} = \begin{vmatrix} n^2 & 0 & 0 \\ 0 & n^2 & 0 \\ 0 & 0 & n^2 \end{vmatrix}$$

and the state error covariance matrix is

$$E\{\bar{e}_S\,\bar{e}_S^T\} = n^2\,(A^T A)^{-1}$$

For Phase II, $(A^T A)^{-1} =$

| | | |
|---|---|---|
| 704.9 | 1968.5 | 4670.6 |
| 1968.5 | 8201.8 | 11918.2 |
| 4670.6 | 11918.2 | 31419.3 |

The standard deviation of the position error magnitude may be taken as the square root of the trace of the state error covariance matrix, i.e., $\sigma_x$ = 200.8 ns, for n = 1 ns.

11.2 Effects of Station Co-ordinate Errors

A similar approach could be followed either analytically or numerically to ascertain the sensitivity of $\bar{S}$ to changes in ground station co-ordinates. A numerical sensitivity determination was performed, with consistent results. For the same set of $T_1+T_K$ as in 11.1, station co-ordinates were increased by 10m, a single co-ordinate for a single station, at a time. Algo 1 was used to generate a new parameter set, and then Algo 2 applied it to the constant $T_1+T_K$.

For the co-ordinate frame orientation employed (x through the prime meridian), $|\Delta\bar{S}|$ varied from 1300m to near zero. With the co-ordinate frame rotated so that x lay along the nominal satellite direction, a 10m change in a station x co-ordinate caused a change of up to 1466m in $|\bar{S}|$, while the same increment along the new y co-ordinate caused only a 41m change in $|\bar{S}|$. The solved-for value of $\bar{S}$ is much more sensitive to 'radial' station co-ordinate errors than to East-West errors.

12. TRANSPONDER DELAY PREDICTION

The provision of the additional station permits a redundant observation parameter, $T_1+T_5$, which might permit the solution of one more unknown, the transponder delay. This concept was explored, with negative results; for feasible station-to-satellite geometries, one may not solve simultaneously for satellite position and transponder delay. Numerically this became evident when an algorithm was written to operate on the difference between $T_1+T_5$ actual and predicted. Simulations showed that a transponder delay 'D' added simultaneously to each of $T_1+T_K$ shifted $\bar{S}$ outward almost radially. Thus $T_1+T_5$ predicted increased by D as well, for a very small discrepancy between $T_1+T_5$ predicted and actual.

Analytic support was provided for this conclusion by considering Equation (2) with the range of K increased to (2,3,4,5), with $D_K$ fixed as the transponder delay, now treated as the fourth state vector component. The state covariance and correlation matrices were evaluated, and the corre-

lation coefficient of transponder delay with spacecraft radial co-ordinate was found to be in the order of 0.9999 (Canadian Astronautics Limited, 1977). For such a high correlation coefficient between two state vector components, only a linear combination of the two may be found, as already observed numerically.

An effort to operate on differences between the $T_1+T_K$ (and thereby eliminate the common transponder delay element) resulted in the need to solve simultaneously three transcendental equations describing three hyperboloids of revolution intersecting at $\overline{S}$. These equations proved even more ill-conditioned than for the ellipsoids, and in subsequent work an 'engineering guesstimate' of 20 ns was used for the transponder delay.

## 13. PRELIMINARY RESULTS OF POSITION DETERMINATION

Before being processed by Algo 2, synchronization delay data was read from magnetic storage, decommutated, and passed through a pre-processor. The main functions of the pre-processor were to convert measurements to an appropriate unit, reject bad data according to flags or $\sigma$ rejection levels, correct for predictable delay errors and perform curve fitting for data compaction and smoothing. Using the parameter set generated by Algo 1, the pre-processed data was operated upon by Algo 2 to yield $\overline{S}$. The results for one run are plotted in figure 5 for comparison with the $\overline{S}$ values predicted from a previously-performed orbit determination.

Agreement is observed here for all three components of absolute position to within the accuracies of the orbit prediction. Relative motion predictions and observations are seen to agree closely, although some noise in the experimental data is apparent. The results of another run on a different date also demonstrated close x and y agreements, but with a significant z component difference.

Effort is continuing to allocate the discrepancy to experimental parameter errors (equipment delays, locations) and to errors in the orbit predictions. Further results will be published as they become available.

## 14. CONCLUSIONS AND REMARKS

The CENSAR concept has been shown to be valid and the objectives of the experiment with Hermes have been met. The experiment has demonstrated the technical feasibility of the selected implementation. The work has revealed that further technical improvements can be obtained and that reductions in the cost of TDMA synchronization may be realized by using open-loop methods. The experiment has also identified new areas for research or development.

The high resolution and frequency of delay data from the CENSAR system show great promise for accurate satellite position and motion determination. This process offers the

advantage of employing existing signals in this type of TDMA system, with no further hardware or satellite transponder time requirements. Sensitivities of the solved-for position to errors in station co-ordinates or delays have been described, and are of considerable interest for designing future systems for orbit determination. The potential ability to track the fine motion of a satellite in three dimensions should permit the improvement of existing orbit perturbation models. Some of the concepts in this paper may be fruitfully employed in other than satellite applications, for example, in terrestrial navigation.

## ACKNOWLEDGEMENTS

These experiments were the work of a large team of dedicated individuals. The authors acknowledge the support from DOC during this long project, and in the co-ordination and operations with Hermes and the ground stations. The authors are grateful to each member of the project, and particularly to S.M. Chow, D.A. Hill, K.E. Brown, H.H. Chan, and L. Green. The project team at Canadian Marconi Company is appreciatively thanked for the construction of the hardware equipment.

## REFERENCES

Canadian Astronautics Limited
1977 *OPME Users Guide*, Communications Research Centre, June.

deBuda
1972 Synchronization for Time Division Multiple Access Experiments, *Technical Report* RQ72EE4, Canadian General Electric Company Limited, June.
1973 Position Tracking a Spot-Beam Satellite from Delay Data, Canadian General Electric Company Limited, *Technical Report* RQ73EE1, January.

Dill, G.D.
1977 TDMA, The State-of-the-Art, *EASCON '77*, paper #31-5A, Washington, D.C.

Nuspl, P.P. and deBuda, R.
1974 TDMA Synchronization Algorithms, *EASCON '74 Record*, Washington, D.C., pp 656-663.

Nuspl, P.P. Davies, N.G., and Olsen, R.L.
1975 Ranging and Synchronization Accuracies in a Regional TDMA Experiment, *INTELSAT/IECE/ITE, Third International Conference on Digital Satellite Communications*, Kyoto, Japan, November, pp 292-300.

# HERMES DAMA EXPERIMENT

R.J. Campbell

Communications Research Centre, Ottawa, Canada

*Le satellite technologique de télécommunications Hermès a servi pour la mise à l'épreuve d'un système d'accès multiple par assignation en fonction de la demande (Demand-Assignment-Multiple-Access (DAMA)). Le satellite fonctionnait sur une seule voie par signal porteur (Single-Channel-per-Carrier (SCPC)), en mode d'accès-multiple par répartition des fréquences (Frequency-Division-Multiple-Access (FDMA)) à double bond. Le contrôle du système DAMA était centralisé, avec une voie de commande à accès aléatoire, et était relié au réseau téléphonique à commutation au poste de contrôle central (Central Control Station (CCS)). Les dispositifs DAMA ont été ajoutés au système de télécommunication du satellite sans modification préalable à ce dernier.*

*On a réussi à identifier plusieurs problèmes de mise en application tels la difficulté à établir les niveaux d'atténuement des échos, la lenteur du réseau quitté à céder le canal et le manque de sureté des appels venus d'un code régional autre que celui du CCS. Les inconvénients algorithmiques comprenaient notamment des difficultés de procédures pour placer des appels spéciaux ainsi que la ligne d'attente causée par la lenteur à déconnecter le réseau quitté. Toutefois, la réaction des usagers du système éprouvé a été favorable.*

## 1. Introduction

The purpose of this paper is to describe the demand-assignment multiple-access (DAMA) experiment carried out at the Communications Research Centre (CRC) from May to August 1976, using the joint U.S./Canadian Communications Technology Satellite (CTS) which has been renamed Hermes. A real-time simulation facility, developed for earlier DAMA research, became an essential element in the implementation of this experiment.

Work in demand assignment of audio channels for voice and/or data began at CRC just prior to 1970 when it was recognized that other systems such as the Single channel per carrier

PCM Multiple Access Demand Assignment Equipment (SPADE) (Werth, 1969) did not meet Canadian requirements for low traffic-capacity systems. In such systems, dedicated channels to each earth terminal cannot be justified. Consequently, a project was begun to develop a DAMA system for use in Canadian satellite communication systems which could be implemented in the late 1970's and early 1980's.

The characteristics of low capacity Canadian satellite communication systems for which demand assignment is well suited can be summarized as follows:

- low-cost earth terminals transmit and receive short-duration messages every day;
- the number of available satellite channels is substantially less than the number of terminals;
- all terminals are integrated into the switched-telephone network;
- all calls are billed automatically;
- calls may be pre-empted in emergencies.

As a result of various studies at CRC, a system with the following characteristics was chosen for further investigation using Hermes:

- a system in which a central control station (CCS) is responsible for system control, administration and billing functions;
- random access request channel(s);
- single-channel-per-carrier Frequency Division Multiple Access (FDMA);
- signalling to suit communication system employed, i.e., no special signalling modems;
- station addressing based on telephone system;
- double hop.

This centrally-controlled system reduces overall costs (in comparison with SPADE-type systems) by greatly reducing the complexity and cost of the remote terminals.

After some background work, it was decided to conduct an experiment using Hermes and a plan and schedule were prepared. The objectives can be summarized as follows:

- to demonstrate a working DAMA system in a real satellite communications environment to establish its capability of providing improved communications to remote communities;

- to obtain user reaction to the system;
- to test at least one DAMA algorithm;
- to ascertain DAMA implementation problems;
- to verify engineering calculations;
- to acquire information on the engineering and production requirements of DAMA equipment.

## 2. SYSTEM DESCRIPTION

### 2.1 Hermes DAMA System

The DAMA system studied utilizes central control. A block diagram of the overall experimental configuration is shown in figure 1. The central control, station (CCS) equipment located on the CRC site performs the functions of processing requests for channels, terminating calls, baseband switching for call connections between stations and the telephone network, logging and billing of calls and providing diagnostic messages to aid in trouble-shooting.

The experimental system used 5 of the 14 two-way voice channels available on Hermes for this project. One of these was used for control purposes - a one-way request (REQ) channel from the remote stations to the CCS and a one-way assignment (ASS) channel from the CCS to the remote stations. The remaining 4 were used as two-way voice channels. The selection of these 5 channels was not fixed; the total of 14 was divided into 3 pools - one for control, one for DAMA communications, and one for fixed-assignment communications. Channel pool assignments were made via a keyboard and during an experiment channels were frequently exchanged between the DAMA pool and the fixed assignment pool.

The Hermes experiment plan proposed the use of 5 remote terminals thus giving a system which had one more terminal than available channels. However, due to difficulties experienced by the contractor in developing and programming the DAMA controllers for the remote stations and due to problems encountered in commissioning the RCA terminals, the maximum number of terminals ever equipped with a DAMA capability was three. A simple block diagram of the remote stations is included in figure 1.

The numbering scheme and call set-up procedure was based on the telephone system, as far as the user is concerned, to minimize user training requirements. Thus, each remote station has its own 7-digit telephone number and all stations were considered to be in the same area code but "long distance" from each other. To place a call, a user simply dialed the digit '1' followed by a telephone number.

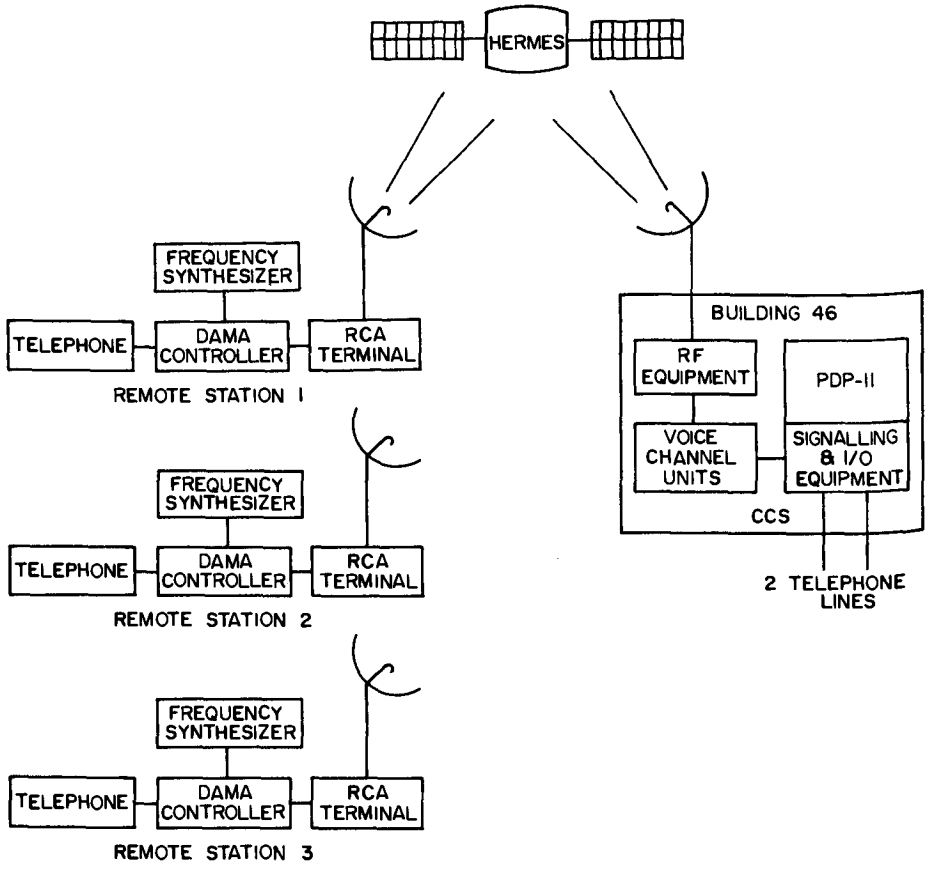


Figure 1. Configuration for DAMA Experiment Using Hermes.

## 2.2 Types of Calls and Billing

Based on conversations with potential users and planners, the following types of calls were implemented on the Hermes system:

- remote-station to remote-station calls;
- remote-station to switched-network calls;
- switched-network to remote-station calls;
- conference calls;
- broadcast calls;
- priority calls with automatic pre-emption of lower priority calls;
- selective drop-out and pre-emption in conference calls.

All the above calls are processed automatically without the intervention of an operator either at the CCS or in the switched network.

The billing procedure for the Hermes segment of calls is carried out by the DAMA central station computer. The portion of the call associated with the switched telephone network is billed by the latter.

## 2.3 Signalling

Baseband signalling suitably encoded with an error-detecting code is used between the remote stations and the central station. The interface for the signalling is made at the regular telephone interface to the remote terminals. Thus, no special signalling equipment is used which might require special high-speed or conditioned channels. Consequently, the DAMA capability can be added to any communication system which can support baseband signalling.

The user enters the telephone number of the party to whom he wishes to talk, as described earlier. Consider now only a remote-station to remote-station call. The remote-station controller processes the digits and transmits a request message over the REQ channel in a short burst. The REQ channel is shared by all remote stations and there is a finite probability of overlap. If the request messages are sufficiently short and the overall call rate is sufficiently low, then this probability can be very small, e.g., $\leq$ 1%. The CCS processes the request and assigns channels to all stations over the ASS channel.

The end-of-call procedure is initiated when one party hangs up. Various signals are transmitted between the remote

stations and the CCS on the channels used for the call, and the remote stations then return to standby.

## 2.4 Equipment

### 2.4.1 CCS Equipment

The CCS is controlled by a PDP-11/20 computer supported by an RK05 disc unit, a line printer, a CRT display with input keyboard, a high-speed paper-tape reader and punch, and 16K of core memory.

Each of the input control channels and the 4 voice channels is basically the same. Each has a buffer amplifier, the receive portion of a digital baseband modem, a programmable serial-to-parallel converter, and a general-purpose interface.

The serial-to-parallel converters are triggered by the first data transition and convert the serial bit stream into either 15-bit or 16-bit words. The length of the word and the number of words to be converted is controlled by the PDP-11 under program control. The PDP-11 is interrupted after each word is converted and has a period of time to respond equal to the time necessary to convert another word.

The peripherals for the output channel ASS and the common signalling line for the voice channels form the reverse of that for the input channels. The parallel-to-serial converters are also programmable. Provision is also made for inclusion of audible ringing, dial, busy and no-circuit tones on each of the voice channels.

The DAMA system allows calls to and from the switched telephone network using two consecutively-numbered private business lines equipped with voice station couplers. (The consecutive numbering of these lines effectively allows the central station to have one telephone number since the switched telephone network automatically routes calls to the second line if the first line is busy.) Thus, to call a remote station from the switched telephone network, a user calls the first number associated with these lines, the central station computer is interrupted by the ringing signal from the coupler, places a dial tone on the line and the user dials the 7-digit telephone number of the station he wants. (The dialing is restricted to *TOUCH-TONES* since the CCS has only *TOUCH-TONE* equipment.) The CCS provides information on the status of the call by the usual audible signals (ringing, busy, etc.). When the call is terminated in the switched network, the CCS uses its dial-tone detectors to initiate an end-of-call procedure. For calls from the remote stations to the switched network, the user dials the area code and 7-digit number of the party he wants and the central station computer seizes one of these lines and dials the area code (if necessary) and the 7-digit number of the called party.

Interconnection to the switched network requires a transition from the 4-wire satellite system to the 2-wire telephone system, using a hybrid transformer. Due to impedance mismatches, part of the signal from the remote station is reflected back to it about half a second later. An echo suppressor in the CCS attenuates this echo by 60 dB.

### 2.4.2 Remote Station Equipment

The basic remote station is a RCA terminal supplied to the experimenters by CRC. A DAMA capability was added by interfacing a DAMA controller at baseband, a frequency synthesizer unit at the low IF (≈ 100 MHz) and a transmitter switch in the transmit portion of the synthesizer circuits. No modifications were made to the RCA terminals.

The use of a PDP-11/10 for the remote station DAMA controllers proved to be adequate for the simulation facility. However, the cost, size, weight and power consumption made it unsuitable as a controller for the individual remote stations which were to be deployed in the field. Since experience had shown that a hardwired controller was just too inflexible even though the size, weight and power consumption were acceptable, it was considered that the time was right to begin the transfer of technology to private industry. Consequently, a contract was let to Digital Devices Limited (DDL), Montreal, to produce 5 microprocessor-controlled prototype remote-station DAMA controllers. A block diagram of the controllers appears in figure 2 and a more complete description can be found in Campbell and Kofsky, 1975.

In order for a remote station to be able to operate in an FDMA DAMA system, it must be able to switch quickly from one channel to another. Frequency converter units were designed and built at CRC (Fig. 3) for use with the terminals since it was not cost-effective to have RCA redesign their synthesizers to reduce the switching time from about 3 to 4 seconds to the required 100 ms. These converters are also controlled by the DAMA controller. Figure 4 is a photograph of the controller and frequency converter units.

## 2.5 Software

The CCS computer (PDP-11/20) was programmed in assembler language and the program resides entirely in core memory during DAMA operations. Although the disc system is used for program development, it is not used in the DAMA mode. The CCS program occupied $33676_8$ memory locations ($7135_{10}$ 16-bit words).

The program was written in modular form and uses a separate software 'processor' for each call in progress. A combination of flag scanning and automatic interrupts carries out input-output control and data-transfer functions.

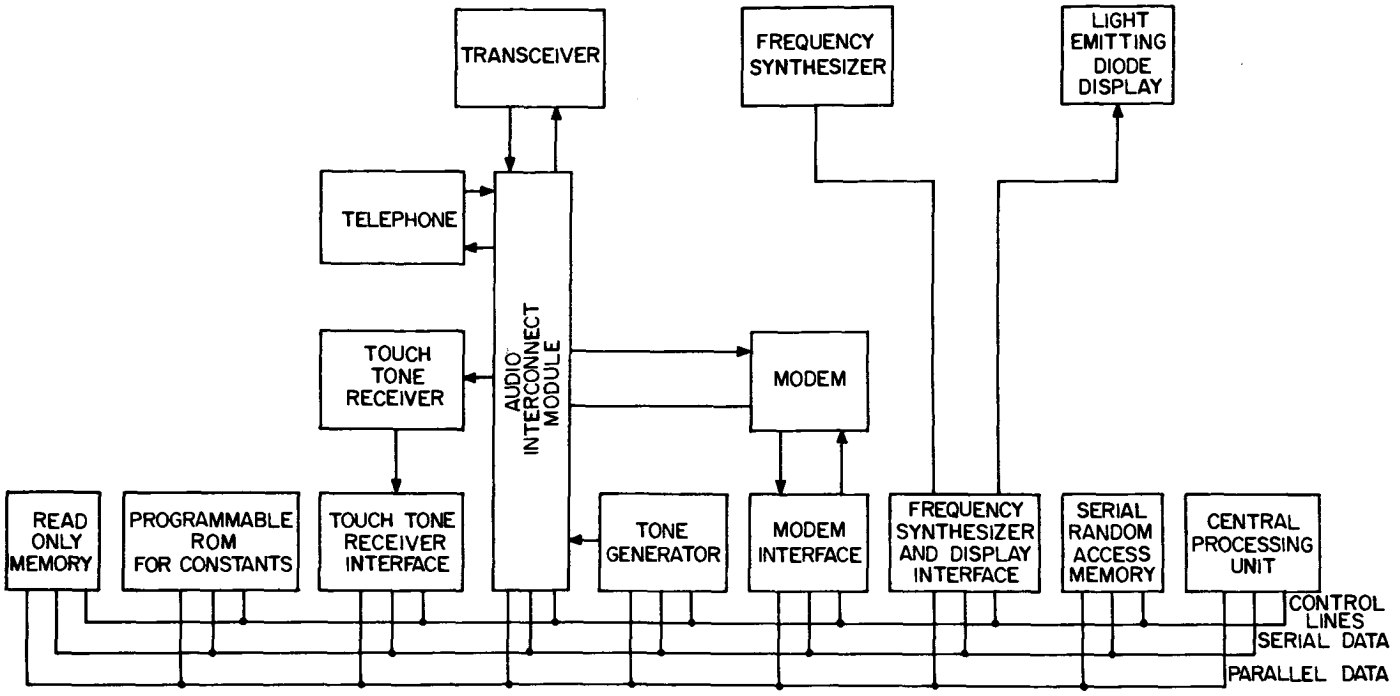


Figure 2. Block Diagram of DAMA Controller.

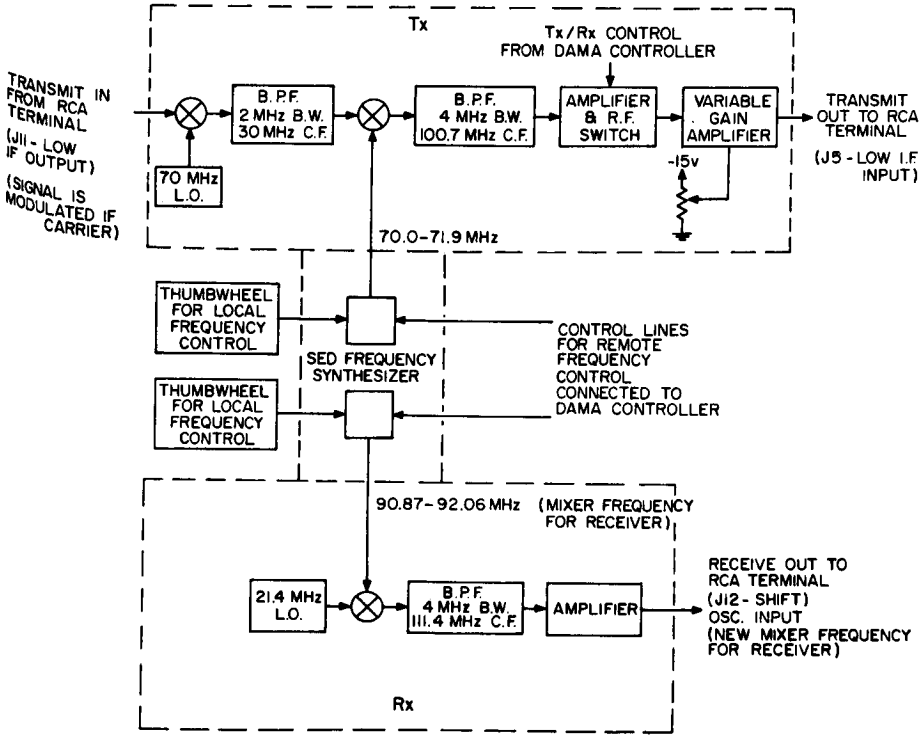


Figure 3. Block Diagram of Frequency Converters.

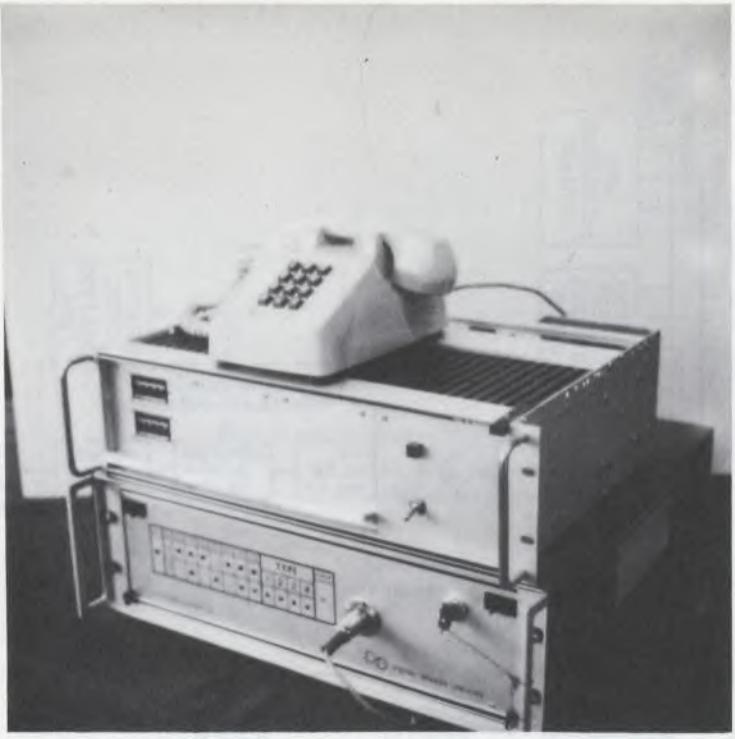

Figure 4. DAMA Controller (lower unit) and Frequency Converter (upper unit).

In general, the PDP-11/20 is fast enough to carry out all processing except for serial-to-parallel and parallel-to-serial conversion. Hardware converters were built to handle these functions; otherwise the CPU would have been too occupied with these tasks to respond to other chores without losing data. It was discovered during the simulation phase that a 16-bit word buffer was required for both serial-to-parallel and parallel-to-serial conversion since the CPU was frequently busy with other tasks and could not respond in an inter-bit time to place a word into or remove a word from the converters.

Records of calls are placed on the line printer after each call. A sample record appears in figure 5.

The remote-station DAMA controllers use custom-made CPU's with discrete TTL logic packs. Program memory was made up of four 1K x 8 programmable, read-only memories (PROM). Scratch-pad memory was made up of a 256 x 8 random-access memory (RAM). A special, serially-addressable memory for processing input-output data was made up of a 256 x 1 RAM. The program consisted of 2176 eight-bit words, which includes 1K for overhead.

```
03401 27035 67601 02540 12164 24022  - CODED ASSIGNMENT TO DESTINATION
37403 02435 34010 76721 76163 56021  - CODED ASSIGNMENT TO SOURCE
DATE  051/73                         - DATE (ROUTINE WOULD NOT ACCEPT CORRECT DATE)
TIME  13:22:56                       - TIME OF DAY (ROUTINE WOULD NOT ACCEPT TIME)
LENGTH  00127 SECS                   - LENGTH OF CALL
OVERHEAD  00011 SECS                 - TIME REQUIRED FOR SIGNALLING AND FOR DESTINATION TO ANSWER
SOURCE  7703                         - ADDRESS OF CALLING PARTY-EXCHANGE IGNORED
DESTN  (000)000-7701                 - ADDRESS OF DESTINATION
PRIORITY  1                          - PRIORITY OF CALL IS 1
CALL TYPE  2TO                       - CALL TYPE IS TOLL QUALITY DUPLEX VOICE
SECURITY  0                          - NO SCRAMBLER USED
************************
37403 02435 34010 24541 12164 56021
DATE  051/73
TIME  13:27:13
LENGTH  00086 SECS
OVERHEAD  00007 SECS
SOURCE  7703
DESTN  (613)820-5053
PRIORITY  1
CALL TYPE  2TO
SECURITY  0
************************
```

Figure 5. Sample Billing Output.

The program language is unique to DDL and is task oriented. The program itself is modular and operates in interrupts mode.

## 3.0 EXPERIMENTAL PROCEDURE

The procedure recommended by the CRC/Hermes personnel for checkout of the experimental system (RCA terminals, satellite link, CCS equipment) had two disadvantages: it occurred during scheduled experiment time, and it required too many operators to conduct non-routine tasks with a substantial probability of human error. To reduce lost experiment time and minimize human error, a modified procedure was developed.

In the new procedure, the Hermes operator did the baseband patching and switched the voice-channel units to the proper frequencies before the start of the experimental period. The remote terminals were converted to the full DAMA configuration, except that the frequency synthesizers were under manual control. At the start of the experiment period, the various types of signals to be used during the experiment were exchanged between the CCS and the remote stations over each channel. This procedure reduced the pre-experiment checkout time from between 15 and 30 minutes to between 5 and 10 minutes.

After checkout, calls were made to and from the remote stations according to a schedule drawn up subsequent to the previous experiment period. The types of call scheduled for any particular experiment varied widely. Occasionally schedules were changed during an experiment to accommodate unforeseen problems such as equipment malfunctions, procedural errors, and/or programming errors.

It became apparent that baseband simulation was inadequate for solving RF equipment problems such as frequency-synthesizer control and RF carrier turn on. Consequently, an RF simulator (Fig. 6) was set up between the remote terminals in trailer T2 near the CCS at CRC. The terminals' 70 MHz cables were disconnected from the up and down converters and were connected to cables running outside T2 to the voice-channel units in the CCS. This arrangement simulated the RF link but not the satellite delay. The baseband signals to and from the voice-channel units were connected to the 7-track tape recorder in essentially the same way as they had been for the baseband simulator, to simulate the delay. Although this arrangement could only be used every other day, when the U.S. experimenters were using Hermes, very large blocks of time became available to carry out changes and/or additions to the DAMA system and test them before using Hermes again.

## 4. OBSERVATIONS

### 4.1 General

The overall quality of the Hermes voice channels was much better than the channels used on the baseband simulator. Paradoxically, this caused a few problems, since a few unwanted signals due to reflections and mixing operations now had a signal-to-noise ratio high enough to trigger some detectors which they had not triggered before when such signals were masked by noise.

The other notable problem was the sensitivity of the echo suppressors in the system. The areas in which the remote stations were operated were so noisy that audible background noise from nearby equipment triggered the suppressors and the user in the remote stations was not able to hear the person in the switched telephone network. Adjustments to eliminate this false triggering reduced the sensitivity of the echo suppressors to the point where echoes were not suppressed. A compromise setting was finally used which allowed some false triggering in the background noise.

### 4.2 Features Tested

The following features and types of voice calls were tested and demonstrated:

- remote-station to remote-station calls;

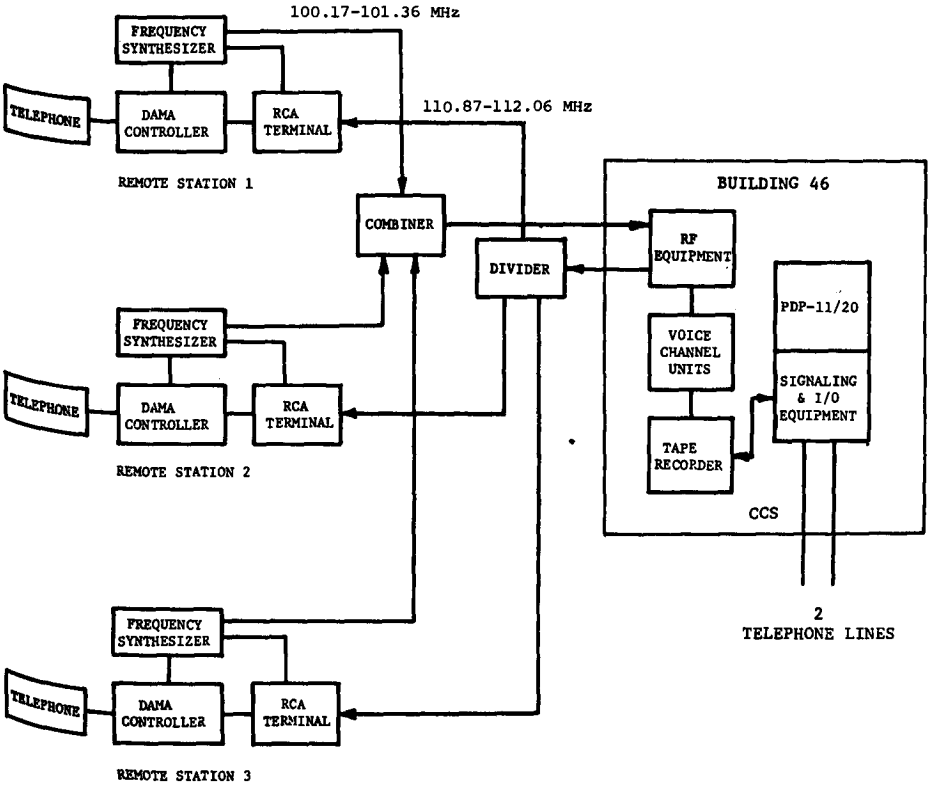


Figure 6. Configuration for DAMA Equipment Using RF Simulator.

- remote-station to switched-telephone network calls;

- switched network to remote-station calls;

- conference calls with selective drop-out, i.e., a member may drop-out without ending conference call;

- broadcast calls to remote stations originating from both remote stations and the switched network;

- priority calls with pre-emption of calls of lower priority already in progress, including pre-emption of members of a conference call without ending the conference call.

Remote-station to remote-station calls were the most difficult to get working since they involve 3 stations (two remotes and the CCS) and 3 CPU's which must all work together at the right times. However, once the initial call set-up difficulties were eliminated, these types of calls were the most reliable, the fastest to set-up (about 2 seconds) and the fastest to release (about one second), since the signalling was optimized for the system and there was no interaction with the switched network.

Remote-station to switched-network calls were slower to set-up since the CCS computer had to seize a telephone line and re-dial the number required in the switched network. This type of call was about as reliable to set-up as the remote-station to remote-station call, although on some occasions wrong numbers were dialled. This was traced to incorrect signal levels to the TOUCH-TONE decoders in the remote stations which caused incorrect detection of the digit 8. By coincidence the digit 8 did not appear in any remote-station to remote-station calls but appeared in most remote-station to switched-telephone-network calls. A cross check of dialled numbers with authorized test numbers was performed by the CCS during checkout. The disconnect time for this type of call was about as long as for the remote-station to remote-station call. However, when the party in the switched network hung up, it took 20 to 30 seconds before the switched network returned a dial tone to the CCS. The CCS then carried out the end-of-call procedure with the remote station.

Switched-network to remote-station calls were the most inconvenient to place due to the dialling procedure. The user had to dial the CCS. After one ring, the CCS seized the line and placed a dial tone on it. At this point the user dialled the 7-digit telephone number of the remote station and the call was set-up. The reliability of call set-up for this type of call depended on the source of the switched network call. A caller in the Ottawa area experienced no difficulty in the second stage of dialling. If, however, the caller were in Montreal, calls placed at night were all successful but none of the daytime calls were com-

pleted. The TOUCH-TONE receivers were checked and found to be functioning normally. One possible explanation is that the telephone lines did not meet the switched network specifications during the day. This problem was not pursued further due to time limitations. This is certainly an area requiring further investigation. The comments about the end-of-call for remote-station to switched-network calls also apply for this type of call.

Special calls, such as conference, broadcast or priority calls require a rather complex dialling sequence. For any calls other than the ordinary priority 1 voice call, the user must perform the following dialling operations:

- an asterisk to indicate to the controller that this is a special call;
- one digit to specify the priority of this call;
- the digits of the telephone number;
- a digit for the type of message;
- a digit for the mode (simplex or duplex);
- a digit for the quality (toll or field);
- a digit for the security (clear or scrambled);
- an asterisk to indicate to the controller that all the call information has been entered.

This procedure was used since only one keypad (on the telephone sets) was available.

Conference calls required the user to dial the special sequence of numbers to reach the first party. After that, additional members could be added to the conference by simply dialling the 7-digit number of the desired party. (This simplification was possible because the CCS monitors the channels for these TOUCH-TONE signals.) The special dialling sequence to initiate the call was very inconvenient and difficult for most users and almost all expressed a desire for a special button for conference calls. The users liked the capability of adding members at any time, of dropping individual members without ending the conference and of reconnecting such members.

Broadcast calls were also set-up with the special dialling sequence, and again the users expressed a desire for a special button. The recipients of a broadcast call were somewhat uncomfortable with this type of call since it is one-way and the recipients could not talk to the 'broadcaster'. They did like the ability to drop out and make other calls while the broadcast was still in progress.

By far the most popular type of call was the priority

call with associated pre-emption of on-going calls if necessary. The pre-emption, which the party pre-empted has no means of preventing, is automatic. The central station commands the pre-empted remote station to return to standby and the user hears a brief tone in the handset just prior to the dial tone. Most users who were pre-empting other users favoured both the pre-emption feature and the way it was carried out and said that they wished they had such a feature in the existing telephone system.

### 4.3 Billing

As each call was processed by the CCS, the parameters necessary for billing the call were stored in a table in core memory. These parameters were: source address, destination address, date, time of start of call, total length of call, overhead time (signalling, ringing, etc. durations), priority, call type, security (automatic insertion of a scrambling device), and any diagnostic messages to aid in the debugging of a call which may not have gone through. A sample of the output produced after each call is given in figure 5. The first line, which is a string of numbers, is a coded version of the assignment message for debugging purposes and would not normally be part of the billing information.

### 4.4 Statistics

It was the intention to gather statistics on the DAMA system, such as percentage of each type of call completed, reliability of the signalling system, performance of the coding system in detecting errors, fastest call rate which the CCS could handle, user reactions to call set-up procedures and system features. However, developmental problems occurred in both the controllers and the earth terminals, such that early in the experiment there was a shortage of controllers and later a shortage of terminals. Consequently, insufficient data was gathered to make statistically meaningful statements about the system. However, the following observations were made.

On 25 August 1976, a demonstration of the types of calls and features described in Section 4.2 was given to government departments and agencies. Twelve out of 55 calls were not completed on first try giving a probability of connection for the system of 78%. On 27 August 1976, two other demonstrations were given to government departments, agencies, and industry, during which 111 calls were made and 16 were not completed on first try giving a connection probability of 86%. It must be noted however, that on both occasions one remote station was producing errors of a type which were not common to all remote stations. Thus the probability of connection for that station was less than that for the system; for other stations, it was better.

There was no instance of the error-detecting code failing to detect an error.

Users were impressed with the speed with which a call was completed in the case of remote-station to remote-station calls, where there was no interaction with the switched network. The people who tried the system made favourable comments about its features as mentioned previously. However, no long-term user reactions were obtained.

The most critical phase of the call procedure is the end of the call, which takes much longer to carry out than the call set-up procedure for calls involving the switched network. The effect of having a longer queue to end a call than to start one is definitely an area requiring further study.

The echo suppressors were difficult to adjust , due to background noise, but since they did not affect the DAMA signalling, little effort was expended in their adjustment. This problem is common to all satellite systems interfacing to the switched network, whether they use DAMA or not.

It was observed that some sort of feedback to the user is required during the set up of a call in a new system such as this. In some instances, the user was allowed to hear some of the signalling in order to give him the impression that the system was still 'alive'.

## 4.5 Sharing of Experiment Time with Other Users

From time to time, the satellite voice channels were shared with other users. This occurred with both narrowband and wideband experiments.

Time was frequently shared with the TDMA experiment which used a digital, wideband signal spread over the entire voice-channel band. No mutual interference was observed. This mode of operation increased the time each experiment had on Hermes and, at the same time, demonstrated that under these circumstances such narrowband and wideband communications services could share a communications band.

Occasionally, the DAMA experiment was conducted while another experiment was using a fixed voice channel (or channels). The DAMA system then excluded these fixed channels from the pool of frequencies available for assignment and control. Both experiments carried on without mutual interference, demonstrating the ability of a DAMA system to operate independently and interference-free from a fixed assignment system using channels placed randomly throughout the same band. At times during the DAMA experiment it became necessary to allot one of the DAMA channels for an experiment using a fixed frequency. Simple commands on the CCS input keyboard removed the required channel from the DAMA pool, demonstrating that a DAMA system can allow temporary transfer of some channels from the DAMA pool to a fixed-channel pool should the need arise.

## 4.6 Reliability of Software Systems

The software system in the CCS was very reliable. Reloads of the program were extremely rare and only required after serious hardware malfunctions or program changes. If the computer had not been used for some other task between experimental periods, it was sufficient to simply turn the computer on and load the starting address before each experiment period.

The software in the remote station microprocessors was also reliable. The program was stored in programmable read-only memories (PROMS). Various sub-routines were incorporated to return the units to standby if something went wrong. A case never arose where it was impossible to initialize the controller by turning it off, and then on again.

## 5.0 CONCLUSIONS

Each of the objectives of the experiment was achieved at least in part.

The main objective of demonstrating a working DAMA system in a real satellite environment was achieved. A centrally-controlled, random-access request channel, single-channel-per-carrier, FDMA, DAMA system using baseband signalling was added to an existing satellite communications system, without any modification to the later system equipment.

User reaction to the system was obtained only during the demonstrations. Although the reaction is somewhat limited, it was in general favourable with respect to the operations the user must perform to set up a call, the feedback given to the user during call set up, the time required to set up a call and the features of the system, e.g., priority, pre-emption conference, etc.. It should be noted that the DAMA system was preferred to the communication system provided for experimenters using the Hermes satellite for two-way voice communications. The Hermes procedure required operator intervention to place calls to and from the switched network. Calls between remote stations required non-standard dialling.

A DAMA algorithm devised at CRC was implemented. Time did not permit its full testing but did allow demonstration of the various calls and features outlined earlier. Shortcomings and areas requiring improvement were identified, e.g., end-of-call procedure, signalling in remote-station to switched-network calls, termination of calls by the user in the switched network. In certain instances, procedures and/or signalling were changed to improve the DAMA system performance.

Various implementation problems were uncovered. Interconnection to the switched network is an area which requires special attention as far as interfacing, billing, and call set up are concerned. In the remote terminals, obtaining

adequate turn-on and turn-off of the RF carrier and frequency agility can be troublesome if the RF equipment is not designed with a DAMA capability in mind.

The engineering calculations, e.g., time delays, time windows for signalling, signal levels, interfacing requirements, etc., were verified. Verification of performance calculations, e.g., probability of call completion first time, probability of error in signalling, call capacity of the CCS, etc., was not possible due to the slippage in the project to the point where time did not permit their testing.

Useful information on the cost of adding this type of DAMA capability to the remote terminals in a satellite communication system of this type has been gathered. The degree of effort and time required to implement a DAMA capability can now be estimated much more accurately. Central station costs, etc., are not as easily estimated, since the CCS was an in-house effort and not on a scale comparable to that of an operational system.

## REFERENCES

Campbell, R.J. and Kofsky, H.
1975 A Low-Cost, Flexible Demand Assignment Multiple Access Controller for Small Terminal Satellite Communications, paper number 75263, *International Electrical, Electronics Conference and Exposition*, 29-30 September, 1 October, Toronto, Canada.

Werth, A.M.
1969 SPADE: A PCM FDMA Demand Assignment System for Satellite Communications, *INTELSAT IEE International Conference on Digital Satellite Communications*, 25-27 November.

# A DIGITALLY IMPLEMENTED COMMUNICATIONS EXPERIMENT UTILIZING THE HERMES (CTS) SATELLITE

H.D. Jackson and J. Fiala

NASA Lewis Research Center, Cleveland, U.S.A.

*Le programme expérimental Hermès (STT) marque un effort significatif en vue de nouveaux développements qui réduiront le coût de la distribution des services par satellites. La technologie avancée des répondeurs de satellite et de petits terminaux terriens peu coûteux ont fait l'objet de démonstrations au cours de l'exécution du programme Hermès. Un autre élément du système qui promet de réduire le coût de la transmission touche la réalisation de la liaison de télécommunications.*

*Cette communication décrit une expérience menée conjointement par les laboratoires NASA-Lewis et COMSAT et qui utilisent le STT pour démontrer la réalisation d'une liaison de transmission numérique et ses avantages par rapport aux systèmes analogiques conventionnels. On y décrit une expérience de transmission par réalisation numérique (DICE) qui démontre la souplesse et l'efficacité de la transmission numérique des signaux son et image de la télévision, des signaux téléphoniques et des données à débit binaire élevé.*

*La présentation du concept de cette expérience qui se concentre sur l'évaluation de la télévision numérique en duplex intégral dans la représentation à n éléments des téléconférences est suivie d'une description de l'équipement unique mis au point pour produire:*

1. *Des signaux de télévision de haute qualité NTSC (National Television System Committee - Comité national du système de télévision des Etats-Unis) à partir d'un codec numérique de TV COMSAT (CODIT) employant un codage MIC différentiel entre deux images à un débit nominal de 43 Mbps. L'équipement CODIT comprend également une fonction de multiplexage par répartition dans le temps pour permettre d'ajouter un train de données externes comme celui que fournit le système phonique COMSAT CODEC (SIDEL).*

2. *Soixante voies de conversation de haute qualité à partir d'un codec (SIDEL) utilisant une combinaison unique de modulation en delta et d'interpolation de signaux vocaux par voie numérique pour obtenir une transmission de haute qualité avec une compression de 4 à 1 des*

*données. Le débit binaire de sortie est d'environ 1 Mbps.*

3. *La transmission optimale de signaux numériques sur la voie de transmission d'un satellite avec une modulation QPSK avec débits binaires de 1, 22, 32, 43 et 49 Mbps. La conception technique particulière du COMSAT rend possible le fonctionnement d'un seul modem avec une vaste gamme de débits binaires en utilisant des modules enfichables permettant ainsi la démonstration de divers systèmes.*

*Les auteurs décrivent le système de multiplexage par répartition dans le temps à duplex total du DICE et présentent des considérations sur la mise en oeuvre de l'expérience, notamment l'effet des convertisseurs élévateurs et abaisseurs, les exigences relatives à l'émission et à la réception des terminaux terriens avec et sans codage des erreurs, ainsi que les budgets de la liaison du secteur spatial.*

## Introduction

The demand for satellite communications services is rapidly expanding. As stated by U.S. Federal Communications Commission Commissioner Abbot Washburn (1976) - Bringing together the various techniques in the advancing communications satellite technology will result in considerably lower overall costs to the users. Increasing use of digital communications techniques should mean an increase in the number of usable channels per pound in orbit.

In this light, the advanced technology provided by the CTS experimental satellite high-power transponder and small inexpensive earth terminals has been extensively demonstrated.

A natural extension of the communications link experimentation on Hermes is associated with the methods of transmission. Digital transmission of voice (Su et al, 1976; Syderhoud, et al, 1974; and Goldberg, 1976) as well as television (Gatfield et al, 1977 and Gatfield, 1977) has been investigated worldwide and a variety of techniques have evolved. In an attempt to obtain an assessment of the feasibility and implementation problems associated with different techniques of simultaneous transmission of video, voice, and data in digital form, an experimental program using CTS was proposed.

The proposed Digitally Implemented Communications Experiment (DICE) was designed to focus on the development and performance evaluation of a variety of video, audio, and data digital communications techniques. The primary configuration for the experiment uses the small earth terminals at NASA/LeRC and COMSAT. Full digital duplex operation is being

demonstrated using both the 200W and 20W channels on Hermes. Data such as carrier-to-noise ratios bit error rates and baseband signal quality are being measured and correlated with up/downlink transmission variables in order to define levels of performance for a variety of digital configurations. Operational/economic data are also being compiled to show the cost effectiveness and practicality of the digitally compressed video voice/data system.

This paper concentrates on the development, integration, and operation of a flexible communication system for digital satellite transmission. The primary communication medium considered is high-quality color television augmented by multichannel voice and data. The system concept as well as preliminary results are described in the following sections.

## SYSTEM DESCRIPTION

Figure 1 shows the basic communication system for a DICE demonstration. The LeRC Portable Earth Terminal shown in the figure was configured to support DICE demonstrations in the field while a fixed terminal at LeRC is used for in-house demonstrations and experimentation. Figure 2 is a more detailed breakdown of the baseband-to-microwave system configuration. Using figure 2 as a reference, the signal flow and DICE system description follow.

## UPLINK

### DICE Transmit System

Program color video and the associated audio are inputs to the CODIT analog-to-digital PCM converter. The PCM video data stream (8 bits per sample) is converted to DPCM (4 bits per sample and a sample rate of 10.7 MHz) to provide a baseband video data rate reduction of 2:1 (before input to the multiplexer). This rate reduction is accomplished by a circuit which uses preceding samples to predict the value of the next sample. The more accurate the prediction, the less bits required to represent the information.

The DPCM video output bit stream is then fed to the multiplexer which formats the data to allow for the addition of line and frame synchronizing unique words, program audio and SIDEL audio within the horizontal sync interval. Figure 3 shows the timing of the time-division multiplexer. The four traces show the time-division multiplex format for the composite video (near the horizontal sync) and the time slots during the horizontal sync period for the unique word, program audio, control-channel audio, and SIDEL audio data. (These schematic curves are *not* drawn to the same time scales). The inserted digital bits have also been timed to avoid interference with the other video synchronizing pulse edges.

The SIDEL system is a 60-channel digital speech interpolation (DSI) system. The audio input signals are digitally

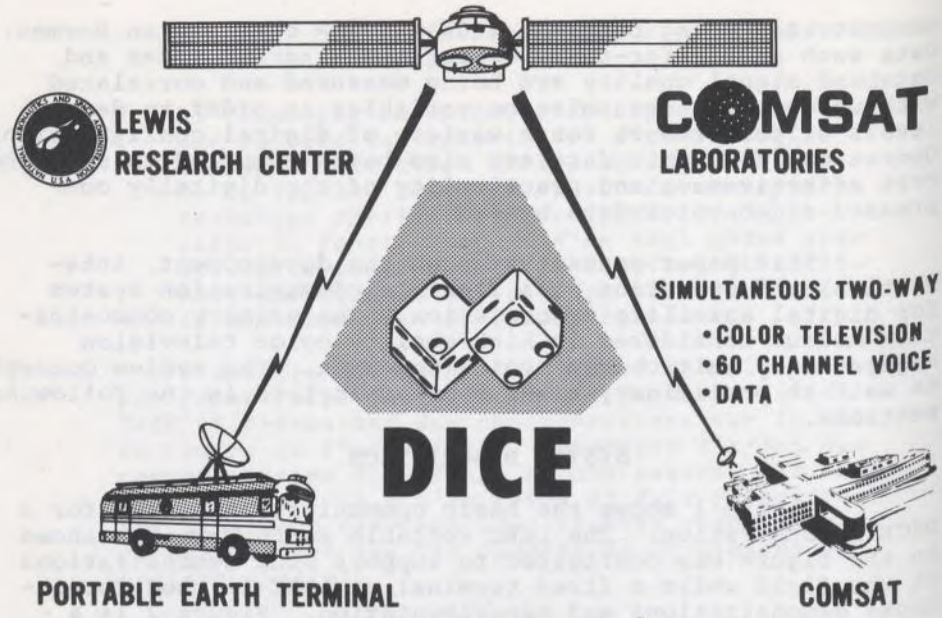


Figure 1. Digitally implemented communications experiment.

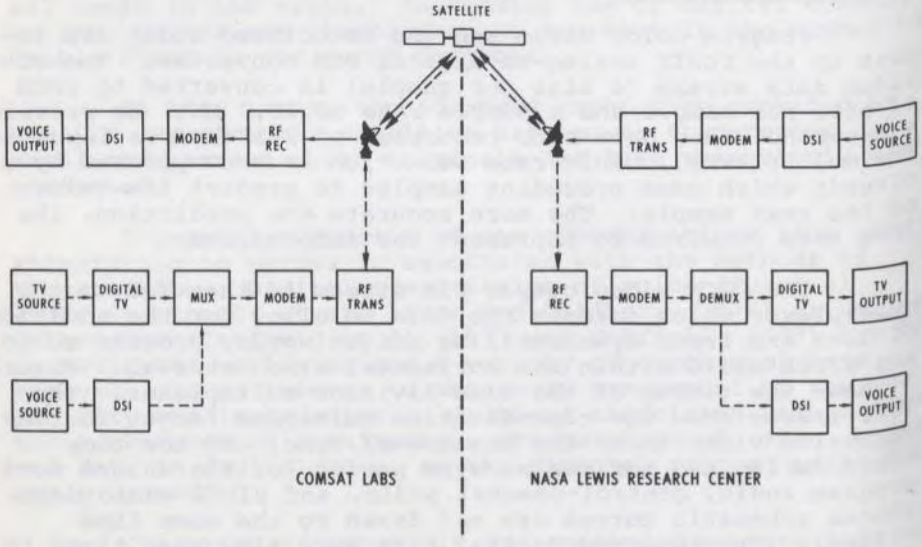


Figure 2. Communications Technology Satellite digitally implemented communications experiment.

encoded using variable-rate delta modulation and are time-division multiplexed into a serial bit stream. The rate of delta modulation is controlled by a speech detector which periodically determines the channels that are active. The information as to which channels are active is then stored in a 60 bit speech spurt assignment word (SSAW). Based on SSAW, the active channel speech data is then stored in memory. By using the speech detector and variable-rate delta modulation, the needless transmission of inactive channel noise is prevented and an effective bit-rate compression ratio of approximately 4:1 over conventional 64 Kbps PCM is achieved. Both the SSAW with error encoding and the active channel information are multiplexed into the frame structure. The SIDEL frame timing format is shown in figure 4. A 6 bit unique word is added for frame synchronization. The bit rate is 1.0227 Mbps and the frame rate is approximately 1 KHz. The SIDEL output is then fed to the CODIT multiplexer and time-division multiplexed as shown in figure 3 to form one data stream at approximately 43 Mbps.

The DICE experiment utilizes a COMSAT Labs developed universal QPSK modem which can be used over a wide range of bit rates and multiple-access methods (TDMA or FDMA). The universal modem is designed to cover the bit rates of 4 to 60 Mbps with a maximum of common circuitry over the entire range. Five operating bit rates were chosen over the above range with plug-in modules designed to operate at 1, 22, 33, 43, and 49 Mbps. Each module contains the channel filters and a clock recovery circuit for simplicity in changing from one rate to another. The 43 Mbps DICE input to the uplink modulator is processed into two parallel streams that are differentially encoded and filtered. The output of each filter is fed to two double balanced mixers that are driven in quadrature by a 70 MHz carrier oscillator. The 70 MHz carrier is routed to the up/down converter located at the transmitter site.

The Lewis RF system incorporates a variable-frequency double conversion up/down converter. The DICE input and output frequency is 70 MHz. The converter translates to and from the link frequencies using an intermediate frequency of 1.5 GHz, and can be tuned to any frequency in either of the two Hermes bands for transmit or receive (Fig. 5). Tuning and stability are accomplished with synthesizer-controlled local oscillators and manually-tuned phased-locked loop circuitry.

The converter output at the chosen transmit frequency is applied directly to a 2 watt TWT intermediate-power amplifier and then to the high-power amplifier stage. Due to the different configurations of available transmit sites, both portable and permanent, a limited parametric analysis of TB1 and TB2 link characteristics was integrated with the required bit-error-rate (BER) (Table I) to define the transmit system configuration.

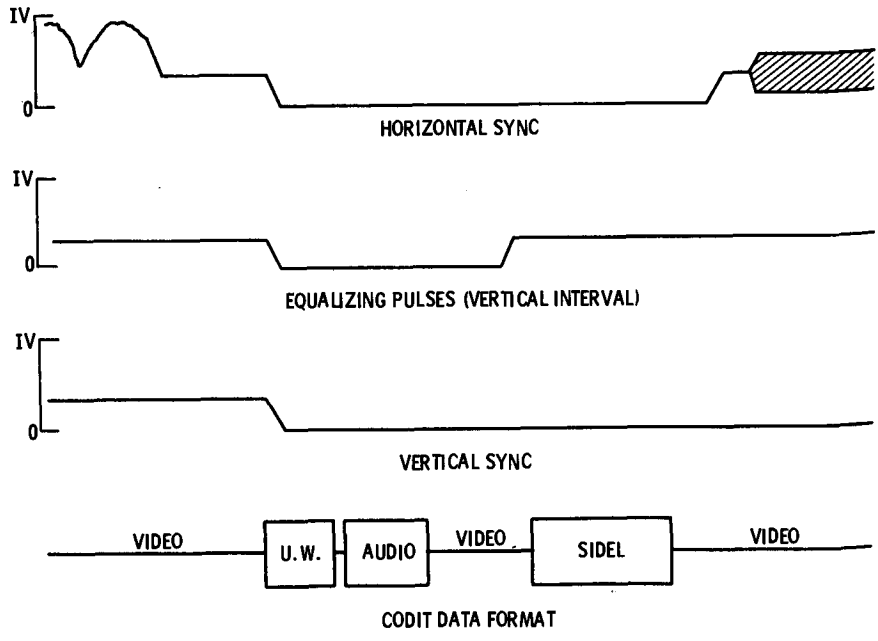


Figure 3. Time-division multiplex format.

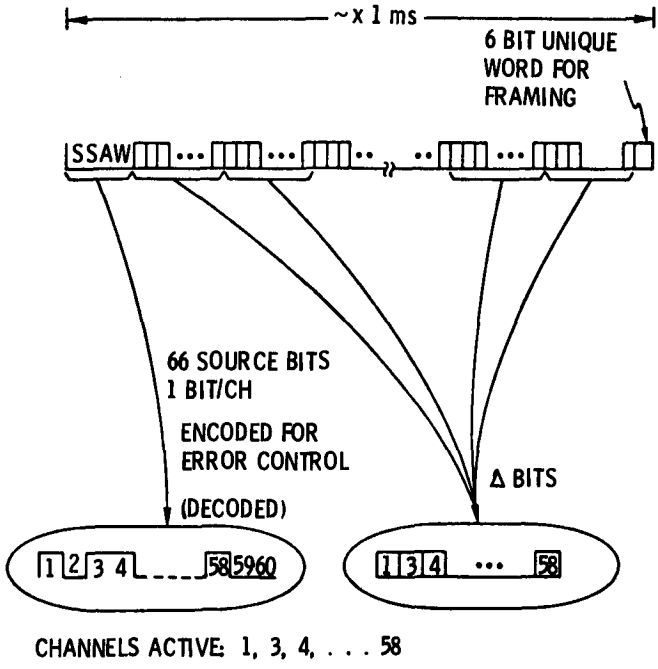


Figure 4. SIDEL-1 frame format.

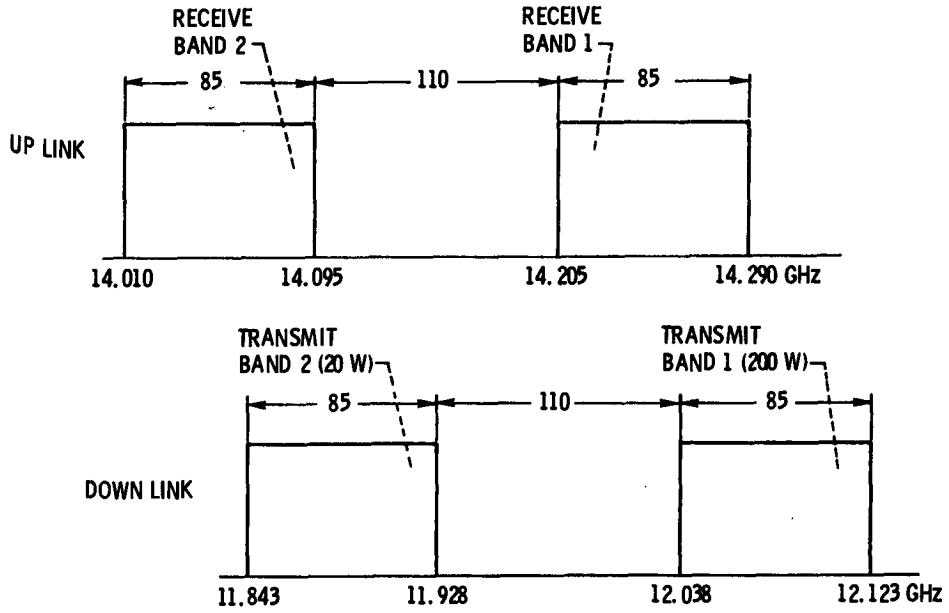


Figure 5. Communications technology satellite frequency plan.

TABLE I

$C/N_o$ REQUIREMENTS

| | |
|---|---|
| Limiting error rate | $10^{-8}$ |
| Bit rate, Mbps | 42.9 |
| *$E_b/N_o$ (back-to-back) required to achieve $10^{-8}$ error rate, dB | 15.0 |
| **$C/N_o$ $E_b/N_o$ + 10 log (bit rate) = 15.0 + 76.3, dBHz | 91.3 |
| C/T - carrier/temperature 228.6 - $C/N_o$, dBW/K | -137.3 |

*$E_b/N_o$ - bit energy/noise power density.

**$C/N_o$ - carrier power/noise density limiting error rate = error rate above which video impairments are perceptible.

The link budgets (Table II) were based on the following assumptions: that the experiment would be conducted in a two-way transmission of digital video, data and voice using the two Hermes transponders, and that the Hermes antennas would be pointed at the positions of the participating earth stations under clear sky conditions.

TABLE II

LINK BUDGET TB-2 (with the 20W channel)

| | |
|---|---|
| **Uplink** | |
| $P_T$ - transmitted power at earth station, dBW | 22.0 |
| $G_T$ - gain, 3m earth station, dB | 49.0 |
| EIRP, dBW | 71.0 |
| Path loss, dB | -207.6 |
| $G_R$(S/C antenna gain), dB | 37.6 |
| $P_r$ received power, dBW | -99.0 |
| G/T(S.C.), dB/°K | 6.6 |
| C/T (uplink), dBW/°K | -130.0 |
| **Downlink** | |
| $P_T$ - transmission power S/C, dBW | 11.0 |
| $G_T$ - S/C antenna gain, dB | 36.3 |
| EIRP, dBW | 47.3 |
| Path loss, dB | -206.4 |
| $P_r$, dBW | -159.1 |
| $G_A$ - 2.4m earth station, dB | 47.8 |
| System temperature, dB (°K) | 24.8 (300) |
| G/T, dBW/°K | 23.0 |
| C/T (downlink), dBW/°K | -136.1 |
| **Combined link** | |
| C/T combined, dBW/°K | -137.1 |
| C/T required, dBW/°K | -137.3 |
| Margin, dB | 0.2 |

TABLE II - continued
(with the 200W channel)

| | |
|---|---|
| **Uplink** | |
| $P_T$, dBW | 23.0 |
| $G_T$ - gain, 2.4m earth station, dB | 48.0 |
| EIRP, dBW | 71.0 |
| Path loss, dB | -207.6 |
| $G_R$, dB | 37.6 |
| $P_r$, dBW | -99.0 |
| $G_T$, dB/°K | 6.6 |
| C/T uplink, dBW/°K | -130.0 |
| **Downlink** | |
| $P_T$, dBW | 22.0 |
| $G_T$, dB | 36.3 |
| EIRP, dBW | 58.3 |
| Path loss, dB | -206.4 |
| $P_r$, dBW | -148.1 |
| $G_A$ - 3m earth station, dB | 48.0 |
| System temperature dB (°K) | 27.0 (600) |
| G/T, dB/°K | 21.0 |
| C/T (downlink), dBW/°K | -127.1 |
| **Combined link** | |
| C/T combined, dBW/°K | -131.7 |
| C/T required, dBW/°K | -137.3 |
| Margin, dB | 5.6 |

## Terminal Characteristics

The LeRC portable earth terminal had a 2.4m diameter antenna (48 dB gain) and 500w transmitter with an instantaneous bandwidth of 50 MHz. The maximum net EIRP was 74 dBW. Demonstrations to date have used the LeRC signal through the satellite 200w channel and the COMSAT signal through the satellite 20w channel. The COMSAT terminal has a 3m diameter antenna (49 dB gain) and a 200w transmitter with a maximum net EIRP of 71 dBW. The receive G/T for both terminals is approximately 22 dBW/°K.

The link budget calculations (Table II) based on the LeRC and COMSAT terminals show link margins of 0.2 and 5.6 dB respectively, using the 20w and 200w channels.

## DOWNLINK

The receive downlink signal, either TB1 or TB2, is input to the downconverter whose input dynamic range is -70 to -30 dBm. The internal gain of 60 dB provides a 70 MHz signal at 0 dBm level to the demodulator.

Demodulation is achieved by coherent detection. The local carrier signal is recovered by a separate carrier recovery circuit (Fig. 6). Regeneration is performed by instantaneous sampling by the clock signal which is recovered by the clock recovery circuit.

The demodulation consists of two double balanced mixers followed by two passive low-pass baseband filters. The mixers act as multipliers with the in-phase and quadrature phase carriers supplied from the carrier recovery circuit.

Carrier and clock recovery circuits complete the basic demodulation system which supplies the data bit stream to the CODIT Buffer and Demultiplexer, which in turn separates the various video, program audio, and SIDEL bit streams.

The CODIT DPCM receiver (Fig. 7) uses a predictor identical to that of the transmitter, and a decoder which is the complement of the coder.

The received DPCM signal is decoded to recover the PCM difference which is then added to the prediction for the sample to form the reconstructed video. The SIDEL receiver (Fig. 8), like the transmitter, demultiplexes the SSAW and delta encoded speech samples, and stores them in memory. After error checking, the samples are routed to their respective channels.

## DEMONSTRATION AND TESTS

### Demonstration Concept

The experimental demonstration concentrates on the

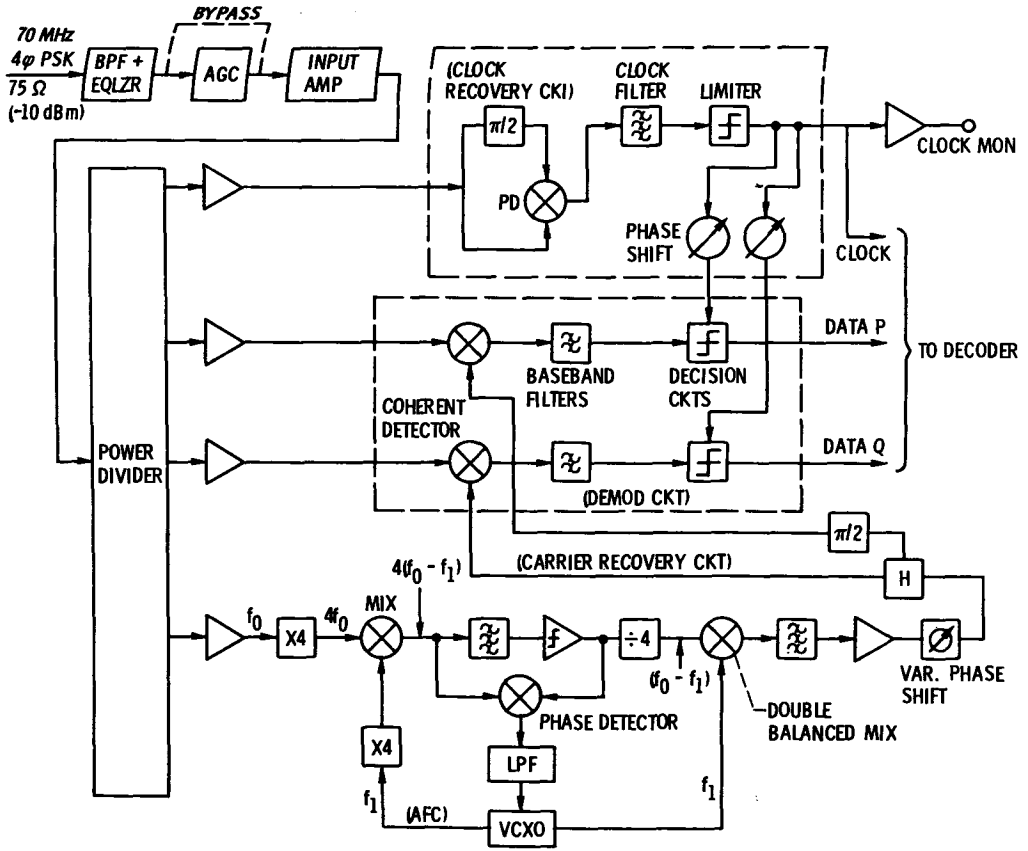


Figure 6. Demodulator block diagram.

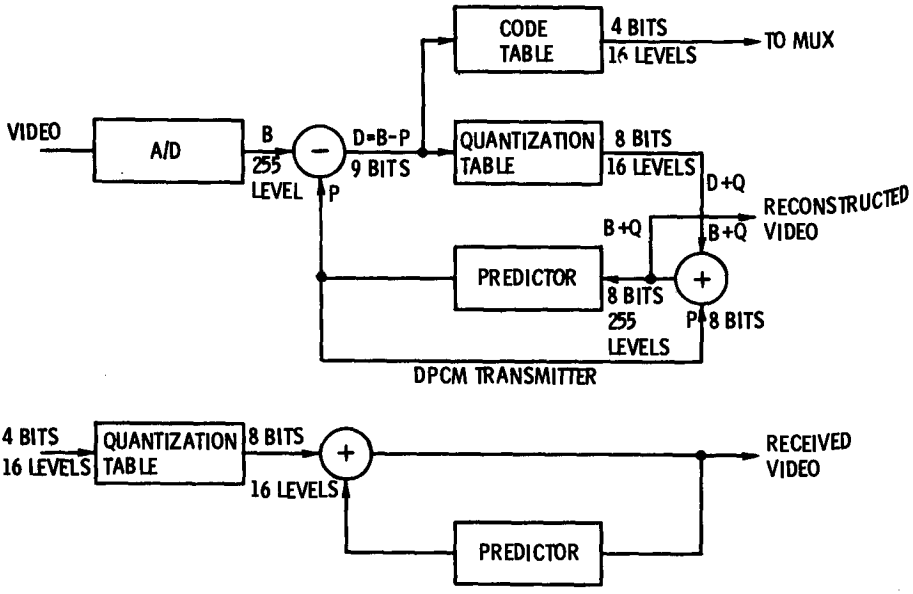


Figure 7. The CODIT DPCM receiver.

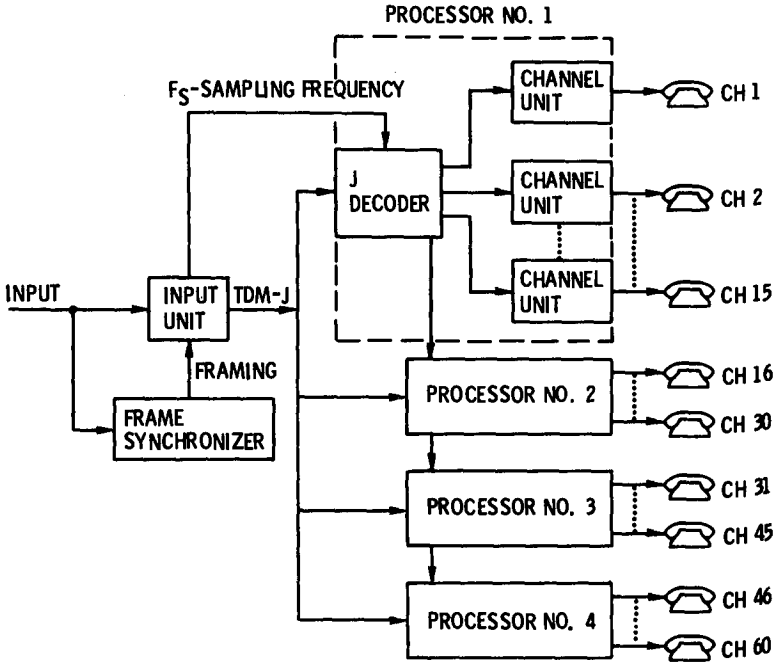


Figure 8. SIDEL receiver.

evaluation of full-duplex digital television in a teleconferencing environment. This environment was configured to provide feedback on digital system quality and performance from a user's rather than observer's perspective. A variety of digital transmission methods which are nearing commercial availability are intended to be comparatively evaluated. The specific television experimental hardware previously described (i.e., CODIT-1 DPCM system) as well as digital television processors using frame storage and transform methods will be included.

Baseband Tests

CODIT - Video and audio test signals are used to characterize CODIT. The video tests are as follows:

(1) Video insertion test to measure the insertion loss of the system

(2) Differential gain and phase test to measure nonlinear distortion

(3) Signal-to-weighted-noise-ratio tests to measure the systems thermal noise contribution to the output signal

(4) Chromanance signal's relative amplitude and delay compared to those of the lumanance signal

The audio tests are as follows:

(1) Audio insertion test to measure the insertion loss of the system

(2) Audio frequency response test

(3) Audio signal-to-distortion ratio test to measure the distortion in the program audio channel

SIDEL - The following tests are used to evaluate SIDEL:

(1) Signal-to-distortion (S/D) ratio of each channel unit

(2) S/D ratio of a test tone in a channel with the DSI fully loaded

(3) Bit-error-rate (BER) measurement of the data circuit

(4) Determine proper operation of SIDEL when multiplexed with a video signal

(5) Echo suppression tests

MODEM - The following tests are used to evaluate the MODEM:

(1) A modulator balance test to determine the proper PSK and QPSK modulation

(2) BER measurements to determine BER versus C/N, BER versus AGC, and BER versus IF variations

SYSTEM - On a system level, the following data are being compiled:

(1) For all operational bit rates, BER and C/N ratios are measured and correlated with up and downlink transmission variables to define levels for acceptable performance.

(2) For a given system configuration and operating conditions, a subjective evaluation will be made by participants who will be asked to fill in questionnaires on their perception of the system effectiveness as a communications medium.

## RESULTS AND DISCUSSION

### Demonstration

The first utilization of the DICE experimental system was for a communications convention, the International Conference on Communications, June 1977, Chicago. The exhibit was structured as a full-duplex video teleconference/open discussion between convention attendees and COMSAT personnel using their video teleconference facilities at Clarksburg, MD.

Concurrent with the videoconference open discussion, the SIDEL system was loaded with taped conversations on 59 of 60 channels. The remaining channel was used extensively by convention attendees.

Quality of the CODIT-1 and SIDEL was subjectively judged as excellent to better than network quality by approximately 250 communications media personnel in attendance.

### Baseband

CODIT and SIDEL performance parameters are compiled in Tables III and IV respectively. Measured data equalled or exceeded all pretest limits for excellent quality television (CODIT) and audio (SIDEL) communications.

As stated earlier, two tests are performed to evaluate the modem: the modulator balance test and the BER test. For the modulator balance test, measurements are made for proper PSK and QPSK modulation. For proper PSK modulation, the suppression of the carrier component should be $\geq$40 dB. Measurement showed it to be $\geq$40 dB. For proper QPSK modulation,

TABLE III

CODIT TEST DATA

| Measurement | Limits | Measured value |
|---|---|---|
| 1. Video insertion gain | 96 to 104 IRE | 100 IRE |
| Video insertion sync | 38 to 42 IRE | 40 IRE |
| 2. Differential gain | 5 percent | 2 percent |
| Differential phase | ±5° | 1.5° |
| 3. Video S/N weighted | >48 dB | 55 dB |
| 4. Chroma gain inequality | 10 percent | 0 percent |
| Chroma delay inequality | 100 ns | 40 ns |
| 5. Audio gain response | ±1 dB | ±0.1 dB |
| 6. Audio frequency response | 1 to 14 kHz ± 1 dB | ±0.15 dB |
| 7. Audio S/D | >47 dB | 50 dB |

TABLE IV

SIDEL TEST DATA

| Measurement | Limits | Measured value |
|---|---|---|
| 1. S/D ratio of each channel unit | >30 dB | >33 dB and >30 dB[a] |
| 2. S/D ratio for a channel, DSI loaded | >25 dB | >29 dB and >27 dB[a] |
| 3. BER of data circuit | $\geq 10^{-7}$ | 0 |
| 4. Echo suppression | >55 dB | >59 dB |

[a]With and without a message weighting filter.

side band components of the carriers are such that the upper side bands are enhanced and the lower side bands cancelled after the signals are combined. Suppression of the lower side band should be $\geq$35 dB. Measurement showed it to be 38 dB. The BER measurements are performed by connecting the modem back-to-back. For the BER versus C/N ratio test, the C/N was converted to the energy per bit to noise power density ratio ($E_b/N_o$) by using the expression

$$\frac{E_b}{N_o} = \frac{C}{N} - 10 \log \frac{R}{B_n}$$

where R is the bit rate and $B_n$ is the noise bandwidth of the receive band pass filter.

The data is shown plotted in figure 9. Measured $E_b/N_o$ values exceeded the theoretical curve by 1 dB. For the BER versus AGC test, no measurable variations in the BER were observed for input level variations from -5 dB to -15 dBm.

The BER versus IF variations test is to check out the performance of the AFC loop. The AFC loop is designed to track between 70 MHz ± 50 kHz. BER variations between these limits were approximately one order of magnitude which is within design limits.

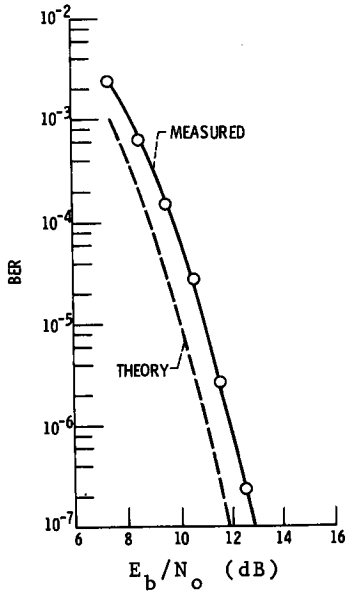


Figure 9. $E_b/N_o$ vs BER, for a 43 Mbps data rate with 33 MHz bandwidth.

System

Preliminary system level duplex video tests have been performed utilizing Hermes and the LeRC/COMSAT terminals. For band 2 (20w channel backed off to 10w) operation, the uplink EIRP was approximately 70 dBW and S/C EIRP 46 dBW to achieve a BER of $10^{-8}$. For band 1 (200w channel backed off to 160w) operation, the uplink EIRP was 71 dBW (approximately 4 dB S/C gain suppression) and the S/C EIRP 58.3 dBW to achieve a BER of $10^{-8}$. Simplex and duplex testing is continuing to define generalized terminal and S/C parameters required for $10^{-8}$ BER performance with DICE. Subjective evaluation tests have not begun on a systematic basis; however, results from our demonstration activities have been very encouraging.

## CONCLUDING REMARKS

The system design described provided full duplex teleconference capability in addition to 60 channels of digital voice and 1 Mbps data. The CODIT and SIDEL compression of approximately 2:1 and 4:1, respectively, provided excellent quality transmission equivalent to NTSC standards.

The CTS link performance provided by small earth terminals using either the 200w or 20w channels (at backed off levels 160w and 10w respectively) is sufficient to provide system BERS of $10^{-8}$ or less, without additional error-encoding equipment.

## REFERENCES

Gatfield, A.
1977 CODIT, A Digital TV System for Communication Satellites. *Intelcom 77, International Telecommunication Exposition*, Atlanta, Ga., Oct. 9-15. Paper 3. 8. 2.

Gatfield, Allen G., Suyderhoud, Henri G., and Wolejsza, Chester J.
1977 System Design for the Digitally Implemented Communications Experiment (DICE). Conference Record, *International Conference on Communications, ICC 77, IEEE*, vol. 1, pp. 1.1-1 - 1.1-5.

Goldberg, A.A.
1976 Digital Techniques Promise to Clarify the Television Picture. *Electronics*, vol. 49, no. 3, Feb. 5, pp. 94-100.

Su, J.C., Suyderhoud, H.G., and Campanella, S.J.
1976 A Strategy for Delta Modulation in Speech Reconstruction. *COMSAT Technical Review*, vol. 6, no. 2, pp. 339-355.

Suyderhoud, H.G., Jankowski, J.A. and Ridings, R.P.
1974 Results and Analysis of the Speech Predictive Encoding Communications System Field Trial. *COMSAT Technical Review*, vol. 4, no. 2, pp. 371-390.

Washburn, Abbot
1976 Bringing Together Satellite Techniques Can Reduce Costs. *Telecommunications Reports*, vol. 42, no. 15, p. 19.

# THE CRL 60 Mb/s FFSK MODEM: ITS DEVELOPMENT AND ITS PERFORMANCE ON THE HERMES SYSTEM

D.P. Taylor and S.S. Haykin

McMaster University

Hamilton, Canada

*En 1973, le Laboratoire de recherche en communications (CRL) de l'Université McMaster entreprenait une étude comparative minutieuse des techniques de modulation numérique à haute vitesse pour les télécommunications par satellite. L'un des buts de cette étude était d'établir des critères de sélection à partir desquels on pourrait choisir la meilleure technique de modulation pour le développement d'un modem d'usage expérimental sur le système Hermès, soit l'expérience U-4. Cette étude préliminaire consistait en une étude du comportement simulé de divers types de modulation numérique y compris une étude comparative de leur performance sur des voies à largeur de bande limitée de type satellite.*

*La simulation révéla que les deux meilleures techniques étaient la manipulation par déplacement de phase quaternaire décalé (OQPSK) et la manipulation par déplacement de fréquence rapide (FFSK). A cause de sa nouveauté, on a décidé de développer un modem à haut débit utilisant la technique FFSK selon un débit binaire nominal de 60 Mb/s. Pendant les essais préliminaires, le modem fonctionnant selon un mode dos-à-dos se maintint en-deçà de 1.5 dB de la performance théoriquement possible; était produite par suite du passage des signaux dans produite par suite du passage des signaux dans un convertisseur élévateur de la fréquence intermédiaire (de 70 MHz à 735 MHz) des terminaux terriens utilisés avec le satellite Hermès.*

*Au cours de 1975, le modem a fait l'objet d'un programme de vérifications nombreuses en laboratoire. Ce programme comprenait des essais de taux d'erreurs sur les bits en fonction des bruits additifs, de la gamme dynamique et des mesures spectrales, et des vérifications des effets de la distorsion non-linéaire du genre qu'on trouve dans les répondeurs de satellite. En outre, on a fait de nombreux tests sur les effets d'une*

*sérieuse limitation de bande sur la performance du modem. Tous ces essais ont été effectués à la fréquence intermédiaire de 735 MHz ainsi qu'à la fréquence centrale de 11,265 Ghz d'un répondeur simulé. Ces essais indiquèrent que le modem fonctionnait de la manière indiquée par les simulations antérieures. De petites dégradations étaient produites par l'équipement, principalement dans les diverses conversions de fréquences.*

*A partir de ce programme d'essais, on a développé un plan détaillé pour des essais pratiques sur le système Hermès. A l'exception de quelques essais de transmission vidéo et de quelques mesures de statistiques d'erreurs, ces essais ont eu lieu avec succès en juin 1976 et mai 1977. Les résultats indiquent que la qualité de rendement du modem est approximativement (en deçà de 2 dB) celle qu'on avait prévue en fonction des simulations sur ordinateur et des essais sur banc.*

## Introduction

In 1973 the Communications Research Laboratory (CRL) of McMaster University undertook a study, under contract to the Communications Research Centre, of high speed digital-modulation techniques for satellite communications. The initial phase of this work consisted of a simulation study of eight different digital modulation types (Chan et al, 1974, 1975; Taylor et al, 1976) including a detailed comparison of their performance over a satellite type of channel. The results of this study indicated that the two best modulation types for use on such channels were the offset quaternary phase-keyed (OQPSK) signal and the fast frequency-shift keyed (FFSK) signal.

On the basis of this first study, a decision was taken to pursue the development of a high-rate FFSK modem. This modem would then be field tested as experiment U-4 during 1976-'77 using the Communications Technology Satellite (CTS), later renamed Hermes. Thus in 1974, under contract to the Communications Research Centre, the design, construction and testing of an FFSK modem at a nominal data rate of 60 Mb/s was carried out (Ogletree et al, 1975; Taylor et al, 1976; Taylor et al, 1977). During preliminary testing the modem, when operated in a back to back mode, was within 1.5 dB of the theoretically achievable performance; an additional 0.8 dB degradation was introduced by up-conversion to the 735 MHz, IF frequency required by the Hermes ground terminals.

During 1975, an extensive laboratory test program (Taylor et al, 1976) was performed on the modem using a bench

simulator of a satellite transponder at a centre frequency of 11.265 GHz. On the basis of this program a detailed test plan for use in field testing the modem on Hermes was evolved. Then during June 1976 and May 1977, these field tests were carried out. During June 1976, the majority of the tests used the high-power (200 W) satellite transponder, whereas in May 1977 all of the tests used the low-power (20 W) transponder. The field testing included measurements of bit error-rate as a function of bit energy to noise spectral density ratio $E_b/N_o$, the effects of severe band-limiting on the bit error-rate, the received signal spectra, and system sensitivity tests. All of these measurements were performed at a number of input levels to the satellite transponder.

Section 2 of this paper describes the initial simulation study and presents the results of and conclusions obtained from the comparative evaluation of the different modulation techniques. Section 3, summarizes the design philosophy and implementation of the 60 Mb/s FFSK modem. In section 4, we deal with the testing of the modem, beginning with preliminary back-to-back testing and extending through the tests carried out using a transponder simulator to the actual field testing on the Hermes system. Finally in section 5, we draw some conclusions concerning the use of FFSK modulation for high data-rate satellite communication.

## 2. The Simulation Study

In this initial phase, we employed digital computer simulation to evaluate system performance degradation due to intersymbol interference (ISI), nonlinear distortion and additive noise, for a variety of digital modulation schemes. Simulations of this type have previously been reported (Muratani et al, 1972; Hedderly and Lundquist, 1973) for certain coherent phase-shift keying (CPSK) schemes and also in the evaluation of ISI and co-channel interference effects in multicarrier systems (Eric, 1972), but these studies have in the main been restricted to very specific situations. In our work, a unified approach has been taken which facilitates direct comparisons of the performance of different modulation types under a variety of operating conditions.

High-frequency signal transmission can, in all cases of interest, be investigated using pre-envelope functions of the form

$$s(t) = u(t)\, e^{j\omega_c t} = [x(t) + j\, y(t)]\, e^{j\omega_c t}$$

The actual transmitted signal is then just the real part of $s(t)$:

$$\mathrm{Re}\,\{s(t)\} = x(t) \cos \omega_c t - y(t) \sin \omega_c t$$

where $\omega_c$ is the angular carrier frequency. The information to be transmitted is entirely contained in the real baseband signals $x(t)$ and $y(t)$, and thus with no loss in generality

the modulation systems under study may be investigated by means of the complex baseband signal $x(t) + j\,y(t)$. This is the basic philosophy behind our simulation which is entirely carried out in complex baseband form. The baseband signals $x(t)$ and $y(t)$ are referred to as in-phase and quadrature signals, respectively.

A general block diagram of the system being simulated is shown in figure 1. The main portions of the signal path including the transmit filter, the nonlinear Travelling Wave Tube (TWT) and the receive filter are modelled in complex baseband form. (All uplink and downlink filtering action is included in the transmit and receive filters respectively). These portions of the simulation program are written as a self-contained set of subroutines. They are used in simulating all of the various modulation schemes. To simulate a particular modulation scheme it is then necessary only to write programs for the signal generation and receiver portions of the model.

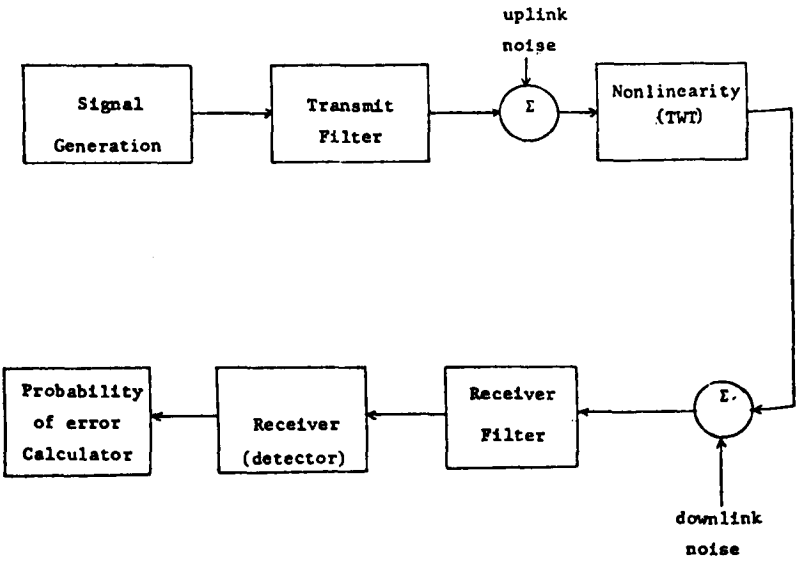


Figure 1: Basic Block Diagram of System Simulation

To simulate digital data sources, fairly long repetitive, pseudo-random (PN) sequences are used. In most of the work sequences of length 127 were used. (The exception is 8-phase CPSK where sequences of length 2047 were used.) To study the effects of ISI, all possible patterns of consecutive transmitted digits should be present with equal frequency. In practice, of course, this requirement depends directly on the characteristics of the transmit and receive filters. In virtually all of our work we found it sufficient to ensure equal representation of all possible singlet, doublet and triplet patterns of digits.

In the simulation, the signal generation portion of the program converts the input PN sequences into the quadrature baseband signals x(t) and y(t) according to the desired modulation law. Fast Fourier Transform techniques convert the complex baseband signal x(t) + j y(t) to the frequency-domain form X(f) + j Y(f). Filtering is performed by multiplying X(f) + j Y(f) by the complex baseband transfer function of the transmit filter. The resultant is then transformed back to the time-domain to be processed by the nonlinear TWT. (At this point up-link Gaussian noise samples may be added. In this study, this was not done because of limitations on computer time).

The TWT may be represented as a combination of two nonlinear effects, namely;

a) an amplitude compression or soft-limiting effect often referred to as AM/AM conversion

b) a nonlinear amplitude-dependent phase-shift often called AM/PM conversion.

The TWT is modelled, following Eric (1972), in quadrature form. It is thus represented as the additive combination of two essentially soft-limiting envelope nonlinearities which are 90° out of phase with each other. This is illustrated in figure 2 which shows a general bandpass nonlinearity modelled in quadrature form.

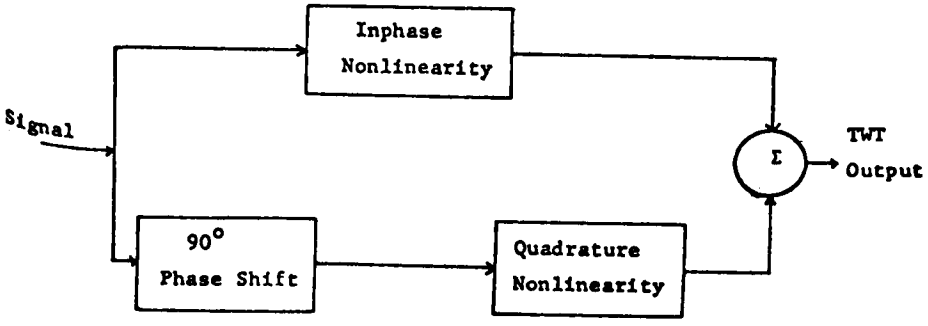


Figure 2: Quadrature model of a bandpass device with nonlinear phase and amplitude characteristics.

After processing by the TWT, the Fast Fourier Transform is again used to transform the signal into the frequency-domain. Receiver filtering is performed in a similar manner to that described above for the transmit filter. The resulting frequency-domain signal is then transformed back into the time-domain for passage through the receiver.

The receiver portion of the simulation is modulation-dependent and must be separately programmed for each type of modulation. In general, it consists of in-phase and quadrature channels each containing appropriate matched filters for the given modulation law. The energy of each received symbol is evaluated at the outputs of these filters.

Rather than simulate the downlink additive noise, we account for its effect by computing the noise power at the output of the receive filter using well known results (Davenport, Jr. and Root, 1958), where we assume white additive noise at its input. The calculated noise power is then used in conjunction with the received symbol energy to calculate the probability of error for each symbol conditioned on the transmitted symbol value.

The average of these conditional probabilities of error taken over the entire transmitted symbol sequence then forms the estimate of error probability for the given simulated system. This error probability is the basic measure of performance used in comparing the various digital modulation schemes. Other measures of performance, namely the degradation in required signal-to-noise ratio (SNR) at a given error-rate as a function of the data rate and the well known eye diagram (Lucky et al, 1968) are available from the simulation and are also useful in making comparisons of different systems.

Detailed simulations of eight different digital modulations were conducted. These were:

coherent 2-phase PSK (phase-shift keying)
coherent 4-phase PSK,
coherent 8-phase PSK,
differential 2-phase PSK,
differential 4-phase PSK,
offset 4-phase PSK,
fast frequency-shift keying (FFSK) and
octal amplitude-phase keying (APK).

The first seven of these yielded results which indicated in general that on a given channel a) they are usable over a wide range of bit rates depending on the available SNR. b) they are relatively insensitive to the operating point of the TWT. Typically a 1 dB variation in required SNR was observed over a wide range of operating points.

The last one, APK, yielded relatively poor results. With the TWT operating at 12 dB input power backoff and at 60 Mb/s we obtained a SNR degradation of 3.1 dB from the theoretical curve. (By theoretical curve, we mean the calculated probability of error as a function of the bit energy to noise ratio $E_b/N_o$ on an additive noise channel.) At 120 Mb/s (corresponding to 40 megabauds) the degradation from the theoretical curve was 6.4 dB at the same error-rate. This performance is acceptable provided there is sufficient SNR margin in the system. However, it must be remembered

that at 12 dB input power backoff the TWT operates linearly and is much less efficient than when it is operated near saturation.

At 1 dB input power backoff, the TWT is essentially in saturation, where it is most efficient, but here the performance degradation in APK becomes very severe. In fact the system becomes useless for communications. For example, at a data rate of 60 Mb/s and a TWT backoff of 3 dB we found the SNR degradation was 15.3 dB at an error-rate of $2 \times 10^{-4}$. It therefore appears to us that when the TWT is operating near saturation APK is not a useful modulation technique. Therefore, we did not give APK any further consideration for this experiment.

One of the primary aims of the initial study was to choose a modulation method for implementation in a modem and for later experimental use on the Hermes system. The nominal data-rate for the satellite was specified as 65.5 Mb/s when a binary modulation technique is used. For binary modulation this is equivalent to a symbol rate (or pulse rate) of 65.5 megabauds. To aid us in our choice of a modulation method the symbol probability of error versus the bit energy to noise ratio $E_b/N_o$ at a transmission rate of 65.5 megabauds was plotted (Fig. 3).

From these curves, it is obvious that, at this baud-rate, the best performance is obtained using the FFSK and offset PSK systems. Moreover, we found that both these systems perform effectively over the channel being simulated at data-rates in excess of 160 Mb/s. That is, for the assumed channel model, the binary eye was still open at this rate, although with a much reduced noise margin. (In all our investigations the channel was modelled as the combination of 85 MHz 3 dB bandwidth, 4-pole, ½ dB ripple Chebychev filters and a Hughes 261-H TWT).

For both these modulation systems, the theoretical error-rate curve is the same as the 2-phase CPSK theoretical curve. Thus at the nominal rate of 65.5 Mb/s both these systems suffer a degradation of approximately 1 dB in SNR at an error-rate of $10^{-5}$ with the TWT operating at an input power backoff of 1 dB.

Performance of the various modulation systems is again compared in figures 4 and 5 by plotting the degradation in required signal-to-noise ratio versus the parameter BT where B is the bandwidth and T is the symbol duration. At values of BT less than 2 the offset PSK and fast FSK systems are superior in performance to any of the others, and the superiority increases as BT is reduced.

In the Hermes system, the maximum available channel bandwidth is 85 MHz. From figures 4 and 5, we see that in the range $0.75 \leq BT \leq 1.4$ the fast FSK system yields performance which is as good as or slightly better than that of

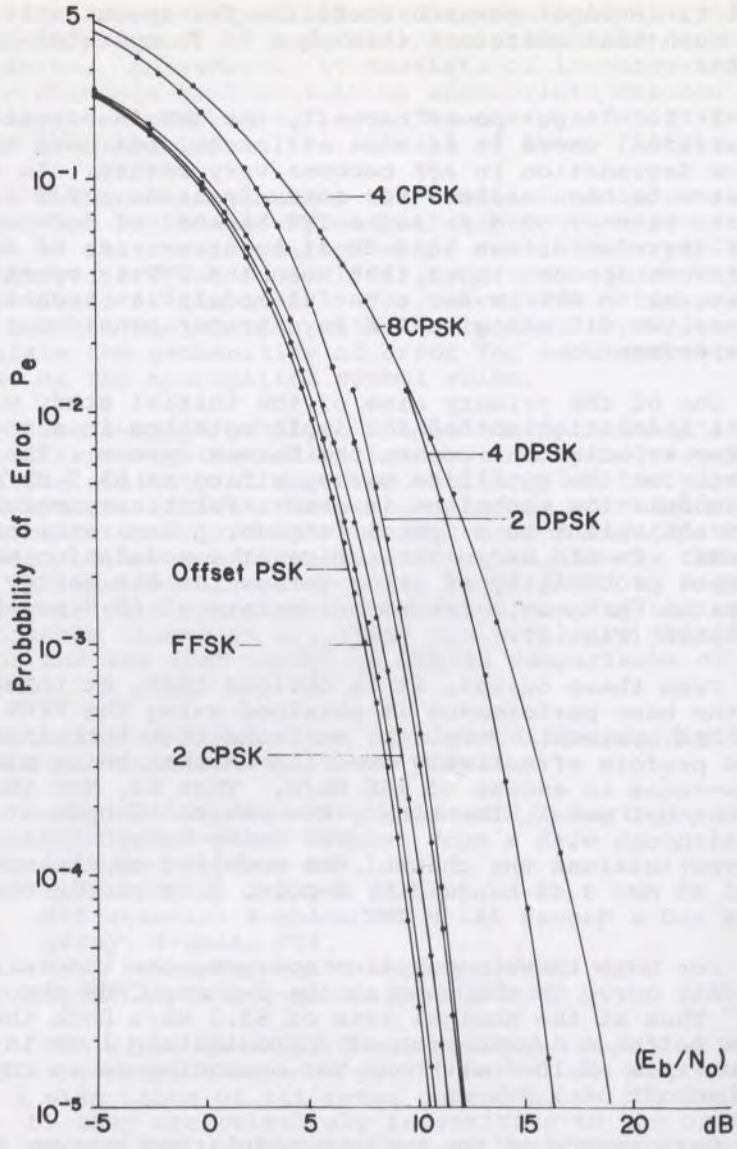


Figure 3: Comparative error-rates obtained at a rate of 65.5 megabauds by computer simulation.

the offset PSK system. This range of BT corresponds to a baud-rate range of 60.8 to 113 megabauds. This range of rates includes the range of interest for high-rate data experiments on Hermes.

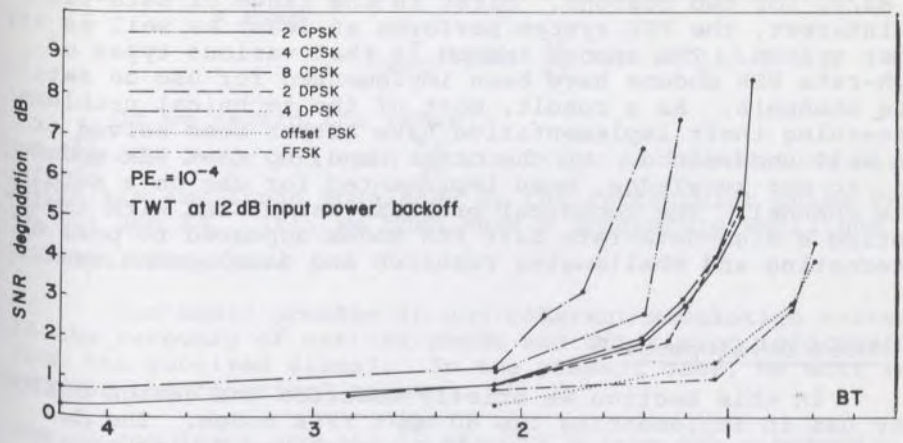


Figure 4. Degradation in SNR from theoretical as a function of time-bandwidth product BT. The TWT is operated at 12 dB input backoff.

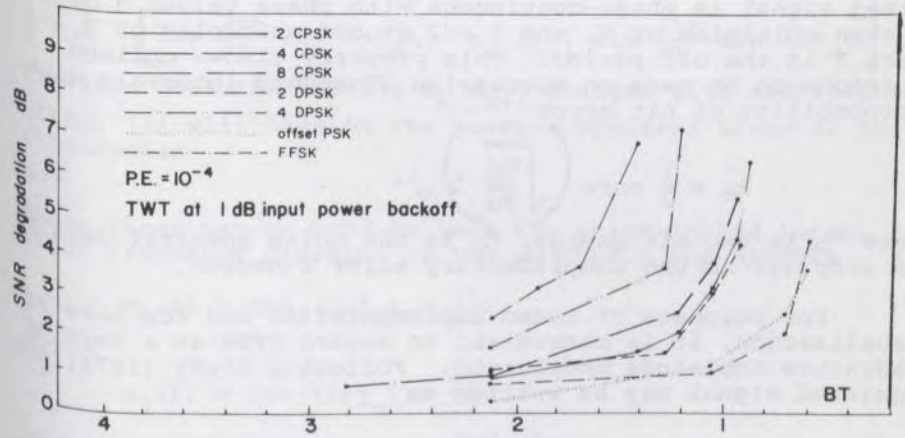


Figure 5. Degradation in SNR from theoretical as a function of time-bandwidth product BT. The TWT is operated at 1 dB input backoff.

Thus, the two best candidate modulation types for implementation in a high-performance, high data-rate modem are the offset PSK and the FFSK systems. The CRL at McMaster decided to implement a FFSK modem at a nominal data rate of 60 Mb/s, for two reasons. First in the range of data-rates of interest, the FSK system performs at least as well as any other system. The second reason is that various types of high-rate PSK modems have been implemented for use on satellite channels. As a result, most of the technical problems concerning their implementation have either been solved or are well understood. On the other hand, no fast FSK modem has, to our knowledge, been implemented for use on a satellite channel. The technical problems associated with implementing a high-data-rate fast FSK modem appeared to pose an interesting and challenging research and development task.

## 3. Modem Development

In this section we briefly describe the design philosophy use in implementing the 60 Mb/s FFSK modem. The details of the design are available elsewhere (Taylor et al, 1976; Taylor et al, 1977). Because it is an experimental design, coaxial cable technology was used for the analog portion of the system and Schottky TTL circuitry was used for the digital portion. This provided maximum flexibility for both modification and measurement.

FFSK is a coherent frequency-shift keyed modulation with a frequency deviation ratio or modulation index of $h = 0.5$ (deBuda, 1972; deBuda and Anto, 1969; de Buda, 1971; Sass and Hannum, 1973). It has the property that the transmitted signal is phase-continuous with phase values 0 or $\pi$ at even multiples of T, and $\pm \pi/2$ at odd multiples of T, where T is the bit period. This property allows optimum decisions to be made on successive 2T-second intervals with a probability of bit error

$$P_e = \frac{1}{2} \operatorname{erfc}\left(\sqrt{\frac{E_b}{N_o}}\right) \qquad (1)$$

where $E_b$ is the bit energy, $N_o$ is the noise spectral density and erfc (.) is the complimentary error function.

For purposes of modem implementation and for ease of visualization, it is convenient to regard FFSK as a form of quadrature amplitude modulation. Following Brady (1974) the modulated signal may be written as

$$s(t) = \Sigma\, a_k \cos\left(\frac{\pi(t-kT)}{2T}\right) \cos\left(2\pi f_c t + \frac{k\pi}{2}\right) \qquad (2)$$

where the $\{a_k\}$ represent the data sequence having the values $\pm 1$ and $1/T$ is the transmitted bit rate. Then, if we define

$A_k(t)$ as a rectangular pulse of amplitude $a_k$ and width $2T$ centered on $t=kT$, we may write (2) as

$$s(t) = \sum_{k \text{ even}} \{ A_k(t)\cos \frac{\pi t}{2T} \cos 2\pi f_c t - A_{k+1}(t)\sin \frac{\pi t}{2T} \sin 2\pi f_c t\} \quad (3)$$

If we regard the terms $\cos \frac{\pi t}{2T} \cos 2\pi f_c t$ and $-\sin \frac{\pi t}{2T} \sin 2\pi f_c t$ as "quadrature carriers" which are amplitude modulated by the rectangular pulse train $\Sigma A_k(t)$ and $\Sigma A_{k+1}(t)$, we then have a quadrature amplitude modulation system.

One basic problem in any coherent modulation system is the recovery of carrier phase and bit timing information from the received signal. In the present case, we want to recover the "carrier" terms $\cos \frac{\pi t}{2T} \cos 2\pi f_c t$ and $\sin \frac{\pi t}{2T} \sin 2\pi f_c t$ from the received modulated signal.

Let us consider the signal in the interval $kT \leq t \leq kT+T$ for $k$ even, i.e.,

$$a_k \cos \frac{\pi t}{2T} \cos 2\pi f_c t - a_{k+1} \sin \frac{\pi t}{2T} \sin 2\pi f_c t.$$

If this is passed through a squaring device, then after some manipulation we obtain

$$\frac{1}{2} + \frac{1}{2} \left[\cos \frac{2\pi t}{2T} \cos 4\pi f_c t - a_k\, a_{k+1} \sin \frac{2\pi t}{2T} \sin 4\pi f_c t\right] \quad (4)$$

Provided that the product $a_k\, a_{k+1}$ changes sign sufficiently often, (4) will have on the average spectral lines at the frequencies

$$2f_c \pm \frac{1}{2T}$$

These lines may be used to lock two phase-locked loops, and after frequency division by two we obtain the signals

$$m_1(t) = \cos (2\pi f_c t + \frac{\pi t}{2T}) \quad (5)$$

and

$$m_2(t) = \cos (2\pi f_c t - \frac{\pi t}{2T}) \quad (6)$$

Forming the sum and difference of these signals, we obtain

$$m_1(t)+m_2(t) = 2 \cos \frac{\pi t}{2T} \cos 2\pi f_c t \quad (7)$$

and

$$m_2(t)-m_1(t) = 2 \sin \frac{\pi t}{2T} \sin 2\pi f_c t \quad (8)$$

which, except for a 180° phase ambiguity, are the "carrier" signals required for coherent demodulation of the fast FSK signal of equation (3).

In order to recover the clock signal, we form the product of $m_1(t)$ and $m_2(t)$ and after low-pass filtering to remove the double-frequency component, we obtain

$$\frac{1}{2} \cos \frac{2\pi t}{2T}$$

which is the desired bit-timing (1/2 clock frequency) signal. The 180° phase ambiguity which remains can be catered for by suitable coding and decoding. This problem has been examined in considerable detail by deBuda (1975) and will not be discussed further here. The effect of the encoding/decoding process is to change the theoretical system error-rate from $P_e$ to $2P_e - P^2_e$ where $P_e$ is given by (1).

A block diagram of the modulator is given in figure 6. The FSK centre frequency $\omega_0$ is generated by means of a stable, temperature-compensated, crystal-controlled oscillator. From this it is necessary to generate two phase-coherent carriers such that the spacing between the two frequencies is exactly one-half the bit rate. This is accomplished by taking the external clock signal, dividing it by four and multiplying it with the FSK center frequency. This operation gives two-phase coherent carriers separated by one half the bit rate, resulting in a deviation ratio of exactly 0.5. The advantage of deriving the binary FSK carriers in this fashion is that variations in the data rate do not change the deviation ratio nor do they affect the coherence of the carriers. The binary FSK carriers are separated by means of bandpass filters.

The quadrature carrier components, $\cos \frac{\pi t}{2T} \cos \omega_0 t$ and $\sin \frac{\pi t}{2T} \sin \omega_0 t$, required to generate the modulated FFSK signal are generated by a hybrid coupler as suggested by Brady (1974). In the present case $\omega_0$ corresponds to 135 MHz. These quadrature carriers are then amplitude modulated with alternate data bits to produce the modulated signal.

A block diagram of the demodulator is shown in figure 7. After down-conversion from the IF frequency to the FSK centre frequency of 135 MHz, the received FFSK signal is amplified and passed through a four-channel signal splitter. Two of the four channels are used in a squaring operation to obtain a signal which is predominantly a double frequency version of the inputs. This squared signal is the so-called Sunde FSK signal which has spectral lines at twice the modulator FSK carrier frequencies. Recovery of these carriers is accomplished by means of two phase-locked loop circuits. The voltage-controlled oscillators in the phase-locked loops are designed to operate, one at the upper FFSK carrier fre-

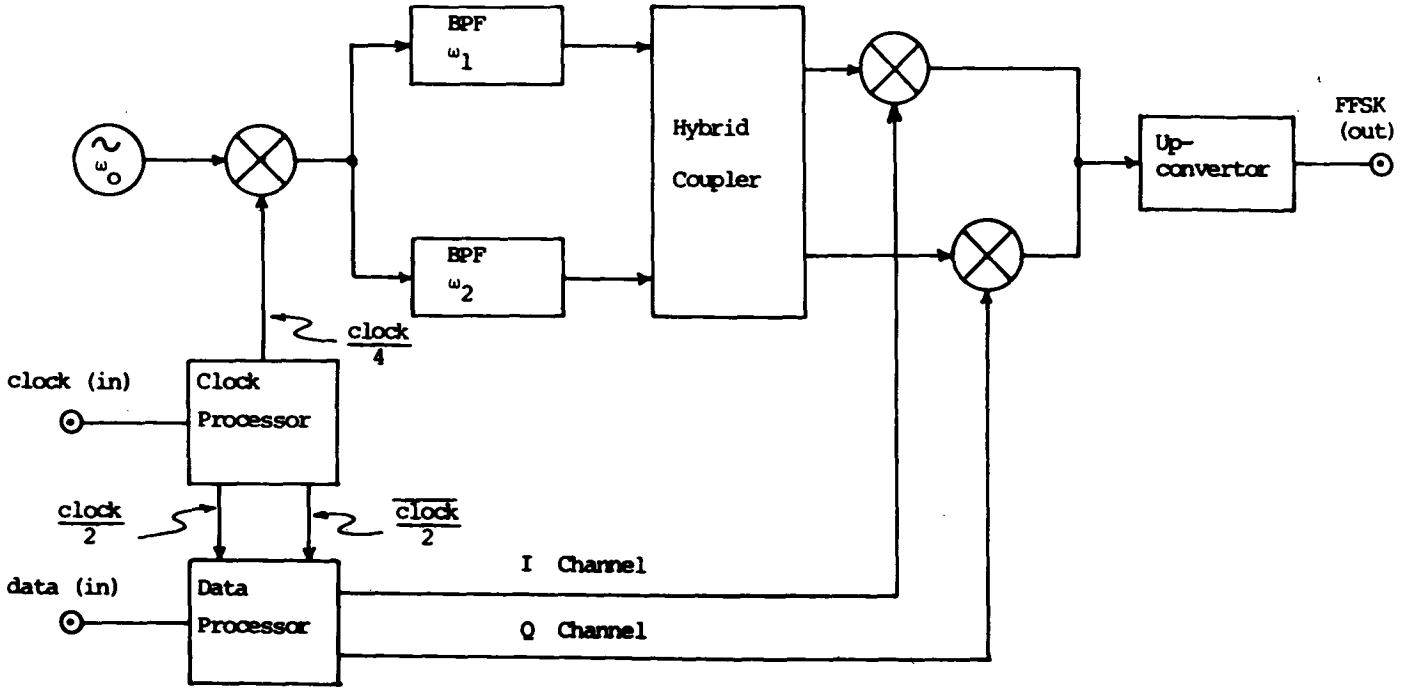


Figure 6: Modulator block diagram

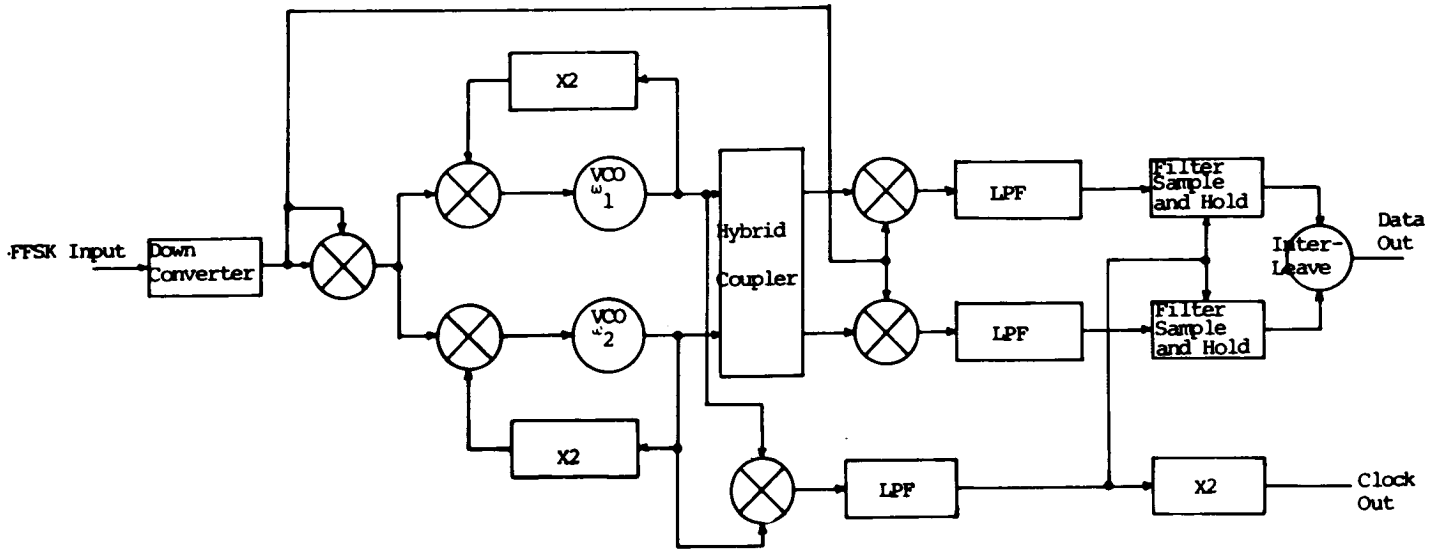


Figure 7. Demodulator block diagram.

quency and the other at the lower FFSK carrier frequency. The VCO outputs are added and subtracted with a hybrid coupler, in a similar fashion to that at the modulator to generate the quadrature "carrier" signals to equations (7) and (8) which are used in the coherent detector.

Clock timing recovery is accomplished by mixing the VCO outputs which are separated by 1/2 the clock frequency. By low-pass filtering the mixer output, a half-clock frequency signal is obtained for data bit synchronization after detection. A times-two multiplier is used to convert the half-clock signal to the clock rate for external synchronization.

The FFSK signal is coherently detected using the regenerated "quadrature" carrier signals. Two parallel channels of data are formed, each channel being at one-half the original data rate (i.e. 30 Mb/s each channel). The pulse shape of the demodulated signals is a raised cosine.

The classic approach to signal detection in the presence of noise is the use of a matched filter. The most common matched filter implementation used in the detection of digital data is an "integrate and dump" type of circuit. However, it was found that the time required to "zero" the integrator was too long for the bit rate involved. It was thus decided in the interests of simplicity to design a low-pass filter which could be optimized experimentally. An active, second order, Butterworth filter was chosen (Taylor et al, 1976; Taylor et al, 1977), and its performance was optimized by choosing its time-constant to obtain minimum error-rate as a function of $E_b/N_o$.

## 4. Performance Testing

The FFSK modem described in section 3 has been subjected to an extensive test program. This program was carried out in three stages, namely, preliminary back-to-back testing at the time of construction (Ogletree et al, 1975), a laboratory test program using a satellite transponder simulator (Taylor et al, 1976) and finally a set of field tests using the Hermes satellite (experiment U-4) during 1976 and 1977.

The results of the back-to-back testing are shown in figure 8. The curve labelled baseband indicates the results obtained when the up- and down-converters shown in Figures 6 and 7 were bypassed, and the only source of interference was additive Gaussian noise injected at the demodulator input, as shown in the test set-up of figure 9. It is of interest to note that, at a probability of error of $10^{-5}$, the performance is within 1.1 dB of the theoretical curve and at $10^{-6}$ within 1.3 dB, indicating that the modem implementation is very close to being optimum. The second curve in figure 8, labelled "CTS IF converters enabled", indicates the back-to-back results obtained when the up- and down-converters are enabled. These converters translated the

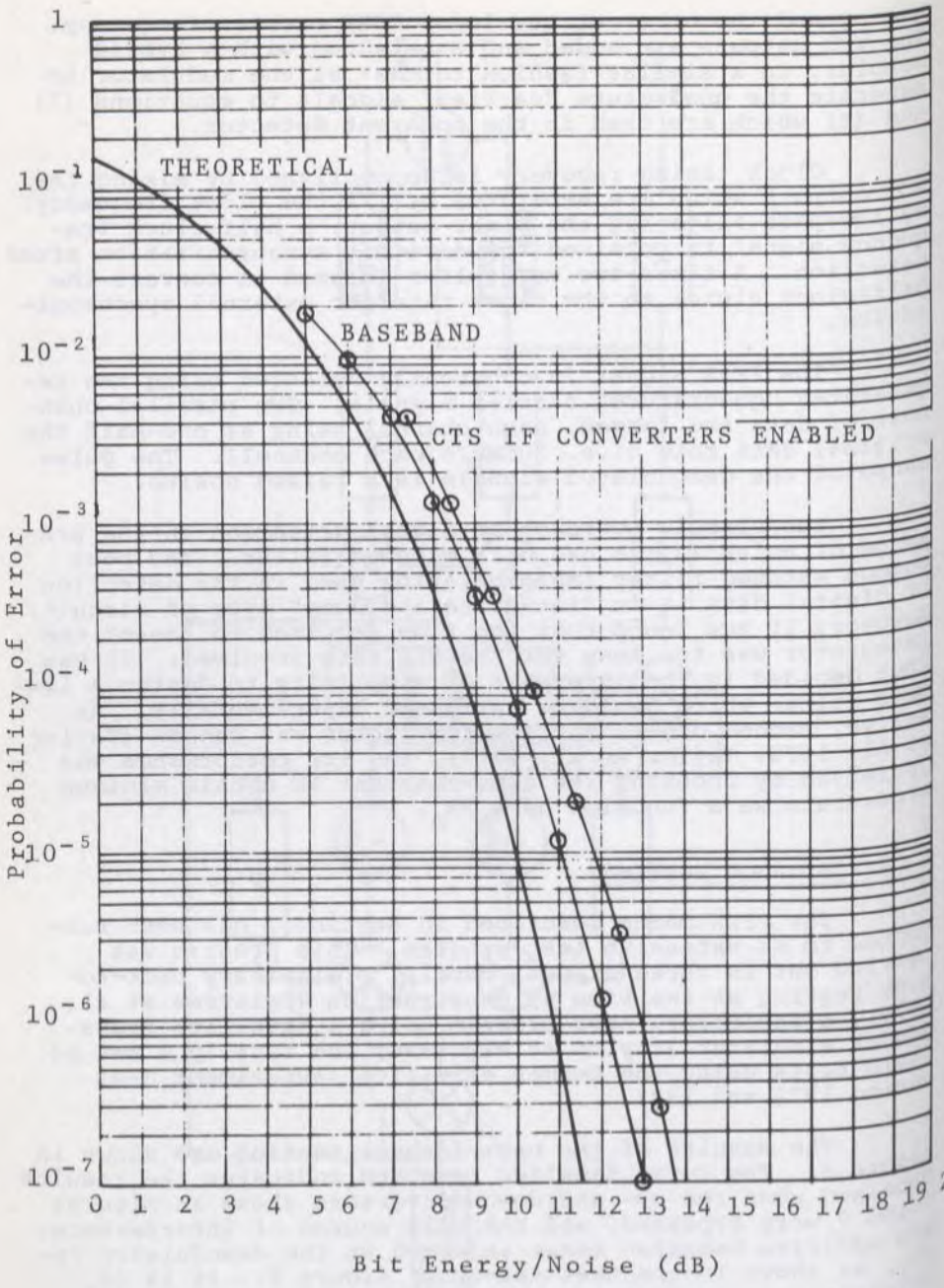


Figure 8: Measured back-to-back error-rate results for the FFSK modem.

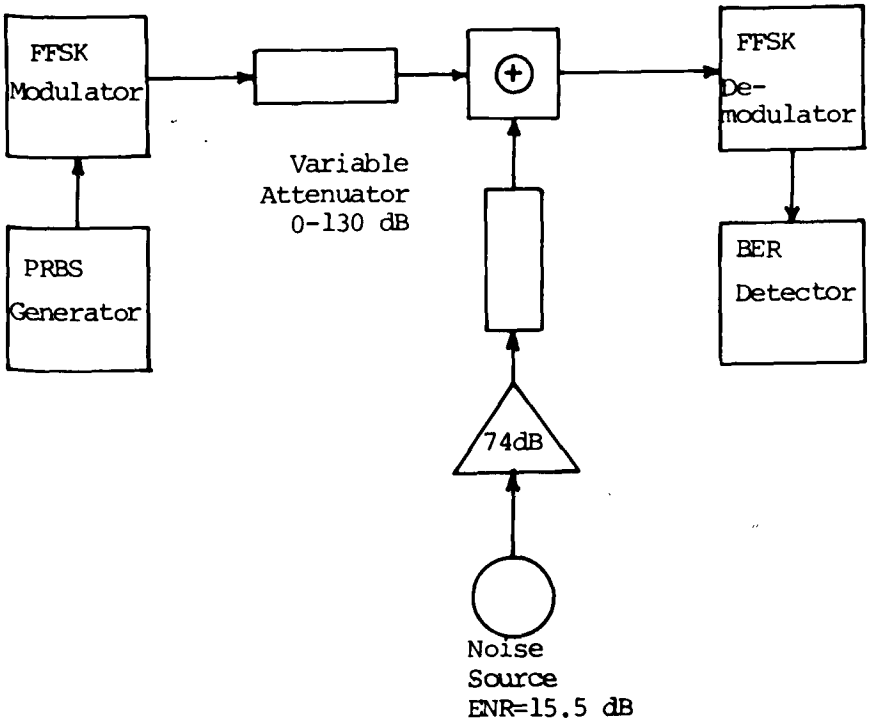


Figure 9. Test set-up used to obtain back-to-back error-rate results.

signal from a centre frequency of 135 MHz, the modem's internal carrier frequency, to 735 MHz, the IF frequency used in the Hermes system ground terminals, and in so doing, introduced an additional degradation of 0.7 dB at $10^{-5}$ and 0.8 dB at $10^{-6}$.

The second stage of the test program consisted of measurements of bit error-rate (BER) or probability of error as a function of $E_b/N_o$ after the signals had been passed through a transponder simulator operating at a centre frequency of 11.265 GHz. During these tests a detailed operational test plan was evolved for use in experiment U-4 (Taylor et al, 1976) on the Hermes system. A block diagram of the simulator is shown in figure 10, and the results of the tests are shown in figure 11. The curve labelled "TWTA in saturation" indicates a degradation of 1.2 dB from the IF result at a BER of $10^{-5}$ and 1.8 dB at a BER of $10^{-6}$. These curves were obtained for a demodulator input level of -5.5 dBm, the highest that could be obtained with the available equipment. Other tests (Taylor et al, 1976) have shown that about 0.7 dB of the degradation can be recovered if the demodulator input level is raised to approximately 0 dBm, which was the level used in the field testing described below.

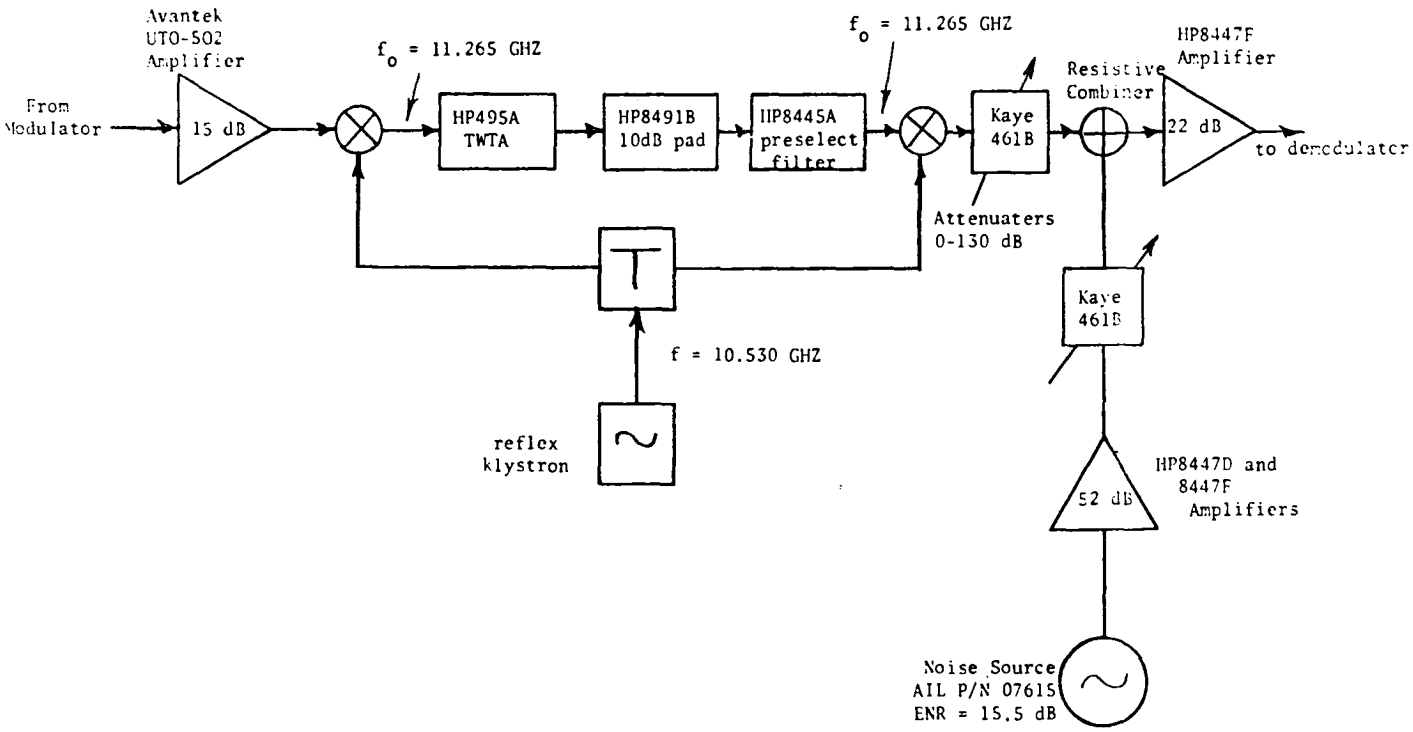


Figure 10. Block diagram of the transponder simulator.

The curve in figure 11 labelled "with 36 MHz filter" shows the result of interposing a 36 MHz bandwidth filter between the modulator and the input to the transponder simulator. This causes a performance degradation due to the presence of intersymbol interference (ISI) of approximately 2.4 dB at a BER of $10^{-5}$ and almost 4 dB at $10^{-6}$.

The third and final stage in the testing of the modem consisted of field tests using Hermes. During June 1976, the majority of the tests used the high-power (200 W) transponder. These tests consisted largely of measurements of BER as a function of $E_b/N_o$ using a number of different channel configurations. The detailed results are given elsewhere (Taylor et al, 1977). Typical results with the 200 watt transponder operating in saturation are shown in figure 12. Curves A and B show the results when the full 85 MHz transponder bandwidth was used, with curve A for a demodulator input level of 0 dBm and curve B for a level of -4 dBm. As can be seen, curve A is degraded from theoretical by only 2.4 dB at a BER of $10^{-6}$ and curve B by an additional 0.5 dB. Curves D and E represent the results obtained when 45 and 36 MHz bandwidth filters are placed at the demodulator input; they show the expected additional degradation due to ISI of between 3 and 4 dB. Curve C was obtained when the 45 MHz filter was placed at the modulator output. The somewhat more severe degradation encountered here is probably due to the AM/PM conversion effects of the satellite transponder (Huck and Nuspl, 1975) on the bandlimited signal.

A second set of tests during May 1976 used the Hermes low-power (20 W) transponder. These tests have not been reported previously but again, because of space limitations, only a few of the results are presented here. Figure 13 shows bit error-rate as a function of $E_b/N_o$ under three different channel conditions, but in all cases with the 20 watt transponder operating in saturation. Also shown for purposes of comparison are the back-to-back results of Figure 8. Curve number 1, with the full 85 MHz transponder bandwidth, shows a degradation from the back-to-back IF curve of only 2.4 dB at a BER of $10^{-6}$. The received signal spectrum for this case (Fig. 14) shows small spectral spreading and the spectral sidelobes are approximately 23 dB below the peak value. This value is the same as the theoretical value for the first spectral sidelobe of FFSK.

Curve number 2 in figure 13 is for the case when a 45 MHz bandwidth filter is placed at the modulator output, and curve number 3 is for the case of a 36 MHz filter. As expected, rather severe degradation is caused by the bandlimiting. It is of some interest to compare curve 3 in figure 13 with curve C of figure 12 which was obtained using the same filter and the high-power transponder. As can be seen the two curves are virtually identical and we may conclude that the effects of the two transponders on the bandlimited signals are approximately the same.

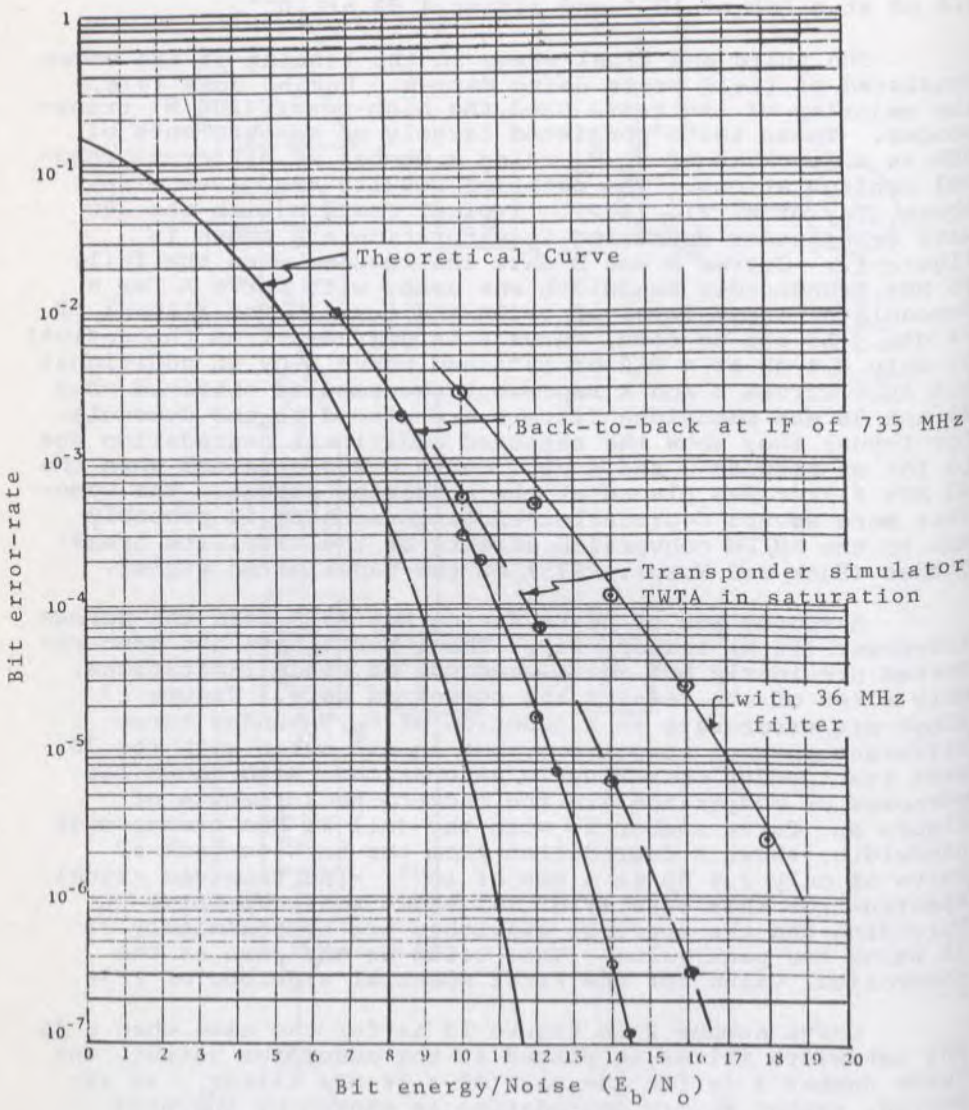


Figure 11. Error-rate curves obtained using the transponder simulator.

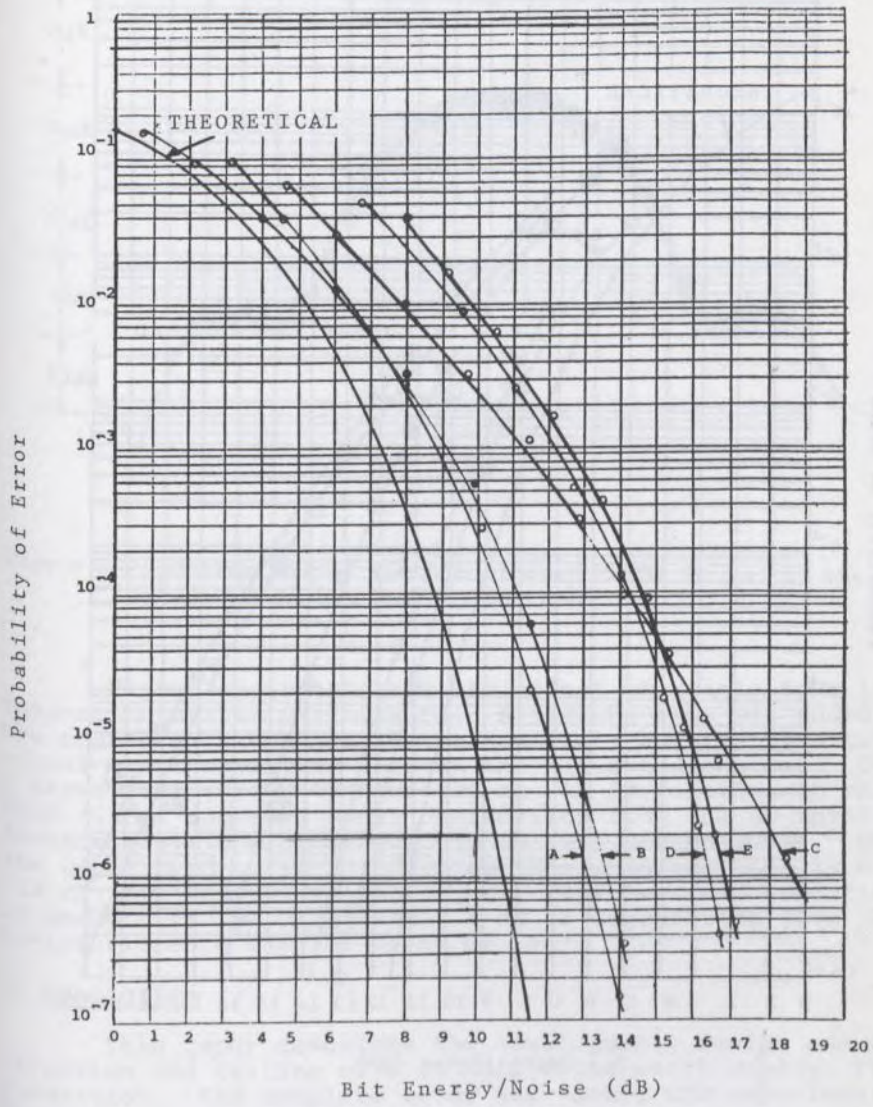


Figure 12. Error-rate curves obtained on 22 June 1976 with high power transponder in saturation.

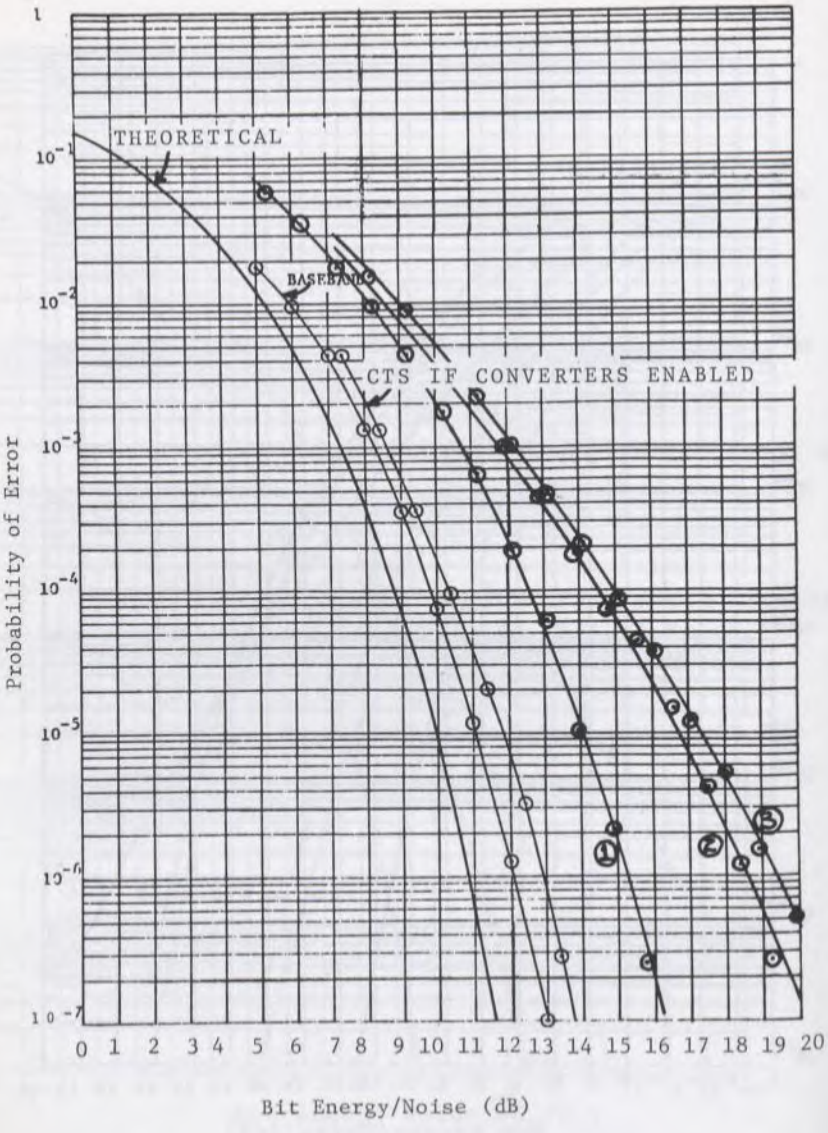


Figure 13. Bit error-rate as a function of $E_b/N_o$. Curve 1 is for the wideband configuration. Curve 2 was obtained using the 45 MHz filter and curve 3 was obtained using the 36 MHz filter. In all cases, the CTS 20 watt transponder was operated in saturation.

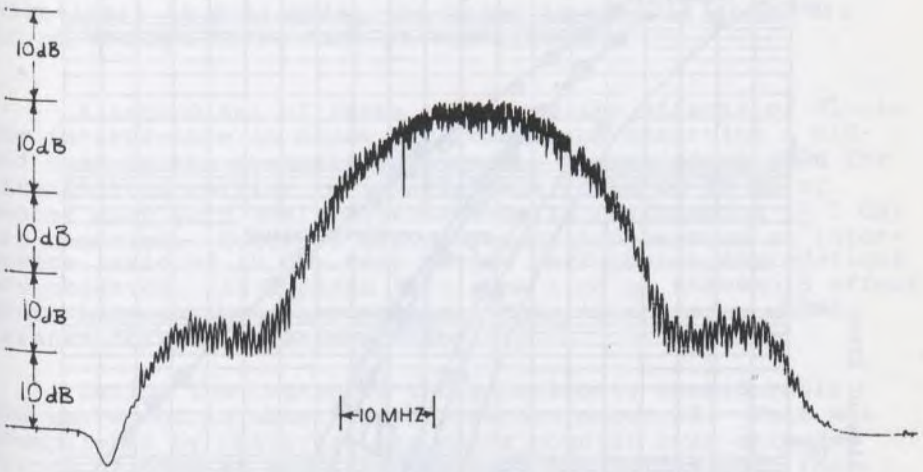


Figure 14. Received signal spectrum at the 735 MHz IF port in the wideband case. (Curve 1 on figure 13).

Figure 15 illustrates the effect of single-tone interference on system performance. A midband tone was added to the modulated signal at the transmitter, and the resultant signal was transmitted through the saturated channel. Curve 3 shows that a tone transmitted at -15 dB relative to the FFSK signal causes a small degradation from the no-interference case (approximately 0.9 dB at a BER of $10^{-6}$). On the other hand curve 2 indicates that when the tone is at -10 dB with respect to the signal, very severe degradation is encountered, approximately 6 dB of degradation from the no-interference case at a BER of $10^{-4}$.

## 5. Conclusion

This paper describes the development, design and construction and testing of a 60 Mb/s modem which employs FFSK modulation. The complete study has formed CTS experiment U-4 which culminated in field testing the modem using the Hermes satellite during 1976 and 1977.

In the wideband testing of the modem on Hermes excellent performance was obtained, with degradations of the order of 2 dB from back-to-back- performance. This compares favorably with the performance of conventional quaternary phase-shift keying modems over similar channels.

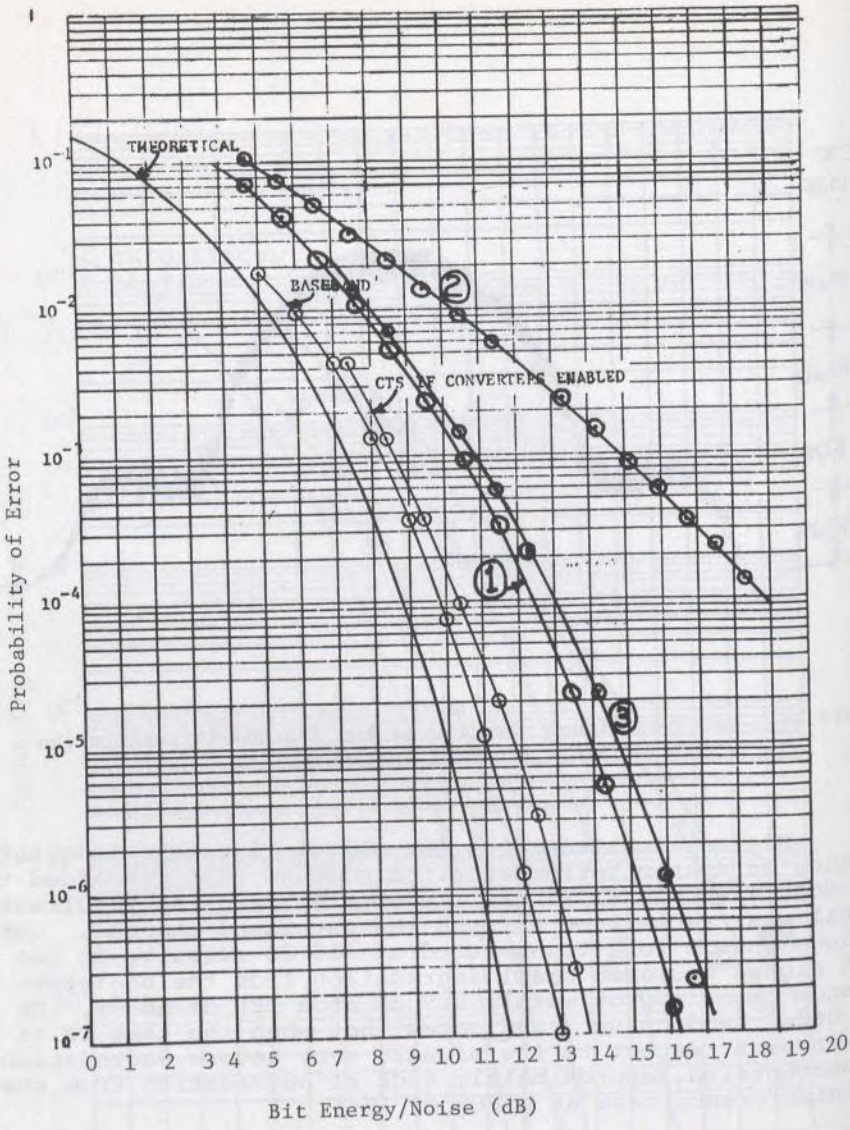


Figure 15. Bit error-rate vs $E_b/N_o$ in the presence of single tone interference. Curve 1 is wideband result with no interference. Curve 2 is result for a tone-transmitted at -10 dB with respect to the FFSK carriers and curve 3 for a tone-transmitted at -15 dB with respect to the FFSK carriers.

One set of field tests concentrated on evaluating the performance of the modem under severely bandlimited conditions. As a result of these tests, it appears that for BT as low as 0.6, modem performance degrades fairly gracefully and that provided sufficient noise margin (about 9 dB from theoretical) is available, the modem is useable at BT=0.6 with no attempt being made at equalization.

A second set of tests evaluated the effects of single tone interference on modem performance by inserting a mid-band tone in the transmitted stream. It was found that for a transmitted carrier to interference ratio of 15 dB or greater only very small degradations in performance ($\leq$ 1 dB) were observed. However, for a transmitted carrier to interference ratio of 10 dB, very severe performance degradations were observed. It appears that some kind of threshold effect occurs between these two values. This is an issue which warrants further experimentation.

During the course of the experiment, considerable time was spent in observing how errors occurred. This was accomplished by observing the error counter over extended periods of time at sufficiently high SNR values such that errors occurred only once a second or less. In all cases, errors occurred only in pairs. Thus instead of considering single error behavior, it appears that we should be considering the error event or burst error behavior of the modem. It is hoped to at least partially resolve this issue by measuring word error-rates and mean-time between errors later this year, using equipment developed by the Communications Research Centre.

The overall conclusion of the study is that the FFSK modulation technique offers superior performance and a simpler implementation than a conventional PSK system, and that further development should be carried out to produce complete high-performance digital satellite communications systems employing FFSK.

## 6. Acknowledgement

The authors wish to thank K.E. Brown, N.G. Davies and P.P. Nuspl all of the Communications Research Centre for their very valuable guidance throughout the course of the study.

## REFERENCES


Brady, D.M.
1974 A constant envelope digital modulation technique for millimeter-wave satellite systems, presented at *Int. Conf. on Comm.*, Minneapolis, Minn., June.

Chan, H.C., Taylor, D.P. and Haykin, S.S.
1974 Comparative evaluation of digital modulation techniques, *CRL Internal Report No. CRL-18, part III*, Communications Research Laboratory, McMaster University, Hamilton, Canada. April.
1975 A comparative study of digital modulation techniques for single carrier satellite communications, *Proc. 3rd International Conference* on Digital Satellite Communications, Kyoto, Japan, 11-13 November.

Davenport, W.B., Jr., and Root, W.L.
1958 An introduction to the theory of random signals in noise, McGraw-Hill Book Company, Chapter 6.

deBuda, R.
1971 The fast FSK - a new modulation system, Canadian General Electric Co., Ltd., *CGE Report No. RQ71EE2*, February.
1972 Coherent demodulation of frequency-shift keying with low deviation ratio, *IEEE Trans. Comm.*, vol. COM-20, pp. 429-435, June.
1975 Binary encoding for the fast FSK, Communications Research Laboratory, McMaster University, Hamilton, Canada, *CRL Internal Report Series No. CRL-27*, January.

deBuda, R. and Anto, H.
1969 About FSK with low and modulation index, Canadian General Electric Co., Ltd., *CGE Report No. RQ 69EE11*, December.

Eric, M.J.
1972 Intermodulation analysis of nonlinear devices for multiple-carrier inputs, Communications Research Centre, Ottawa, Canada, *CRC Report No. 1234*, November.

Hedderly, D.L. and Lundquist, L.
1973 Computer-simulation of a digital satellite communications link, *IEEE Trans. Comm.*, vol. COM-21, pp. 321-325, April.

Huch, R.W. and Nuspl, P.P.
1975 CTS transponder protoflight model communications test report, Dept. of Communications, Space Programs Branch, *Report No. CS-04-04*, 13 August.

Lucky, R.W., Salz, J. and Weldon, E.J., Jr.
1968 Principles of data communication, McGraw-Hill Book Company, Chapter 4.

Muratani, T., Matsushita, I., Tsuji, Y. and Hara, T.
1972 Simulation of a PSK transmission system including the nonlinear satellite channel, *2nd Int. Symp.* on Digital Satellite Communication, Paris, November, pp. 184-192.

Ogletree, S.T., Taylor, D.P. and Haykin, S.S.
1975 Design and implementation of a 60 Mb/s fast frequency-shift keying modem, *CRL Internal Report No. CRL-30*, Communications Research Laboratory, McMaster University, Hamilton, Canada, March.

Sass, E.J. and Hannum, J.R.
1973 An MSK modem, presented at *Int. Conf. on Comm.*, Seattle, Wash., U.S.A., June 12.

Taylor, D.P., Chan, H.C. and Haykin, S.S.
1976 A simulation study of digital modulation methods for wideband satellite communications, *IEEE Trans., Comm.*, vol. COM-24, pp. 1351-1354, December.

Taylor, D.P., Horvai, G. and Haykin, S.S.
1976 Laboratory test program for the CRL 60 Mb/s fast frequency-shift keying modem, *CRL Internal Report No. CRL-36*, Communications Research Laboratory, McMaster Univeristy, Hamilton, Canada, May.
1977 Field testing a 60 Mb/s FFSK modem on the Hermes satellite: phase I, *CRL Report No. CRL-46*, Communications Research Laboratory, McMaster University, Hamilton, Canada, March.

Taylor, D.P., Ogletree, S.T., Chan, H.C. and Haykin, S.S.
1977 A high speed digital modem for experimental work on the communications technology satellite, *Canadian Electrical Engineering Journal*, vol. 2, pp. 21-30, January.

Taylor, D.P., Ogletree, S.T. and Haykin, S.S.
1976 A prototype 60 Mb/s fast frequency-shift keying modem, *Conf. Rec., Int. Conf. on Comm., ICC '76*, Philadelphia, Penn., U.S.A., pp. 51-26 to 51-30, 14-16 June.

# DATA TRANSMISSION VIA THE HERMES SATELLITE: MEASUREMENT AND EVALUATION

J.W. Mark and I.F. Blake

Computer Communications Networks Group

University of Waterloo, Waterloo, Canada

*La largeur de bande effective de la voie de communication à notre disposition est celle de la bande de base téléphonique reçue par la station terrienne de 1m du Hermès, soit environ 2 400 Hz. Par conséquent, les caractéristiques décrites dans le présent article découlent principalement de la restriction imposée à la largeur de bande par le fait de la jonction avec la bande de base téléphonique plutôt que par la voie de transmission par satellite car le taux d'erreurs est pratiquement nul lorsque la vitesse de transmission est inférieure à 7,200 bps. Par contre, lorsque la voie n'est pas codée, des erreurs se produisent à 9,600 bps.*

*Les erreurs calculées semblent intermittentes et dispersées. On estime que la voie de transmission pourrait être établie sur le modèle d'un canal binaire symétrique, le nombre d'erreurs à chaque passage devenant alors une variable aléatoire binômiale. Toutefois, l'approximation de la loi binômiale par la loi de Poisson n'est pas vérifiée par le test de validité de l'ajustement au chi carré. Nous concluons que la jonction de l'interface et de la voie de transmission du satellite ne peut se fonder uniquement sur la distribution de Poisson.*

*Les résultats indiquent que la transmission de données au rythme de 9,600 bps sur la voie de transmission du satellite reliée à la bande de base téléphonique nécessiterait un codage de la voie de transmission afin d'éviter une multiplication catastrophique des erreurs.*

## 1. INTRODUCTION

The original purpose of this Hermes experiment was three-fold: 1) to examine the effect of certain signal processing techniques on compressed-video data transmitted on a satellite channel, 2) to examine the usefulness of convolu-

tional coding, and methods of implementing such coding techniques, on a combined land and satellite channel, and 3) to model the combined land and terrestrial channel for data communication by measurement in a manner similar to Fuchs and Jackson, 1969, who modelled terrestrial computer communication systems. These objectives assumed we would have an IF interface to Hermes. Initially, much effort was expended in developing software for the network of four PDP-11 computers of the University of Waterloo Computer Communications Networks Group Laboratory. However, this coding software was not fast enough for real-time application.

At about this time, we first realized that, although a Hermes interface at 70 MHz could be provided by CRC, a high-speed digital modem could not be made available. This meant that the effective channel bandwidth for our experiment would be limited by the telephone interface. Accordingly, early in 1976, it was decided to concentrate on more basic measurements related to the error process, which would be relevant to further work on the satellite channel. Software for the minicomputers was prepared which allowed flexible and effective use of the channel for this purpose. With these limited objectives, we were successful.

Section 2 reports on our attempts to characterize the channel, by measuring only two of the parameters: spectral shape (amplitude) and path length. Measurements on the phase jitter and time delay would also have been useful. Considerable variation in the error statistics was observed between early morning and mid-morning and this was attributed to the shifting beam pattern caused by satellite movement. A novel method for attempting to detect this movement is described in Section 2.

Section 3 reports on the error measurements and the configuration used to obtain them. The sophisticated modem used (a Codex 9600) introduced some problems in the analysis of this data, but these were largely overcome.

In Section 4 the results of transmitting slow-scan video data are given. Because of equipment limitations, we have not yet drawn conclusions on the effect of errors on the various compression techniques for such pictures.

The final section comments on the usefulness of the experiment and the conclusions reached. In particular, it examines how the results of this effort would affect the planning of possible future experiments.

## 2. CHANNEL CHARACTERIZATION

### 2.1 Objectives

The main objective of the entire experiment was to gain insight into the error process on the channel. Much of

the planning for this objective centered on software for the minicomputers to process and compile errors and error statistics.

A diagram of the experimental system is given in figure 2.1. The signal was transmitted from Waterloo through a portable 1m antenna up to the satellite. For the first four weeks of the experiment the signal was received by the 3m antenna at Moose Factory, Ontario. It was attenuated through a 23 db pad to compensate for preset gains, and then returned through the satellite to Waterloo. For the last two weeks of the experiment the signal was received at Ottawa using the 9m dish.

## 2.2 Channel Spectral Characteristics

It was mentioned previously that considerable variation was noted in the error statistics from early morning transmissions to mid-day transmissions. It was felt that this was probably a result of satellite movement and beam shift and to see if this was reflected in signal amplitude characteristics both early morning (8:30 a.m.) and mid-morning (11:30 a.m.) readings were taken. Surprisingly, no detectable variations were found. Only two sets of readings are shown in figure 2.2.

## 2.3 Path Length Measurements

Because of the observed variation in error statistics, an attempt was made to see if co-related satellite movements could be detected by path length measurements, using the equipment shown in figure 2.3. A short train of square pulses was initiated manually for transmission on the channel. Simultaneously the 10 MHz timer of the programmable hardware monitor was started. The return signal, detected by a level-crossing circuit, stopped the timer. Almost all the inaccuracy of the method is due to the distorted pulse shape of the return signal and determining precisely where the circuit was triggering. Experience with this method suggested that, after this adjustment, the absolute readings are accurate to ± 35 μsecs while the differential measurements are accurate to at least ± 10 μsecs and possibly better.

Consider the data for March 11th, 1977 only. At 9:25 a.m. the average measured time delay was 0.531401 ($\pm$ 35 x $10^{-6}$) s. At 10:38 a.m. the average measured time delay was 0.531455 ( $\pm$ 35 x $10^{-6}$) s. The differential of the two readings is 53.7 ± 10 μsecs or 16.11 ± 3.00 kms, in the total path length.

# 3. DATA EXPERIMENT

## 3.1 Description of Experiment Configuration

The experiment configuration was as in figure 2.1. The Codex 9600 modem is capable of data rates 4800, 7200 and

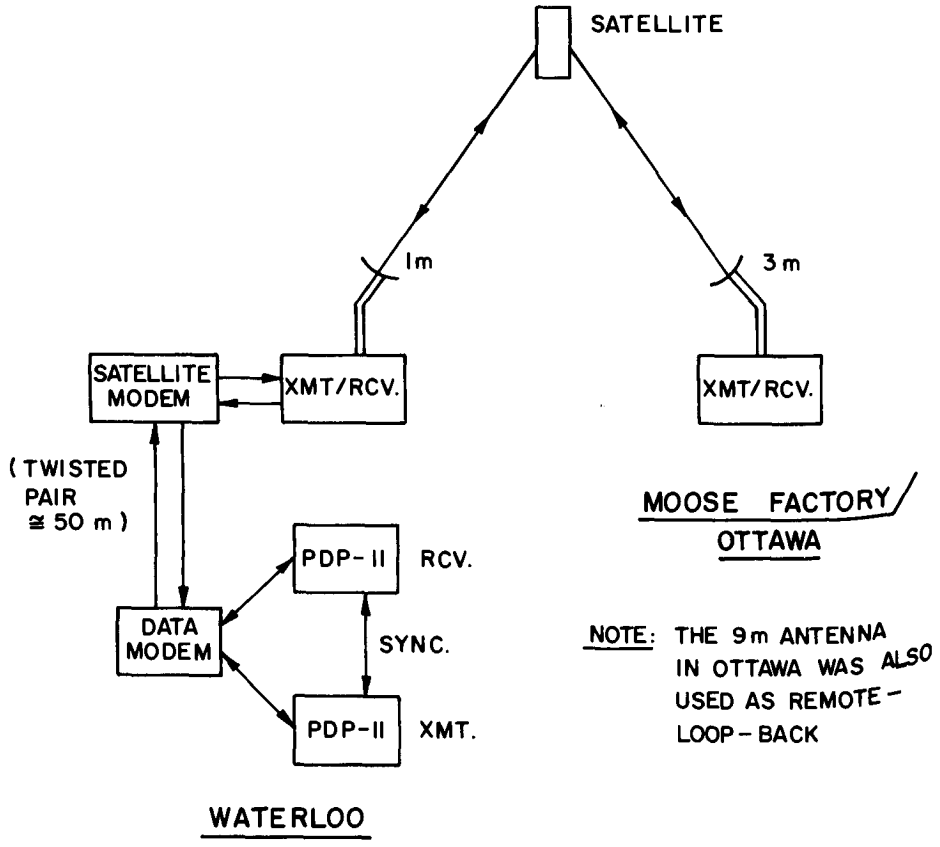


Figure 2.1 Hermes experiment configuration.

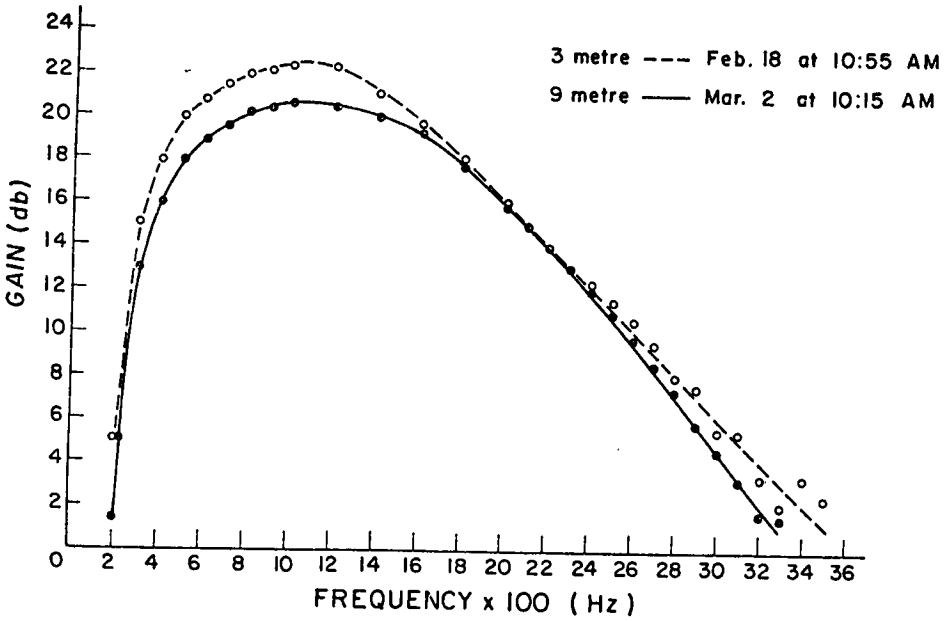


Figure 2.2 Measured amplitude characteristics of telephone-baseband-interfaced satellite channel.

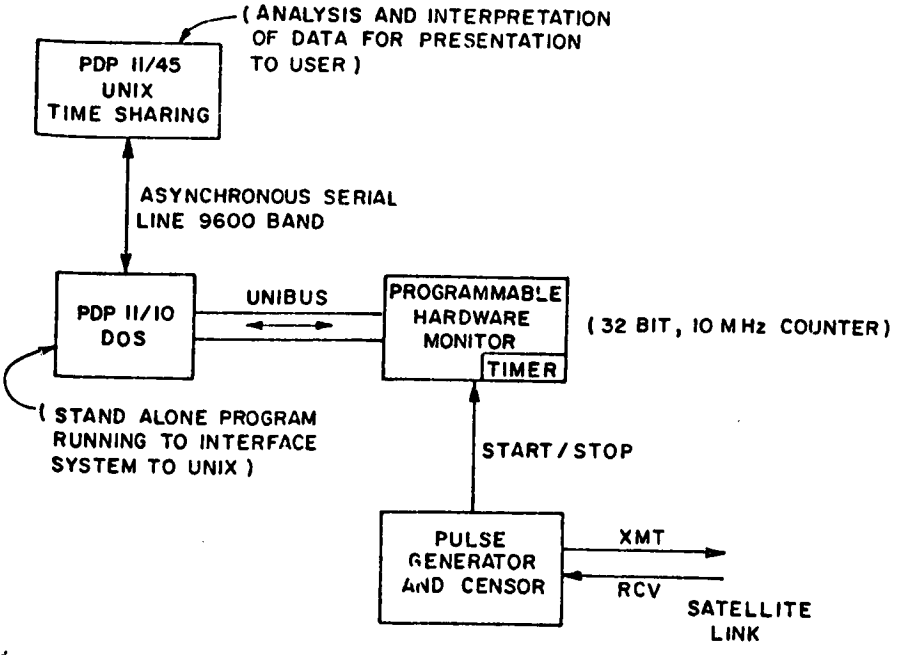


Figure 2.3 Data measurement configuration.

9600 bps. Briefly stated, at 9600 bps a 4-bit register is loaded with data. Each such 4-bit sequence corresponds to one of 16 phase and amplitude-modulated symbols. At 4800 and 7200 bps, 2 and 3 bits respectively are taken from the data and the 4-bit register is completed with zeros.

Part of our interest in the modem operation was to determine, for a given input sequence, which errors were more likely to occur. This would, of course, be a function of the signal configuration used by the modem. Because of the maximum length sequence and Gray coding operation, such studies were virtually impossible.

## 3.2 Comments on the Data

The appearance of the data was very much of a random, non-burst, nature and this is illustrated by the fact that, in the burst length total record, the predominant figure is always for bursts of length 1. When an error occurred, however, it was sometimes accompanied by errors in the same or adjacent half byte. This was attributed as much to the modem operation as to burst noise, and as alluded to earlier, it was difficult to interpret the effect of the modem on the channel.

Due to the random appearance of the data it was felt that the channel might be modelled as a binary symmetric channel in which case the number of errors per pass would be a binomial random variable. To test this hypothesis, the Poisson approximation to the binomial was used and the chi-square test to determine the goodness of fit of the data to a Poisson distribution tried (for the errors per pass data).

As an illustration, the chi-square variable

$$\chi^2 = \sum_{i=1}^{k} \frac{n_i - \ell_i^{\,2}}{\ell_i}$$

where $n_i$ is the number of passes in which $s_i$ errors were obtained, and $\ell_i$ the expected number of such errors if the Poisson distribution were in effect. Here $s_i$, which could be a range of error values, was chosen so that $\ell_i \geq 5$. For example, for one file containing 100 passes, $s_1$ was chosen to be the range 0 to 11 and $n_1 = 27$, $s_i = 10 + i$, $i = 2, \cdots, 13$, $s_{14}$ was chosen as the range 24 to 63. The average number of errors per pass was 17.31 and the quantities $\ell_i$ calculated from the Poisson distribution with parameter $\lambda = 17.31$. The variable $\chi^2$ was calculated as 69.98 and, since $\lambda$ was estimated from the data, it has $k - 2$ or 12 degrees of freedom. Consulting $\chi^2$ tables we conclude quickly that it is highly unlikely that the data was generated according to a Poisson distribution. We attribute that to

the fact that the error process is more complicated than anticipated and that some dependencies, not apparent from its appearance, exist. The same test was done on other files with the same result.

Similarly, chi-square tests were applied to the burst-length totals, excluding zero length, this time testing whether the burst mechanism could be modelled as an exponential random variable X, with distribution

$$P(X=k) = p^{k-1}(1-p), \quad k = 1, 2, \ldots$$

The mean of such a distribution is $1/(1-p)$ and from this parameter p was estimated from the data for each file. The chi-square test was then applied and again, for each file tested the hypothesis that the burst length was an exponential random variable was rejected.

The results of these tests, while disappointing from a modelling point of view, simply reflect the fact that the process causing errors on the channel and in the modem operation is more complicated than the simple models assumed. It was decided not to pursue the modelling aspect of the experiment at this time and no further tests have been performed on the data as yet.

## 4. VIDEO DATA EXPERIMENT

### 4.1 System Configuration

The useful bandwidth seen by our transmitted data was approximately 2400 HZ (Fig. 2.2). The experiment configuration was as shown in figure 4.1. Black and white images were scanned by a Sony camera digitized to 6 bits per picture element (pel) and inputted into the PDP 11/45 computer at a slow-scan rate using a CVI Model 260 video compressor. Computer programs were written to perform data compression/decompression and error detection in the PDP 11/45. Decompressed images were displayed on the video monitor via the CVI Model 261 video expander.

The CVI 260 video compressor executed vertical scanning. Each image frame consists of two interlaced fields with 200 vertical lines per field and 240 pels vertical scan line (Fig. 4.2). Thus, there are a total of 96,000 pels or 576,000 bits per frame. Interlaced sampling yields an effective sampling rate of approximately 3.8 MHz.

We have investigated many different data compression algorithms. Here we employed an adaptive predictive coding algorithm (Mark, 1976) depicted in figure 4.3. Both the quantizer and predictor are adaptive. A salient feature of the predictive coder of figure 4.3 lies in the fact that the adaptive predictor and quantizer are coupled together in their adaptive operation. A three-point predictor with the pels used for prediction as in figure 4.4 was used.

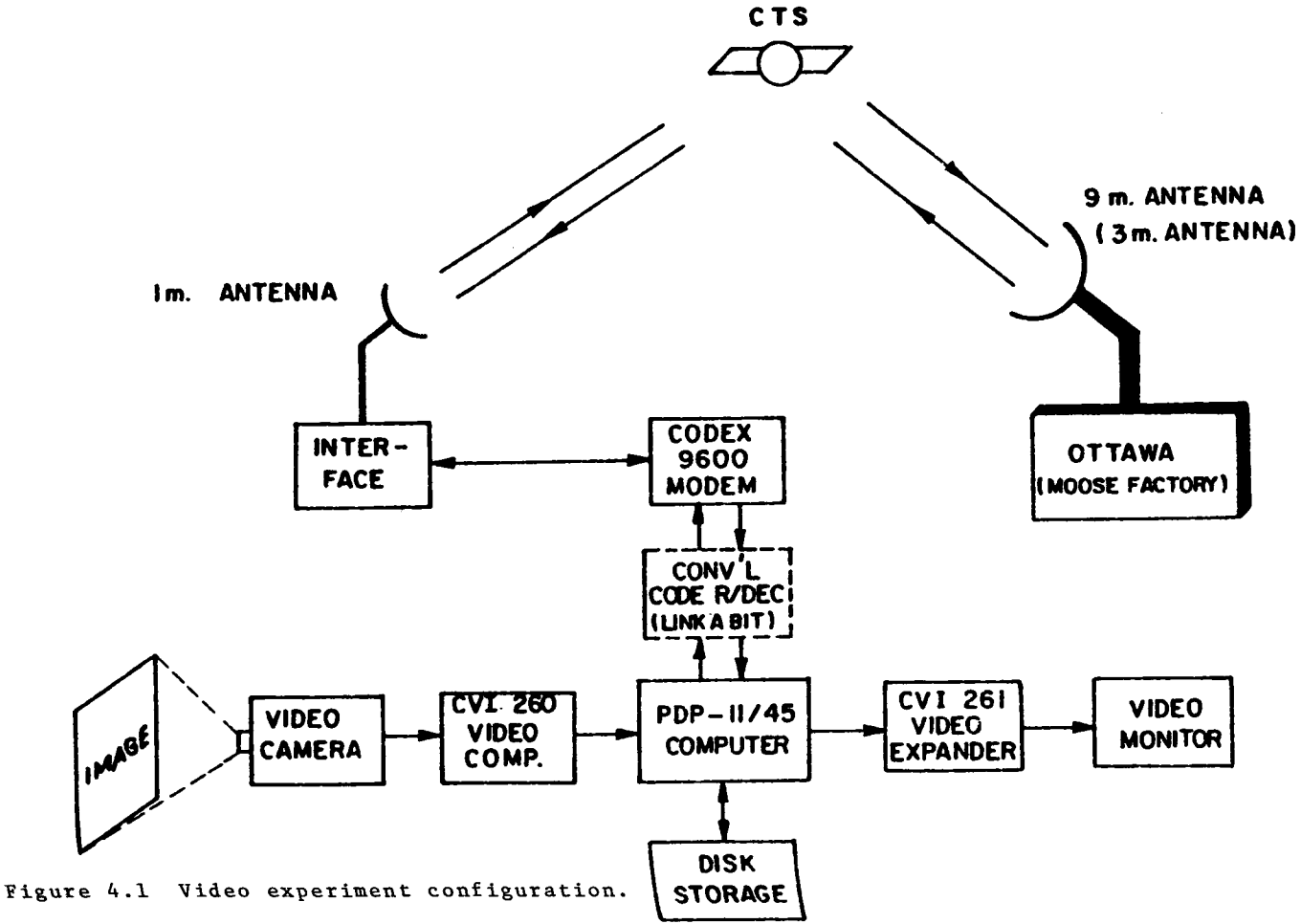


Figure 4.1 Video experiment configuration.

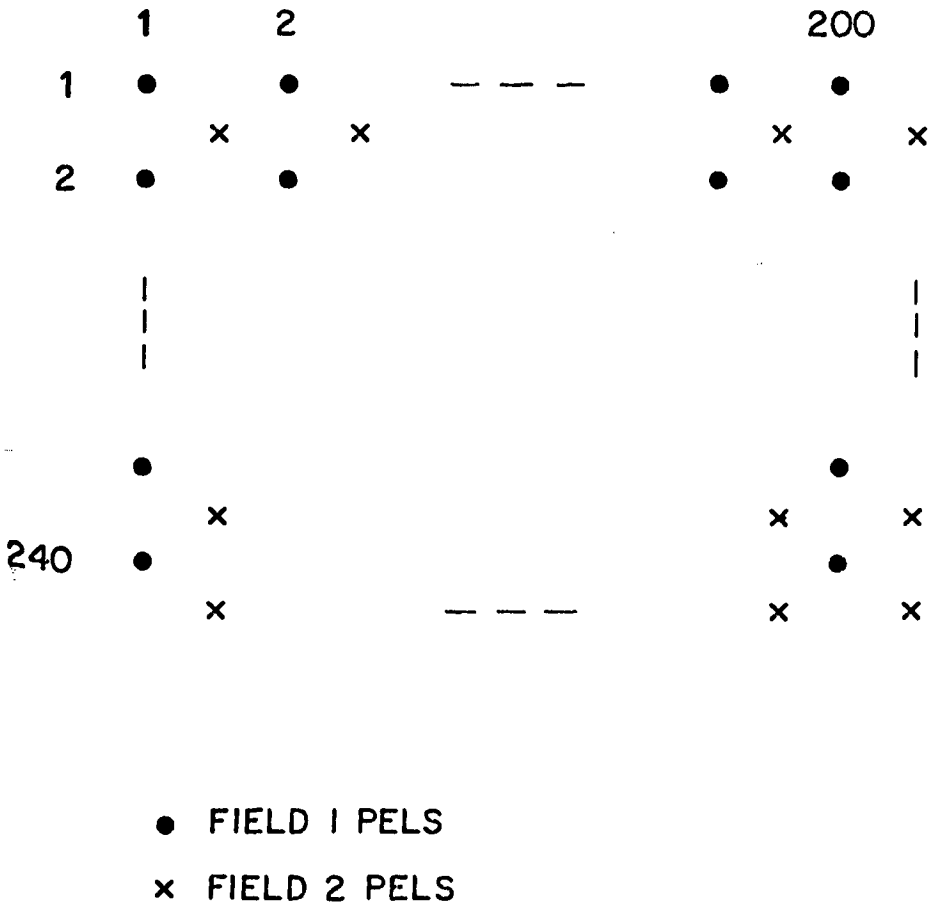


Figure 4.2 Interlace-scanned image array.

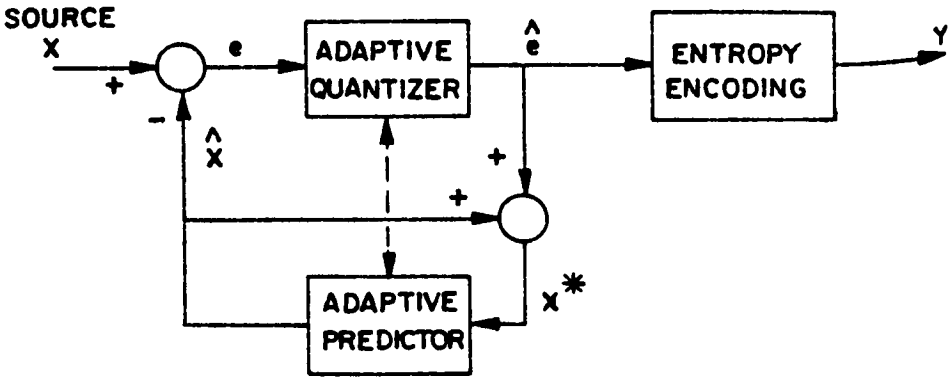


Figure 4.3 Adaptive predictive encoding.

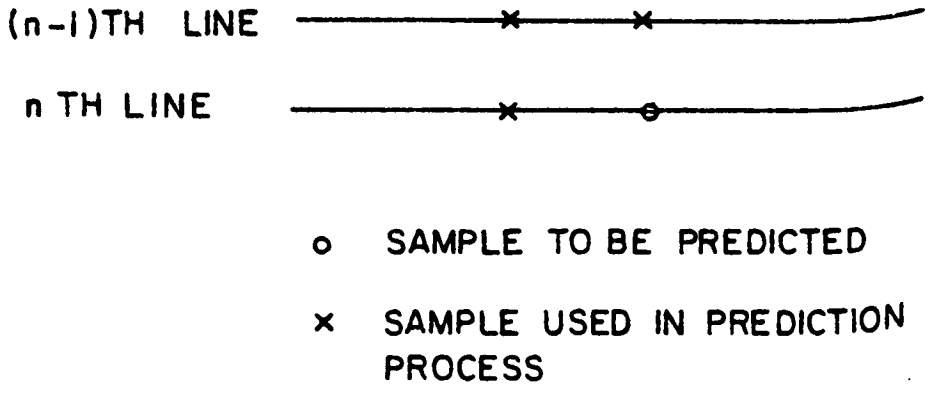


Figure 4.4 3-point predictor configuration.

Three images were used in the experiment. Images GIRL, LAB, and CROWD, which were sampled and quantized to 64 levels, represent respectively, low density, medium density and high density scenes.

## 4.2 Effects of Channel Errors

We transmitted coded image data at different transmission rates and different code rates. No errors were observed for data transmitted at 4800 bps. Even at a 7200 bps rate the amount of error is negligibly small. While a vast amount of data is logged in a separate volume (Mark and Blake, 1977), here we report on only the 5-level predictive coded and the 64-level uncoded image data transmitted at 9600 bps.

With transmissions at 9600 bps through a rate 1/2 convolutional encoder/threshold decoder, there was virtually no error in the received data. In the absence of the convolution encoder/threshold decoder, errors were observed.

Figure 4.5 shows the received 64-level uncoded images of GIRL and CROWD in which the transmission errors occurred in a particular scan line and the line containing errors was replaced by the preceding "good" scan line. Errors of this nature do not cause observable degradation. To illustrate the effects of transmission errors on compressed data, we display in figure 4.6 the decompressed 5-level coded images of the CROWD scene. Because of the recursive characteristics of the adaptive predictive coder, once an error has been encountered, it persists over many lines. With the memory of the predictive coder refreshed at the start of each scan line, it is possible to confine transmission errors within a scan line to avoid error propagation.

## 5. COMMENTS AND CONCLUSIONS

While the spectrum and path length measurements proved to be interesting, the most useful contribution of the experiment is undoubtedly in the data and video experiment results (Mark and Blake, 1977). Further analysis of these results would be of interest, and various directions are possible. From a personal point of view, the experimenters gained considerable experience with the satellite channel and equipment and a good appreciation of their capabilities. This experience was very satisfying and would prove extremely useful in the planning of any further satellite work.

## ACKNOWLEDGEMENTS

The authors wish to thank J. Runge, P.P. Dasiewicz and A. Bowler of the Computer Communications Networks Group for their assistance and participation in the preparation and data collection of the experiment.

The also wish to thank the staff and engineers at the

a) 43 bits in error occuring in line 116, field 1. Line 116 replaced by line 115.

b) 57 bits in error in line 67, field 2. Line 67 replaced by line 66.

Fig. 4.5 Received 64-Level Uncoded Image with Errors at Transmission rate = 9600 bps

Fig. 4.6 Decompressed 5-Level Coded Image at Transmission Rate = 9600 bps (46 bits in error)

Communications Research Centre for their excellent co-operation throughout all phases of the experiment. Special thanks are due to Doris Jelly and John Day for their help and guidance in the planning of the experiment.

## REFERENCES

Fuchs, E. and Jackson, P.E.
1969 Estimates of distributions of random variables for certain computer communications traffic models, *Proc. ACM Symp. Problems on the optimization of data Communications Systems*, Pine Mountain, GA, Oct. pp. 202-225.

Mark, J.W.
1976 Adaptive predictive run-length encoding for analogue sources, *Proc. Inst. Elec. Eng.*, vol. 123, pp. 1189-1196, Nov.

Mark, J.W. and Blake, I.F.
1977 Signal processing techniques for data communication by satellite, *CCNG E-Report E-66, Computer Communications Networks Group*, University of Waterloo, September.

# SCIENCE AND TECHNICAL APPLICATIONS


# LA SCIENCE ET LES APPLICATIONS TECHNIQUES

# SMALL HIGHLY TRANSPORTABLE TERMINALS FOR USE IN DISASTER RELIEF COMMUNICATIONS VIA THE HERMES SATELLITE

Joachim Kaiser

COMSAT Laboratories

Clarksburg, U.S.A.

*La Communications Satellite Corporation (COMSAT), en coopération avec l'American National Red Cross, a effectué une expérience de communications en état d'urgence à l'aide du satellite technologique de télécommunications (STT) ou Hermès. Le but de l'expérience était d'évaluer l'acceptabilité et l'efficacité des télécommunications par satellite entre des équipes de secours à l'action et leur quartier-général.*

*La COMSAT a dessiné et fabriqué un terminal miniature portatif équipé d'une antenne de 1,2 mètres de diamètre qu'il est possible d'amener jusqu'à une zone sinistrée. Ledit terminal est relié à un autre équipé d'une antenne de 4,7 mètres de diamètre et situé aux COMSAT Laboratories, à Clarksburg dans le Maryland. Aux fins de l'expérience, on a mis au point un système de conversion verticale très souple et on a fait appel à des assemblages particuliers de l'émetteur à tube à ondes progressives (Travelling Wave Tube) (TWT)) et du récepteur à faible bruit.*

*Le terminal miniature peut être relié via Hermès à celui de la COMSAT qui est lui-même relié, via les installations de communication terrestres, au quartier-général de la Croix rouge qui coordonne les opérations de secours. Le système opère généralement sur trois voies bidirectionnelles pouvant transmettre des sons, des textes en fac-similé et des messages télétypés. Le système de télécommunication a été mis à l'essai dans plusieurs simulations de sinistres et au cours d'un désastre réel à Johnstown (Pennsylvanie), en juillet 1977, au cours duquel il s'est avéré inestimable. L'article qui suit décrit les caractéristiques techniques des stations terrestres et l'utilisation partagée des répondeurs de Hermès; il fait état aussi des résultats de l'expérience.*

## Introduction

The Communications Satellite Corporation (COMSAT), in cooperation with the American National Red Cross, participated in a disaster communications experiment (designated #6). COMSAT Laboratories constructed a highly-transportable earth terminal with a 1.2m diameter antenna for field use and a stationary terminal with a 4.7m antenna at COMSAT Laboratories, Clarksburg, Maryland.

COMSAT terminals, among the first to use the Communications Technology Satellite (CTS) or Hermes spacecraft (Franklin and Davison, 1974), were designed for a variety of uses in addition to the experiment's primary mission, disaster-relief communications. The terminals were used in simulated-disaster exercises and in one real disaster, as well as to transmit video programs on a number of special occasions.

## SMALL TERMINAL DESIGN

### General Considerations

The proposed use of the small terminal called for a design which would provide a rugged terminal, readily transportable by road or air, and simple to erect and operate on site. At least two voice-grade channels were required with the ability to interconnect with the public dialed telephone network.

The final configuration for the terminal electronics met all the requirements and was capable of transmitting and receiving high-speed digital TV, analog TV, and data. Table I summarizes the pertinent characteristics. The terminal consists of a 1.2m tripod-mounted antenna with a Cassegrain feed system, a 20W (nominal) TWT transmitter, and a low-noise parametric amplifier receiver, all of which are weatherized. An IF baseband unit is supplied for use in a shelter. The two subsystems are connected by cables up to about 20m long.

The antenna reflector is made of fiberglass, and the subreflector is supported by sturdy aluminum tubing. The corrugated feed horn is inserted from the rear of the reflector during terminal assembly on site. The reflector, feed, transmitter, and receiver are fastened to a lightweight backup structure which, in turn, is mounted on a modified TV-camera tripod. The antenna can be pointed 360° in azimuth and from 0° to 70° in elevation with a smoothly turning hand wheel elevation vernier control. The power-supply unit for the TWT transmitter is in a waterproof box and is connected to the transmitter by a waterproof high-voltage cable about 6m long. Primary power for the terminal is 110 VAC 60 Hz.

TABLE I

Small Terminal Characteristics

| | |
|---|---|
| Antenna | Diameter 1.2m; tripod mounted |
| Feed system | Dual, linear-polarized Cassegrain |
| TWT Transmitter power | 30W maximum (nominal 20W TWT) at full saturation |
| Low-noise paramp receiver | 260 K system noise temperature |
| Antenna | |
| Transmit gain | 41.3 dB |
| Receive gain | 40.2 dB |
| G/T | 16.1 dB/K |
| Maximum e.i.r.p. | 55.8 dBW |
| Weight for air shipment | 250 kg |
| Primary power | 110 V/AC, 60 Hz, 1.5 kW |
| Communications capability | 3 two-way channels (3.0 kHz baseband bandwidth each), that can carry voice, facsimile, and full-duplex teletype messages. |
| Alternate capability | Receive TV and 2 program audio channels |
| Terminal Units | The outdoor units of the terminal are waterproof and operate from -20°C to +40°C. The antenna can be secured to the ground to operate in winds in excess of 50 km/hr. |
| | The indoor units can be separated from outdoor units by RG-214N cables up to 20m long, or low-loss spiroflex cables up to 50m long. |
| Transmit/receive | Switch control selects transmit and/or receive in either of the CTS bands. Frequency increments exist within each band in steps of 0.5 MHz, selectable by thumbwheel switch. |
| TWT operation | Controlled remotely from indoor unit. |
| Pointing | Maintained by hand-operated controls based on received beacon signal strength. |

The terminal can be packaged in several containers. The reflector can be shipped with the subreflector assembled or, if required, with the subreflector removed. The front surface of the reflector must be protected from damage during shipment. The transmitter, receiver, and feed assemblies fit into a container measuring 2 ft x 2 ft x 14 in. The backup structure and tripod require no packing, and the transmitter power supply operates from its shipping case.

The baseband and IF interface unit is mounted in a sturdy container that has covers and handles for transportation and requires no special packing. The entire terminal weighs 250 kg and has been shipped by commercial air lines.

## Electronics Design

Figure 1 shows the signal flow. The system consists of a dual frequency conversion between 70 MHz and the transmitted and received frequencies of 14 and 12 GHz, respectively. Baseband-to-70-MHz frequency conversion is accomplished with standard multiplex and mod/demod equipment.

In the transmit path, each telephone channel is multiplexed by a standard Lenkurt unit, and the combined signal modulates a Farinon video modulator adapted for low-deviation application. Total deviation is less than 500 kHz peak-to-peak. The 70 MHz signal is mixed with a synthesizer-controlled local oscillator to produce a nominal 1.5 GHz signal. Transmit bands (TB) 1 or 2 are selected by switching the signal through bandpass filters centered on 1,669 MHz for TB1 and 1,474 MHz for TB2. TB1 uses the upper sideband, and TB2 uses the lower sideband of the mixing process. The bandpass filters are 85 MHz wide; therefore, the transmitted signals can be placed anywhere within the two transmit bands--from 14.205 to 14.290 GHz for TB1, and 14.010 to 14.095 GHz for TB2. The different mixer sidebands for the two transmit bands were selected to reduce the frequency range of operation of the synthesizers.

After passing through the appropriate filter, the transmit signal is amplified at 1.5 GHz and sent to the transmitter, which consists of a high-level mixer, local oscillator operating at 12.578167 GHz, and bandpass filters. The high-level mixer, combined with the high gain of the TWT (59 dB for small signals and 53 dB saturated), eliminates the need for a driver stage in the transmitter. Before the TWT, the bandpass filter eliminates unwanted signals from the mixing process; following the TWT, the bandpass filter restricts the output to the band from 14.0 to 14.5 GHz.

The transmitter is connected to the feed by a short piece of flexible waveguide with a quick-disconnect flange. This permits rapid assembly of the transmitter

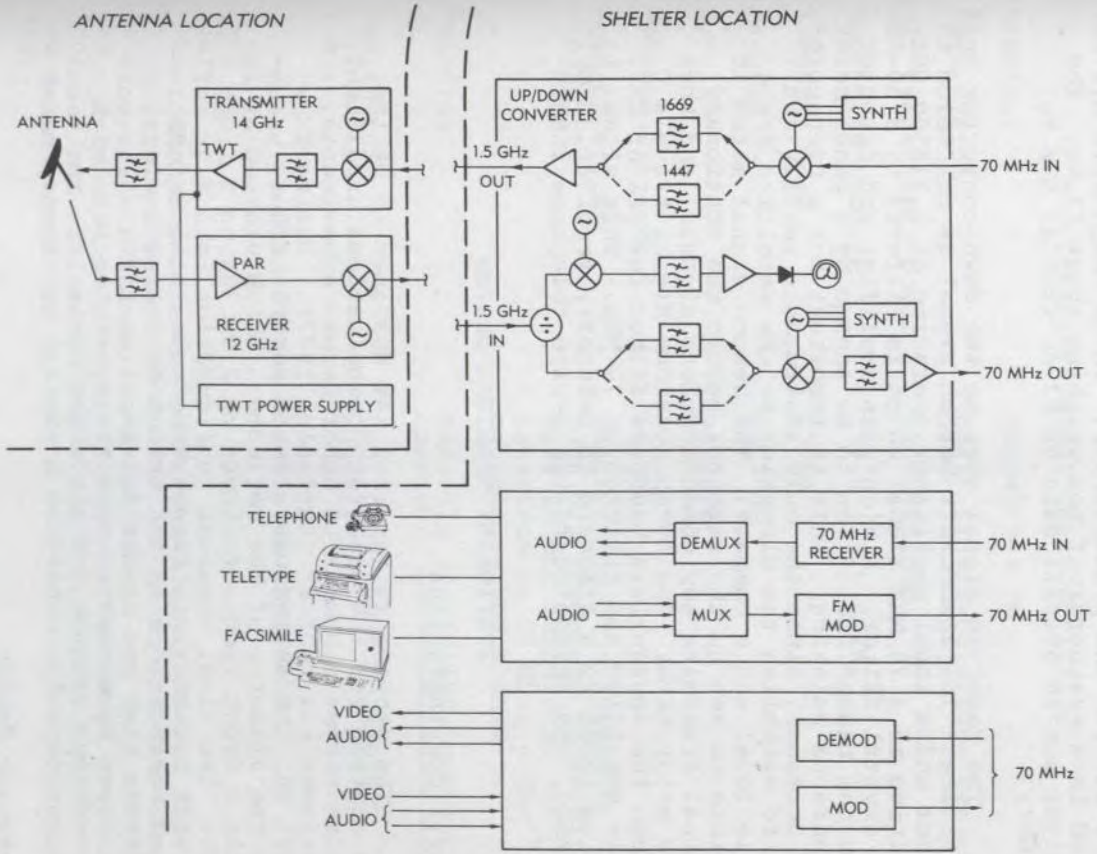


Figure 1. Signal Flow Diagram

to the feed and rotation of the feed horn to adjust the polarization axis. The receive path starts at the feed followed by a filter with bandpass between 11.7 to 12.2 GHz. The signal then travels, via a short piece of flexible waveguide, to the low-noise parametric amplifier receiver which contains a fixed-frequency oscillator at 10.411500 Ghz, mixer, and 1.5 GHz preamplifier. These components are contained in a weatherproof box weighing about 13 kg. The receiver has an overall gain of 63 dB from 12 GHz to 1.5 GHz.

The received signal goes to the down-converter unit via cables. The spacecraft beacon signal is channeled to a mixer and a local oscillator operating at 1.218500 GHz, resulting in a 70 MHz signal which is filtered by a 30-KHz-wide crystal filter. A high-gain amplifier and detector allow the beacon indication to be sensed by a panel meter for antenna pointing. This is important for a transportable terminal, since the only instruments readily available to establish the direction to the satellite are a bubble level and a compass. The beacon signal makes it possible to set up the terminal before the stationary terminal transmits any communications signals, and thus saves setup time. The communications signal travels through the appropriate bandpass filter for TR1 or TR2, and is amplified and filtered at 70 MHz. This signal is used as input to a standard FM telemetry receiver, demultiplexed, and channeled to the 4-wire telephone instruments.

## STATIONARY TERMINAL DESIGN

### General Considerations

The stationary terminal was designed to be the base station for the disaster communications experiment. It also serves a number of other Hermes experiments, i.e., Experiment #24, "DICE" (Gatfield, 1977). During Experiment #6, the design was altered several times, primarily the diameter of the reflector, which started at 2m (using a front feed), followed by 2.4m (using a front feed). The final terminal configuration is a 4.7m reflector with a Cassegrain feed system containing a COMSAT-designed corrugated horn and orthomode transducer system. This reflector size was needed for Experiment #24. The various reflectors were mounted on a transportable base with motor-driven azimuth and elevation controls. The final configuration is mounted on a similar stationary mount.

### Electronic Design

The stationary terminal, whose characteristics are given in Table II, is similar to the small terminal except that the antenna reflector has a diameter of 4.7m, and the transmitter has a maximum power output of 200W. The terminal is mounted in the roof of the COMSAT Laboratories building in Clarksburg, Maryland. The antenna unit is

connected to the IF and baseband equipment by 50m long low-loss spiroflex cables. Remote control systems located at the IF equipment control the transmitter and antenna pointing.

TABLE II

Stationary Terminal Characteristics

| | |
|---|---|
| Antenna | Diameter 4.7m |
| Feed system | Dual, linear-polarized Cassegrain |
| TWT transmitter power | 200W maximum |
| Low-noise receiver | 230 K (23.6 dB/K) |
| Transmit gain | 53 dB |
| Receive gain | 51.7 dB |
| G/T | 28 dB/K |
| Maximum e.i.r.p. | 75 dBW |
| Communications capability | Receive and/or transmit on both CTS frequency bands with full 85 MHz bandwidth. IF interface at 70 MHz, 0 dBm on receive and transmit. |
| Pointing | Manually controlled, motor operated |
| Monitoring | Continuous beacon-receiver monitoring |

## OPERATIONAL USE OF THE TERMINALS

### General

The small terminal and several versions of the large terminal were used in various tests and demonstrations, including three simulated and one real emergency-communications events, and in a number of special applications of transportable earth terminals. These are described in the following sections in chronological order.

### Emergency Simulation - Washington National Forest

On July 29, 1976, the 1.2m terminal was deployed at Luray, Virginia, in the Washington National Forest to provide communications for a simulated emergency. This demonstration was held at the request of the U.S. Forest Service with the assistance of the National Red Cross.

The goal of this test was to demonstrate that the small terminal could be set up at an unprepared site to furnish emergency communications to headquarters during a major forest fire. As a companion effort, the Red Cross Headquarters in Washington, D.C., was connected to the small terminal using voice and teletype circuits.

The test was completely successful. About one hour after arrival at the site, telephone communications were established via Hermes between the 1.2m terminal and the 2m terminal at COMSAT Laboratories. A number of telephone calls were placed to forest-service officials in San Diego, California. A teletype circuit was established with the National Red Cross Headquarters and previously prepared messages were sent in the full-duplex mode between the headquarters and the terminal in the field. Figures 2, 3, and 4 show the terminal in the field; figure 5 shows the teletype terminal at the Red Cross Headquarters.

For this test, the RF transmitter power into the antenna feed at each earth station was about 10W. The center frequency of each transponder was used in the two-way transmissions. No unusual problems were encountered during the test period.

Special Demonstration - Yellowstone Park, Grandfather Mountain

Two special demonstrations were conducted using variants of the COMSAT transportable terminals. By special arrangement, the transportable terminal with a 2m antenna was taken to Yellowstone National Park on July 4, 1976, to send a TV picture of Old Faithful Geyser via Hermes to the receiving station at NASA Lewis Research Center in Cleveland, Ohio. From there, the signal went by terrestrial links to the NBC Studios in New York and was incorporated into the "Glorious Fourth" program to illustrate the technological progress in this bi-centennial year.

For this demonstration, the transportable terminal was carried within a General Motors "Recreation Vehicle" from Maryland to Yellowstone and was erected in about 4 hours. NBC furnished a transportable TV studio which was interconnected with the CTS terminal. The communications links provided were the following: TB1, from Yellowstone to Cleveland, consisted of one video signal with 43-dB S/N and two voice channels of good quality. TB2, from Cleveland to Yellowstone for monitoring purposes, consisted of one medium video signal and two voice channels.

A two-way video link program and monitor channels was established. The return link to Yellowstone was kept at a low power level to avoid degrading the primary path link from Yellowstone to Cleveland. About 30W of RF power was obtained for the antenna feed from the nominal 20W Varian TWT amplifier and provided a good quality video

Figure 2. The small terminal in the field.

Figure 3. Emergency communications.

Figure 4. Field terminal set-up.

Figure 5. Teletype terminal of Red Cross Disaster Relief Headquarters.

signal from Yellowstone to Cleveland. The link was uplink power limited because of the small antenna size of the earth station. Table III is a link budget calculation for the primary video link.

The terrestrial facilities were provided by conventional telephone company arrangements. The transmission was successful and lasted 10 hours on July 4, in addition to the test periods of the previous day.

Another special demonstration was held on July 11, 1976, in conjunction with Experiment #19 of the South Eastern Communications Association (SECA). A live TV broadcast of the annual Scottish games was transmitted from Grandfather Mountain, North Carolina, via Hermes to Columbia, South Carolina, for transmission in the SECA network. The 2m antenna was used at the transmit site and the COMSAT 1.2m antenna was positioned next to the South Carolina Public TV Building at the receive site in Columbia, South Carolina.

A one-hour program was transmitted using one-way TV with a program channel and a voice order wire. The return link for monitoring purposes used terrestrial faci-

TABLE III

Link Power Budget TV from Yellowstone to Cleveland

| | | |
|---|---|---|
| Power Transmitted $P_T$ = 30W | 14.8 | dBW |
| Antenna gain (2m) $G_T$ | 46 | dB |
| Earth Stations e.i.r.p. | 60.8 | dBW |
| Path Loss | -207.6 | dB |
| Power received into spacecraft antenna | -46.8 | dBW |
| Spacecraft G/T | +6.1 | dB/K |
| $C/T_{up}$ | -140.7 | dB/K |
| Spacecraft antenna gain | 37.4 | dB |
| $P_r$ | -103.5 | dBW |
| Spacecraft transponder gain | 127 | dB |
| Spacecraft transmitted power | 19.8 | dBW |
| Spacecraft antenna gain | 36.3 | dB |
| Spacecraft e.i.r.p. | 56.1 | dBW |
| Path loss | -206.4 | dB |
| $P_r$ into earth station antenna | -150.3 | dBW |
| NASA Lewis earth station G/T | 22 | dB/K |
| C/T down | -128.3 | dBW/K |
| C/T total | -141.0 | dBW/K |
| Power bandwidth product, $C/N_o$ | 87.6 | dB (Hz) |
| Bandwidth, 20 MHz | 73.0 | dB (Hz) |
| C/N | 14.6 | dB |
| Video S/N* | 45 | dB |

*Computed from:

Video S/N (weighted luminance signal/noise) = 236.4 + 20 log d + C/T - 10 log fvn + Q in dB.

where d = deviation index = fd/fv = $\frac{5.8 \text{ MHz}}{4.2 \text{ MHz}}$ = 1.4

fd = highest peak deviation

fv = fvn = highest modulation frequency = 4.2 MHz

Q = weighting factor = 13 dB

lities since the 1.2m terminal with a 20W TWT does not produce sufficient e.i.r.p. to transmit video signals via Hermes. The demonstration was successful and the video quality was adequate for use in the educational network.

The link parameters for this demonstration are the same as shown in Table IV for the uplink. However, the downlink parameters given in Table IV differed because of the small 1.2m receiving antenna.

TABLE IV

Downlink Power Budget TV from Grandfather Mountain North Carolina to Columbia, South Carolina (For uplink, refer to Table III)

| | |
|---|---|
| Spacecraft e.i.r.p. | 56.1 dBW |
| Path loss | -206.4 dB |
| $P_r$ with the earth station antenna | -150.3 dBW |
| 1.2m antenna G/T (T = 260K) | 16.1 dB |
| C/T down | -134.2 dBW |
| C/T total | -141.7 dBW |
| $C/N_o$ | 86.9 dB (Hz) |
| C/N in 20 MHz | 13.9 dB |
| Video S/N | 44 dB |

## Ohio River Flood Watch Simulation

In February 1977, a simulated-disaster exercise for a possible flooding of the Ohio River Valley was held in conjunction with the American Red Cross Chapter in Cincinnati, Ohio, and the National Disaster Headquarters in Alexandria, Virginia. The small terminal, which was transported to Cincinnati in the back of a station wagon and a small rental trailer, was set up in downtown Cincinnati. During the exercise, simulated emergency traffic was sent between the two headquarters using telephone, facsimile, and high-speed teletype. The exercise was judged successful and it demonstrated the ability of only two voice channels to handle considerable traffic. Messages were pretyped on the teletypewriters with magnetic tape cassette storage and sent in the full-duplex mode at 300 words per minute when the circuits were not occupied with telephone traffic. The operators at both ends of the link were astonished at the message-handling ability of this system.

## Transponder Sharing

During this exercise, the spacecraft transponders were shared with another experiment by separating the signals in frequency. All of the traffic was carried in transponder #1 (using the spacecraft 200W TWT) including a TV broadcast for SECA, Experiment #19, originating in Cleveland and received in the South Eastern U.S. The resulting spacecraft antenna pointing allowed the signals from Experiment #6 to share the transponder. The TV signal was monitored in Cincinnati using the 1.2m terminal to ensure that the video signal had no interference. The video transmission was made at a somewhat reduced level not saturating the S/C transponder to avoid suppressing the much weaker narrowband signals from Experiment #6. The video output from the transponder was about 150W, representing a 1.25 dB output backoff. Transponder #2, containing the spacecraft's 20W TWT, was not carrying any of the signals in the above case. Sharing of spacecraft transponders by many signals, is, of course, common in the commercial communications satellites. The unique time-scheduling and antenna-pointing requirements for the CTS users made sharing of the spacecraft difficult. The present experiment illustrated that in some cases, sharing CTS is also possible and yields efficient use of the crowded experiment time availability.

## Effects of Rain on an Operating System

A severe thunderstorm occurred at Clarksburg, Maryland, during the exercise. The rain attenuation was sufficient to disrupt the communications signals completely for about ten minutes. Based on the C/N measurements, the attenuations are believed to have been 20 dB or more. Significant rain attenuation was also observed during a disaster communications test described in a later subsection. Attenuation in that instance was overcome by switching all signals to transponder #1 (200W TWT) and increasing the power at both ends of the link. These results are not intended to develop data on rain attenuation, but only to demonstrate that severe rain can and did disrupt an operating link for an appreciable period of time.

## Texas Hurricane Simulation Exercise

On July 21, 1977, the American National Red Cross and COMSAT planned a hurricane disaster exercise in Texas. Two terminals were to be used: one at Houston, Texas, and the other at Corpus Christi, Texas. Disaster relief headquarters were in Austin, Texas. Communications links were to be established via Hermes between Houston and Clarksburg and Corpus Christi and Clarksburg; two land lines were dialed between Clarksburg and Austin to complete the link.

The 1.2m terminal and a 2.4m terminal were used in the field with the 4.7m terminal at COMSAT Labs. The two small terminals were taken to Texas by a Red Cross van and

a boat trailer, with the small reflector nested inside the larger one. The stations were deployed as planned and the exercise was very successful. However, the transmission parameters were altered. Actually, 4 voice channels were established between Clarksburg and the field stations; two channels served as engineering order wires to link the 3 earth terminals and the other two were routed via the land lines to Austin. The transmission format used two channels multiplexed on one carrier and two separate channels in a single channel per carrier (SCPC) mode. This was accomplished using the audio subcarrier modules in the Farinon video equipment in a non-standard way as SCPC mod/demod units.

## Johnstown Flood Disaster Communications

On Saturday, July 23, the Red Cross requested emergency communications for the disaster at Johnstown, Pennsylvania. The small 1.2m terminal was flown by commercial airliner to Pittsburg and transported by small van to Johnstown. On Monday morning, July 25, the terminal was in operation and was furnishing two voice channels between Johnstown and Clarksburg, which routed the channels into the commercial telephone network. The communications link was maintained for two days until the Johnstown telephone system was sufficiently restored. The small terminal carried voice and facsimile traffic for the American Red Cross Disaster Relief Unit to the Washington Red Cross Headquarters and many other points. The facilities were used to transmit requests for emergency supplies, nurses, and volunteers and to notify relatives of flood victims. On Monday, July 25, the Johnstown Telephone Plan was evacuated for several hours due to a nearby explosion, and the satellite link was the only means of communication into or out of the Johnstown area.

The response to the emergency at Johnstown demonstrated that the small transportable terminal was able to fulfill its mission. This success was also attributable to the cooperation of the U.S. and Canadian agencies who control the spacecraft experiments and made Hermes available for this purpose on very short notice.

## CONCLUSION

The small, highly transportable emergency communications terminal, which was used for simulated and real emergency communications, accomplished its goal. The portability, reliability, and ease of field operation, as well as frequency flexibility of the equipment, has made it possible to provide a communications services in remote locations under emergency conditions. The design and implementation of the Hermes spacecraft and its operational control contributed immeasurably to the success of Experiment #6.

ACKNOWLEDGEMENTS

The following contributed to the design and operation of the equipment of Experiment #6. E. Ackerman, N. Helm, F. Seidel, L. Veenstra of COMSAT Laboratories, D. Lehman, D. Reiser, J. Steinhorn, formerly of COMSAT, R. Davis, M. Fink, E. Matherly, B. Torrence, American Red Cross. This paper is based upon work performed in COMSAT Laboratories under the sponsorship of the Communications Satellite Corporation.

REFERENCES

Franklin, C.A. and E.H. Davison
1974 A High Power Communications Technology Satellite for the 12- and 14-GHz Bands, *(Communication Satellite Systems Technology (Advances in Astronautics and Aeronautics*, Vol. 32), edited by P.L. Bargellini, Cambridge, Massachusetts: MIT Press, pp. 87-121.

Gatfield, A., et al
1977 System Design for the Digitally Implemented Communications Equipment (DICE), ICC '77 Chicago, Ill. *Conference Record*, Vol. 1, IEEE Catalog No. 77 CH 1209-6 CSCB, June.

South Eastern Communications Association (SECA), "Television Distribution by Satellite", Experiment #19.

# EXPERIMENTAL TELEVISION BROADCASTING FOR COMMUNITY AND INDIVIDUAL RECEPTION

C.A. Siocos

The Canadian Broadcasting Corporation

Montreal, Canada

*Radio-Canada (R.-C.) a effectué des expériences de radiodiffusion télévisée au moyen du satellite technologique de télécommunications (STT) Hermès, du 26 juillet au 25 novembre 1976. Il s'agissait d'évaluer la qualité de la réception d'images télévisées dans la bande de 12 GHz en milieu urbain, en utilisant:*

*(i) un équipement de réception collective consistant en une antenne de 2 mètres de diamètre reliée à un poste de télévision professionel;*

*(ii) des appareils de réception individuelle dotés d'antennes plus petites et reliés à des postes de télévision ordinaires.*

*La transmission expérimentale de signaux télévisés a été réalisée à partir des studios de R.-C. à Ottawa. Ont été diffusés dans le cadre de ce projet, des mires, des diapositives en couleur, ainsi qu'un programme spécial de démonstration décrivant en termes simples le fonctionnement de Hermès et les expériences de R.-C. et insistant sur la description de l'évaluation et des essais eux-mêmes. La transmission comportait également des signaux audio d'essai et quelques extraits d'émissions disponibles aux studios d'Ottawa au moment de l'expérience.*

*Les essais ont prouvé que la télévision par satellite, du point de vue de la réception collective ou individuelle, est techniquement réalisable et qu'elle permet d'offrir un service fiable, facilement accessible et de très haute qualité dans une aire de diffusion relativement vaste (comme dans une des plus grandes provinces du Canada).*

## INTRODUCTION

The Canadian Broadcasting Corporation (CBC) conducted experimental broadcasts using the Communications Technology Satellite (CTS) or Hermes, from 26 July to 25 November 1976, with the objective of evaluating television reception in the 12 GHz band in a metropolitan environment, using:

(i) community-reception type of equipment, with a 2m diameter antenna and a professional receiver.

(ii) direct-to-home type of equipment, with smaller antennas and simpler receivers.

For various reasons, Hermes time was available for only 31 days during the scheduled period, and only for a short time each day; specifically 1½ hours in the morning from July 26 to August 27 and 2 hours in the early afternoon from October 19 to November 25. In addition, a special demonstration with the complete terminal inside a building was arranged during the week of November 28.

Television signals for this experiment originated at the CBC studios in Ottawa. They included video test signals, a variety of color still slides, and a specially produced demonstration program featuring simple explanations of Hermes and the CBC experiments performed with it, with emphasis on the description of the present evaluation and demonstrations. The transmissions also included audio test signals and segments of running programs, as available at the Ottawa CBC Studios during the time of the experiment.

## EXPERIMENTAL CONDITIONS

These signals were transmitted from the CBC Studios via a specially set up microwave link, to the main transmitting earth station for Hermes in Canada, some 12 km away, at the Communications Research Centre (CRC) of the federal Department of Communications (DOC). During the summer of 1976, due to large demands generated by the Olympic Games in Montreal, the only equipment available for a temporary radio relay link to CRC was a relatively old 7 GHz microwave system. Its basic performance was acceptable but its stability left something to be desired and so did its record of outages. During the fall of 1976, the link to CRC was supplied and maintained by Bell Canada, and its performance and reliability were fully satisfactory. The main earth station at CRC is a permanent installation with a 9m antenna. The uplink transmission was in the 14 GHz band, and the transmitter power was 32W. The calculated uplink carrier-to-noise ratio was 24.8 dB in clear weather.

## RECEPTION BY THE 12-GHz COMMUNITY-TYPE STATION

The terminal for community-type reception was in Montreal, at the Maison de Radio-Canada, the headquarters

and broadcasting center of the French-language networks of the CBC, situated at 1400 Dorchester Boulevard East, near the center of the city. From this site Hermes is at an azimuth of 232.0° and an elevation of 23.2°.

The earth terminal (Fig. 1) was manufactured by RCA Ltd. of Montreal for DOC. The 2m antenna and associated preamplifier (tunnel-diode) and first down-converter (to 735 MHz) were located on a lower-level, southern roof of the building at a height of, roughly, 10m above street level. This package was interconnected by some 50m of cable with the indoor package consisting of a second down-converter, video and audio demodulators, output electronics, and a separate power-supply unit. The figure of merit (G/T) of this receiving terminal is 16.6 dB.

The indoor unit of the receiver was in a special equipment room that contained video and audio monitoring and test equipment, to assess the link characteristics. The experimental system, and the associated control room and theatre are shown schematically in figure 2.

Measurements of the distortion of the video signal were made with test equipment and test signals as follows:

a) *Frequency response* - Tektronix 1480 Waveform Monitor, multiburst signal.

b) *Short time distortion* - Tektronix 1480 Waveform Monitor, 2 T sine-squared pulse, 2 T pulse and bar signal.

   The K factor (from 2 T pulse) and pulse-to-bar ratio give a measure of overshoot, ringing, and relative low and high frequency response. Excessive short time distortion will give rise to echoes or ghosts.

c) *Differential gain* - Tektronix 1480 Waveform Monitor, modulated staircase signal.

   Differential gain is the difference in amplitude response at the colour subcarrier frequency at various levels of the signal.

d) *Differential phase* - Tektronix 520 A Vectorscope, modulated staircase signal.

   Differential phase is a change in phase of the colour subcarrier with changes in the luminance level.

e) *Chrominance to luminance gain and delay* - Tektronix 1480 Waveform Monitor, Tektronix 1478 Calibrated Chrominance Corrector, modulated 12½ T sine-squared pulse.

   Unequal chrominance to luminance gain affects the colour saturation of the picture and unequal delay can cause colour smearing or colour ghosts.

f) *Video signal-to-noise ratio* - Rhode and Schwarz UPSF Video Noise meter, 50 IRE unit pedestal.

(a) Antenna and outdoor units.

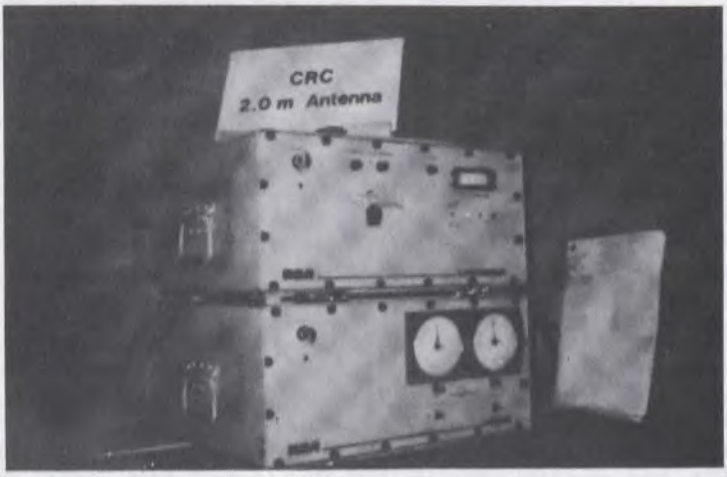


(b) Indoor units.

Figure 1. The RCA 2-meter station at Maison de Radio Canada, Montreal.

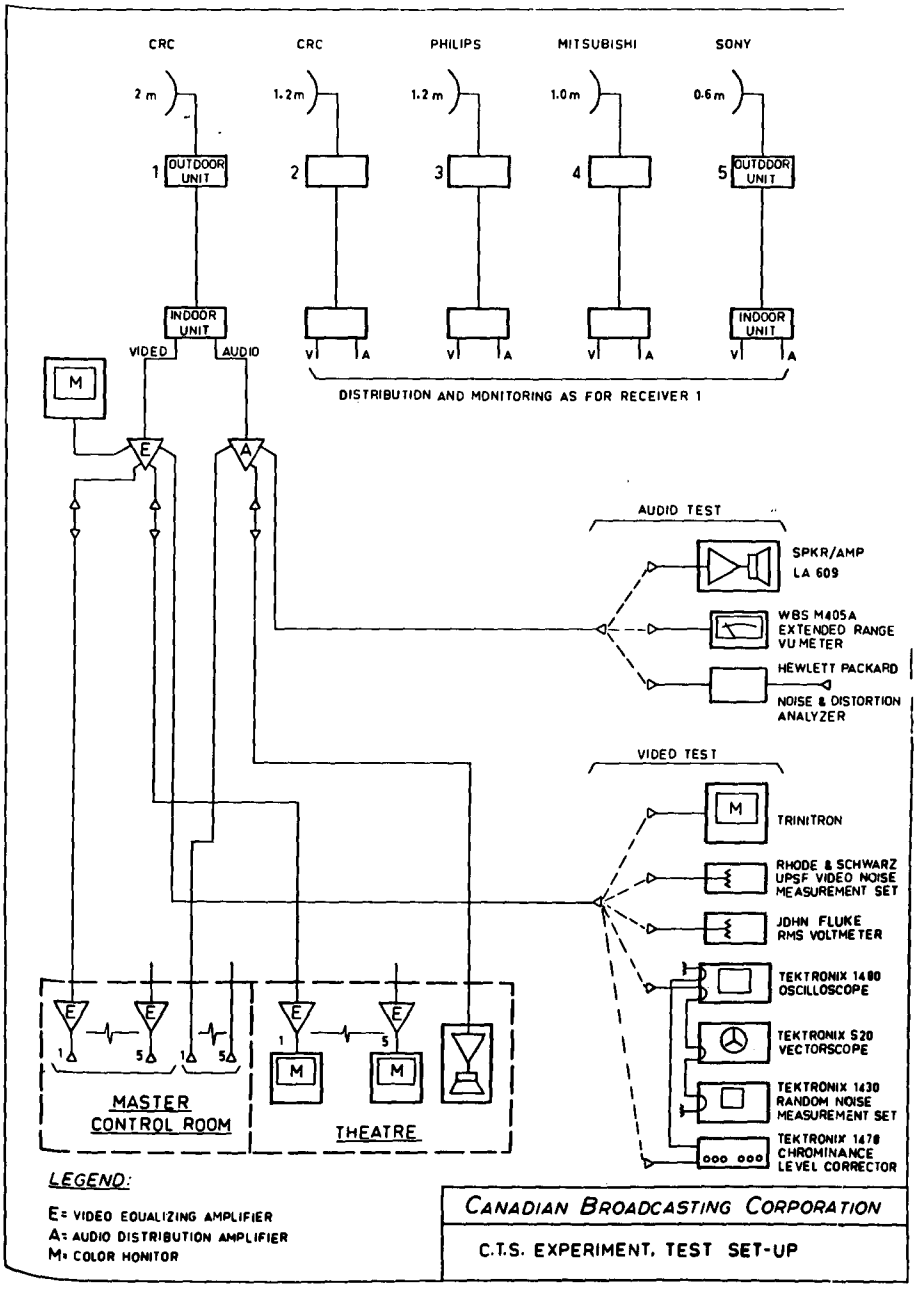
CRC
CRC
PHILIPS
MITSUBISHI
SONY
2 m
1.2 m
1.2 m
1.0 m
0.6 m
1 OUTDOOR UNIT
2
3
4
5 OUTDOOR UNIT
INDOOR UNIT
INDOOR UNIT
VIDEO
AUDIO
V
A
DISTRIBUTION AND MONITORING AS FOR RECEIVER 1
M
E
A
AUDIO TEST
SPKR/AMP LA 609
WBS M405A EXTENDED RANGE VU METER
HEWLETT PACKARD
NOISE & DISTORTION ANALYZER
VIDEO TEST
TRINITRON
RHODE & SCHWARZ UPSF VIDEO NOISE MEASUREMENT SET
JOHN FLUKE RMS VOLTMETER
TEKTRONIX 1480 OSCILLOSCOPE
TEKTRONIX S20 VECTORSCOPE
TEKTRONIX 1430 RANDOM NOISE MEASUREMENT SET
TEKTRONIX 1478 CHROMINANCE LEVEL CORRECTOR
MASTER CONTROL ROOM
THEATRE
LEGEND:
E= VIDEO EQUALIZING AMPLIFIER
A= AUDIO DISTRIBUTION AMPLIFIER
M= COLOR MONITOR
CANADIAN BROADCASTING CORPORATION
C.T.S. EXPERIMENT, TEST SET-UP

Figure 2

As control, during the second phase of the experiment, terminated input S/N measurements were also taken using a John Fluke 910A True-RMS Voltmeter. Weighted-noise measurements were made, using weighting according to CCIR Recommendations 421-3. Again, as a control, unweighted-noise measurements were also made during the second phase.

The *video transmission quality* of the link was very good (Fig. 3) and displayed small variation with time, as follows:

| | |
|---|---|
| Frequency Response | Less than 0.7 dB |
| K Factor | Approx. 2.5% |
| Chrom./Lum. Gain Inequality | Less than 0.8 dB |
| Chrom./Lum. Delay Inequality | Approx. 0 ns |
| Diff. Gain | Approx. 2.5% |
| Diff. Phase | Approx. 1.7% |
| Signal-to-Weighted Noise Ratio | Average 51.5 dB |

Television pictures were totally free from ghosting and were judged between "good" and "excellent" on the CCIR scale of subjective quality.

*Audio transmission quality* was lower with Signal-to-Unweighted Noise Ratio of about 36 dB, and 4% distortion. The Carrier-to-Noise Ratio (C/N) calculated for this terminal is 21.7 dB and this affords a margin-over-FM-threshold of 11.5 dB for fades. The largest fades due to rain, or to snow accumulation on the antenna, during the short experimental duration, were much smaller than this margin.

## RECEPTION BY THE 12 GHz HOME-TYPE STATIONS

Terminals for direct-to-home type reception were sited in the downtown areas of Montreal (2), Ottawa (2) and Toronto (1). The azimuth and elevation of Hermes from all sites was within the range 227° - 232° and 23° - 28° respectively.

Five terminals were tested at the *Maison de Radio-Canada in Montreal. Two terminals from Japan*, were supplied courtesy of Nippon Hoso Kyokai (NHK) who participated actively in this experiment with personnel and equipment. One terminal had a 1.0m antenna by Sumitomo Electric Industries Ltd., and a receiver with a Noise-Figure (NF) specification of 5.0 dB. (Initially, this was a Mitsubishi (Melco) receiver, later replaced by Sony.) The second terminal had a 0.6m antenna by Sumitomo and a Sony receiver with NF specification of 4.3 dB. (See Figs. 6 & 7).

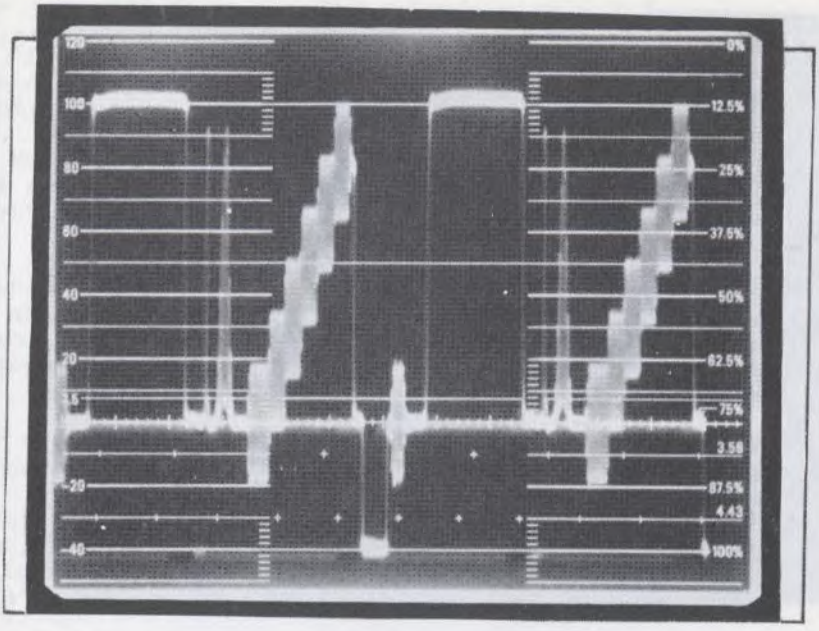


Figure 3a. Response to Test Signal CCIR No. 1.

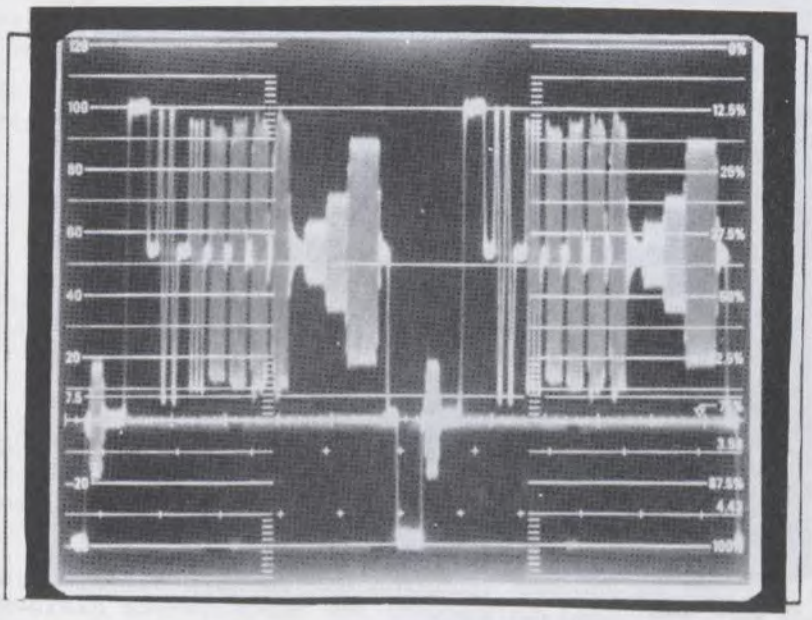


Figure 3b. Response to Test Signal CCIR No. 2.

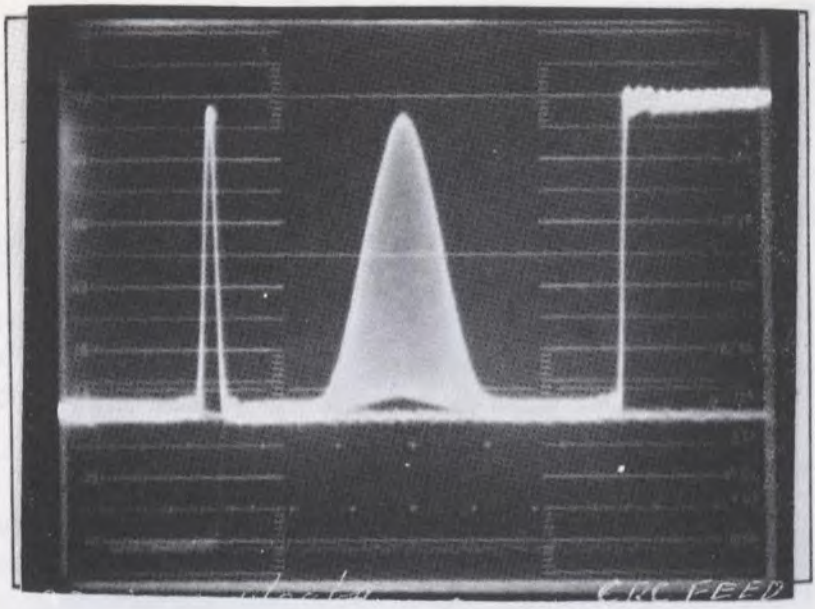

Figure 3c. Response to Sine Squared Test Signals.

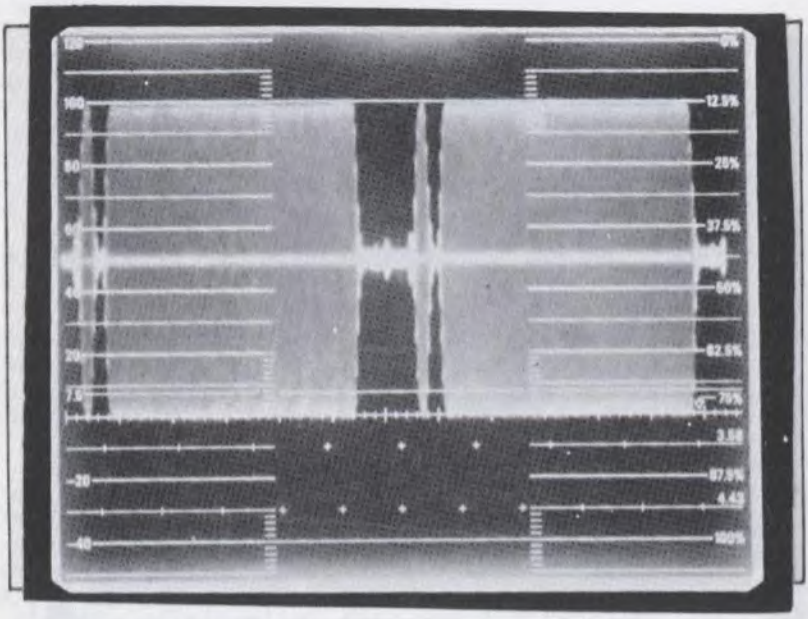


Figure 3d. Differential Gain.

*One terminal from the Netherlands* with a 1.2m antenna (Fig. 4), was supplied courtesy of Philips, who also participated in this experiment, mainly with equipment and by providing technical personnel during installation and initial adjustment. The Philips receiver had a NF specification of 7.6 dB. *Two terminals from Canada* were supplied by the CRC and by RCA Ltd., Montreal; both have 1.2m antennas (Fig. 8). The receivers have NF specifications of 6.3 and 5.8 dB respectively.

One terminal was tested at *CBC Engineering Headquarters in Montreal, a Philips terminal* of semi-professional nature. It is characterized by a 1.6m antenna, a more elaborate antenna mount and a indoor receiver that incorporates a signal-strength meter. (See Figs. 4 & 5).

Two terminals were tested in Ottawa. One, at the *CBC Head Office* was a *1.0m Japanese terminal* with Sumitomo antenna and Hitachi receiver, with NF specification at 5.0 dB. One, at the *CBC Television Studios*, was a *1.6m Japanese terminal* with Sumitomo antenna and Toshiba receiver with NF specification of 5.3 dB. During the second phase of the experiment, the Sumitomo receiver mentioned below was used in this terminal.

Two terminals were tested at the *Jarvis Street Television Studios of the CBC in Toronto*. One was a *Philips 1.6m semi-professional terminal* as above. The second was a *Japanese terminal*, with Sumitomo antenna and Sumitomo receiver with a NF specification of 6.3 dB. During the second phase of the experiment, this receiver was replaced with one by OKI of Japan with a lower NF.

*Additional Information on the Satellite Broadcast Receiving Terminals*

Details of the Philips terminals have been published by Edens, 1977, and details of the Mullard by Freeman, 1977.

Regarding the Japanese terminals, the antenna-mounted SHF unit of all receivers was of the well-known NHK type (Konishi et al, 1973) with a NF from 4.3 to 6.3 dB, depending on the make.

Likewise the antennas and their mounts were all of the "Pretcher" type by Sumitomo Electric Industries Ltd. The indoor units were of conventional type, made by 6 different manufacturers. Figure 7 shows, as an example, the Sony unit which, like most of the Japanese receivers, has a signal-strength meter and a video pre-emphasis on-off switch.

Of the Canadian 1.2m terminals, two had the SHF unit mounted in the back of the antenna; the one by CRC having a Cassegrain subreflector and corrugated feed, and the RCA one having a horn focal feed. The third, also by CRC, had the SHF unit mounted in front of the antenna at the focal point. Figure 8 shows the Cassegrain antenna used with the

1.6 METER ANTENNA (Community Reception)
Motorized mount, Engineering Headquarters, Montreal

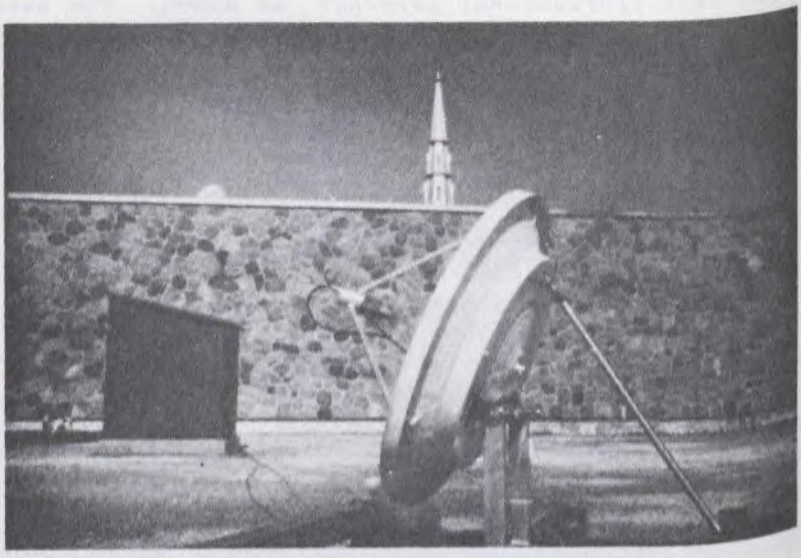

1.2 METER ANTENNA (Individual Reception Mount)
Maison de Radio Canada, Montreal

Figure 4. PHILIPS STATIONS (with down-converter at focal point)


PHILIPS INDOOR UNITS

Figure 5


FRONT VIEW

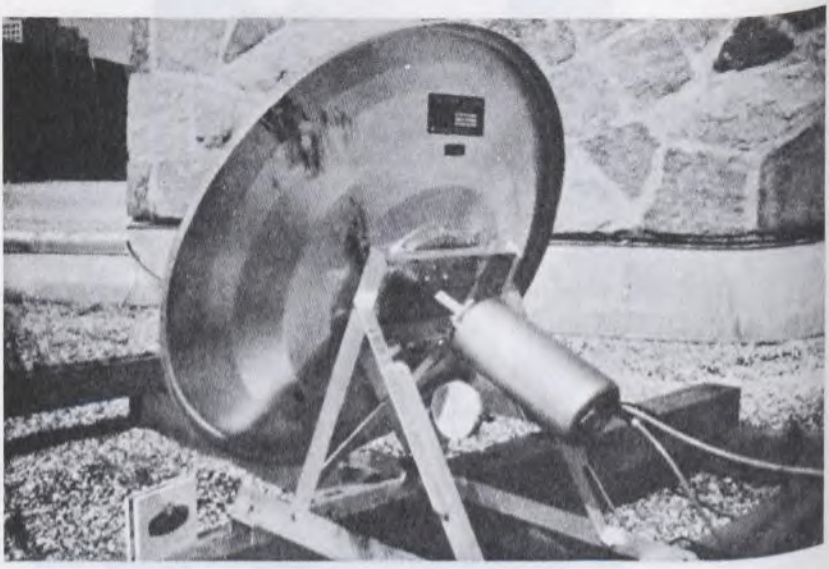

REAR VIEW, Showing down-converter unit

Figure 6. NHK 0.6 METER STATION. Installation at the Maison de Radio Canada, Montreal.

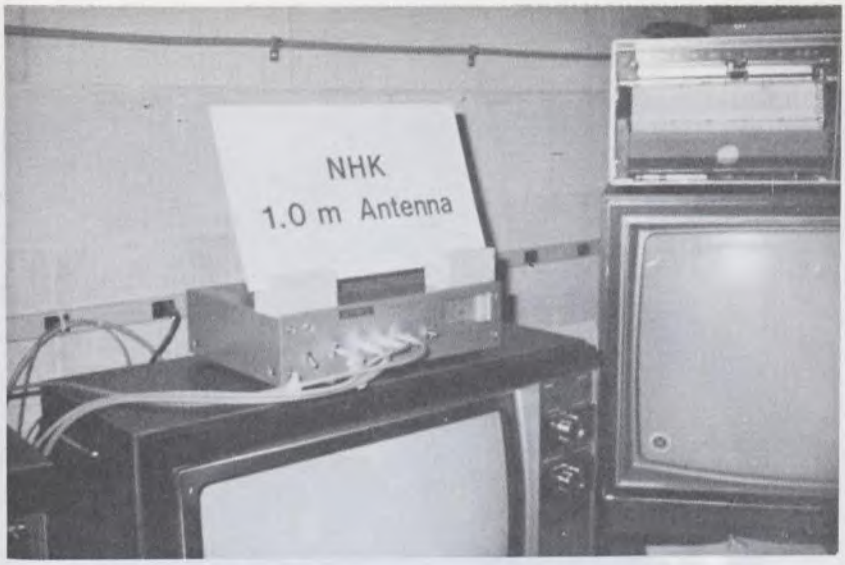


Figure 7. Indoor unit by Sony

CRC receiving installation in the Maison de Radio-Canada in Montreal. Figure 9 shows the other CRC antenna with the focally-mounted SHF unit.

*Summary of results for home-type stations*

The average transmission quality of the links using some of the home-type terminals at the Maison de Radio-Canada is summarized in Table I.

The performance at other sites was comparable, taking into account the effect of the G/T on the signal-to-noise ratio.

## OBSERVATIONS REGARDING AVAILABILITY

The experiment was deliberately scheduled during a period when rain storms are prevalent in Eastern Canada. However, during the brief transmission times, weather conditions were more clement than anticipated. On the very few occasions when heavy rain cells affected the downlink path, diminutions in carrier-to-noise ratio exceeding 5 dB were observed. In the case of the 0.6m terminal, reception on these occasions became rather noisy. To the extent that the C/N of the other installations was higher, the effect of heavy rain was less pronounced subjectively. The C/N of the uplink was practically 25 dB, and appreciable subjective change in noise was not observed during rain storms in the uplink path. On one occasion, accumulated snow on the antennas decreased the S/N ratio by 3 to 4 dB.

Figure 8. CRC 1.2 METER CASSEGRAIN ANTENNA.
Indoor unit shown at foot of mount.


Figure 9. CRC 1.2 METER ANTENNA With focally mounted outdoor unit.

TABLE I

TRANSMISSION QUALITY, HOME-TYPE TERMINALS
(MONTREAL STUDIOS)

| Terminal antenna diameter and origin | 0.6m (Japan) | 1.0m (Japan) | 1.2m (Holland) | 1.2m (Can.CRC) |
|---|---|---|---|---|
| Frequency Response measured by multi-burst | -0.1 dB | -0.6 dB | +0.7 dB | -1.5 dB |
| K Factor | 2% | 2% | 2% | |
| Chrom./Lum. Gain Inequality | +0.1 dB | 0 dB | +0.4 dB | -1.1 dB |
| Chrom./Lum. Delay Inequality | 175 ns | 165 ns | 155 ns | 170 ns |
| Diff. Gain | 5% | 5% | 6% | 7% |
| Diff. Phase | 1.4° | 1.6° | 7.0° | 5.9° |
| Signal-to-Weighted Noise Ratio (Video) | 45.1 dB | 47.2 dB | 46.8 dB | 47.8 dB |
| Audio Distortion | 4.9% | 4.0% | 4.0% | |
| Signal-to-Unweighted Noise Ratio (audio) | 35.6 dB | 37.6 dB | 36.2 dB | |

The C/N ratio of the Philips 1.2m terminals in Montreal and Toronto was above 10 dB for 98% of the 76.4 hours of data taken during this "rainy" period. One may therefore anticipate that the data for year-round operations would be much better.

An interesting event occurred one day, when considerable snow fell just before the measurement period. The observed decrease of 3 to 4 dB in signal-to-noise ratio was cured by removing the snow that piled up on the lower part of the antenna dishes. This experience suggests that in areas subject to snow, the antenna should have a radome shaped to prevent the accumulation of snow, given that melting and de-icing heaters are likely to be too expensive for broadcasting-satellite receiving antennas.

## SPECIAL DEMONSTRATION INSIDE A BUILDING

Following the end of the main experiment, special arrangements were made for a demonstration of home reception inside a building, for 1 to 2 hours around noon on two days during the week of November 28, 1976. A 0.6m terminal was in a room on the 18th floor of a building in downtown Ottawa,

behind a window facing southwest. The window had double-plated thermal-glass panes with aluminum partitions spaced approximately 1.4m apart. In figure 10, the picture on the monitor is being received directly from Hermes.

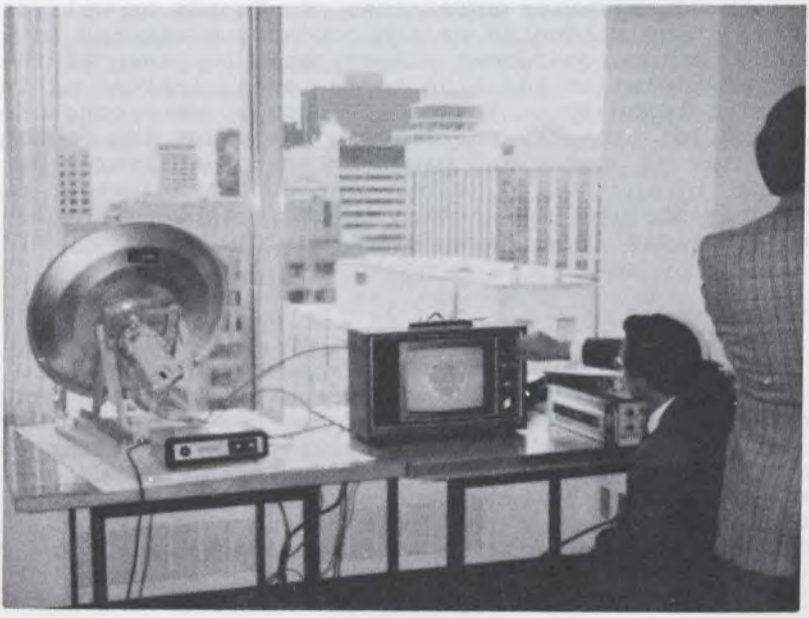

Figure 10. Indoor reception of CTS with 0.6 meter antenna.

The Canadian Radio and Telecommunication Commission (CRTC) engineers who conducted this demonstration reported a S/N ratio of 43 dB indicating that the loss due to the glass pane was approximately 2 dB.

## DEMONSTRATIONS TO VISITORS

A viewing theatre in the Maison de Radio-Canada in Montreal, with a capacity of 50 seats (Fig. 2), was used to demonstrate direct-to-home reception to a large number of persons in the engineering and executive branches of the broadcasting industry, from Canada, U.S.A., France, West Germany, Denmark, Japan, Czechoslovakia, Poland, England, Hungary, etc.. This viewing theatre was equipped with picture monitors, each fed by one of the Hermes receivers. A single loudspeaker was fed from one receiver, to avoid confusion.

## CONCLUSION

This successful experiment leaves no doubt that satellite broadcasting, whether for "community" or for individual reception, is technically feasible and can provide a television service of very good picture quality quite uniformly over an extensive service area (such as one of the larger Provinces of Canada) and of very good availability. What remains to be seen is if this new technological capability can be used to economical and cultural advantage. Several broadcasting organizations, in Canada as well as elsewhere, have conducted or are conducting studies on this question. A more confident answer could be given if the next experiments, in addition to or, even, instead of investigating technological aspects further, were conducted, also, as pilot projects for finding out about the economical realities of operation, gauging the possibilities for acceptance by the public, estimating cultural impact, testing the possibility of introducing new or special broadcasting services (e.g. high-definition, large-screen TV), etc..

## ACKNOWLEDGEMENTS

The special-program video tape used during these experiments and demonstrations was prepared at the CBC studios in Ottawa under the supervision of Mr. Del MacKenzie, TV producer. Installation of the facilities and associated technical matters were under the supervision of Mr. John Dickson of CBC Engineering Headquarters. Arrangements for visitors and associated public-relations matters were supervised by Mr. Charles Kirkman of CBC Engineering Headquarters.

## REFERENCES

Edens, J.W.
1977 Experience With and Some Aspects of Reception of Direct Television Broadcasts from satellites. *A.B.U. Review Technical* no. 162, April.

Freeman, K.G.
1977 Experimental Direct Broadcast Reception of 12 GHz Television Signals from the Canadian Communications Technology Satellite. *Radio and Electronics Engineer*, vol. 47, #5, May.

Konishi, Y. et al.
1973 Simplified 12 GHz Low-noise Converter with Mounted Planar Circuit in Waveguide. NHK Laboratories, note 161, March.

# ADVANCED GROUND RECEIVING EQUIPMENT EXPERIMENT

John Chitwood

NASA-Goddard Space Flight Center

Greenbelt, U.S.A.

*L'Advanced Ground Receiving Equipment Experiment (AGREE) est destinée à mesurer et évaluer le rendement de stations terminales relativement économiques recevant des signaux du satellite technologique de télécommunications (STT) Hermès dans des conditions simulant le milieu opérationnel d'un système de radiodiffusion par satellite. Il s'agit d'une expérience conjointe de la NASA et des laboratoires de recherches techniques de la Nippon Hoso Kyokai (NHK) du Japon. La participation de la NHK est parrainée par les laboratoires de recherches en radiocommunications du ministère des Postes et Télécommunications du Japon.*

*La première phase de l'expérience est terminée et les données recueillies jusqu'à présent indiquent que les récepteurs mis à l'essai conviennent parfaitement à la réception de signaux de télévision satisfaisants transmis par le STT. De plus, on ne prévoit pas de problèmes lorsque les stations seront opérationnelles.*

*Tous les récepteurs doivent être retournés au Centre Goddard de la NASA à la fin de janvier 1978. Ils y subiront alors d'autres tests portant notamment sur le facteur de bruit, le niveau de seuil, le contrôle automatique d'amplification (Automatic Gain Control (AGC)) par rapport à la puissance d'entrée, le gain différentiel et la phase différentielle. Un rapport suivra ces tests.*

## OBJECTIVES AND PURPOSE

The Advanced Ground Receiving Equipment Experiment (AGREE) is designed to measure and evaluate the performance of relatively low-cost ground terminals operating with the Communications Technology Satellite (CTS) or Hermes, under conditions simulating an operational broadcasting satellite

system environment. This is a joint experiment by NASA and the Technical Research Laboratories of Nippon Hoso Kyokai (NHK), Japan. The participation of NHK is being sponsored by the Radio Research Laboratories of the Ministry of Posts of Telecommunications, Japan.

There is world-wide interest in the application of communication satellite technology for broadcasting instructional, educational and entertainment television. Studies and several experimental projects have been undertaken to determine the feasibility and cost of such applications. Most notable of the experimental projects have been the Health, Education Telecommunications (HET) Experiment conducted in this country and the Satellite Instructional Television Experiment (SITE) conducted in India. Both experiments used NASA's Applications Technology Satellite (ATS-6) which operates in lower frequency bands than CTS.

The transition of these and similar experiments from the experimental to the operational stage could eventually require thousands, and even millions of ground receiving equipments. The cost and reliability of such equipments is expected to be a major factor in how fast operational systems will evolve.

Development of low-cost ground receiving equipment has been underway in this and other countries for some time. In particular, several manufacturers in Japan have developed low-cost ground receiving equipment under the guidance of the Technical Research Laboratories of NHK. These equipments are representative of ground stations that might be used in an experimental satellite broadcasting system using the 12 GHz band. This CTS Experiment will provide an early opportunity to evaluate such ground receivers under actual field conditions.

## EXPERIMENTAL TECHNIQUE

A simplified configuration of the experiment is shown in figure 1. Thirteen sets of ground receiving equipments are being used; diameters of the paraboloid antennas are 2.4m(2), 1.6m(10) and 1.0m(1). A wideband frequency-modulated carrier containing the picture and one audio channel is transmitted to the CTS in the 14GHz band from an earth station. CTS translates this carrier to the 12GHz band and relays it to the ground terminals. The system and receivers have been designed to meet goals that will insure satisfactory performance for most educational and commercial applications. The quality of the picture should exceed 43 dB peak-to-peak picture to RMS weighted-noise (TASO 1.5) and the audio channel should exceed 50 dB test-tone-to-noise ratio.

The performance and reliability of the ground receiving equipments are being measured using techniques which are accepted as standard practice by the television broadcasting industry.

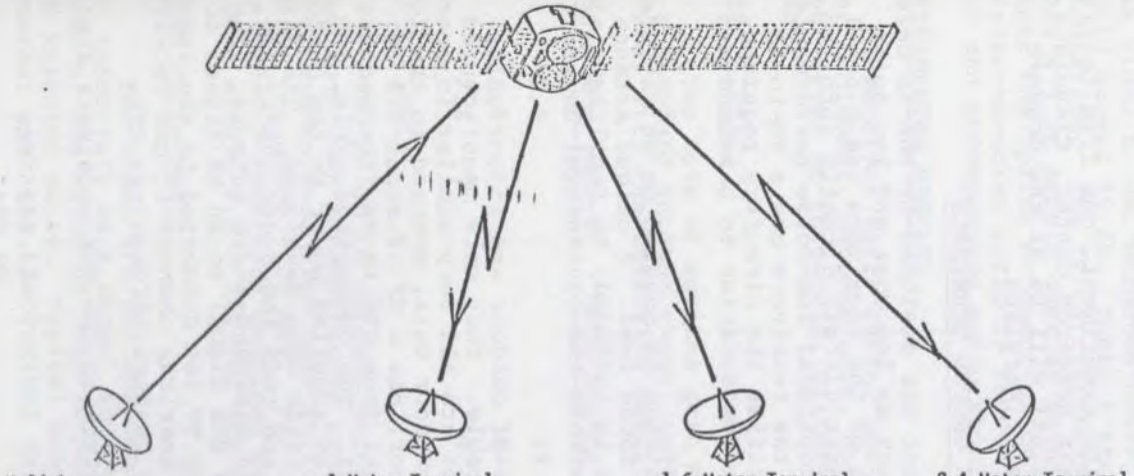


PHASE I

- Series of 18 comprehensive tests to be performed
- Uplink at Goddard or Lewis
- All 13 receiving terminals at Goddard

PHASE II

- Two receiving terminals at Goddard
- One receiving terminal at Lewis
- Ten receiving terminals to be loaned to approved CTS Experimenters
- Uplink will be that associated with appropriate CTS User Experiment
- Limited data taken over a one (1) year period

Figure 1. AGREE experiment configuration.

The experiment has two phases. The first phase, an intensive evaluation of the ground receiving equipments at the Goddard Space Flight Centre, was completed in about two months. For the second phase, 10 of the 1.6m terminals are being loaned for about one year to approved CTS Experimenters. In return, they will take and record limited data on the performance of the receiving equipment.

For the duration of the experiment, one 2.4m terminal will be installed at the Lewis Research Center, Cleveland, while one 2.4m and 1.0m terminal will be at the Goddard Space Flight Center, Greenbelt, Maryland.

## TECHNICAL DESCRIPTION OF THE GROUND TERMINALS

The receiving equipment was designed by NHK to have desirable characteristics such as low cost and low noise figure (NF). The front ends of the receivers use a novel technique of inserting a planar circuit directly into the waveguide which exhibits exceptional low-noise performance. The indoor units of some of the receivers use a FM-to-AM direct converter which simplifies the circuitry required, as this removes the need for demodulation to baseband and the AM remodulation process.

The parabolic dish antenna is mounted on an extruded metal frame and has a prime focus feed. A unique antenna elevation pointing mechanism is included, to facilitate elevation adjustment anywhere within the continental United States.

The receivers consist of outdoor and indoor units, with a flexible connecting cable. They were manufactured by 5 different companies, yet are all very similar in operation and performance. The outdoor unit, mounted to the feed behind the parabolic reflector, has a NF of about 5.0 dB, and converts the 12 GHz signal from CTS to an intermediate frequency (IF) around 400 MHz. The connecting cable, 30m long and 6mm in diameter, also supplies power to the outdoor units. Two types of indoor units were developed. The first demodulates the 400 MHz IF, and then the audio subcarrier, to provide baseband-video and baseband-audio outputs. The second type converts the 400 MHz signal to an AM signal to drive a standard TV set. Any TV set connected to the indoor unit and tuned to the North American channel 12 can receive the video and a single audio channel through the CTS.

The modulation parameters of the NHK receivers are:

| | |
|---|---|
| Center Frequency | 12.0805 GHz |
| Bandwidth | 30 MHz |
| Sense of Modulation | Positive |
| Deviation of Carrier by Video | 12 MHz peak-to-peak |
| Audio Subcarrier Frequency | 4.5 MHz |
| Deviation of carrier by subcarrier | 2 MHz peak-to-peak |
| Deviation of subcarrier by audio | 50 KHz peak-to-peak |

The principal difference from the parameters used by most of the CTS Experimenters is the subcarrier frequency of 4.5 MHz.

With the above parameters, clear-weather video performance of the NHK receivers should exceed 50 dB peak-to-peak video to RMS weighted noise, and the audio S/N ratio should exceed 60 dB. Table I shows a typical clear-sky link calculation. The TV carrier-to-noise ratio of 19 dB provides a 9 dB margin over an assumed 10 dB threshold. Should either the uplink or downlink degrade so that the effective carrier-to-noise ratio is reduced by 9 dB or more, the picture and accompanying audio should be very noisy.

## EXPERIMENTAL RESULTS

Receiver tests during the first phase of the experiment included: antenna gain, noise figure, video S/N ratio, input level at threshold, differential gain, and differential phase.

### Antenna Gain

Two sets of antenna gain measurements were made, one on a standard antenna range, another using the CTS as a source, with the following results:

| Antenna Size (meters) | Using Antenna Range (dB) | Using CTS (dB) |
|---|---|---|
| 1.0 | 39.0 | 39.5 |
| 1.6 | 43.0 | 43.2 |
| 2.4 | 47.0 | 47.0 |

### Noise Figure

The NF of 16 outdoor units was measured at center frequency over a temperature range of -20°C to 40°C. NF measurements were also made at room temperature at the center frequency ± 20 MHz. For the above test conditions, the NF of 7 receivers remained within the range 4.4 - 5.9 dB, 8 were within 4.2 - 5.5 dB, and one was within 3.8 - 4.3 dB.

### Video Performance

The video S/N was measured from the receivers using the spacecraft as a signal source. The data is expressed in terms of the ratio of peak-to-peak video excluding sync to RMS weighted noise. Typical measurements are shown below together with the theoretical calculated values:

| | Video S/N (dB) | |
|---|---|---|
| Antenna Size (meters) | Measured | Calculated |
| 1.0 | 43.8 | 45.6 |
| 1.6 | 45.6 | 49.1 |
| 2.4 | 46.7 | 52.6 |

TABLE I

Sample Link Calculation for NHK Receiver

| | | | |
|---|---|---|---|
| **UPLINK** | | | |
| Transmit EIRP | | 74.8 | dBw |
| Subsatellite Path Loss | -206.6 dB | | |
| Correction for 30° Elevation | - 0.5 dB | | |
| Total Path Loss | -207.1 dB | -207.1 | dB |
| S/C Antenna Gain | 37.9 dB | | |
| Beam Edge | - 3.0 dB | | |
| Pointing Error (±.25°) | - 0.2 dB | | |
| Net Antenna Gain | 34.7 dB | | |
| S/C Receiver Temperature | 1285°K | 31.1 | dB |
| System G/T | | 3.6 | dB/°K |
| Uplink Carrier-to-Noise Power Density | | 99.9 | dB-Hz |
| **DOWNLINK** | | | |
| Spacecraft Power to Antenna Input | 22.4 dBw | | |
| Spacecraft Antenna Gain | 36.9 dB | | |
| EIRP | 59.3 dBw | 59.3 | dBw |
| Subsatellite Path Loss | -205.1 dB | | |
| Correction for 30° Elevation | - 0.5 dB | | |
| Off-axis Loss | - 3.0 dB | | |
| Total Losses | -208.6 dB | -208.6 | dB |
| Earth Station G/T | | 15.6 | dB/°K |
| Downlink carrier-to-noise power density | | 94.9 | dB-Hz |

TABLE I (Cont'd)

FM TELEVISION SYSTEM PARAMETERS

| | | |
|---|---|---|
| Uplink C/n | | 99.9 dB-Hz |
| Downlink C/n | | 94.9 dB-Hz |
| Effective C/n | | 93.7 dB-Hz |
| Bandwidth (30 MHz) | | 74.7 dB |
| Carrier-to-noise ratio | | 19.0 dB |
| VIDEO: | Bandwidth | 4.2 MHz |
| | Peak Deviation | 6.0 MHz |
| | FM Improvement | 19.4 dB |
| | De-emphasis advantage | 2.5 dB |
| | Noise Weighting | 10.2 dB |
| | P-P Picture/RMS WTG noise | 51.1 dB |
| AUDIO: | Subcarrier Frequency | 4.5 MHz |
| | Peak Deviation (c by Sc) | 1 MHz |
| | Subcarrier Bandwidth | 80 KHz |
| | Subcarrier Improvement | 9.7 dB |
| | Subcarrier-to-noise ratio | 28.7 dB |
| | Audio Bandwidth | 15.0 KHz |
| | Peak Deviation | 25.0 KHz |
| | FM Improvement | 22.2 dB |
| | De-emphasis Advantage | 12.7 dB |
| | Test-tone-to-noise ratio | 63.6 dB |

## Input Level at Threshold

The input level at threshold was measured for 17 receivers. Here, threshold is the input carrier level for which the output S/N is 1 dB less than the calculated value. The threshold for 12 receivers was in the range 82 - 84 dBm, and for the remaining 5 receivers was in the range 78 - 82 dBm.

## Differential Gain and Phase

Using conventional measurement techniques, differential gain and phase was measured on all receivers with the following results:

| RECEIVER | DIFF. GAIN (%) | DIFF. PHASE (Degrees) |
|---|---|---|
| 1 | 10 | 5 |
| 2 | 4 | 9 |
| 3 | 5 | 5 |
| 4 | 2 | 2 |
| 5 | 5 | 2 |
| 6 | 2 | 2 |
| 7 | 2 | 5 |
| 8 | 2 | 4 |
| 9 | 3 | 1 |
| 10 | 4 | 11 |
| 11 | 4 | 4 |
| 12 | 25 | 10 |
| 13 | 1 | 1 |
| 14 | 3 | 1 |
| 15 | 2 | 1 |
| 16 | 4 | 3 |
| 17 | 2 | 2 |

As of this writing, data is being taken in phase two of the experiment. Ground stations have been loaned to host experimenters, including the Federal Communications Commission, NASA's Lewis Research Center, the Public Service Satellite Consortium, and the Virginia Polytechnic Institute and State University. Two ground stations remain at NASA-Goddard for further measurements. All experimenters are requested to maintain a strip-chart recording of the received AGC level, and make entries on a data sheet regarding local weather conditions and the quality of the signals received.

## CONCLUSIONS AND FUTURE PLANS

To date, only phase one of the experiment has been completed. The data taken during this phase indicates that low-cost receivers tested are quite adequate for receiving good quality TV signals from the CTS. Furthermore, no problems are anticipated while the ground stations are set up in the field.

All of the terminals are scheduled to be returned to NASA-Goddard around the end of January 1978. At this time further tests will be conducted on the receivers. These tests will include NF, threshold, AGC vs input level, differential gain, and differential phase. After these measurements, a final report will be prepared.

# A SATELLITE LINK RADIO INTERFEROMETER

J.L. Yen, University of Toronto, Toronto, Canada
N.W. Broten, D.N. Fort and R.S. Richard, National Research Council, Ottawa, Canada
K.I. Kellerman and B. Rayhrer, National Radio Astronomy Observatory, Green Bank, West Virginia, U.S.A.
S.H. Knowles and W.B. Waltman, E.U. Hulburt Centre for Space Research, Naval Research Laboratory, Wasington, D.C., U.S.A.
G.W. Swenson, University of Illinois, Urbana, Illinois, U.S.A.

*Un interféromètre-radio, employant des radiotélescopes situés à Lake Traverse (Ontario), Green Bank (West Virginia) et Owen's Valley (California) et reliés entre eux par le satellite Hermès, fonctionne depuis novembre 1976. Cet appareil est un modèle nouveau d'interféromètre à grande base (Very Long Base Interferometer (VLBI)) qui constitue le principal instrument d'étude des éléments compacts des quasars, des radiogalaxies et de l'effet maser des nuages moléculaires. L'interféromètre à liaison par satellite remplace l'enregistrement des signaux sur bandes magnétiques et la corrélation des données après observation (méthodes utilisées dans les systèmes existant d'interférométrie à grande base) par l'observation et la corrélation en temps réel.*

*Le signal d'une radiosource capté par un radiotéléscope est transmis via le Hermès à un autre observatoire utilisant une paire d'antennes de télécommunication. Ce signal est ensuite comparé à celui reçu par le deuxième radiotélescope afin d'obtenir ses franges d'interférence.*

*Ce modèle d'interféromètre a servi à l'étude d'un échantillon sans biais de radiosources et du noyau dense de certaines galaxies, en plus de permettre le calcul en temps réel d'étalons de fréquence. On a également entrepris de comparer les phases en temps réel à l'aide d'une liaison bidirectionnelle permettant la synchronisation d'un interféromètre à grande base.*

Since November 1976 a radio interferometer using radio telescopes located at Lake Traverse, Ontario, Green Bank, West Virginia and Owen's Valley, California linked together by the Hermes Satellite has been in successful operation (Yen, et al, 1977). The interferometer is a new form of the Very Long Baseline Interferometer (VLBI) which is the principal instrument for the study of compact components of quasars, radio galaxies and masering molecular clouds as

well as a promising new tool for geophysical investigations. The Satellite Link Interferometer replaces signal recording on magnetic tapes and post-observation data correlation used in previous VLBI systems by real-time correlation and observation. In addition, the Hermes link provides a means of synchronizing the independent frequency standards used at each radio telescope, making it possible to implement, for the first time, a phase coherent VLBI.

Although a great deal is known about galaxies, we understand very little about why they behave as they do. Many anomalies have been found in optically-normal galaxies, galaxies that emit mainly radio waves, and quasars. Very compact cores, explosions, wisps and jets, rapid fluctuations in intensities, as well as components seemingly separating at several times the velocity of light, have been discovered. Many of these discoveries were the result of radio, infrared, ultraviolet and x-ray observations. In particular, the study of compact components in the nucleus of galaxies and quasars, and their sometimes violent structural variations, lie in the domain of VLBI. Using radio telescopes separated by continental or intercontinental distances in synchronism, angular resolution approaching $10^{-4}$ arcsecond can now be achieved (Cohen, 1973). With such high resolution we can also investigate the peculiar localized masering molecular clouds excited by nearby very luminous stars, to help in understanding some aspects of interstellar molecules (Moran, 1976). In addition, the positions of all such compact sources in the sky as well as the positions of the telescopes on earth used for the observations can be determined. As a result, significant advances in astrometry (Counselman, 1976), geodetic measurements (Shapiro et al, 1974) and precision time transfer (Clark and Shapiro, 1973) using VLBI appear to be imminent. Observational programs using as many as 8 radio telescopes distributed over North America and Europe are being vigorously pursued.

A telescope forms an image by combining waves from one part of an object incident on different parts of the telescope aperture, with appropriate time delays to compensate for the differences in path lengths, such that all the waves interfere constructively. A neighbouring part of the object is resolved if the waves are combined out of phase so as to interfere destructively. Since the maximum path phase difference is proportional to the dimension of the aperture measured in terms of wavelengths, so is the resolution of the telescope. To obtain sufficient angular resolution to study compact radio sources, aperture sizes in excess of $10^8$ wavelengths are required. At wavelengths of a few cm this requires telescopes with diameters of a few thousand km. Fortunately, if the object remains unchanged during the measurement, the image produced by a large telescope can be synthesized by using two small telescopes, one fixed and one moveable, to cover the entire aperture area of the large telescope. The two small telescopes form an interferometer whose outputs when correlated form inter-

ference fringes depending on the relative positions of the two telescopes or the interferometer baseline. By combining the interference-fringe amplitude and phase vs baseline length and orientation, an image of the object equivalent to that obtained from a large telescope filling the entire aperture can be synthesized. In fact, if enough small telescopes are available, the rotation of the earth can be used to move the interferometer baselines relative to an extraterrestrial object without repositioning the telescopes. For his development of this, "the synthesis radio telescope", (Ryle, 1975), Ryle was awarded a Nobel prize.

To extend the synthesis radio telescope to continental and intercontinental baselines VLBI was introduced in 1967 (Broten et al, 1967; Bare et al, 1973). In this technique the signal received from each telescope is first converted to video frequencies by mixing with a local oscillator, timing information is inserted, and the composite data is recorded on magnetic tape at each station. The recorded data from two or more telescopes are correlated later to obtain interference fringes. Since the original signal emitted at a specific instant by the radio source is received by several different telescopes, and the received signals must be combined, the clocks at each station must be synchronized to a high degree of accuracy. In addition, the local oscillators in each station must be highly stable, otherwise the very weak interference fringe will be spread out in frequency, making it difficult to measure. Unfortunately, even with the most stable atomic frequency and time standards available, it is not possible to determine the phase of the interference fringes from different baselines because the various local oscillators are not synchronized, i.e., not phase-coherent. Thus, from a knowledge of the fringe amplitude alone, as a function of baseline length and orientation, a model of the radio source and its position are derived. The lack of fringe phase information, however, introduces ambiguities in source models and large errors in source positions.

A major difficulty with the tape recording system is that post-observational tape processing is usually very time consuming, especially for multibaseline observations, requiring an inordinately large amount of scientific labour. Also, a major observing program consumes large amounts of magnetic tape creating logistic problems. Furthermore, no information is available on the performance of the individual telescopes and peripheral equipment during the observations. Frequently a subtle failure of a minor yet vital component will not be recognized until after tape processing has commenced, resulting in much wasted observing time and effort. Finally, using independent local oscillators, the fringe phase is undetermined. The advent of Hermes provided an opportunity to replace tape recordings by a communication link, to form a real-time VLBI. Furthermore, phase comparison between individual oscillators can also be performed via Hermes leading to a phase-coherent VLBI.

The VLBI system designed to utilize the Hermes satellite is illustrated in figure 1. Astronomical signals from two radio telescopes are clipped and sampled under the control of clock pulses derived from two independent hydrogen-maser oscillators, to obtain two binary signals. Synchronization words are inserted into the data stream every second at station 1. The binary signal thus formatted modulates a 150 MHz IF carrier phase locked to the hydrogen-maser oscillator. The modulation employed is differential phase-shift keying (DPSK). This modulated IF carrier is then converted to 14 GHz for transmission to Hermes, which translates it to 12 GHz and relays it to the communications antenna at station 2.

The received signal is demodulated and a phase-locked loop recovers the clock pulses. The data and clock pulses from station 1 are combined with the processed astronomical signal from telescope 2 in the delay and correlation system. The two astronomical signals must be exactly synchronized before being cross-correlated. As the signal arriving via the satellite path suffers a delay of approximately 0.25 s, it is necessary to delay the signal from telescope 2 by a corresponding amount. A sampling rate of 20 Mbps was chosen as a compromise between the desire for increased sensitivity and the need to restrict the delay line to a reasonable size. At this sampling rate, the DPSK signal occupies a bandwidth of 40 MHz, about half of the 85 MHz Hermes channel.

The local 20 Mbps data stream is delayed up to 270 ms. It contains 5500 shift registers of 1024 bits each and a small but fast 32 K-bit read/write memory which is used as a first in - first out register. The memory writes at the rate of the station 2 clock, and reads at the rate received via Hermes, which compensates for the motion of the satellite. This arrangement also aligns the two data streams to an accuracy of 1 bit. The amount of delay is set by control circuitry which detects sync words in the received data stream and compares them with a 1 second pulse from the local clock. The amount of delay can be modified by as much as ± 26.2 ms to account for geometrical delay under program control.

The control computer calculates the geometric delay and relative Doppler shift for the two stations. After both data streams are aligned in time a 3-level digital fringe rotator reduces the natural fringe rate to a rate near zero. Cross correlation is then performed in a 64-channel digital correlator with a total delay range of 3.2 μs. Data are accumulated in the correlator for 100 ms, read into the control computer and further accumulated for one second. Then the 64 complex numbers are stored in a core-memory buffer. After 60 such samples the whole buffer, along with all other necessary information is dumped onto magnetic tape. These data are intended for detailed post-experiment analysis. In addition, each minute of data is analysed on-line to provide a real-time display of fringe amplitude vs delay and residual rate. These three quantities are also printed out at this time.

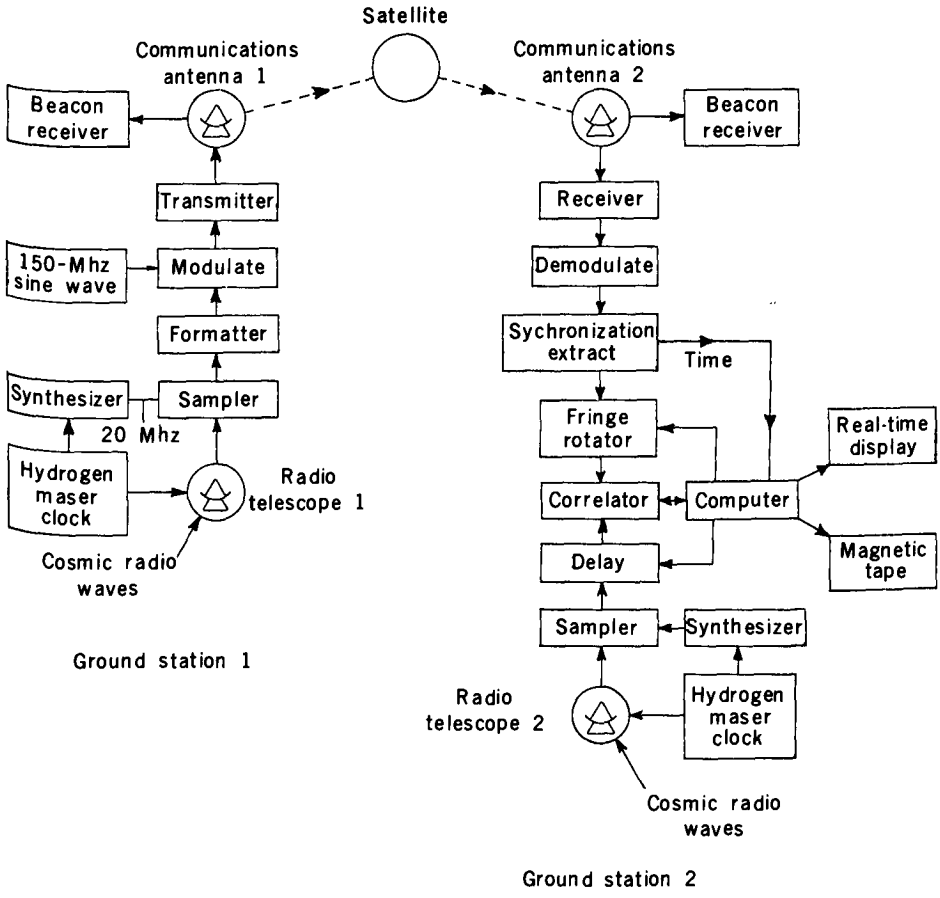


Figure 1. Very Long Baseline Interferometer (VLBI).

The system was first successfully used for astronomical observation on November 27, 1976, in conjunction with the 43-meter radio telescope of the National Radio Astronomy Observatory at Green Bank, West Virginia and the 46-meter instrument of the Algonquin Radio Observatory at Lake Traverse, Ontario. The wavelength was 2.8 cm, the video bandwidth was 10 MHz, and the system noise was about 120°K at each telescope. The West Virginia station served as station 1 in the diagram of figure 1 and the Ontario station as station 2. The uplink transmitter (at Green Bank) utilized a 26-meter parabolic antenna and the downlink receiver a 10-meter antenna, each of which was provided with a receiver for the 14 GHz beacon transmitter on Hermes. The beacon receivers permitted precision pointing of the narrow-beam communication antennas. With an uplink transmitter power of 5 w and a downlink receiver noise temperature of 900°K, the received energy per bit to noise-power density ratio E/N is 14 dB. With this E/N the error probability, including the clock error, is less than $10^{-5}$. The satellite link therefore does not impair the sensitivity of the interferometer. The ground terminal of station 1 has also been moved to the Owen's Valley Radio Observatory, California using a 27.5 m antenna for data transmission to achieve a transcontinental baseline.

Figure 2 shows a typical real-time display of one minute integration of radio source 3C120. The lower trace is the fringe amplitude vs delay (channel separation is 50 ns) while the upper trace is fringe amplitude of the strongest delay channel vs fringe frequency (channel separation 16 millihertz). The spectral purity of the two hydrogen-maser oscillators used in the experiment is evident in the sharpness in fringe frequency and the broader but still concentrated distribution of fringe amplitude vs delay.

Using the Green Bank - Algonquin baseline a survey of all radio sources with 1400 MHz flux above 3 Jansky in a statistically-complete sample of sources (Bridle et al, 1972) was conducted. Each source was observed once without regard to baseline orientation. Among the approximately 130 sources observed, 34 show fringe amplitude above 0.3 Jansky. These data are important in determining the incidence and the intensity of self-absorbed components in a representative sample of sources. Several normal galaxies have also been investigated; the results from one of these, NGC4278, show that a large fraction of the radiation originated from a very compact core. The compact radio source at the Galactic Centre has also been observed. The result supports the presence of scattering of radio emission originating from a component with intrinsic size less than one milli arcsecond in diameter by a surrounding medium.

A demonstration of real-time precision time transfer was performed between Green Bank and Algonquin using the radio source 3C84 (Knowles et al, 1977). The centroid of the fringe amplitude vs delay was measured with an error of about 10 ns. This measurement was then corrected for the

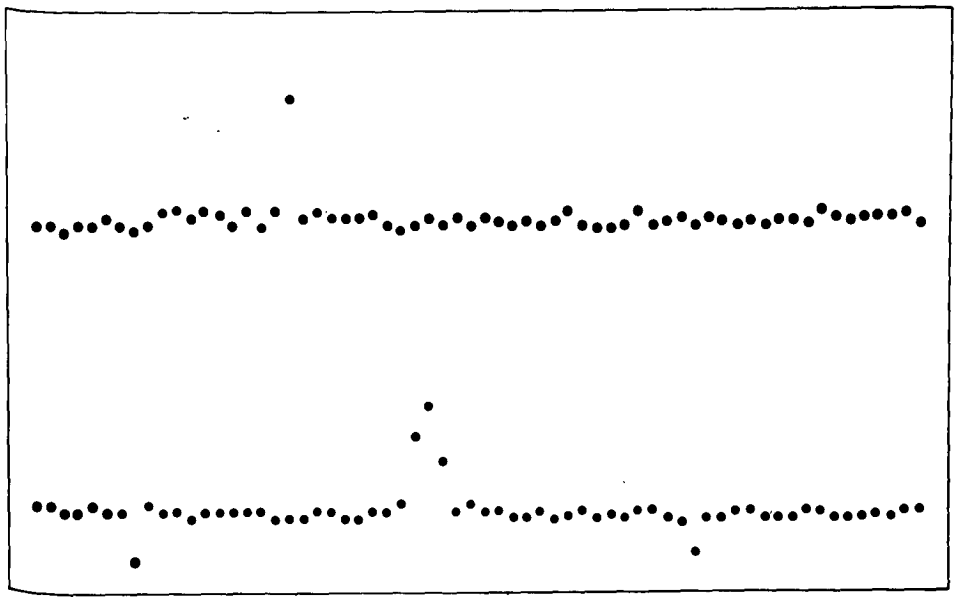

Figure 2. Typical real-time display.

cable delays at each station and compared with that predicted from a pair of calibrated cesium standards transported from the U.S. Naval Observatory to each station. The resulting agreement indicates the feasibility of this mode of time transfer. The stability of several samples of atomic frequency standards was also evaluated by substituting them in turn as local oscillator at one station. The results show that a high-quality rubidium standard is nearly as stable as a hydrogen-maser over a 1 minute interval.

To remove the major difficulty, namely, the lack of phase information in current VLBI techniques, a local oscillator phase-comparison link was introduced. The received phase of a signal transmitted from one station through the satellite to the other depends on the satellite position, the propagation medium and the translation oscillator in the satellite transponder. Fortunately, the Hermes beacon transmission is generated from the same source as the translation oscillator. In the phase-comparison system, each station receives the Hermes beacon, and each station transmits a pilot tone to the other. The received pilot tone and the beacon are first converted to intermediate frequencies. The pilot tone is then mixed with a signal that is phase locked to an appropriate fraction (5/27) of the beacon. By choosing the upper sideband, the effect of satellite transponder frequency down conversion is completely cancelled. What remains at each station is the Doppler-shifted version of the distant oscillator which can be compared with the station oscillator. The smoothed phase dif-

ference is measured once a second at each station. The measured value of station 1 is coded and inserted onto the astronomical signal data stream and transmitted to station 2 where it is extracted and decoded. By comparing the two differences, the Doppler effect on the two pilot tones can also be cancelled. What remains is the uncontaminated phase-comparison of the two local oscillators. When appropriate calibrations are implemented the fringe phase of the interferometer can be derived, thus achieving a phase-coherent VLBI.

Advances in technology are increasingly lowering the cost of satellite communication channels and ground terminals. The Hermes experiment has demonstrated that a phase-coherent satellite-linked VLBI network is technically feasible and may indeed become a real possibility.

## ACKNOWLEDGEMENTS

The National Radio Astronomy Observatory is operated by Associated Universities, Inc. under contract with the National Science Foundation. The Algonquin Radio Observatory is operated as a national facility by the National Research Council of Canada. The Owen's Valley Radio Observatory of California Institute of Technology is supported by Grants from the National Science Foundation.

The experiment was made possible by time on Hermes granted by the Canadian Department of Communications. The cooperation and assistance given by N.G. Davies and D. Jelly are gratefully acknowledged. We also thank the following persons for their contributions: A.W. Woodsworth, P. Kremer, D. Morland, W. Wireman, D.B. Shaffer, G. Grove, B.J. Geldzahler, D.L. Thacker, J.W. Johnson and J.F. Laroye. We also thank Prof. A.T. Moffet and the staff of the Owen's Valley Radio Observatory of California Institute of Technology.

## REFERENCES

Bare, C.C., Clark, B.G., Kellermann, K.I., Cohen, M.H., and Jauncey, D.L.
1973 *Science* 157, 189.

Bridle, A.H., Davis, M.M., Fomalont, E.B., and Lequeux, J.
1972 *Astronomical Journal*, 77, 406.

Broten, N.W., Legg, P.H., McLeish, C.W., Yen, J.L., Richards, R.S., Chisholm, R.M., and Gush, H.P.
1967 *Science* 156, 1592.

Clark, T.A. and Shapiro, I.I.
1973 *Proceedings of the Fifth Annual NASA and Department of Defense Precise Time and Time Interval (PTTI) Planning Meeting.*

Cohen, M.H.
1973 *Proc. IEEE* 61, 1192.

Counselman, C.C. III
1976 In *Annual Review of Astronomy and Astrophysics*, vol. 14, Annual Reviews, Inc. (Palo Alto, Cal.) p. 197.

Knowles, S.H., Waltman, W.B., Broten, N.W., Fort, D.N., Kellermann, K.I., Rayhrer, B., Yen, J.L., and Swenson, G.W., Jr.
1977 *Proceedings of the Ninth Annual NASA and Department of Defense Precise Time and Time Interval Planning Meeting.*

Moran, J.M.
1976 In *Frontiers of Astrophysics*, E.H. Avrett ed., Harvard University Press (Cambridge).

Ryle, M.
1975 *Science* 188, 1071.

Shapiro, I.I., Robertson, D.S., Knight, C.A., Clark, T.A., Counselman, C.C. III, Rodgers, A.E.E., Neil, A.E., Hinteregger, H.F., Lippincott, S., Whitney, A.R., and Sptizmesser, D.J.
1977 *Science* 186, 920.

Yen, J.L., Kellermann, K.I., Rayhrer, B., Broten, N.W., Fort, D.N., Knowles, S.H., Waltman, W.B., and Swenson, G.W., Jr.
1977 *Science* 198, 289.

# ALASKAN NORTH SHORE ICE INFORMATION DEMONSTRATION

Ronald J. Schertler, Robert C. Evans
and Richard T. Gedney

NASA Lewis Research Center

Robert J. Hlivak

Case Western Reserve University

Cleveland, U.S.A.

*Le développement commercial des réserves de pétrole du versant nord de l'Alaska a accéléré le besoin non seulement de renseignements plus complets sur l'état des glaces, mais aussi d'une diffusion plus rapide de ces renseignements pour faciliter les opérations maritimes de réapprovisionnement. Traditionnellement, c'est à partir d'observations visuelles d'aéronefs et de satellites qu'on a recueilli jusqu'ici les renseignements sur l'état des glaces. Les nuages et particulièrement le brouillard qui est général dans l'Arctique durant les mois d'été, empêchent sérieusement ces observations visuelles pendant plusieurs jours à la fois. Les vents changeants communiquent un mouvement dynamique au pack qui, pour cette raison, constitue une menace continuelle à la navigation. Pour fournir une information suffisante sur les glaces afin de venir en aide aux expéditions maritimes, il faut communiquer deux éléments essentiels: (1) une information sur l'état des glaces par tous les temps et (2) une diffusion presque immédiate de l'information à ceux qui s'en servent.*

*Cette communication décrit l'essai par la NASA, la Garde côtière, la NOAA et la Marine d'un système d'information tous temps, presque en temps réel sur l'état des glaces, destiné à guider la navigation côtière arctique le long du versant nord de l'Alaska, en août et septembre 1976. Le système utilise un radar aéroporté à balayage latéral (SLAR) dans la bande X, tous temps monté sur un appareil HC-130B de la Garde côtière américaine. A l'origine, les procédés de cartographie par radar indiquant le type, la distribution en surface et la concentration des glaces ont été mis au point par le Centre de recherche Lewis de la NASA pour faciliter la navigation*

*d'hiver sur les Grands lacs. Les données d'image en temps réel du radar étaient transmises directement de l'aéronef à Cleveland, Ohio, via le satellite NOAA-GOES. Les images radar développées à Cleveland étaient subséquemment transmises par fac-similé à un centre d'opérations maritimes à Barrow, Alaska, via le satellite technologique de télécommunications (STT) ou Hermès.*

*Les résultats de cette expérience d'information de 1976 sur l'état des glaces dans l'Arctique ont montré que ce système peut donner une information complète et immédiate, par tous les temps, sur la formation des glaces, facilitant ainsi les opérations de réapprovisionnement par chalands. Cette communication comprend une évaluation des résultats de la transmission par fac-similé et par télévision via Hermès.*

## Introduction

Commercial development of the petroleum reserves of the Alaskan North Slope has accelerated the need not only for more comprehensive ice information but also for the near real-time distribution of such information, especially to facilitate Arctic shipping resupply operations. Resupply of the commercial oil and gas drilling facilities, as well as the various DEW line military sites and native villages along the North Slope, is generally accomplished by tug and barge convoys. Such sealift operations are the most economic mode of resupply and are the only means available for transporting large building units and modules used in the oil and gas development operations. Figure 1 is a photograph of the lead elements of the 1976 resupply convoy north of Barrow, Alaska. Barge resupply operations are scheduled for July, August and September when the Arctic pack ice traditionally recedes from the northern coastline, creating navigable leads and openings. Shifting winds accompanying weather system frontal passages impart a dynamic movement to the Arctic pack ice. Leads and openings can be closed by ice in a matter of hours. It is therefore extremely difficult to forecast accurately just when and where leads, openings and melting will permit safe navigation.

Ice information for Alaska North Slope barge operations has traditionally been gathered via observations in

Figure 1. Photograph of the lead elements of Alaskan tug-barge resupply convoy off Barrow, Alaska.

the visible spectrum from either aircraft or satellite. Clouds and especially fog, which is prevalent in the Arctic during the summer months, severely hamper such observations, frequently for days at a time. The 1975 North Slope resupply sealift was a near disaster. Twenty-two of the forty-seven barges destined for Prudhoe Bay, as well as all the barges destined for DEW line resupply, were unable to reach their destination because of unseasonable ice conditions. During this 1975 resupply effort, decisions on barge movements were inhibited by lack of adequate ice information. As a result of this failure of traditional methods both to obtain and/or distribute in near real-time satisfactory ice information, organizations associated with Arctic shipping requested the U.S. Coast Guard and NASA to demonstrate in Alaska the all-weather near real-time microwave ice-information system which had been developed for winter navigation in the Great Lakes. As a result of this user initiative, a joint Coast Guard/NASA/NOAA/Navy demonstration using the Great Lakes Ice Information System was conducted during August and September of 1976 for Alaskan barge resupply. The objective of this demonstration was to provide comprehensive near real-time ice information to support vessel operational movements.

## ALASKAN ICE INFORMATION DEMONSTRATION SYSTEM

An adequate ice information system to support any shipping operations must include two key elements: (1) all-weather ice information and (2) near real-time distribution of this information to the user.

### A. ALL-WEATHER ICE INFORMATION

Side Looking Airborne Radar (SLAR) can penetrate all but the most severe weather to map broad areas from aircraft altitudes. Previous investigations in the Arctic (Anderson, 1966; Rouse, 1969; Johnson and Farmer, 1971; Loshchilov and Voyevodin, 1972) have already demonstrated the ability of such SLAR systems to provide essentially all-weather ice information over a broad geographic area. However, only limited attempts have been made to provide operational users with near real-time all-weather ice information over an extended period of time.

A SLAR system was mounted aboard a Coast Guard HC-130B aircraft for the Alaskan demonstration. This system was originally developed for the Great Lakes (Schertler et al, 1976).

A schematic of this radar system is presented in figure 2. For ice reconnaissance missions, the aircraft was flown at an altitude of 3.35 kilometers (11,000 feet) and simultaneously mapped the ice cover out to 50 kilometers on both sides of the aircraft. The SLAR transmission were back-scattered from the ground to the aircraft. The received data were processed and distributed, as outlined in the following

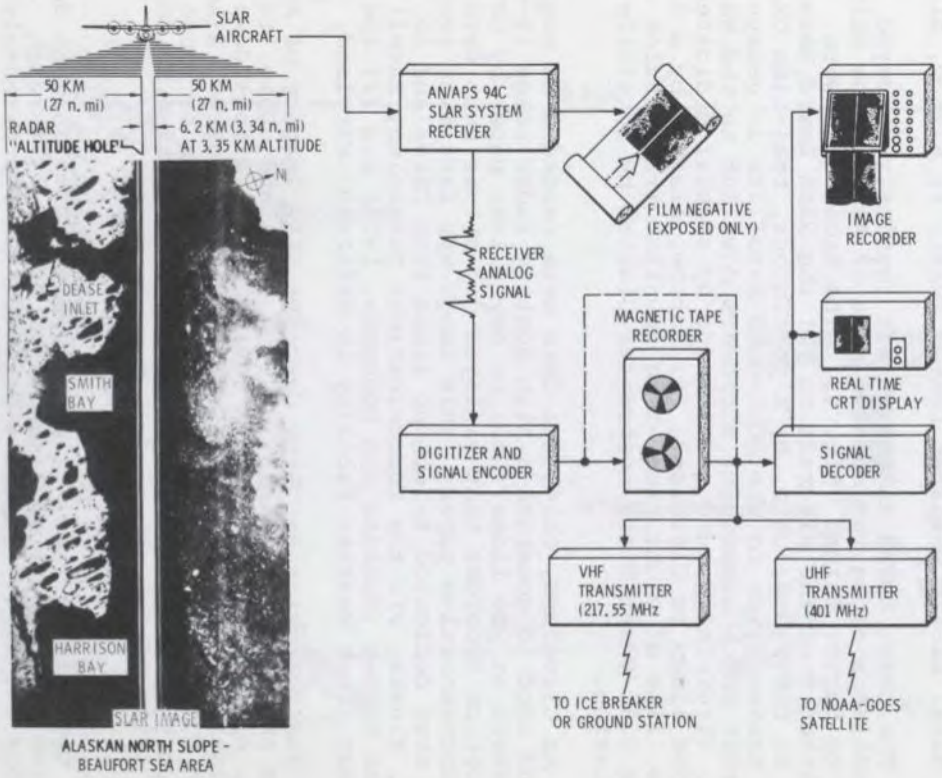


Figure 2. Schematic of side-looking-airborne-radar (SLAR) system.

section. An altitude "hole" exists in the imagery along the aircraft flight track directly beneath the aircraft only as a display artifact.

## B. DATA DISTRIBUTION

The various communication elements associated with the Alaskan Ice Information System are depicted in figure 3. For the 1976 Arctic Sealift, Crowley Maritime Corporation controlled all vessel operations from an operations center at the Naval Arctic Research Center (NARL) in Barrow, Alaska.

The Coast Guard SLAR aircraft routinely surveyed the ice conditions along the coastal area of Alaska from Wainwright to Barter Island (Fig. 4). The radar data were transmitted from the aircraft to (1) the NASA Lewis Research Center in Cleveland, Ohio, by a continuous, real-time UHF uplink transmission to the NOAA-GOES Satellite in geosynchronous orbit and a subsequent microwave downlink to the Wallops Island, Virginia, ground station and by special dedicated telephone lines to Cleveland, (2) Barrow, Alaska, by a continuous, line of sight, real-time downlink transmission and (3) the U.S. Coast Guard icebreaker Glacier by facsimile transmission.

At Cleveland, Ohio, the data were recorded on magnetic tape and used to generate a high quality radar image (9-12 grey levels at 200 lines/inch) on dry silver paper by CRT-Fiber Optics Recorder that employed dry-silver heat developed photosensitive paper. This image was facsimile transmitted over dedicated telephone lines from Cleveland to (1) Barrow, Alaska, via the Communications Technology Satellite (CTS) or Hermes (Robbins and Donoughe, 1976) and (2) the U.S. Navy Fleet Weather Facility in Suitland, Maryland.

The following sections describe SLAR imagery of Arctic sea ice and data retransmission from Cleveland, Ohio, to Barrow, Alaska, via Hermes. A review of the direct downlink transmissions from the SLAR aircraft to both Barrow, Alaska, and the U.S. Coast Guard icebreaker Glacier can be found in the report by the NASA Lewis Research Center and U.S. Coast Guard, 1977.

### SLAR IMAGERY OF ARCTIC SEA ICE

Operational radar flights were conducted almost daily along the north coast of Alaska from August 27 through September 17, 1976. Figure 4 portrays the approximately 100 km wide areas surveyed by the SLAR aircraft. The area south-east of Wainwright was ice free during this period. Only limited ship operations were conducted east of Prudhoe Bay.

A radar image depicting typical ice conditions found during this demonstration period is presented in figure 5. The image portrays near-shore ice conditions in the Beaufort Sea between the Colville River Delta to just east of Prudhoe

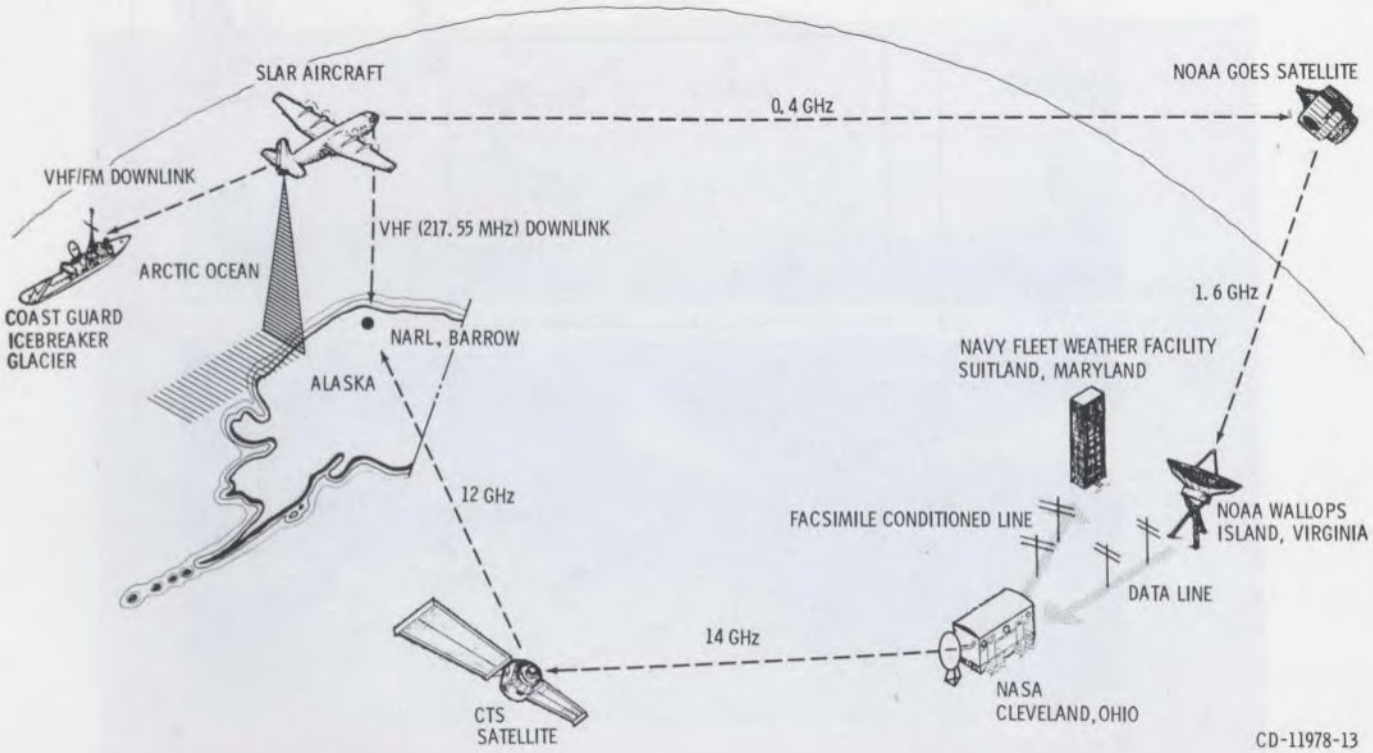


Figure 3. Schematic of Alaskan ice information system.

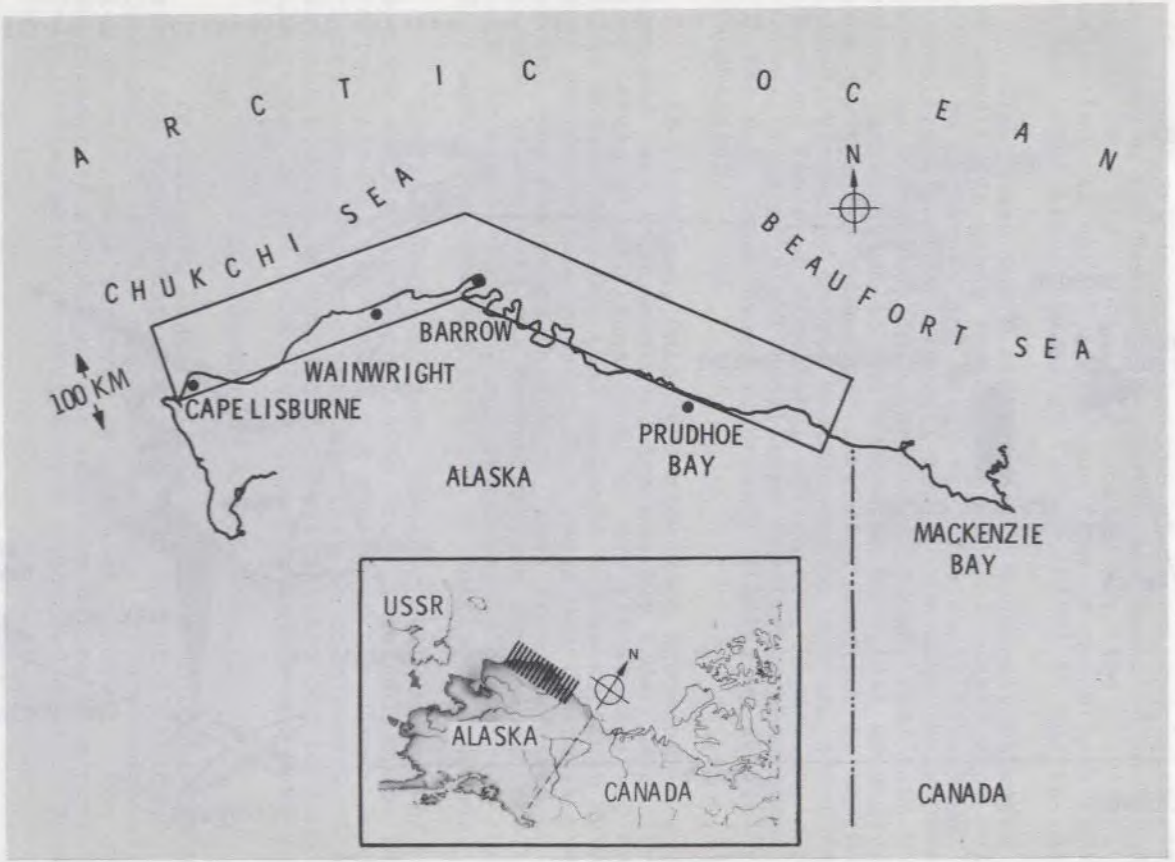


Figure 4. Areas of radar coverage.

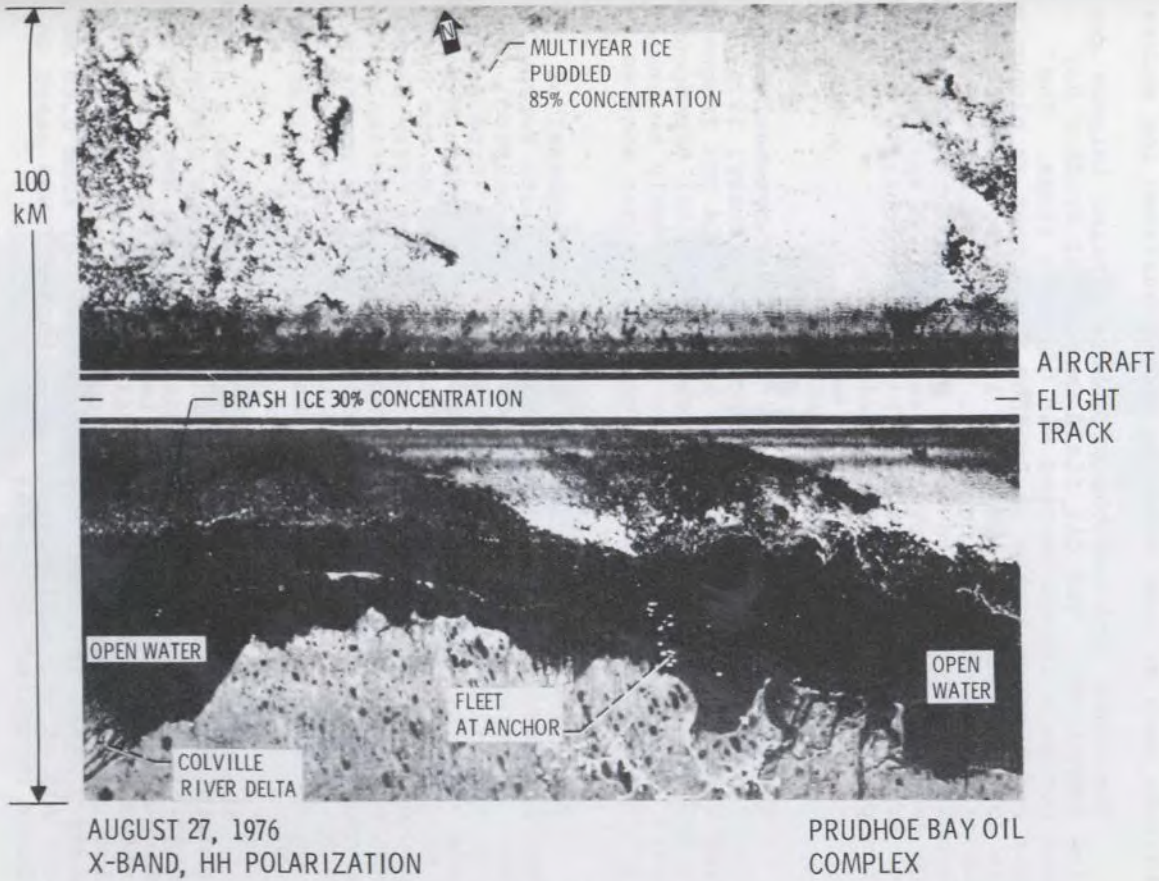


Figure 5. Radar image of Beaufort Sea ice conditions on August 17, 1976.

Bay. The various shades of gray in the radar image correspond to the intensity of backscattered microwave radiation. Light toned, white areas indicate high-intensity backscattered radiation, as might be expected from ice features with multiple edges or rough surfaces. Dark toned, black areas on the other hand represent areas of minimal backscattered radiation, such as open water or smooth-surfaced ice sheets.

The coast line and the off-shore barrier islands are easily identified. The oil field complex at Prudhoe Bay stands out as a interconnected web of white lines. The barges and tugs at anchor in Prudhoe Bay appear as elongated white dots. Within the ice field itself various concentrations of ice can be distinguished. The ice in this area was broken into many small and medium size floes that provided a large amount of backscattering, resulting in a very white toned area on the radar image. This is particularly evident in the pack ice area of 85% concentration.

## HERMES DATA RELAY

The Hermes satellite, a joint project between the United States and Canada, was launched in January, 1976. It is the first satellite to operate in the 12-14 GHz frequency band and it incorporates a high power (200 watt) transponder capable of transmitting television video directly to small, inexpensive ground receivers in remote locations such as Barrow.

For this demonstration the high power channel of Hermes provided a high-quality audio channel into Barrow, Alaska, (an area of the world where none then existed) for the transmission of facsimile ice information. From Barrow, Hermes was very low on the horizon (5.77°). Although Hermes had been used at low receive elevation angles, no one had attempted to operate so close to the so-called "five degree elevation angle cutoff". Furthermore, no propagation data were available for the 12 GHz downlink path into northern Alaska. And finally, both ground terminals were as simple and inexpensive as possible and therefore used small antennas (3m diameter transmit, 0.6m receive).

The Hermes Alaskan Earth Terminal (AKET) was a direct outgrowth of the efforts of the NASA CTS Project Office to demonstrate small terminal applications at its Small Earth Terminals Station (SETS), at the Lewis Research Center in Cleveland, Ohio. The SETS (Fig. 6) consists of a field office type trailer along with a collection of super high frequency (SHF) antennas, ranging in diameter from 0.6m to 4.5m. All of the equipment used for the AKET was based on hardware installed and tested at the SETS.

A diagram of the CTS Data Communication System used for this Alaskan Demonstration is shown in figure 7. The SETS provided the 14.290 GHz uplink to Hermes. Using a standard vestigial-sideband AM modulation scheme, the facsi-


Figure 6. Photograph of the CTS small earth terminal station, NASA/LeRC, Cleveland, Ohio.

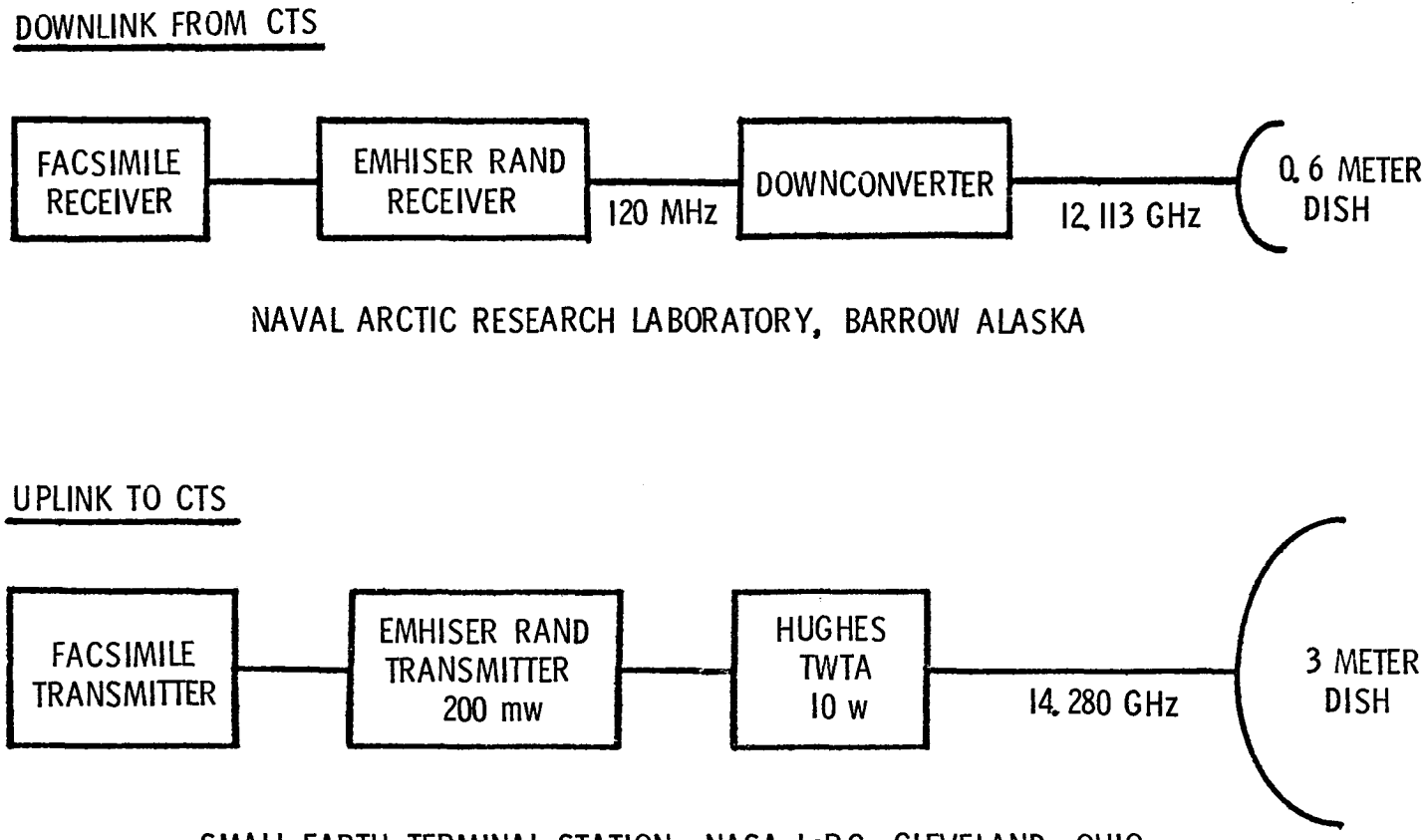


Figure 7. Diagram of CTS data communication system used for Alaskan ice information demonstration.

mile signals of the radar ice imagery were encoded into a 0.3 to 3.0 KHz audio channel. This signal was then fed into the voice signal input of a prototype multi-frequency single channel voice link transmitter. The transmitter produced a 180 KHz wide FM signal at SHF by successive multiplication of a modulated high-frequency signal source. This output drove a high-gain TWTA that provided the uplink power of 10 watts. Although the TWTA used was capable of a saturated output power of 15 watts, the unit was operated at ten watts (as measured at the amplifier output). The TWTA was connected to a 3m dish antenna with a section of helical waveguide (0.7 dB loss). The antenna gain at 14.290 GHz was 49.0 dB.

Hermes is in geosynchronous orbit, stationed at 116° W longitude. The path lengths to Hermes from the SETS (Cleveland) and the AKET (Barrow) are 38,500 and 41,050 km. respectively. The ground station look angles from Barrow were 5.77° elevation and 237.91° azimuth.

The 200W transponder was used for the narrowband downlink. The paramp front end on the spacecraft receiver made the uplink contribution to overall S/N degradation minimal. The SETS had insufficient Effective Isotropic Radiated Power (EIRP) to saturate the transponder TWTA, but due to the high small-signal gain inherent in the channel, a nominal spacecraft output power of 40 watts was achieved. The spacecraft loses 0.85 dB in feed losses, but gains 36.9 dB gain in its antenna. During the demonstration, the spacecraft downlink antenna was boresighted to a point to the south of Barrow so as not to force the antenna gimbals to their stops. As a consequence, the Barrow site was placed at the antenna's 1 dB down contour.

The AKET consisted of a 0.6 meter parabolic dish antenna, an outdoor downconverter, and an indoor receiver and power supply. The antenna was mounted 9.3 meters above ground on a utility pole adjacent to the main science building at the Naval Arctic Research Laboratory (NARL) (Fig. 8). The larger antenna shown in this figure is a 1.2 m parabolic dish antenna used in a separate video teleconference demonstration (Appendix A). From their vantage point well above the building's roof the antennas had an unobstructed view of the flat, wet tundra to the south and the Arctic Ocean several hundred yards to the northwest. The antenna-mounted downconverter used a tunnel diode amplifier (TDA) to achieve an input noise figure of 7.5 dB. The first downconversion of the 12.113 GHz downlink occurred immediately following the TDA, allowing the signal to be cabled indoors at an I.F. of 250 MHz. After conversion to a second I.F., the signal was modulated by a phase-locked loop with a predetection bandwidth of 220 KHz. The recovered baseband signal was then amplified to levels sufficient to drive a standard facsimile receiving unit.

Figure 8. CTS receive facility at Naval Arctic Research Laboratory, Barrow, Alaska.

## SUMMARY OF RESULTS USING HERMES DATA LINK

Hermes transmissions to Alaska ran from August 14 through August 28, 1976. The SETS would begin uplinking and adjust its ground antenna position to maximize the spacecraft output power. Spacecraft movement in orbit during this time was so small that once peaked, the ground antenna did not require further adjustment. The 0.6 meter receiving antenna, lacking the remote-controlled step-track mechanism of its transmitting counterpart, once adjusted was locked in place for the duration of the experiment. The feedhorn polarization had a significant effect on received signal strength.

The successive frequency multiplication scheme used in the uplink transmitter was plagued by drifts in the multiplier chain that resulted in erratic output power. Fortunately, output frequency remained stable, so that the unit was able to drive a high-gain TWTA that provided the uplink power. A modern implementation using directly modulated SHF sources to drive a TWTA would certainly be more reliable and cost effective.

Two sets of narrowband link performance data are pre sented in Table I. The first are the results acquired at Barrow. The second set details the performance of the very same equipment installed at the SETS and operated in the same manner as they were in Barrow. The signal-to-noise (S/N) ratio measured at 1000 Hz are presented for spacecraft output power (TPRF) ranging from approximately 8 to 40 watts.

TABLE I

NARROWBAND VOICE CHANNEL PERFORMANCE

| NARL, BARROW, ALASKA | | SETS, CLEVELAND, OHIO | |
|---|---|---|---|
| Spacecraft Transmitter Output Power (TPRF), Watts | $\frac{S}{N}$ | Spacecraft Transmitter Output Power (TPRF), Watts | $\frac{S}{N}$ |
| 40.3 | 38.2 dB | 40.1 | 44.6 dB |
| 24.0 | 32.8 dB | 21.1 | 37.6 dB |
| 15.4 | 29.4 dB | 15.4 | 33.9 dB |
| 9.5 | 25.4 dB | 8.3 | 29.3 dB |

Even at the lower spacecraft output power levels, the S/N ratio provided an ample margin for the ice-imagery facsimile transmissions. During this demonstration, the arid climate of Barrow featured an almost steady mid-thirties Fahrenheit temperature with no bouts of precipitation. The heavy ground

fog at Barrow during at least half of the periods of data collection had no noticeable effect on system performance. It is felt that data presented herein was acquired under the optimum circumstances of transmission paths and operating techniques (e.g. ground antenna pointing).

Due to prior operational commitments the SLAR aircraft did not conduct its first radar flight in Alaska until August 27, 1976. Shut down of the Hermes communication system during the then upcoming solar eclipse period was scheduled to begin August 29. Therefore, only one near real-time data transmission using Hermes was accomplished. Prior to this flight, a number of facsimile test transmissions were conducted. However, at the time of the August 27 flight, deteriorating weather and fog had prevented visual ice-reconnaissance flights for the previous few days. The SLAR aircraft was unable to land at Barrow to deliver the radar downlink receiving equipment, due to poor weather. Radar data, however, were successfully relayed to Cleveland via the GOES Satellite link and a radar image was facsimile transmitted back to Barrow from Cleveland via the Hermes link.

Ice observers from the U.S. Navy and the Arctic Institute of North America (AINA) stationed at Barrow used this radar imagery and subsequent real-time imagery generated using the radar downlink recorder to develop interpretative ice charts. Figure 9 is an example of a SLAR Image/Ice Chart Product generated for August 27, 1976, in the Beaufort Sea between Smith Bay and Prudhoe Bay. The ice chart outlines the various ice concentration boundaries and identifies the open-water areas. Ice Concentrations are presented in eighths, i.e., 3/8 indicates that the area is 37.5 percent covered by ice.

## CONCLUDING REMARKS

The radar downlink equipment was installed at Barrow on August 19 and provided real-time radar imagery on an almost daily basis through September 10 in continued support of the tug and barge movements. After September 10, additional radar flights were conducted through September 19 in support of the scientific activities of the Coast Guard icebreaker Glacier.

This demonstration was extremely useful in (1) revealing the ice information requirements to support barge operations along the North Slope (NASA Lewis Research Center and U.S. Coast Guard, 1977); (2) verifying that the all-weather near real-time ice information system developed for the Great Lakes could successfully meet these requirements.

The audio circuit provided by the Hermes narrowband communications link provided many hours of dependable high-quality facsimile transmission. The system operated with a satellite viewing angle of 5.77° with no apparent ground-reflection impairments nor insurmountable slant-path losses.

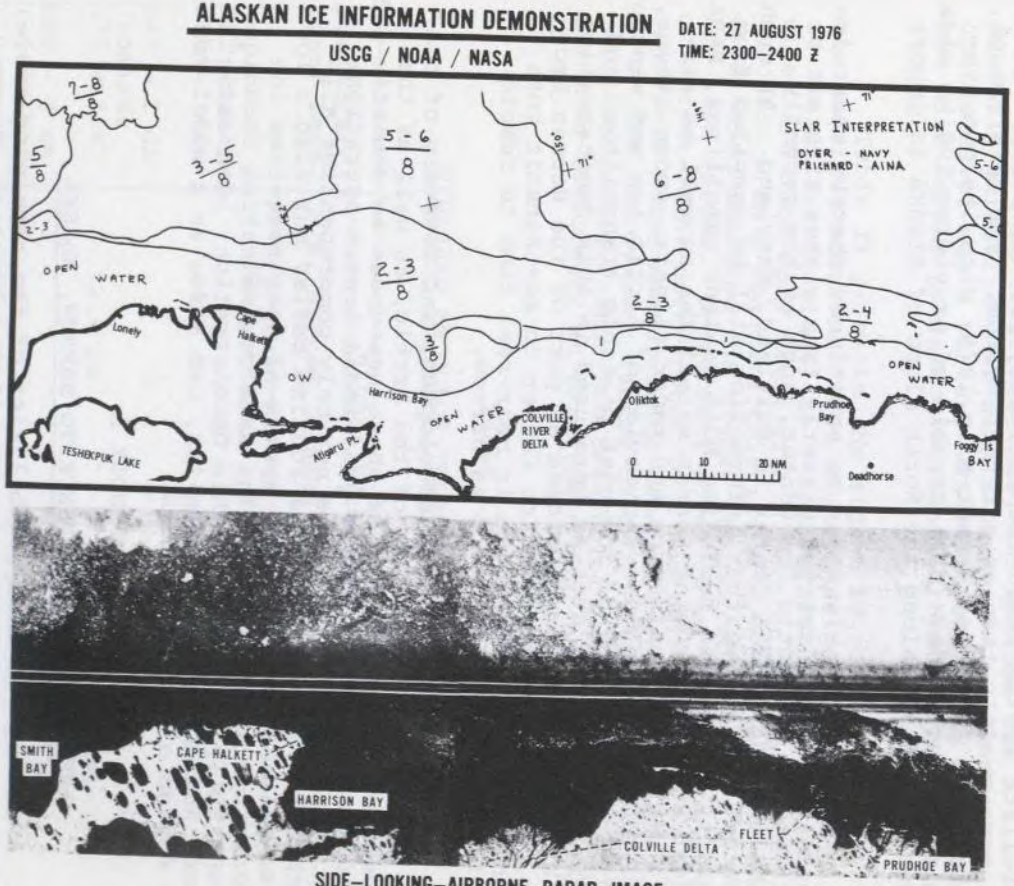


Figure 9. SLAR image/ice chart product of Alaskan North slope on August 27, 1976.

The small terminal configuration allowed a rapid, easy deployment. The high-power of the Hermes transponder allowed small terminals to be used at both ends of the link, keeping system costs within reason.

The SLAR used in the demonstration was mounted on a Coast Guard HC-130B aircraft. Future radars mounted aboard a satellite system could theoretically provide more frequent data more readily than an aircraft system. For this reason, the upcoming launch of Seasat-A in 1978, with its own synthetic aperture radar (SAR) capable of providing 100 km wide images of the ice along the North Slope of Alaska is important.

Future operations can be envisioned whereby radar ice information is transmitted directly from either aircraft or satellite to an Arctic Ice Center, such as the recently established Navy/NOAA Center in Suitland, Maryland. At such a center, ice and weather information will be compiled from a variety of sources including NOAA weather satellites, NASA Landsat and the upcoming Seasat satellites as well as aircraft visual reconnaissance and radar flights, among others, to develop a comprehensive overview of Arctic ice and weather conditions. The use of low-cost portable transmitting and receiving stations, such as were used in this demonstration and are being further developed as part of the Hermes Program, would allow such an Ice Center to re-transmit both weather and ice information in near-real time to remote Arctic field locations such as Barrow.

The future economic development and recovery of the vast oil and gas resources of the Arctic, as well as the subsequent transportation of these resources to domestic and world markets, will require year-round Arctic operations. Such operations will require not only comprehensive all-weather ice information on a routine basis, but also a low cost, reliable and flexible system of near real-time ice information distribution. The data communication technique successfully pioneered in this Demonstration, both using Hermes and direct radar downlink, can serve as a model for the design of future systems.

## APPENDIX A

## HERMES TELECONFERENCE TO BARROW, ALASKA

To explore the possibilities of the receiving environment presented by the Barrow, Alaska location, Hermes personnel carried along wideband FM color television receiving equipment. The installed system featured a 1.2 m dish antenna mounted 8.5 m high and a receiver with a relatively modest front-end noise figure. Surprisingly, the system was able to receive quite useable signals. Using the noisy commercial telephone circuits to return comments and questions, Barrow residents were able to participate in a live color teleconference between Barrow, Alaska and Cleveland, Ohio. The color programming originated at the Lewis Research

Center. It was transmitted to the CTS by the powerful Lewis Ground Station so as to obtain full spacecraft output power of greater than 200 watts. This historic color teleconference, the first between the conterminous U.S. and Alaska's North Slope, occurred on the evening of August 14, 1976, Alaskan local time.

For this teleconference, the antenna was a 1.2 m Prodelin parabolic dish with a gain of 41.1 dB (Fig. 8). The receiver was a Varian, VSX-9951, operating at 12.0805 GHz with 36 MHz predetection bandwidth and a noise figure of 6.3 dB.

Table II presents the signal to noise ratio (S/N) of the received color-bar test signals using the same equipment at two different sites, at 3 spacecraft power levels. All video S/N data were taken with a Tektronix Model 1430 in conjunction with a standard television waveform monitor. Before being measured the signal was passed through a 4.5 MHz low pass filter. Spacecraft power level of SAT (saturation of output TWTA) corresponds to a nominal 220 watts. The signal-to-noise measurements were weighted which corresponded to a CCIR improvement factor of 10.1 dB. This factor is a noise-weighting factor for triangular noise. Picture quality degraded noticeably at weighted signal-to-noise levels below 40 dB.

TABLE II

WIDEBAND FM COLOR TELEVISION RECEPTION

| Spacecraft Power Level | Signal to Noise Measurements | |
|---|---|---|
| | S/N, Barrow, Alaska | S/N, SETS, Cleveland, Ohio |
| | Weighted | Weighted |
| SAT (nominal 220 watts) | 44.9 dB | 51.7 dB |
| SAT - 1 dB (nominal 175 watts) | 42.6 dB | 48.7 dB |
| SAT - 2 dB (nominal 139 watts) | 39.0 dB | 46.0 dB |

## REFERENCES

Anderson, V.H.
1966 High Altitude, Side Looking Radar Images of Sea Ice in the Arctic, *Proceedings of the Fourth Symposium on Remote Sensing of Environment*, University of Michigan, Ann Arbor, pp. 845-857.

Johnson, J.D. and Farmer, L.D.
1971 Use of Side-Looking-Airborne Radar for Sea Ice Identification, *Journal of Geophysical Research* Vol. 76, No. 9, pp. 2138-2155.

Loshchilov, V.S. and Voyevodin, V.A.
1972 Determination of Elements of Ice Cover Drift and Ice Hummock Movement by Means of Toros Airborne Side Looking Radar Imagery Assembly. *Problems of the Arctic and Antarctic*, Gidrometeoizdat Press, Leningrad.

NASA Lewis Research Center and U.S. Coast Guard
1977 All-Weather Ice Information System for Alaskan Arctic Coastal Shipping, NASA TM X-73619.

Robbins, W.H. and Donoughe, P.L.
1976 CTS United States Experiments-A Progress Report NASA TM X-73510.

Rouse, J.W., Jr.
1969 Arctic Ice Type Identification by Radar, *Proceedings IEEE*, vol. 57 pp. 605-614.

Schertler, R.J., Mueller, R.A., Jirberg, R.J., Cooper, D.W., Heighway, J.E., Holmes, A.D., Gedney, R.T., and Mark, H.
1976 Great Lakes All-Weather Ice Information System, *Proceedings of the Symposium on Remote Sensing of Environment*, University of Michigan, Ann Arbor, NASA TM X-71815.

# TRANSMISSION DE DONNEES:

# SEPT-ILES ET QUEBEC

Gilles Missout et Pierre Girard

Institut de Recherche de l'Hydro-Québec

Varennes, Canada

*This paper presents the experiments performed by Hydro-Quebec by means of the Communications Technology Satellite (CTS), or Hermes, as well as the major results obtained. The experiments centered on the measurements of the communications link characteristics, on a method of clock synchronization and the phase measurement of the 735 kV hydro-electric network between Sept-Iles and Boucherville, Québec. The objectives of the experiments were met to everyone's great satisfaction.*

## 1. INTRODUCTION

D'ici quelques années, l'Hydro-Québec prendra la charge de tous les réseaux électriques non reliés au réseau principal de la province. Parmi ceux-ci figurent les postes du Grand Nord québécois actuellement sous la juridiction des gouvernements fédéral et provincial comme par exemple Fort Chimo, Port Harrison, Sugluk. Certains autres, comme ceux de la Côte Nord du fleuve St-Laurent sont déjà sous la tutelle de l'Hydro-Québec.

Ces réseaux non reliés posent un problème de communication assez délicat étant donné les très grandes distances mises en cause. On a eu recours jusqu'à maintenant aux services publics de téléphone (si disponibles) et à la radio HF pour communiquer d'un endroit à l'autre. La fiabilité et la disponibilité de ces liens nous laissent croire qu'ils seront insuffisants compte tenu du développement des prochaines années. La communication par satellite devient alors une solution à ce problème.

C'est dans cet ordre d'idées que l'Hydro-Québec offrit sa participation à l'expérience du Satellite de Technologie de Télécommunication (STT) ou Hermès. L'expérience a comporté trois volets:

1. Mesure de la qualité du lien,

2. Synchronisation d'horloge,

3. Mesure de l'angle de phase entre deux points éloignés d'une ligne à 735 kV.

L'expérience s'est déroulée du 19 octobre à la mi-décembre 1976. L'horaire prévu comptait environ 102½ heures d'antenne. Nous avions comme équipement Hermès à notre disposition:

(a) Deux antennes de 1m de diamètre avec un émetteur et un récepteur de programme sonore (15 KHz de bande passante) situé à l'Institut de Recherche de l'Hydro-Québec (IREQ),

(b) Une antenne de 1m avec un récepteur de programme sonore situé au Poste Arnaud à Sept-Iles.

## 2. MESURE DE LA QUALITE DU LIEN

Afin de caractériser le lien de communication par satellite, nous avons relevé les courbes du temps de propagation de groupe et de réponse en fréquence de chaque canal utilisé. Dans le cas où on désire y transmettre des données numériques, ces caractéristiques deviennent pertinentes particulièrement lorsque le taux de transmission devient élevé. Nous avons également mesuré les niveaux de bruit à la réception pour différentes conditions et pour chacune des liaisons dont nous disposions.

La figure 1 représente schématiquement l'arrangement utilisé pour effectuer ces mesures. Dans tous les cas, ces mesures s'appliquent aux interfaces d'entrée-sortie normalisées (600 ohms équilibrés) telles que décrites dans le manuel "Guide des expérimentateurs de télécommunications" (Huck, 1975). Les figures 2 et 3 concernent le lien téléphonique (TIV/VCU) tandis que les figures 4 et 5 correspondent au programme sonore (APTU). La numérotation des terminaux apparaissant sur les figures est celle du Centre de recherches sur les communications (CRC); D8 et D9 étaient ceux de l'IREQ et D10 celui du Poste Arnaud.

Pour la plupart des cas, les caractéristiques des canaux de transmission prenaient l'allure des figures 2, 3, 4 et 5. D'une expérience à l'autre, nous avons noté de légères variations sur le gain et le délai dans le cas du lien téléphonique. La variation du gain maximal (à 1 KHz ± 100 Hz) était ± 1 dB, et les variations aux fréquences 300 Hz, 1.8 KHz et 3.3 KHz étaient ± 2 dB, ± 1.5 dB et ± 1 dB respectivement. Les délais d'enveloppe aux fréquences 300 Hz et 3.3 KHz étaient 2.0 ± 0.5 ms et - 0.2 ± 0.1 ms respectivement. Ces variations s'expliquent à partir du fait qu'on nous allouait différents VCU (Voice Control Unit) au Terminal de Contrôle du Réseau (TCR) d'une expérience à l'autre pour des raisons de disponibilité d'une part et d'autre part, parce que le TCR n'était pas toujours le même

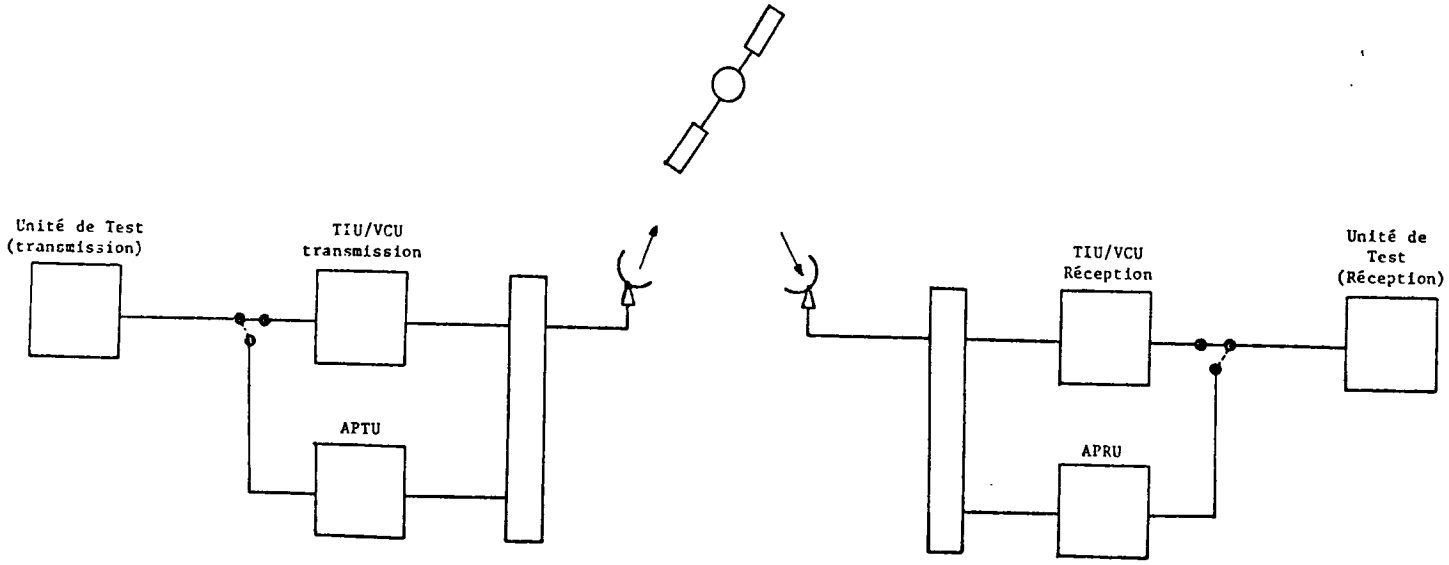
Unité de Test
(transmission)
TIU/VCU
transmission
APTU
TIU/VCU
Réception
APRU
Unité de
Test
(Réception)

Figure 1

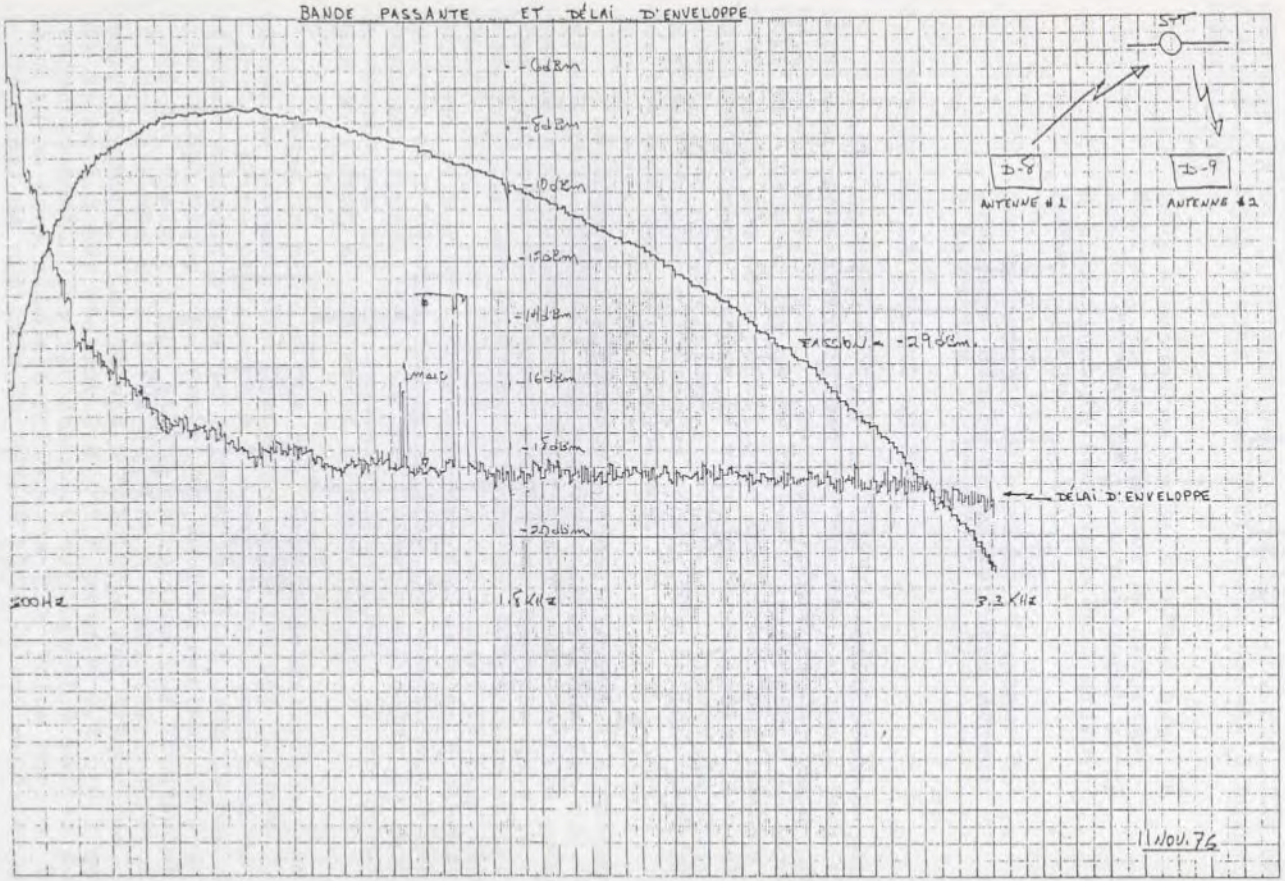
BANDE PASSANTE ET DÉLAI D'ENVELOPPE
-6dBm
-8dBm
-10dBm
-12dBm
-14dBm
-16dBm
-18dBm
-20dBm
FACTEUR = -29dBm
DÉLAI D'ENVELOPPE
500Hz
1.8KHz
3.3KHz
D-8
D-9
ANTENNE #1
ANTENNE #2
11 NOV. 76

Figure 2

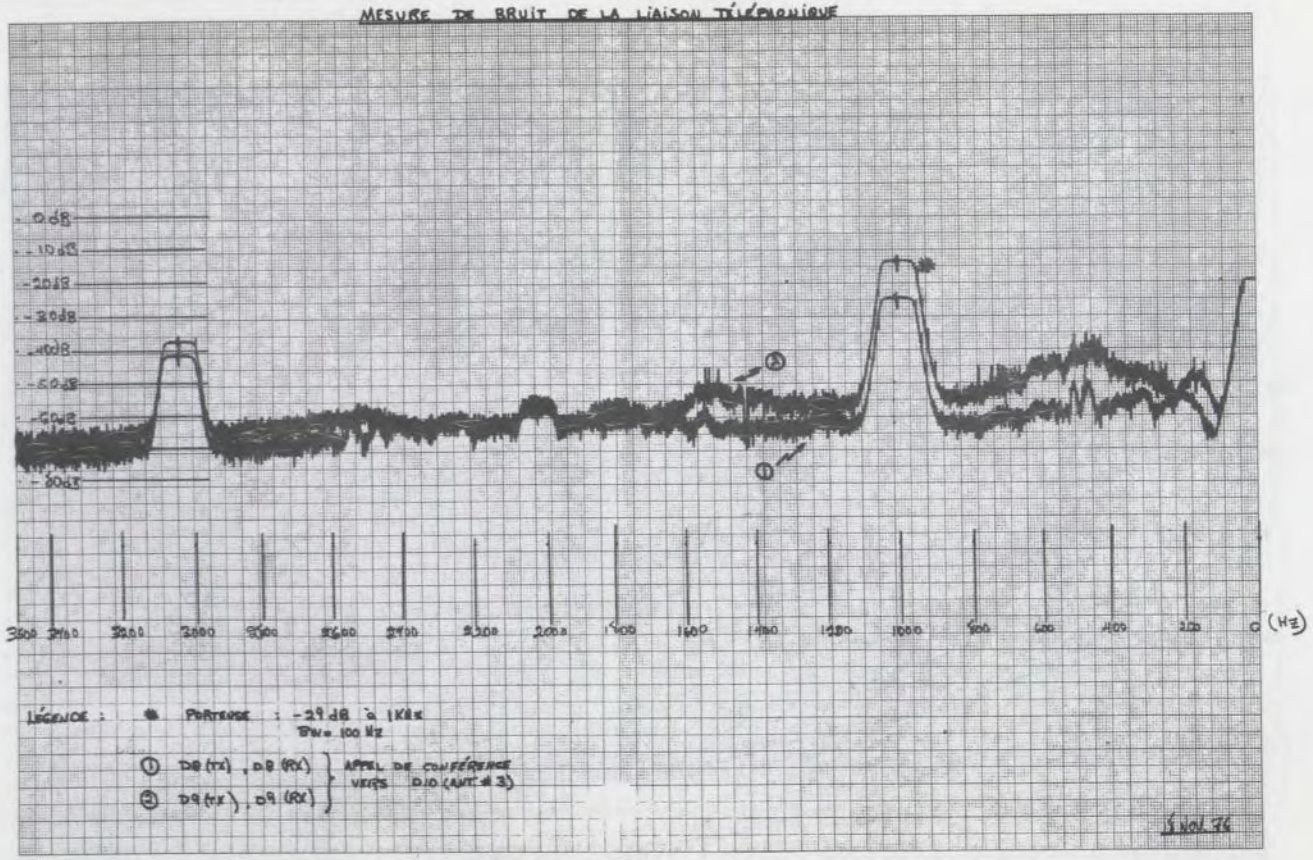
MESURE DE BRUIT DE LA LIAISON TÉLÉPHONIQUE
0 dB
-10 dB
-20 dB
-30 dB
-40 dB
-50 dB
-60 dB
-70 dB
3600
3400
3200
3000
2800
2600
2400
2200
2000
1800
1600
1400
1200
1000
800
600
400
200
0 (Hz)
LÉGENDE :
PORTEUSE : -29 dB à 1 KHz
Bw = 100 Hz
① D8 (TX) , D8 (RX)
② D9 (TX) , D9 (RX)
APPEL DE CONFÉRENCE VERS DJO (ANT. # 3)
5 NOV. 76

figure 3

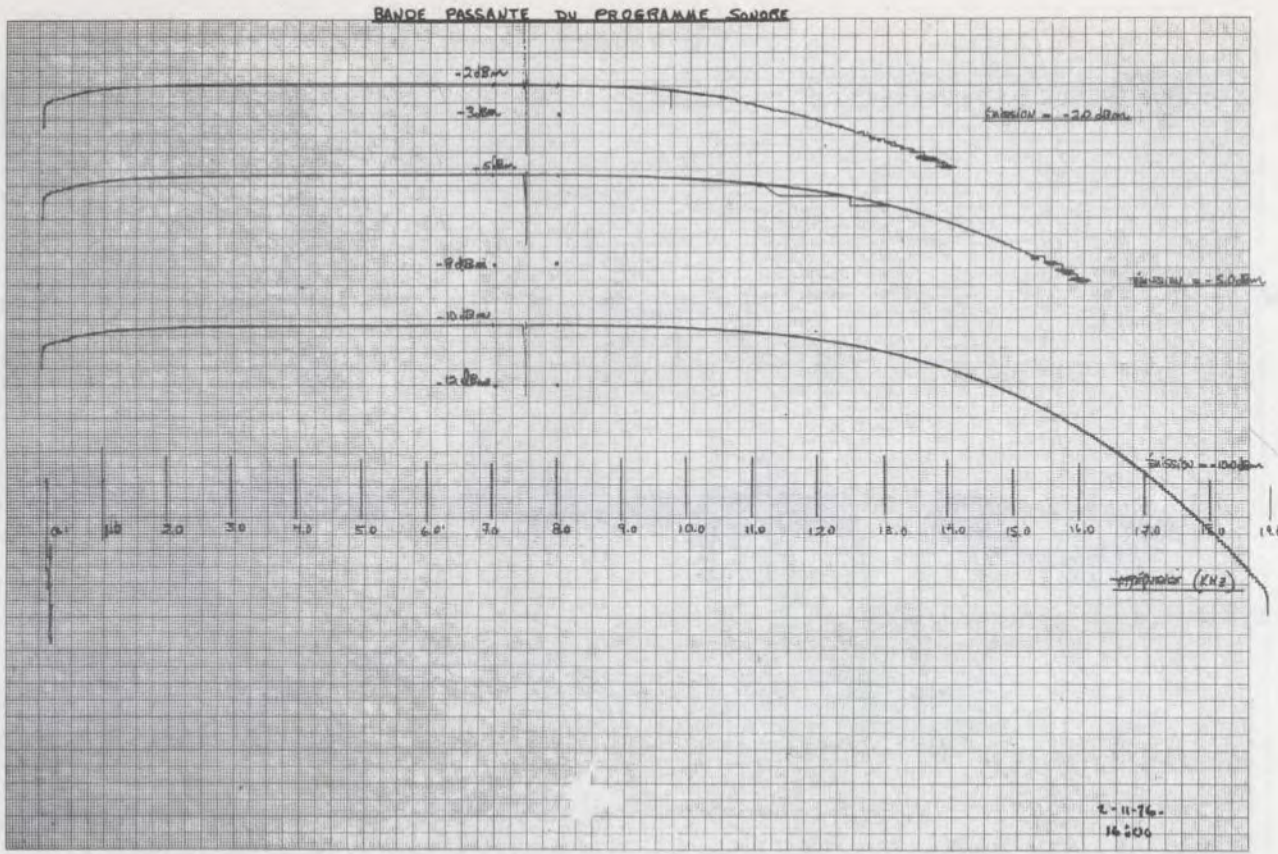
BANDE PASSANTE DU PROGRAMME SONORE
-2dBm
-3dBm
-6dBm
-8dBm
-10dBm
-12dBm
Emission = -20 dBm
Emission = -50 dBm
Emission = -100 dBm
0
1.0
2.0
3.0
4.0
5.0
6.0
7.0
8.0
9.0
10.0
11.0
12.0
13.0
14.0
15.0
16.0
17.0
18.0
Fréquence (KHz)
8-11-76
14:06

figure 4

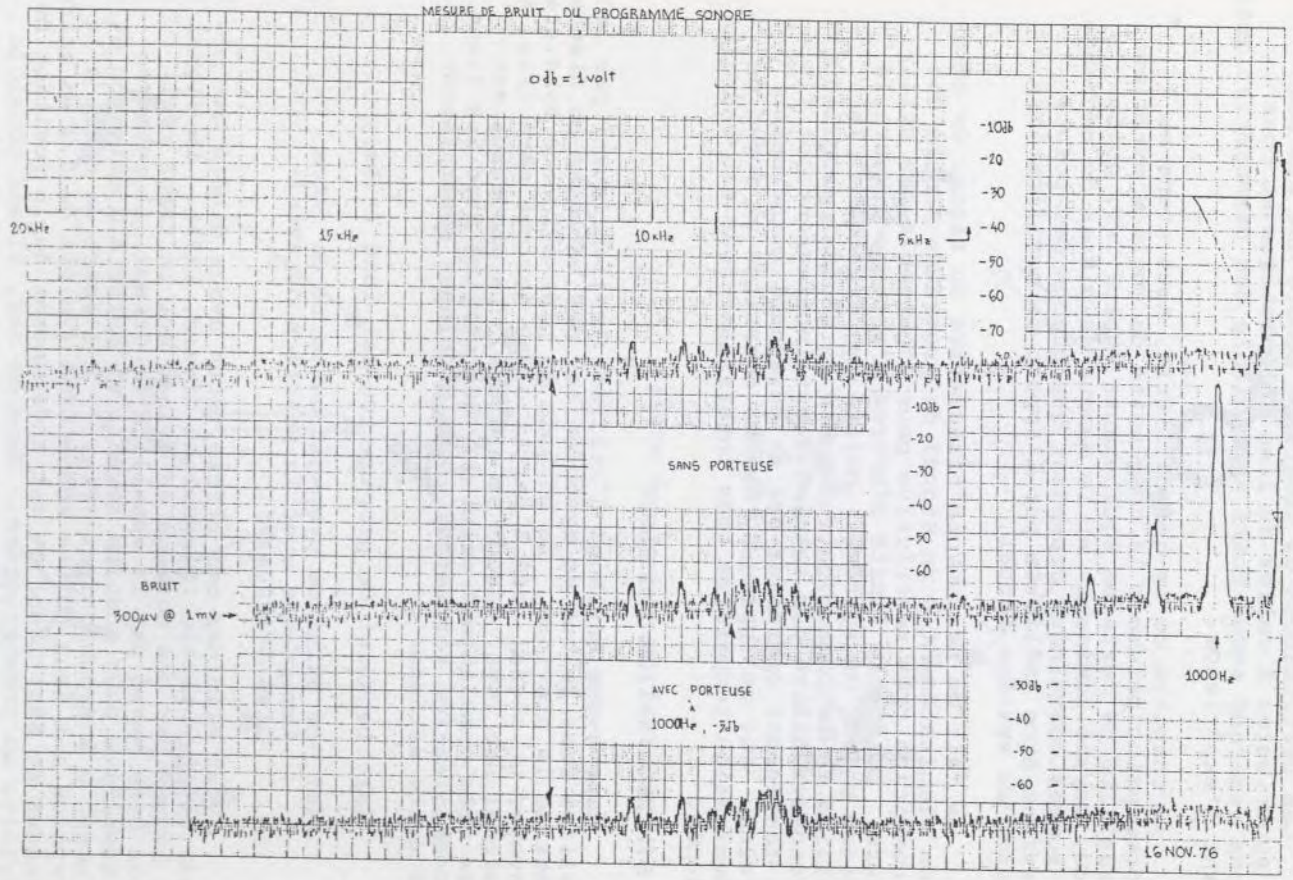
MESURE DE BRUIT DU PROGRAMME SONORE
0 db = 1 volt
20 kHz
15 kHz
10 kHz
5 kHz
-10db
-20
-30
-40
-50
-60
-70
SANS PORTEUSE
BRUIT
300µv @ 1mv
AVEC PORTEUSE
1000Hz, -3db
1000Hz
-30db
16 NOV. 76

Figure 5

(soit le 10m à Ottawa ou le 3m à Montréal, Trois-Rivières ou Québec).

Les performances du programme sonore ont été beaucoup supérieures à celles du lien téléphonique et nous n'avons remarqué aucun écart appréciable des caractéristiques pendant l'expérience.

Au chapitre de la quincaillerie, nous avons eu à déplorer principalement la complexité du montage extérieur, la fragilité de certains équipements (Unité TWT, guide d'onde, voyant lumineux) et le manque de pièces de rechange. Nous sommes convaincus cependant que chacun des points pourraient être améliorés par l'apport de modifications mineures au système actuel.

Le fait de ne pouvoir transmettre un signal de télévision simultanément à un signal de programme sonore est une condition très restrictive pour l'ensemble des utilisateurs. Le nombre limité d'heures d'antenne demeure le handicap majeur du système. Malgré ces remarques, la fiabilité de la communication a été en général excellente. La manoeuvrabilité des terminaux est intéressante et ils sont facilement opérables par un personnel moindrement entraîné. Tel qu'appliqué, Hermès constitue un moyen de communication temporaire très intéressant pour des endroits éloignés.

## 3. SYNCHRONISATION D'HORLOGE

Nous avons envisagé d'utiliser le lien fourni par le satellite dans le but de synchroniser des horloges en divers points de la province. La méthode la plus évidente consiste à envoyer un signal codé à partir d'une horloge mère (Fig. 6). Le signal est reçu, décodé et affiché. Le processus est alors très semblable à celui qui est utilisé avec les liens de communication terrestre. Deux problèmes apparaîtront avec cette méthode:

(a) Le délai de propagation est long ($\simeq$.5s),

(b) Le délai de propagation varie de façon importante avec la position du satellite ($\simeq$100$\mu$s/H).

Pour éliminer ces effets, nous avons étudié une méthode différentielle (Missout et Girard, 1975). Le signal est envoyé par une horloge en avance sur le temps réel. Après être passé par le satellite et Ottawa, il retourne au satellite pour ensuite revenir au point A d'émission et au point B à synchroniser (Fig. 7) à l'écart de délai à la réception aux deux points est minime (voisin de 2.2 ms entre Varennes et Sept-Iles) et est indépendant de la position du satellite au premier ordre. Dans ce cas, il est possible de régler l'horloge d'émission pour que la réception en A soit "à l'heure". La réception en B est alors en retard de 2.2 ms.

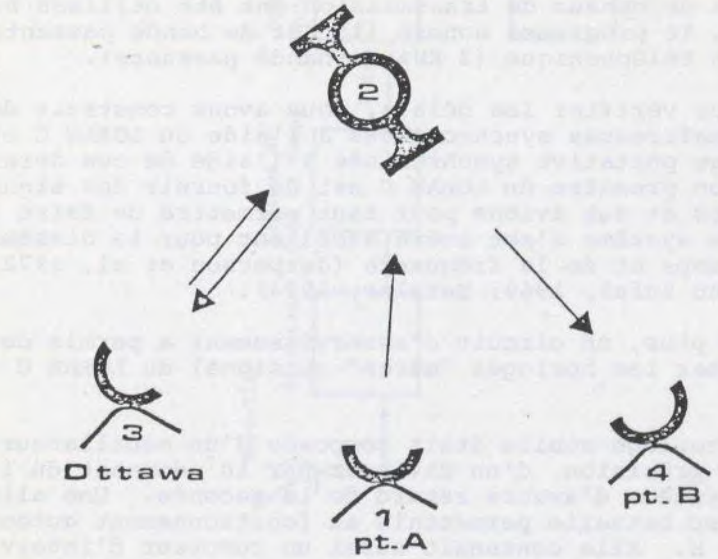


Figure 6

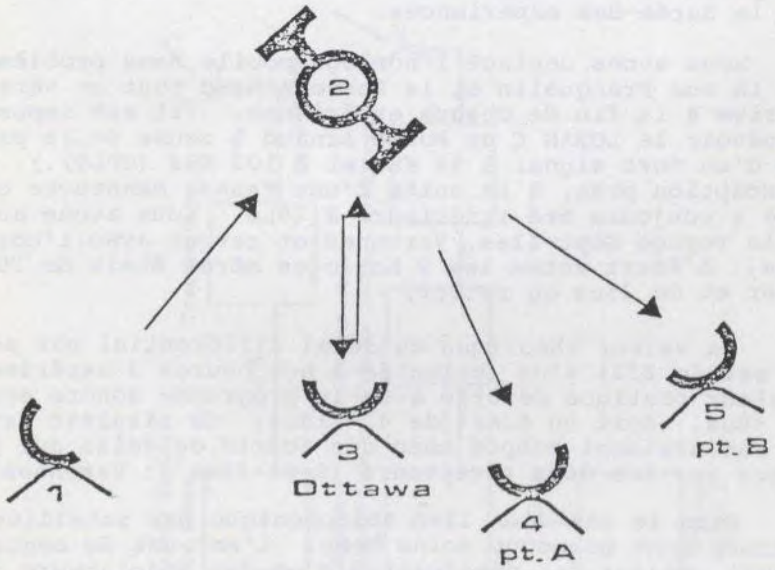


Figure 7

Dans ce but, nous avons utilisé les circuits déjà employés sur le système de communication de l'Hydro-Québec. La modulation est du type IRIG B. La porteuse est à 2 KHz. Deux types de canaux de transmission ont été utilisés sur le satellite, le programme sonore (15 KHz de bande passante) et le lien téléphonique (3 KHz de bande passante).

Pour vérifier les délais, nous avons construit deux horloges maîtresses synchronisées à l'aide du LORAN C et une horloge portative synchronisée à l'aide de ces dernières. La fonction première du LORAN C est de fournir des signaux aux navires et aux avions pour leur permettre de faire le point. Ce système s'est avéré excellent pour la dissémination du temps et de la fréquence (Jesperson et al, 1972; Stetina and Zufal, 1969; Netzler, 1974).

De plus, un circuit d'asservissement a permis de synchroniser les horloges "mères" au signal du LORAN C (Fig. 8).

L'horloge mobile était composée d'un oscillateur à quartz de précision, d'un diviseur par $10^7$ donnant du 1 Hz et d'un système d'avance retard de la seconde. Une alimentation avec batterie permettait au fonctionnement autonome sur 5 à 6 H. Elle contenait aussi un compteur d'intervalle pouvant mesurer le délai entre deux impulsions, la mise à l'heure des horloges et l'observation de leur dérive.

Les deux systèmes basés sur le LORAN C (Sept-Iles, Varennes) ont parfaitement fonctionné. A part deux incidents (une fausse manoeuvre et un convertisseur 28 V à 5 V qui a grillé), l'asservissement est resté accroché pendant toute la durée des expériences.

Nous avons déplacé l'horloge mobile sans problèmes entre la rue Franquelin et le Poste Arnaud tout en vérifiant la dérive à la fin de chaque expérience. (Il est impossible de recevoir le LORAN C au Poste Arnaud à cause de la présence d'un fort signal à 98 KHz et à 102 KHz (OPLT).) A une exception près, à la suite d'une fausse manoeuvre cette dérive a toujours été inférieure à 20µs. Nous avons aussi fait le voyage Sept-Iles, Varennes et retour avec l'horloge mobile. L'écart entre les 2 horloges mères était de 20µs à l'aller et de 25µs au retour.

La valeur théorique du délai différentiel par satellite est de 2221 ±3µs (calculée à nos heures d'expérience). La valeur pratique mesurée avec le programme sonore est de 2179 ±8µs. Soit un écart de 42 ±10µs. Ce résultat est très satisfaisant compte tenu des écarts de délai qui peuvent exister sur les deux récepteurs (Sept-Iles et Varennes).

Dans le cas d'un lien téléphonique par satellite, les résultats sont beaucoup moins bons. L'antenne de contrôle (Ottawa) utilise des démodulateurs et des modulateurs dans le multiplexeur (une paire par antenne de 1m). Ces appareils ont des caractéristiques qui variaient de l'un à l'autre.

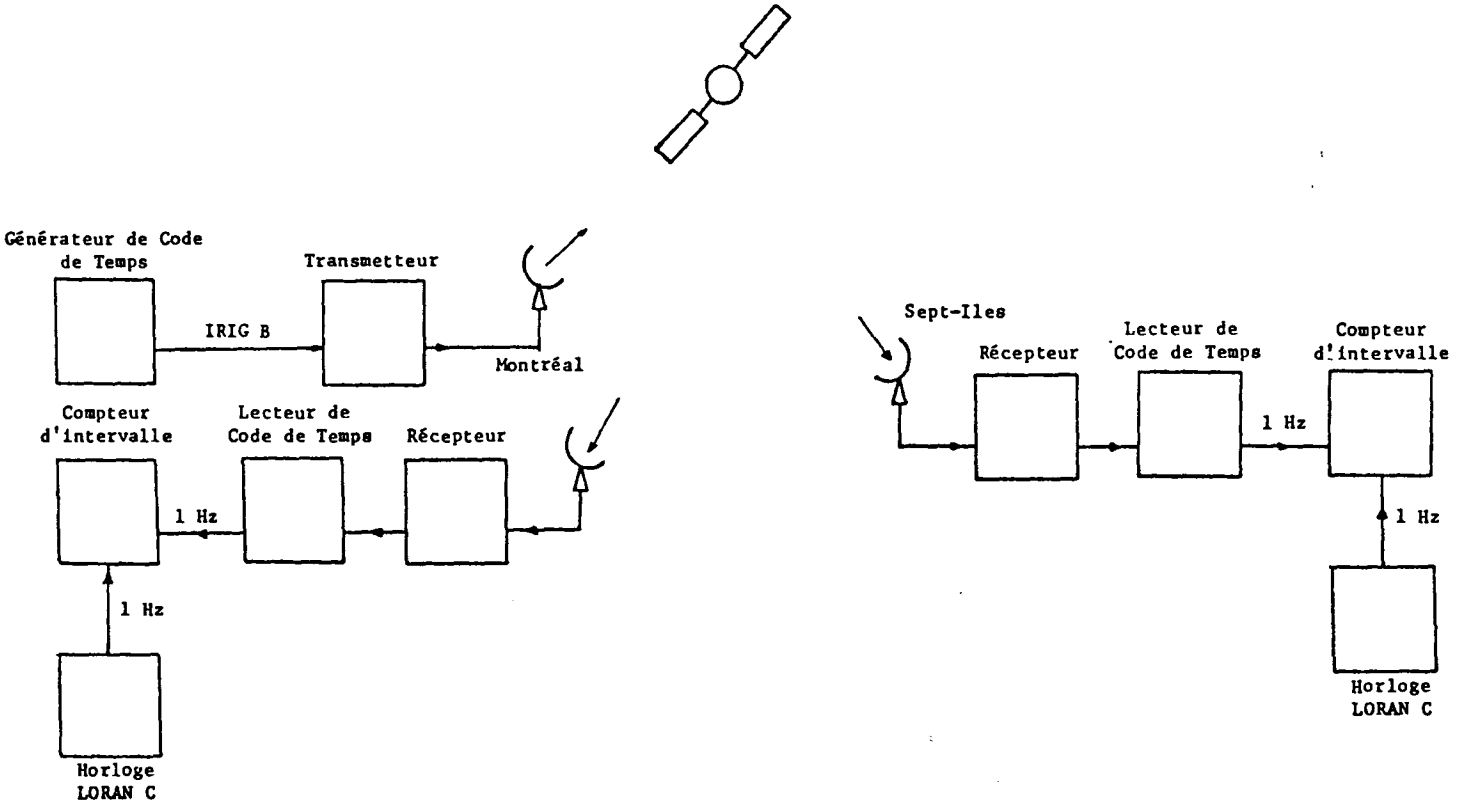
Générateur de Code de Temps
Transmetteur
IRIG B
Montréal
Compteur d'intervalle
Lecteur de Code de Temps
Récepteur
1 Hz
1 Hz
Horloge LORAN C
Sept-Iles
Récepteur
Lecteur de Code de Temps
Compteur d'intervalle
1 Hz
1 Hz
Horloge LORAN C

Figure 8

Ils ont été changés plusieurs fois au cours des expérien . De plus, les récepteurs à Varennes et à Sept-Iles sont aussi différents. Les valeurs obtenues ont varié entre 2.1 ms à 2.3 ms dépendant des expériences. Cependant, au cours d'une même expérience (même appareillage aux deux bouts et à l'antenne de contrôle) le délai était stable à quelques microsecondes près.

## 4. MESURE DE PHASE

L'angle de phase est une bonne mesure de l'indice de sécurité du réseau c.-à-d. de sa stabilité. L'apparition d'oscillation de l'angle de phase peut indiquer le début d'une instabilité ou l'existence d'un incident de réseau. Dans les automatismes, une telle mesure semble intéressante au niveau du contrôle de la tension soit directement, soit en interdisant ou autorisant le fonctionnement de certains automatismes pour des valeurs d'angle de phase jugées critiques.

L'expérience de synchronisation d'horloge nous amène à avoir deux horloges synchronisées à ±20µs à Varennes et à Sept-Iles. Il est alors possible de mesurer la phase du 60 Hz sur une ligne de transport entre les deux points précités (Missout et Girard, 1977).

Pour cela, on peut mesurer le délai qui s'écoule entre un front montant de la seconde et le prochain passage par zéro en montant du 60 Hz (Fig. 9). La mesure est faite

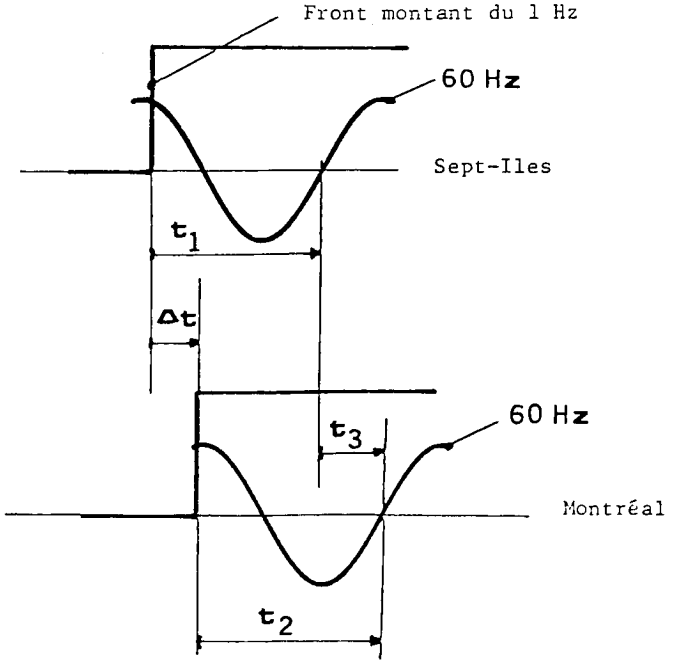


Figure 9

simultanément à Sept-Iles et à Varennes. L'information est expédiée de Sept-Iles à Varennes. La soustraction des deux mesures donne le déphasage en microseconde entre Sept-Iles et Varennes.

Nous avons mesuré la différence de phase entre la phase A de la ligne 735 kVolts reliant Arnaud via le Poste Boucherville. Nous avons compilé plusieurs heures d'enregistrement pendant l'expérience et, quoique incomplets, les résultats montrent que la différence de phase est relativement constante sur une période de plusieurs heures et qu'elle a oscillé de 32° à 42° (cas extrêmes) sur la durée des expériences (≃ 1 mois).

Pour fins de vérification, nous avons fait calculer par les gens de Conduite du Réseau, la valeur de cette phase pour le jeudi 25 novembre 1976 à 15 heures. Leur calcul a donné 33.0°, nous avons mesuré 33.0°! On doit cependant apporter à cette dernière valeur de légères corrections dues principalement au décallage horaire des horloges et au délai du lien téléphonique reliant le transformateur de potentiel du Poste Boucherville à l'instrument de mesure de l'IREQ. Cette correction sera dans le pire des cas, inférieure à 1.5°.

## 5. CONCLUSION

Les buts visés (mesure de qualité du lien, synchronisation d'horloges et mesure d'angle de phase) ont été atteints de façon très satisfaisante. Le lien téléphonique a bien fonctionné pour la voix si l'on écarte quelques problèmes de jeunesse (filtre) qui pourraient être facilement corrigés. Ce moyen pourrait donc parfaitement être utilisé pour communiquer avec des points isolés (Nord du Québec, chantier temporaire, etc.). Le lien du programme sonore fournit un excellent moyen de synchronisation d'horloges (mieux que ±8μs). La mesure de phase a donné d'excellents résultats.

Les applications futures de communication par satellite sont subordonnées à la disponibilité de ce dernier. Il serait cependant judicieux de suivre le dossier car la tendance est à une diffusion de plus en plus grande de ce type de lien.

Côté mesure de phase, nous avons démontré la "faisabilité" de la chose. Rappelons que cette mesure utilise le réseau Hydro et des récepteurs LORAN C et de ce fait, est indépendante du satellite. Un effort devrait être fait pour rendre le système automatique et disponible en tout temps (Netzler, 1974). Une telle mesure semble applicable en conduite du réseau (l'angle de phase peut être fourni à l'opérateur en temps réel, comme une bonne mesure de l'indice de sécurité du réseau).

Au niveau de l'enregistrement chronologique des événements et des oscillo-perturbographes, il serait aussi possible d'améliorer la précision temps des enregistrements. ($\Delta t \leq 40\mu S$) Une telle mesure serait sans doute intéressante entre les points extrêmes du réseau (Baie James, Montréal, Churchill Falls).

## BIBLIOGRAPHIE


Huck, R.W.
1975 *Guide des Expérimentateurs de Télécommunications*, Ministère des Communications, Gouvernement fédéral, Vote Technique du CRC 671 (CS-03-01), février.

Jesperson, J.L., Blair, B.E. et Gatterer, L.E.
1972 "Characterization and Concepts of Time Frequency Dissemination", *Proc. IEEE*, 60 No. 5, pp. 502-521, May.

Missout, G. et Girard, P.
1975 "Study of a Method of Clock Synchronization by Satellite", *International Electrical, Electronics Conference Exhibition*, Sept. 29-30 and Oct. 1. Cat. #75-24901, pp. 124-125, Toronto.

Missout, G. et Girard, P.
1977 "Measurement of Bus Voltage Angle Between Montreal and Sept-Iles", *IEEE PES Summer Meeting*, Mexico, July 7-22.

Netzler, P.R.
1974 "An Automatic Timing Receiver System Based on the LORAN C Navigational Network", *IEEE Trans. on Aerosp. and Electronic Syst.*, AES 10, No. 3, pp. 346, May.

Stetina, F.L. and Zufal, S.Z.
1969 "LORAN C. A Time Synchronization Technique", *Goddard Space Flight Center*, rapport X83269514, September.

# TELECONFERENCING EXPERIMENTATION

# ORIENTED TO NASA APPLICATIONS

John Chitwood, NASA/Goddard Space Flight Center, Greenbelt, Maryland, U.S.A.
Patti Boyce, NASA Headquarters, Washington, D.C., U.S.A.
Erwin Edelman, NASA/Lewis Research Center, Cleveland, Ohio, U.S.A.
Bradford Gibbs, NASA/Ames Research Center, Moffett Field, California, U.S.A.
Michael Richardson, NASA/Lewis Research Center, Cleveland, Ohio, U.S.A.

*Le présent document décrit une expérience de téléconférence vidéo menée actuellement par la NASA au moyen du satellite technologique de télécommunications. On a mis surtout l'accent sur la conception des systèmes et sur les résultats obtenus jusqu'à présent. Divers centres de la NASA participent à l'expérience, notamment le Bureau central à Washington, DC, le NASA Ames Research Center à Moffett Field, en Californie; la NASA Lewis Research Center à Cleveland, dans l'Ohio; et le NASA Goddard Space Flight Center, à Greenbelt, dans le Maryland.*

*La NASA a montré beaucoup d'intérêt pour les études de l'efficacité de la téléconférence dans le but de remplacer et même d'éviter complètement les déplacements des participants. Cet intérêt résulte en partie du désir de la NASA de continuer à diriger ses nombreuses activités dans diverses régions des Etats-Unis, malgré son faible budget pour les déplacements, le coût de plus en plus élevé des voyages et la nécessité de conserver l'énergie. La NASA est désormais en mesure de démontrer à d'autres éléments du gouvernement et aux secteurs de l'industrie comment la téléconférence peut contribuer au maintien d'une coordination efficace des programmes de travail entre groupes éloignés les uns des autres. Cette expérience de téléconférence entreprise par la NASA a été conçue afin d'éprouver l'hypothèse selon laquelle cet organisme peut utiliser la téléconférence vidéo d'une manière concluante, grâce à un puissant satellite de communications. Cette expérience devait permettre de trouver des solutions à certains problèmes bien précis, notamment l'utilisation d'appareils de sécurité efficaces mais peu coûteux sur les circuits sonores et vidéo, ainsi qu'une étude des effets de l'atténuation causée par la pluie sur la qualité des images transmises durant la téléconférence.*

*On examine les considérations d'ordre général dans l'organisation d'une téléconférence vidéo.*

*On étudie également les questions relatives à l'éclairage, aux systèmes vidéo et sonore, à la sécurité et aux stations au sol.*

*L'expérience se poursuit sous deux grands aspects, soit la performance technique et l'efficacité de la téléconférence proprement dite. Du point de vue technique, on évalue dans quelle mesure l'équipement de la station terrestre permet d'atteindre les objectifs de l'expérience. Cette évaluation comprend un inventaire de l'équipement requis pour diriger une téléconférence au moyen d'un satellite géosynchronique de communications, l'utilisation d'un équipement susceptible de permettre des communications de bonne qualité, ainsi que les effets d'une diminution des signaux causée par les précipitations atmosphériques. On évalue au moyen d'un questionnaire l'efficacité de la téléconférence proprement dite.*

*Avec le système de téléconférence vidéo de la NASA, on cherche à obtenir une transparence optimale des images télédiffusées. Malheureusement, il faudra toujours tenir compte de la courbe qui indique la capacité d'absorption de l'information. Par intuition, on croît que plus cette courbe sera courte, ou bien, moins complexe sera le fonctionnement dy système, plus la téléconférence remplacera avantageusement les déplacements.*

## INTRODUCTION

Since June 1976, a teleconferencing experiment has been conducted by the National Aeronautics and Space Administration (NASA) via the joint Canadian-United States Communications Technology Satellite (CTS) or Hermes. The experiment uses ground stations installed at Ames Research Center, California; Lewis Research Center, Cleveland; and Goddard Space Flight Center, Maryland. NASA Headquarters, Washington D.C., has been brought into the loop via land lines from Goddard. The ground stations had been installed initially for other experiments with the Teleconferencing Experiment, becoming a bonus feature at minimum cost.

The CTS is a high-power experimental communications satellite operating in the 12 and 14 GHz bands (see Davies, 1978, for details). With suitable ground stations, the CTS may be used to relay color video plus accompanying audio in a full-duplex mode.

## CONCEPT

For some time now, NASA has shown interest in determining the effectiveness of teleconferencing, as a supplement to and replacement for travel. This interest is due in part to NASA's desire to continue to manage its widespread activities effectively in spite of smaller travel budgets, increased travel costs, and a need for energy conservation. This CTS Teleconferencing Experiment was conceived to test the hypothesis that NASA can effectively use video teleconferencing. Some of the technical problems to be addressed as part of the experiment included the implementation of low-cost effective security apparatus on the video and audio circuits, and an investigation of the effects of rain attenuation on the quality of the teleconferencing.

Our emphasis has been on developing interactive communications facilities where the participant or user is involved as much as possible, so that he is put into a true conference environment as opposed to the television studio arrangements. If participants can operate the system with a minimum of effort and training they will begin to feel as comfortable as they are using their telephone. Accordingly, efforts are being made to optimize system transparency. Unfortunately, there will always be a learning curve associated with using a teleconferencing facility. Intuitively, it is felt that the shorter the learning curve, or the smaller the complexity of the operational system, the more transparent it becomes and the more attractive video teleconferencing will become.

## ENVIRONMENT CONSIDERATIONS

The lighting system used in a video teleconferencing facility is of major concern because of its effect upon the quality of the video picture as well as on the teleconference participants. The esthetics of the lighting system must be considered in order for the teleconferencing participants to look natural and the lighting should not be annoying to the eye. On the other hand, an acceptable picture requires high light levels which are usually annoying to the participants. Many compromises must therefore be made between light levels, camera costs, light placement, picture quality, and comfort to the participant.

We have found that a very low-noise-level air-conditioning system is required for people to be comfortable and get the most out of the communications system. When the air conditioning is not functioning, the productivity of the session drops considerably.

## SYSTEM CONFIGURATION

### General Considerations

Each center assembled a video teleconferencing facil-

ity to best suit its own needs. At Ames, the required hardware was incorporated into an existing Audio/Facsimile Teleconferencing Facility, adding a new dimension in interactive communications. NASA-Lewis also incorporated the video system into a conference room. In order to meet a dual-purpose requirement, however, portions of the equipment are removed during other uses of this conference room. The Video Teleconference Facility at NASA-Goddard was assembled in a room which also serves as a Telecommunications Demonstration Laboratory. NASA Headquarters designed a simple facility specifically for video conferencing incorporating many features found in the other three locations.

Video

Each of the above facilities uses one or two "talent" cameras to cover the prime participants, and an overhead "document" camera, to transmit participant-explained visuals, such as sketches, notes, or printed material.

The Ames Facility is arranged conventionally with a table for the participants, two TV color monitors in front of them, one for the incoming picture and one for the outgoing picture, with the "talent" camera mounted in between. The black and white "document" camera is mounted in the ceiling over the table. Both cameras have been arranged for remote zoom capabilities with the "talent" camera also having remote pan and tilt capability. A small control console to the right of the chairperson or principal speaker provides camera control and selection of the "talent" or "document" camera for the outgoing picture.

The NASA-Lewis facility allows three prime participants to be seated at the table. A number of secondary participants may be seated between these prime participants and the back-drop. A 25-inch color monitor is within easy view of all participants. Two color cameras are located in the facility, one camera is used as a "talent" camera, the other as a color-graphics camera. An overhead-viewing system using two front-surface mirrors allows the "document" camera to remain in a horizontal position, thus eliminating camera pick-up tube damage. One critical factor in this system is mirror alignment. Initial mirror alignment is done using elementary optics, and the fine adjustment is by trial and error.

The video systems at NASA Headquarters and NASA-Goddard are very similar. A 25-inch color monitor is directly in front of the table which can handle three or four prime participants. Secondary participants can be accommodated in chairs along the side of the room. A "document" camera is mounted in the ceiling over the center of the table.

In addition, most locations are equipped to record conferences on video tapes, provide special effects such as screen splitting, subtitles through character generators and other miscellaneous services.

## Audio

The audio system for these facilities is relatively straightforward except that satisfactory echo control is mandatory. Echos arise when audio picked up by the microphone at location "A" is sent via the spacecraft to location "B", where that speaker-microphone combination returns it to "A", delayed one-half second because of the earth-to-satellite transmission time. The echo-suppression circuitry currently available effectively minimizes this problem.

NASA-Lewis and NASA-Ames use unidirectional microphones with a cardioid pattern, placed to minimize pickup of the incoming audio. NASA Headquarters and NASA-Goddard use lapel microphones, which by their very nature are very close to each participant's mouth, thus reducing the microphone gain required and reducing echo problems. It has also been found helpful to separate the incoming audio loudspeaker from the microphones as much as possible.

## Security

There is a need to prevent unauthorized personnel who might have a CTS receiving capability from eavesdropping on some teleconferences. Accordingly, privacy devices that might be suitable for inclusion in the NASA Video Teleconference System have been investigated.

Several reasonably-priced audio-security devices are on the market. Most of these use filtering, frequency heterodyning, and frequency inversion techniques. While such devices are not sophisticated enough to prevent deciphering of the audio, they would be a deterrent to most other CTS users. Plans have been made to include some of these security devices in the NASA Video Teleconferencing System in the near future.

With regard to video security, all of the devices studied were either low-cost devices intended for pay-TV applications, which operate at RF, or high-cost devices employing video digitizing using long pseudo-random codes. As neither type of unit was suitable for the Video Teleconferencing application, devices are currently being built in-house at NASA. These are analog devices which operate by inverting some lines of the video format and by delaying others.

## EXPERIMENTAL RESULTS

The evaluation of the experiment was divided into two areas, technical and system effectiveness; neither is complete at this time.

From the technical point of view, it has been found that good audio is one of the most difficult things to achieve, because of echo problems. For best results, the echo suppressors used in the NASA Video Teleconference

Systems must operate at precisely-controlled levels. Also, speaker and microphone placement is often very critical to prevent excessive pick-up of the received audio by the microphones. Likewise, audio gain to the speakers may have to be reduced to low levels to avoid echo problems.

No serious problems have been experienced with the video equipment. As of this writing, precipitation has not caused signal fades strong enough to seriously affect performance of the system. A few ground-station failures have caused short delays in the beginning of some conferences, until repairs could be made. Likewise, problems sometimes arose with the lines connecting the teleconferencing facility to the ground station, causing delays varying from minutes to days.

It has been difficult to obtain quantitative data on the effectiveness of video conferencing because of the small data base and the large number and variety of unknowns. Therefore, we approached the problem from a slightly different perspective; that of developing systems. Comparisons have been made between audio/facsimile conferencing and video conferencing to assess whether or not video conferencing is needed, and in what circumstances. We look upon these experiments and demonstration projects as an opportunity to get some experience prior to locking oneself into a commercial system which may be very costly to modify. We are still in a data-gathering mode and experimenting with different techniques to get as much data as possible for future evaluation.

We have discovered a few significant points already, such as the value of teleconferences for project reviews. A major project review was conducted via CTS involving a large project group at a field center and a small group of Headquarters program people at the Headquarters Facility. This review by satellite took less time, was more informative, and permitted the active participation of more people. This last point is very significant because travel budgets do not normally allow participation by the individuals doing the work unless the reviews are held on site. Through CTS, more people were able to participate in face-to-face dialogue, thus producing a better and more immediate understanding of problem areas and how they arise. Another rewarding area is seminars involving large audiences at a central location interacting with a small remote panel. The use of video enhances the presentation; faces can be associated with names and the use of visual aids allows for a much better understanding of the material being presented.

Some of the problem areas found in this experimental program include the long lead time required to obtain time on the satellite. Because of this, few conferences can be scheduled very far in advance. Prospective participants like to be able to arrange for a video teleconference in one or two days, otherwise they will find other means of conducting their business.

It has also been observed that many graphics are not satisfactorily prepared for video transmissions. There are two possible solutions: provide training in the preparation of graphics, or provide larger screens for graphics projections.

## REFERENCES

Davies, N.G.
1978 The Hermes Mission, *Royal Society of Canada Hermes Symposium*, November 29, 30, December 1, 1977.

Proceedings of the 20th Symposium

of the Royal Society of Canada

held in Ottawa, Canada

29 - 30 November and 1 December 1977

in cooperation with

the Department of Communications

Canada

and

The National Aeronautics and Space Administration

United States of America

---

Les délibérations du 20e symposium

de la Société royale du Canada

tenu à Ottawa, Canada

les 29 et 30 novembre et le 1er décembre 1977

en collaboration avec

le Ministère des Communications du Canada

et

l'Administration nationale d'aéronautique et spatiale

des Etats-Unis d'Amérique